

TRANSIENT POOL BOILING OF CRYOGENIC LIQUIDS ON WATER

by

Ayodeji Jeje

B.S. Purdue University 1969

M.S. Massachusetts Institute of Technology 1970

Submitted in Partial Fulfillment
of the Requirements for the
Degree of Doctor of Philosophy

at the

MASSACHUSETTS INSTITUTE OF TECHNOLOGY

February, 1974

Signature of Author: _____
Department of Chemical Engineering, Feb. 1974

Certified by: _____
Thesis Supervisor

Accepted by _____
Chairman
Departmental Committee on Graduate Theses





Room 14-0551
77 Massachusetts Avenue
Cambridge, MA 02139
Ph: 617.253.2800
Email: docs@mit.edu
<http://libraries.mit.edu/docs>

DISCLAIMER

**Page has been omitted due to a pagination error
by the author.**

(Pages 77, 104-105, 306, 325, 332-334)

Department of Chemical Engineering
Massachusetts Institute of Technology
Cambridge, Massachusetts 02139
February 15, 1974

Professor David B. Ralston
Secretary of the Faculty
Massachusetts Institute of Technology
Cambridge, Massachusetts 02139

Dear Professor Ralston:

In accordance with the regulations of the Faculty, I herewith submit a thesis, entitled "Transient Pool Boiling of Cryogenic Liquids on Water," in partial fulfillment of the requirements for the degree of Doctor of Philosophy in Chemical Engineering at the Massachusetts Institute of Technology.

Respectfully submitted,

ABSTRACT

TRANSIENT POOL BOILING OF CRYOGENIC LIQUIDS ON WATER

BY

Ayodeji Jeje

Submitted to the Department of Chemical Engineering on February 15, 1974, in partial fulfillment of the requirements for the degree of Doctor of Philosophy

The present study is on heat fluxes to cryogenic liquids boiling on an unheated pool of water. The cryogenes studied were liquid nitrogen, methane, ethane, binary mixtures of the hydrocarbons and typical LNG compositions. The cryogenic liquid composition, initial water temperature, and the quantity of cryogen spilled per unit area were the primary variables.

Initial boiling fluxes for liquid nitrogen ranged from 22 to 35 kW/m² and decreased slowly with time. For pure methane, the initial fluxes were about 35 to 45 kW/m² and they increased slightly with time. When even trace quantities (e.g. 0.1-0.2%) of heavier alkane hydrocarbons were present in liquid methane, significant increases in the boiling flux were noted. With a lean LNG (98.2% CH₄, 1.62% C₂H₆, 0.11% C₃H₈ plus trace butanes), the boiling flux was about twice that noted for pure methane, and the rate of increase of the flux was quite pronounced with time. Very high boiling fluxes were also noted for liquid ethane spills.

The effects of water temperature and quantity of cryogen spilled were less pronounced. In general, the boiling fluxes increased slightly as the initial water temperature was lowered.

Liquid nitrogen and methane apparently evaporated on water in the stable film or transition boiling regime. Any ice particles that were generated at the water surface were recirculated into the bulk and melted. In liquid ethane runs, rapidly growing ice platelets quickly appeared on the water and both film and nucleate boiling resulted. For the hydrocarbon mixtures, significant foaming was noted. Both film and nucleate boiling occurred.

Thesis Supervisor: Robert C. Reid

Title: Professor of Chemical Engineering

Dedicated to my parents
Akinsola and Olanium Jeje

ACKNOWLEDGEMENT

I extend my sincerest gratitude to Professor Robert Reid who suggested the topic of this study. For his patience, inspiration, moral support and constructive criticisms directed towards developing in me more appreciation for the methods of scientific reasoning and research, I am deeply grateful.

The enlightening discussions held with Professors K.A. Smith, E. Drake and I. Davenport are gratefully acknowledged. I also thank Professors G.C. Williams and A.F. Sarofim for permitting me to set-up part of my equipment in their laboratory.

I thank my colleagues at M.I.T., W. Porteous, M. Manning, V. Vilker, K. Griffis, T. Copeland, L. Shanes and A. Desalu for providing stimulating discussions and encouragement. I also wish to thank my friends at Polaroid Corporation, especially R. Wohler and C. Valle, for their encouragement and help.

To Stan Mitchell, Paul Bletzer, Reid Fulton and Charlie Forshey who have extended their services during the construction of the equipment and subsequent work, I extend my gratitude.

I gratefully acknowledge the financial support provided by the American Gas Association and the National Science Foundation. General Electric and Polaroid Corporations have also contributed, at different times, to my stay at M.I.T., in form of tuition refunds.

I thank Mrs. Alice Biladeau for her patience while typing this thesis.

For the woman in my life who shared my ups and downs in the course of the work, Saeeda, and our son, Akinsola, I am thankful. I appreciate their unfailing encouragement, devotion and sacrifices.

VII
TABLE OF CONTENTS

Chapter	<u>Page</u>
1. SUMMARY	1
2. INTRODUCTION	
2.1 General Format of Thesis	36
2.2 Literature	38
2.3 Principal Events Influencing Boiling	51
Pool Boiling Heat Transfer	
Mechanisms of Ice Formation at a Water Surface	
Convective Motions	
2.4 Comparison of Solid-Liquid and Liquid-Liquid Boiling	73
2.5 Objectives of Study	74
3. A PHOTOGRAPHIC STUDY OF LIQUID-LIQUID BOILING INTERFACES	
3.1 Introduction	76
3.2 Experimental	76
3.3 Results	78
3.4 Correlation for Bubble Diameters	98
3.5 Summary	101
4. BOIL-OFF RATES OF CRYOGENIC LIQUIDS ON WATER	
4.1 Introduction	102
4.2 Apparatus	103
4.3 Method	
Procedure	108
Design of Experiments	110
4.4 Preliminary Experiments	110
4.5 Results	
Effect of Quantity Spilled	123
Effect of Initial Water Temperature	127
Effect of Cryogen Composition	131
Comparison of the Effects of Additives	141
Vapor Temperatures	145
Temperatures in the Water	150
4.6 Summary of Results	160

VIII

TABLE OF CONTENTS (Continued)

Chapter	<u>Page</u>
5. DISCUSSION OF RESULTS	
5.1 Introduction	163
5.2 Models of the Boiling Process	163
5.2.1 Bubble Growth Theories	166
5.2.2 Surface Tension Effects on Bubble Growth	177
5.2.3 Concentration Profiles Around a Growing Bubble	187
5.2.4 Film Boiling Theories	190
5.3 Heat Fluxes Across the Water-Cryogen Interfaces	200
5.4 Discussions	
5.4.1 Review of Results	224
5.4.2 Discussion of Results	240
5.5 Comparison of Results with Previous Work	260
6. CONCLUSIONS AND RECOMMENDATIONS	264
APPENDICES	
A. Fog Formation	269
B. Equipment Operational Principles, Design Details and Performance Data	278
C. Auxiliary Results	
Bursting of Bubbles	308
Vapor Hold-Up in Boiling Cryogenics	313
D. Error Estimate (Heat Flux) and Thermocouple Calibration Data	316
E. Sample Data Treatment	324
Computer Program	
Coefficients of Least Square Fit	
F. Experimental Data	336
List of Experiments and Variables Data	
G. Bibliography	
H. Nomenclature	

IX

LIST OF FIGURES

<u>Figure Number</u>		<u>Page</u>
1-1	Apparatus for Boiling Rate Studies	8
1-2	The Boiling Vessel	9
1-3	Photographic Set-Up for the Examination of Liquid-Liquid Interfaces	12
1-4	Vapor Temperatures Above Boiling Pools of Methane (99.98%)	15
1-5	Vapor Temperatures Above Boiling Pools of LNG (98.2% CH ₄ , 1.62% C ₂ H ₆ , 0.11% C ₃ H ₈ Plus Trace Butanes)	17
1-6	Vapor Temperatures Above Boiling Pools of LNG (89.4% CH ₄ , 8.2% C ₂ H ₆ , 2% C ₃ H ₈ Plus Trace Butanes)	18
1-7	Range of Heat Fluxes between Water and Boiling Methane (99.98%)	20
1-8	Heat Fluxes between Water and Boiling Methane-Ethane Binary Mixtures	22
1-9	Heat Fluxes between Water and Boiling Methane-Propane Binary Mixtures	23
1-10	Heat Fluxes between Water and Methane-n-Butane Binary Mixtures	24
1-11	Heat Fluxes between Water and LNG	25
2-1	Boiling of Butadiene-Water Mixtures	40
2-2	Liquid-Liquid Boiling Systems (Sideman, 1966)	43
2-3	The Effect of Water Temperature on LNG Evaporation Rate (Boyle and Kneebone, 1973)	49
2-4	Characteristic Boiling Curve for Water at 1 atm	53
2-5	The Regimes of Boiling	54
2-6	Copper Pentane Test Results: Effect of Surface Cleanliness (Berenson, 1960)	60

LIST OF FIGURES (Continued)

<u>Figure Number</u>		<u>Page</u>
2-7	Copper Pentane Test Results: Effect of Roughness (Berenson, 1960)	60
2-8	Nucleate Boiling of a Mixture of Methylene-Ketone and Water at Atmospheric Pressure (van Wijk et al., 1956)	62
2-9	Film Boiling Curves for Mixtures of CCl_4 and freon-113 on a Horizontal Plate at Atmospheric Pressure (Kautzy and Westwater, 1967)	62
2-10	Homogenous Nucleation of Ice in Water (Mason, 1958)	66
2-11	Hydrate-Forming Conditions for Paraffin Hydrocarbons (Katz et al., 1959)	69
2-12	Heat Transfer Enhancement with Convective Fluid Flows Between Two Horizontal Rigid Plates (Chandrasekhar, 1961)	72
3-1	Photographic Set-Up for the Examination of Liquid-Liquid Interfaces	77
	Sketch of Significant Features of the Photographs	79
3-2	Views of Liquid Nitrogen- Glass Interface	81
3-3	Saturated Liquid Nitrogen Film Boiling on a Water Surface	83
3-4	Close-up Time-Sequenced Images of a Liquid Nitrogen - Water Interface	84
3-5	Liquid Methane Interface with Water	86
3-6	Close-up Time-Sequenced Pictures of the Interface Between Liquid Methane and Water	88
3-7	The Interface of Liquid Ethane and Water ($T_w^\circ \sim 28^\circ\text{C}$)	89
3-8	The Interface of Liquid Ethane and Water ($T_w^\circ \sim 18^\circ\text{C}$)	90
3-9	Close-up Time-Sequenced Bottom Views of the Interface Between LNG (89.2% CH_4 , 1.62% C_2H_6 , 0.11% C_3H_8 Plus Trace Butanes) and Water ($T_w^\circ \sim 32^\circ\text{C}$)	92

LIST OF FIGURES (Continued)

<u>Figure Number</u>		<u>Page</u>
3-10	Close-up Time-Sequenced Bottom Views of the Interface of LNG (same composition as 3-9) on Water ($T_w \sim 18^\circ\text{C}$)	93
3-11	Surface Tension vs. Temperature for Cryogenic Hydrocarbon Liquids (Gallant, 1968)	95
3-12	Bubble Growth	96
4-1	Apparatus for Boiling Rate Studies	104
4-2	The Boiling Vessel	105
4-3	Typical Temperature- Measured by the Sanborn Recorders	111
4-4	Typical Weight-Time Curves for Liquid Methane and Liquid Nitrogen Boiling on Water	113
4-5	Temperatures at Different Levels in Glycerol During n-Butane Boil-Off	114
4-6	Temperature at Different Levels in Glycerol During Ethane Boil-Off	115
4-7	Temperature Profiles in Glycerol Above which n-Butane Boiled Off	117
4-8	Glycerol Surface Temperatures During n-Butane Boil-Off	118
4-9	Temperature Profiles in Glycerol Above which Ethane Boiled-Off	119
4-10	Glycerol Surface Temperatures During Ethane Boil-Off	120
4-11	Dimensionless Glycerol Surface Temperature, ϕ , as a Function of Time	122
4-14	The Effect of Quantity Spilled on Boil-Off Rates of Methane (99.98%)	124
4-15	The Effect of Quantity Spilled on the Boil-Off Rates of Ethane	125

LIST OF FIGURES (Continued)

<u>Figure Number</u>		<u>Page</u>
4-16	The Effect of Quantity Spilled on the Boil-Off Rates of LNG	126
4-17	The Effect of Quantity Spilled on the Boil-Off Rates of Nitrogen	128
4-18	The Effect of Initial Water Temperature on the Boil-Off Rate of Liquid Nitrogen	129
4-19	The Effect of Initial Water Temperature on the Boil-Off Rate of Methane (99.98%)	130
4-20	The Effect of Initial Water Temperature on Boil-Off Rates of Liquid Ethane (99.86%)	132
4-21	Liquid Ethane (99.86%) Boiling on Water	133
4-22	The Effect of Initial Water Temperature on Boil-Off Rates of Mixtures (98% CH ₄ , 2% C ₂ H ₆)	134
4-23	The Effect of Initial Water Temperature on Boil-Off Rates of LNG (98.2% CH ₄ , 1.62% C ₂ H ₆ , 0.11% C ₃ H ₈ and Trace Butanes)	135
4-24	The Effect of Initial Water Temperature on Boil-Off Rates of LNG (89.2% CH ₄ , 8.2% C ₂ H ₆ , 2% C ₃ H ₈ Plus Trace Butanes)	136
4-25	The Effect of Variations in Liquid Composition on Boiling Rates of Binary Methane/Ethane Mixtures	138
4-26	Methane/Ethane Mixture Boiled-Off in First 10s as a Function of % Ethane	139
4-27	The Effect of Composition on Boil-Off Rates of Binary Methane/Propane Mixtures	140
4-28	The Effects of Trace Quantities of Ethane and Propane on Boil-Off Rates of Methane	142
4-29	The Effect of Variations in Liquid Composition on Boiling Rates of Binary Mixtures (0.42 ± 0.004 g cm ⁻² Liquid Spilled)	143
4-30	The Effects of Trace Quantities of Propane and n-Butane on Boil-Off Rates of Methane	144

XIII

LIST OF FIGURES (Continued)

<u>Figure Number</u>		<u>Page</u>
4-31	The Effect of Variations in Liquid Composition on Boiling Rates of LNG (Liquid Spilled $0.42 \pm 0.05 \text{ g cm}^{-2}$)	146
4-32	Vapor Temperatures Above Boiling Pools of Nitrogen	148
4-33	Vapor Temperatures Above Boiling Pools of Methane (99.98%)	149
4-34	Vapor Temperatures Above Boiling Pools of Ethane (99.84%)	151
4-35	Vapor Temperatures Above Boiling Pools of LNG (98.2% CH_4 , 1.62% C_2H_6 , 0.11% C_3H_8 Plus Trace Butanes)	152
4-36	Vapor Temperatures Above Boiling Pools of LNG (98.2% CH_4 , 1.62% C_2H_6 , 0.11% C_3H_8 Plus Trace Butanes)	153
4-37	Vapor Temperatures Above Boiling Pools of Binary Mixtures (98% CH_4 , 2% C_2H_6)	154
4-38	Vapor Temperatures Above Boiling Pools of LNG (89.4% CH_4 , 8.2% C_2H_6 , 2% C_3H_8 Plus Trace Butanes)	155
4-39	Temperature Fluctuations in Water on which Liquid Nitrogen Boiled	157
4-40	Temperature Fluctuations in Water on which Liquid Methane (99.98%) Boiled	158
4-41	Temperature Fluctuations in Water on which LNG Boiled	159
5-1	Saturation Temperatures of LNG (primarily methane and ethane) as a function of composition (derived from the data of Enger and Hartman, 1972)	180
5-2	Dimensionless Bubble Radius (R/R_f) vs. Time	184
5-3	Film Boiling	190

LIST OF FIGURES (Continued)

<u>Figure Number</u>		<u>Page</u>
5-4	Heat Flux Between Water and Boiling Methane (99.98%)	225
5-5	Heat Flux Between Water and Boiling Ethane (99.86%)	228
5-6	Heat Flux Between Water and Boiling Methane-Ethane Binary Mixtures	230
5-7	Heat Flux Between Water and Boiling Methane-Propane Binary Mixtures	231
5-8	Heat Flux Between Water and a Boiling Methane-n-Butane Binary Mixture	232
5-9	Heat Flux Between Water and Boiling LNG (98.2% CH ₄ , 1.62% C ₂ H ₆ , 0.11% C ₃ H ₈ Plus Trace Butanes)	234
5-10	Heat Flux Between Water and Boiling LNG	235
5-11	Heat Flux Between Water and Liquid Nitrogen (Q' vs t)	237
5-12	Heat Flux Between Water and Boiling Liquid Nitrogen (Q' vs w _o)	238

APPENDICES

A-1	Vapor Film Between Water and Cryogen	276
A-2	Vapor Pressures and Pressures and Partial Pressures of Water as a Function of Position Within the Film	277
A-3	Experimental Values of the Critical Saturation Ratio for Homogenous Nucleation of Water Vapor	277
B-1	Block Diagram of Balance	279
B-2	Schematic of Gas Chromatograph	288
B-3	Chromatogram of Low Molecular Weight Hydrocarbons in Durapak Feed G.C. Columns: Flame Ionization Detector	289a

APPENDICES (Continued)

	<u>Page</u>
B-4 Apparatus for Sampling Cryogenic Liquids	291
B-5 Heat Loss From a Circular Well	294
B-6 (a) Thermocouple Probe in Water	293
(b) Vapor Thermocouple; Heat Stationed on Holder	293
B-7 (a) Fluid Directing Double Cone	297
(b) Vapor Thermocouple	297
B-8 Thermocouple Tree	300
B-9 Boiling Vessel	304
B-10 Aluminum Support Plate	306
C-1 Reconstituted Sequence of Sputtering from Helium Bubbles Released in n-Hexane	310
C-2 Void Fraction in Boiling Cryogenic Liquids	315
D-1 Change in Temperature of Cold Water Poured into the Boiling Vessel which was Initially Empty	318

XVI
LIST OF TABLES

<u>Table Number</u>		<u>Page</u>
2-1	Data of Burgess et al. (1970, 1972)	45
3-1	Values of the Prefactor ϕ (equation 3-3) for Different Systems	100
5-1	Bubble Growth Equations	168
5-1	Experimental Data and Calculated Heat Fluxes	206
5-2	Water Loss During Methane Boil-Off	226
5-3	Water Loss During Nitrogen Boil-Off	239
APPENDICES		
A-1	Saturation Ratio Within the Vapor Film	276
B-1	Performance Data for Mettler PE 11 Balance	280
B-2	Sanborn Preamplifier Specifications	283
B-3	Sanborn Recorder Galvanometer Characteristics	284
B-4	H. P. Integrating Digital Voltmeter Specifications	286
D-1	Calibration Data for Thermocouples in Water	321
D-2	Calibration Data for Thermocouples in Vapor	322
D-3	Regression Coefficients for the Thermocouples	323
E-1	Raw Data for Run #161	325
E-2	Processed Data	325a
E-3	Coefficients of Regression Equation Describing $m_L(t)$	327

APPENDICES (Continued)

<u>Table Number</u>		<u>Page</u>
E-4	Computer Program	332
F-1	List of Experiments	337
F-2	Variables of Experiments	338
F-3	Experimental Data	342

NOTATIONS

A	Area
$C, C_A, \text{ etc.}$	Concentration
C_p	Thermal Capacity
D	Diameter
D_{AB}	(or \mathcal{D}) Diffusivity Coefficient
g	Acceleration of Gravity
H	Enthalpy
ΔH_v or f	Latent Heat of Vaporization, Fusion or Sublimation
k	Thermal Conductivity
K	(or K) Surface Dilational Viscosity Coefficient
m	Mass or Wave Number
N_{a_z}	Mass Flux
P	Pressure
ΔP	Pressure Difference
$P(R)$	Pressure Inside a Bubble Radius R
P_o	Pressure Outside a Bubble
P_{A_o}	Partial Pressure of Substance A
P_A	Vapor Pressure of A
Q', Q'', q', q	Heat Flux
Q''	Heat Generated per Unit Volume
R	Radius of Bubble
R'	dR/dt

NOTATIONS (Continued)

R	Universal Gas Constant
r	Radius
s*	Height of Flight of a Droplet
Sc	Schmidt Number (v/D)
t	Time (sometimes θ)
T	Temperature
U	Internal Energy
u	Velocity
x	Shear stress factor, or distance
x_A, X_A	Composition in Liquid (Mole or Mass Fraction)
Y_A	Composition in Vapor
z	Distance
GREEK	
α	($=k/\rho C_p$) thermal diffusivity or, relative volatility or, a constant (in Appendix A)
β	growth constant for bubbles or, a constant (in Appendix A)
γ	($= 3\sigma / (2 \Delta P R_f)$) surface tension: pressure difference ratio
δ	thickness of layer (vapor film, boundary layer, i.e., discs etc.)
ϵ	$= \rho_L - \rho_V / \rho_L$ or, bubble node height or, void fraction
ζ	distance
η	similarity parameter ($= r/2\sqrt{Dt}$)
θ	time
κ	surface dilational viscosity coefficient

NOTATIONS (Continued)

GREEK

λ	wavelength
μ	viscosity
ν	kinematic viscosity (μ/ρ)
ξ	distance
ρ	density
σ	surface tension
τ	time or period
ϕ	prefactor for equation 3-5 or, dimensionless temperature or, pressure constant
ψ	(= R/R_f), a dimensionless radius. Defined differently in Appendix A.

Subscripts

o	Reference point
w	water
v	vapor
L	liquid
c	cryogen
T	total
f	final

Superscript - average

CHAPTER 1

SUMMARY

1-1	INTRODUCTION
1-2	BACKGROUND
1-3	EXPERIMENTAL PROGRAM
1-4	RESULTS
1-5	DISCUSSIONS
1-6	CONCLUSIONS AND RECOMMENDATIONS

1-1 INTRODUCTION

Little is known about the mechanisms and rates of boiling heat transfer between two immiscible liquids, one of which is initially at a temperature exceeding the boiling point of the other. Most of the experimental studies which have been carried out to date (e.g. Gordon et al., 1961; Novakovic and Stefanovic, 1964) have involved boiling water and alcohols off mercury surfaces under steady state conditions. Constant heat fluxes were input into the mercury, and the vapor of the boiling liquid continuously refluxed.

Of interest in the present study is the complex, time-dependent boiling of cryogenic liquids on water under conditions which partially simulate real events, such as a large accidental spill of liquefied natural gas (LNG) on open water. A spilled volatile liquid will simultaneously spread and vaporize. Only the latter phenomenon is examined in this work. Such spills could result from accidents involving tankers or barges transporting the cryogen.

Many cryogenic liquids of commercial importance, besides LNG, are handled in insulated containers on inland waterways and oceans in rapidly increasing volumes. Liquefied petroleum gas (LPG), ammonia and chlorine are some common examples. The hazards associated with accidental spills of such liquids on water are a cause for concern as flammable and/or toxic material are vaporized and dispersed downwind. An evaluation of the possible dangers subsequent to a spill, especially near highly populated areas and in congested harbors, require a knowledge of the source rate of vapor evolution at the spill site.

1-2 BACKGROUND

The boiling of a volatile liquid on the surface of a second liquid has received relatively little attention compared to the more common phenomenon of boiling from a heated solid surface. The former is more difficult to characterize quantitatively since the hot surface is mobile and normally capable of internal heat transfer by convective and conduction mechanisms. In addition, if the volatile liquid boils at a temperature below the freezing temperature of the hot liquid, there is the possibility of a solid phase forming at the surface of, and extending into, the hot liquid. Finally, any real spill of a cryogenic liquid on water will lead to a highly transient situation with the possibility of rapid variations in temperature in the hot liquid and concomitant variations in heat flux.

Early studies of boiling between two immiscible liquids were limited to cases where water was boiled on solid surfaces covered with thin oil films (Jakob and Fritz, 1931). Rather large vapor bubbles were formed and the water vapor evolved was probably superheated (Jakob, 1949). Later, Bonilla and Eisenberg (1948) boiled butadiene on water. By refluxing the hydrocarbon and heating the water, experiments were conducted in a steady-state mode. The presence of the more volatile liquid ($\rho = 0.62 \text{ g/cm}^3$) effectively reduced the bulk water temperature and enhanced the net rate of heat transfer into the water. Similar experiments were made by Bragg and Westwater (1970).

A number of experiments have been conducted in which water and alcohols were boiled on heated mercury pools. These are summarized

by Sideman (1966). As mercury possesses a high thermal conductivity, the boiling heat transfer characteristics would be expected to be intermediate between those represented by a solid surface and water. This was found to be true. Significant scatter between the results of different investigators was, however, noted.

In this thesis, we are concerned with the boiling of cryogenic liquids on water and only a few exploratory studies have been conducted. Burgess et al. (1970, 1972) boiled liquid nitrogen, methane and LNG on water surface and measured the rate of evaporation by noting the changes in the total mass of the boiling system. In a few tests that were reported, boil-off rates were found to be almost constant in the first 20-40 seconds of each run. There was a large scatter in their data which were reproducible to within 50%. For nitrogen, the average initial evaporation rate was about $17 \text{ mg/cm}^2\text{s}$. If one converts this to a heat flux by multiplying by the heat of vaporization of nitrogen, a value of about 33 kW/m^2 ($10,500 \text{ Btu/hr-ft}^2$) is found. Similarly for LNG, vaporization rates of $15 \text{ mg/cm}^2\text{s}$ and 90 kW/m^2 ($28,5000 \text{ Btu/hr-ft}^2$) were noted. This LNG consisted of 84 to 91% methane with the remainder primarily ethane. The heat flux to pure methane differed slightly from the LNG results depending upon the amount initially spilled. For an initial methane depth of about 2.7 cm, the boiling rate was $10 \text{ mg/cm}^2\text{s}$, or the heat flux was 55 kW/m^2 ($17,500 \text{ Btu/hr-ft}^2$), whereas when 7 cm was poured, the values increased to $16 \text{ mg/cm}^2\text{s}$ (or 91.5 kW/m^2). Although the methane boiling fluxes were only approximate, these data suggest that

for equal quantities poured, LNG vaporized much more rapidly than either pure methane or nitrogen. A similar, but less comprehensive study by Nakanishi and Reid (1971) corroborated Burgess' results.

Small scale tests carried out by the Tokyo Gas Co. in 1971 indicated a considerably lower boil-off rate of LNG (of undetermined composition) on water than noted above. Rates did, however, increase significantly with time. Their studies on the effect of initial water temperature were particularly interesting. Little effect was noted for initial water temperatures between 0 and 20°C; at higher temperatures, however, the net rate decreased appreciably. They attributed this change to the fact that ice could more readily form on the surface of the colder water. Such ice would then cool and reduce the temperature difference between the LNG and water thus encouraging nucleate boiling with high rates of heat transfer.

In the most comprehensive study yet on boiling of LNG on water, Boyle and Kneebone of Shell Research, Ltd. (1973) carried out two different types of experiments. In the first, LNG was spilled on restricted brine surfaces of 9 ft² and 40 ft² and they monitored evaporation rates with load cells. The effect of LNG composition, amount spilled, initial water temperature, and agitation rate of water were studied to determine their effect on vaporization rates. In the second type of test, LNG was pumped at a constant rate onto an unrestricted pond and vaporization rates per unit area inferred from the steady-state pool area.

Except for the case of very small spills of pure methane, all

vaporization rates increased with time and, in a few cases, almost an order of magnitude increase from initial values was noted. Boiling rates also increased when larger amounts of LNG were spilled and as the water temperature decreased. In a typical run with LNG (95% CH₄) the initial boil-off rate, determined from taking slopes on a mass-time curve, was about 2-3 mg/s-cm². After a few seconds, there was a dramatic increase in rate to a maximum value between 15 and 20 mg/s-cm². When the residual liquid thickness was about 1.8 mm, break-up of the LNG pool into spheroids were noted and the superficial boiling rate abruptly decreased.

The effect of LNG composition was also examined and it was found that small concentrations of heavier hydrocarbons in methane (particularly ethane and butane) resulted in very marked increase in evaporation rates.

Boyle and Kneebone proposed that the low initial boiling rates were a result of film boiling. As soon as some ice had formed on the surface, however, the temperature difference decreased and nucleate boiling was promoted. Only the very top layer of water cools (temperature measurements 5 mm below the surface usually remained well above 0°C) and low initial water temperatures or an increased hydrostatic head of LNG would favor ice formation. When the water was agitated, lower boil-off rates were measured, and this was attributed to the lower rate of surface ice formation. To explain the enhancement of vaporization rates by addition of heavy hydrocarbons to methane, they propose that there is an enrichment in ethane as methane

is preferentially evolved. The increase in the concentration of heavier hydrocarbons reduces the boiling temperature of the LNG near the interface and encourages collapse of vapor films to form ice (and hydrates?) with subsequent nucleate boiling.

Tests carried out on an open pond (unrestricted) led to constant, and quite low, boil-off rates, i.e., they were similar to those noted early in the restricted area tests, 2-3 mg/s-cm², a value one sixth that noted by investigators at Esso (1973) in similar open pond experiments. The low rate was attributed to the difficulty of forming ice in such spills.

1-3 EXPERIMENTAL PROGRAM

Boil-off Rates

Vaporization experiments were carried out in a well insulated vessel mounted upon a Mettler load cell balance. A schematic sketch of the apparatus is shown on Figure 1 and a more detailed view of the boiling vessel is Figure 2.

Some 5-6 cm depth of water at the desired temperature were poured into the boiling vessel. The test was initiated by tripping the cryogenic Dewar and allowing liquid to impact on the cone and flow down the walls over the surface of the water. The change in system mass was monitored from the output of the load cell on a Hewlett-Packard data acquisition system and on Sanborn recorders. As will be described below, liquid and vapor temperatures were also measured during a test. At the completion of a run, when all the cryogen had

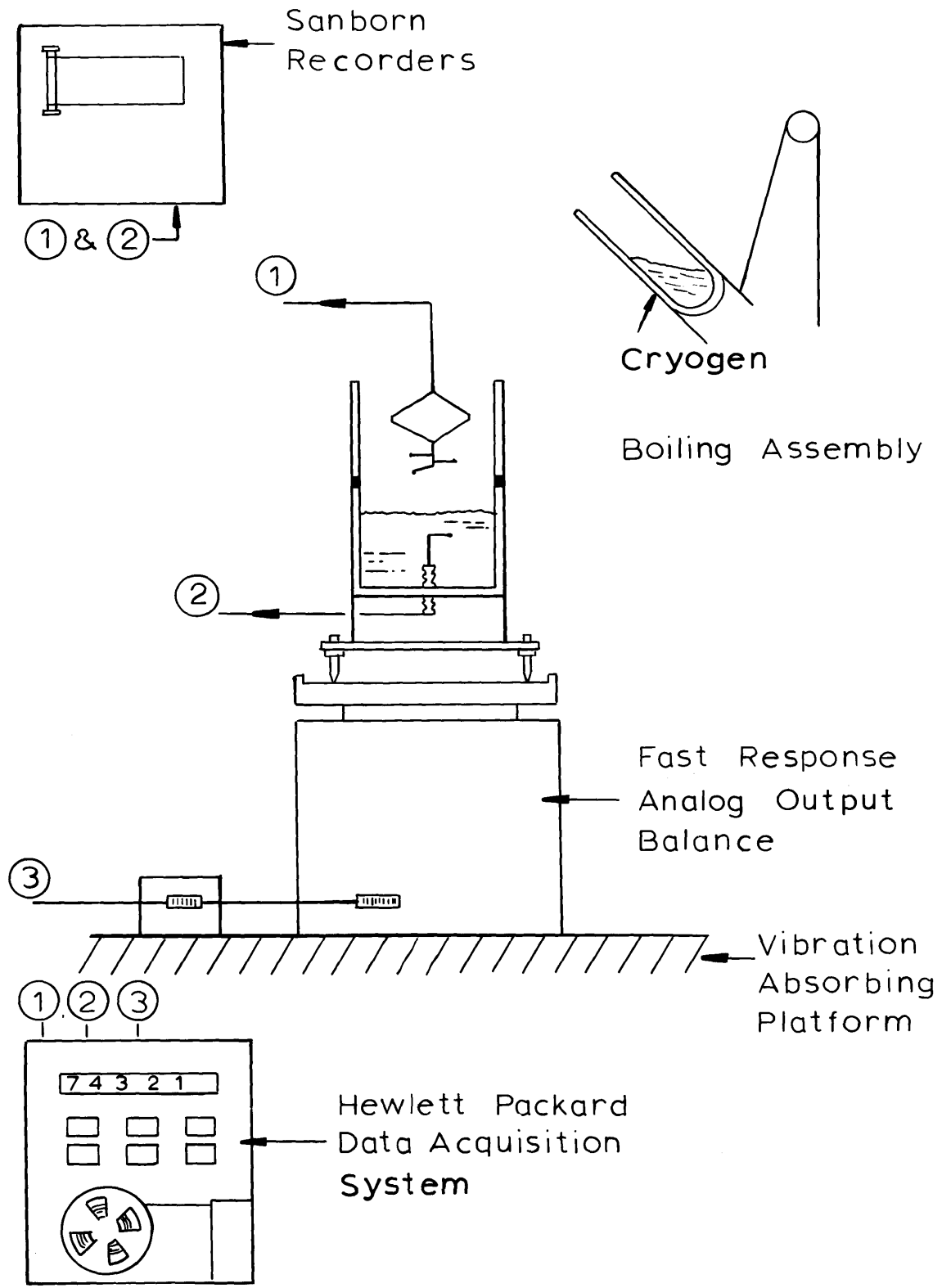


Figure 1 Apparatus for Boiling Rate Studies

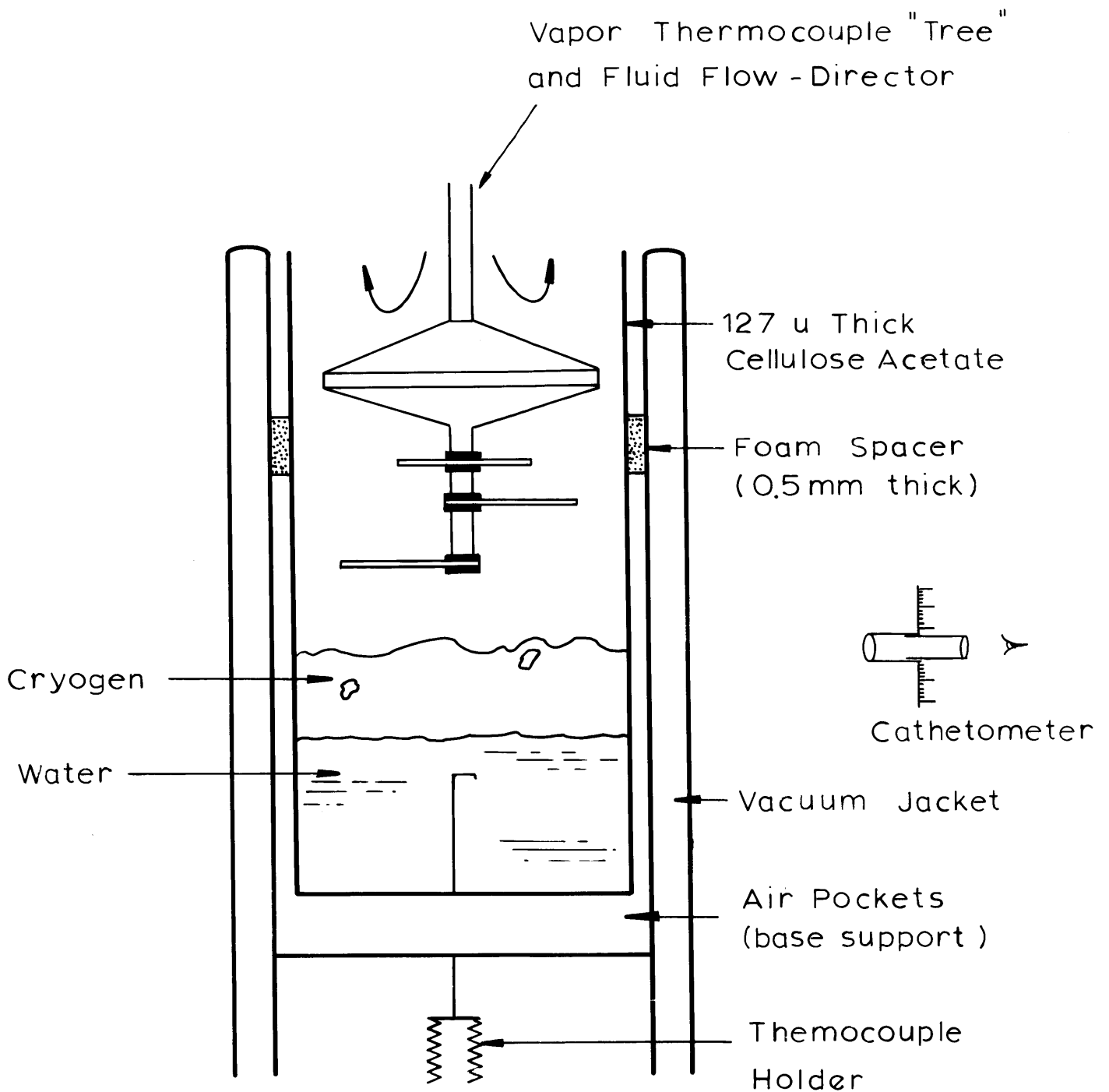


Figure 2 The Boiling Vessel

been boiled away, the residual water was stirred, any ice melted, and a final bulk water temperature measured.

The heart of the apparatus was the boiling vessel (Figure 2). It was actually a triple walled container. The two outer walls were made from acrylic plastic and the annulus was evacuated. The inner wall was fabricated from 127 μm scratch-free cellulose acetate sheets and separated with polyurethane foam spacers from the inner acrylic wall by a 0.5 mm air gap. This cellulose acetate lining covered both the sides and bottom. Heat leak from the environment was negligible over the duration of the experiments (circa 1 minute). The overall dimensions of the boiling vessel were 9.92 cm i.d. and 17.8 cm deep.

An acrylic double-cone (7.6 cm diameter) was hung into the open end of the boiling vessel. This device served several functions. It broke the fall of the cryogen and thus lessened any initial overshoot reading on the load cell. Also, the cryogen liquid was distributed more evenly over the water surface. The cone also served as the support for the thermocouple tree and, finally, it effectively prevented any ambient air from entering the vessel during a test. It did not, however, slow the addition of cryogen appreciably; 100 cm^3 of liquid could be poured into the boiling vessel in about 0.5 s.

The vapor thermocouple tree consisted of three copper constantan thermocouples fabricated from 25 μm wires. Each was heat-stationed with 10 cm lengths wound in a spider web perpendicular to the direction of gas flow. Three other heat-stationed 25 μm thermocouples wire were inserted into the water. In this case, the wires

entered the boiling vessel through the bottom.

Each of the six thermocouples as well as the system mass was sampled every second by the data acquisition system. The values were digitalized and stored on paper tape for later recall and calculations. The Sanborn recorders were used to obtain continuous plots of the same variable noted above.

The location of the thermocouples were varied in different experiments. In most cases, however, one thermocouple in the water was located so that its bead (56 μm diameter) just touched the water surface. As placed, it effectively rode with the surface and was used to monitor the water surface temperature.

During a test, an observer recorded the actual height of cryogen at various times. This was accomplished with a side-mounted cathetometer.

Photographic Study

Photographs were taken of the actual interface between the boiling cryogenic liquid and water. The pictures obtained provided valuable information relating to ice formation and bubble sizes.

The apparatus is shown schematically in Figure 3. It basically consisted of a 14.5 cm diameter glass boiling vessel (with an optically flat bottom and insulated on the side); a Nikkormat camera set to view the interface from beneath the vessel; and high intensity illumination sources. The infra-red portion of the radiation from the light sources was effectively removed in a cold layer of water located

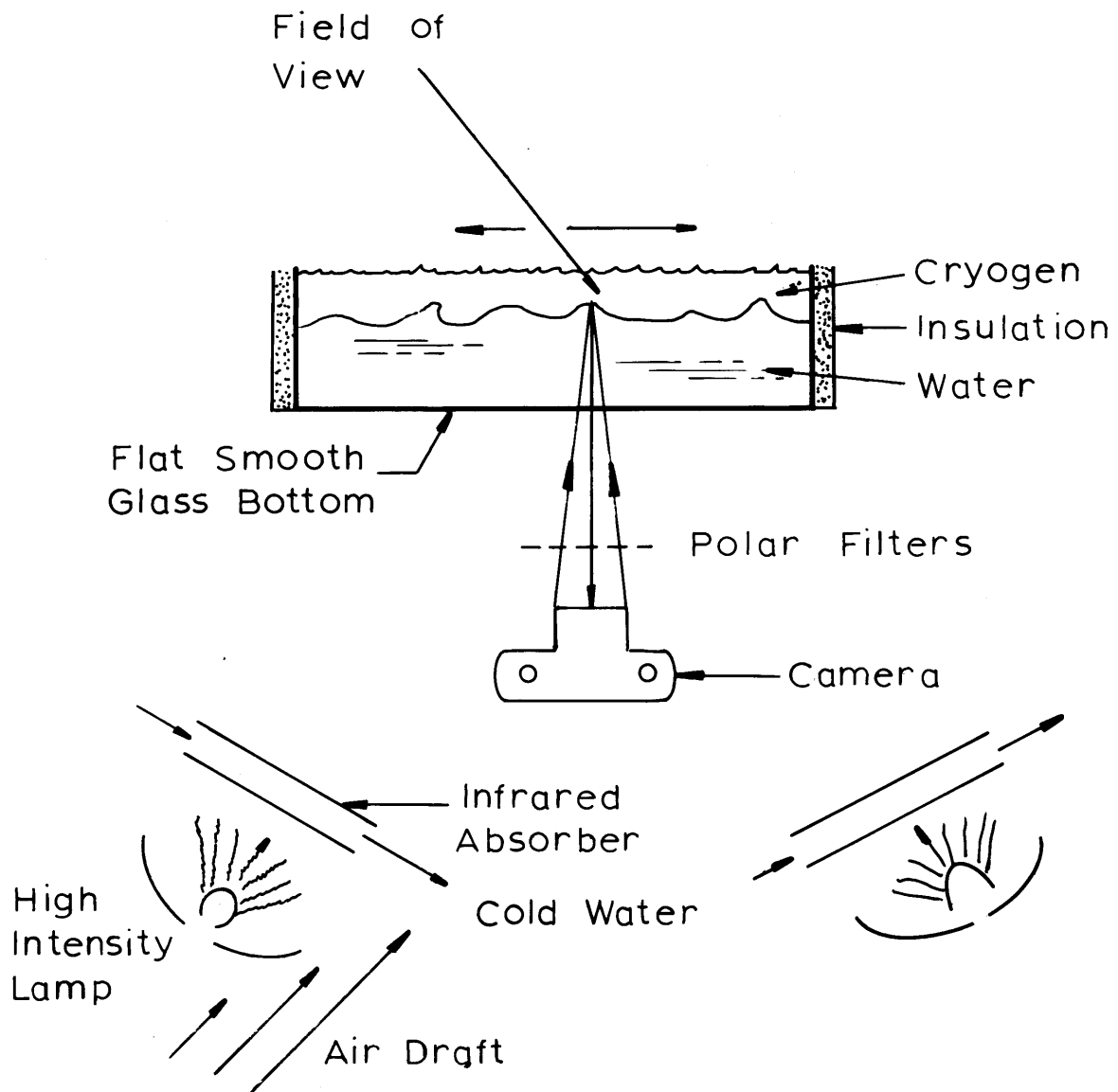


Figure 3 Photographic Set-up for the Examination of Liquid-Liquid Interfaces

between each source and the test vessel.

In the runs, the cryogenic liquids were boiled-off 3 to 5 cm water in the vessel, and the interfacial patterns were recorded every 2 to 3 seconds with the camera exposure set at 1 millisecond.

1-4 RESULTS

Ninety one experiments were carried out and three independent variables were studied: initial water temperature, quantity of cryogen spilled, and chemical make-up of the cryogen. The variables measured were weight of the cryogen-water system as well as vapor and liquid temperatures--all as functions of time. The cryogen-water weight-time data were fitted with fourth degree regression polynomials and variance analyses were carried out. Derivatives of the resulting polynomials are the time-smoothed boil-off rates.

Vapor Temperatures

Vapor temperatures are seldom measured in a boiling experiment. In cases where film boiling might be expected, and where the boiling liquid depth is low, there is the possibility that the vapors may be superheated. To close an energy balance on the overall system, it is obvious that the superheat question must be answered. In addition, the degree of superheat must be ascertained to compute heat fluxes. (Other investigators have obtained heat fluxes from the product of the mass boil-off rate times the appropriate heat of vaporization. Should the vapor leave in a superheated state, some latent energy

is lost that could have been used to vaporize more liquid.) The heat fluxes reported in this thesis represent the energy required to transform liquid cryogen to saturated vapor and to superheat the vapor to the temperature measured by the vapor phase thermocouples.

The vapor temperatures showed no axial nor radial gradients within the boiling vessel. This is what one should anticipate if the boiling vessel were adiabatic and if no liquid cryogenic spray were entrained in the vapor. However, in many experiments the vapor temperature were considerably warmer than the saturation temperature. The highest superheating was found with liquid nitrogen; seldom was it below 50°C, and as the amount spilled decreased (or as the water temperature was increased), the amount of superheat increased. For pure methane, little superheat was noted when the initial charge was above about 1 cm. This depth apparently allows equilibration between the rising vapor bubbles and the residual liquid. Also, in large spills, the probability of ice formation is enhanced. The subsequent nucleate boiling would then depress any superheating. For spills of liquid methane below 1 cm, superheat temperatures of 30-50°C were measured. On Figure 4, some typical measurements are plotted for 3 W_0 size ranges. The abscissa represents the hydrostatic head of cryogen and one moves from right to left as the vaporization proceeds. The odd "V" shaped curve for very small charges was also noted in liquid nitrogen runs. At present, no satisfactory explanation can be offered.

Little superheat was noted in boiling tests with pure ethane

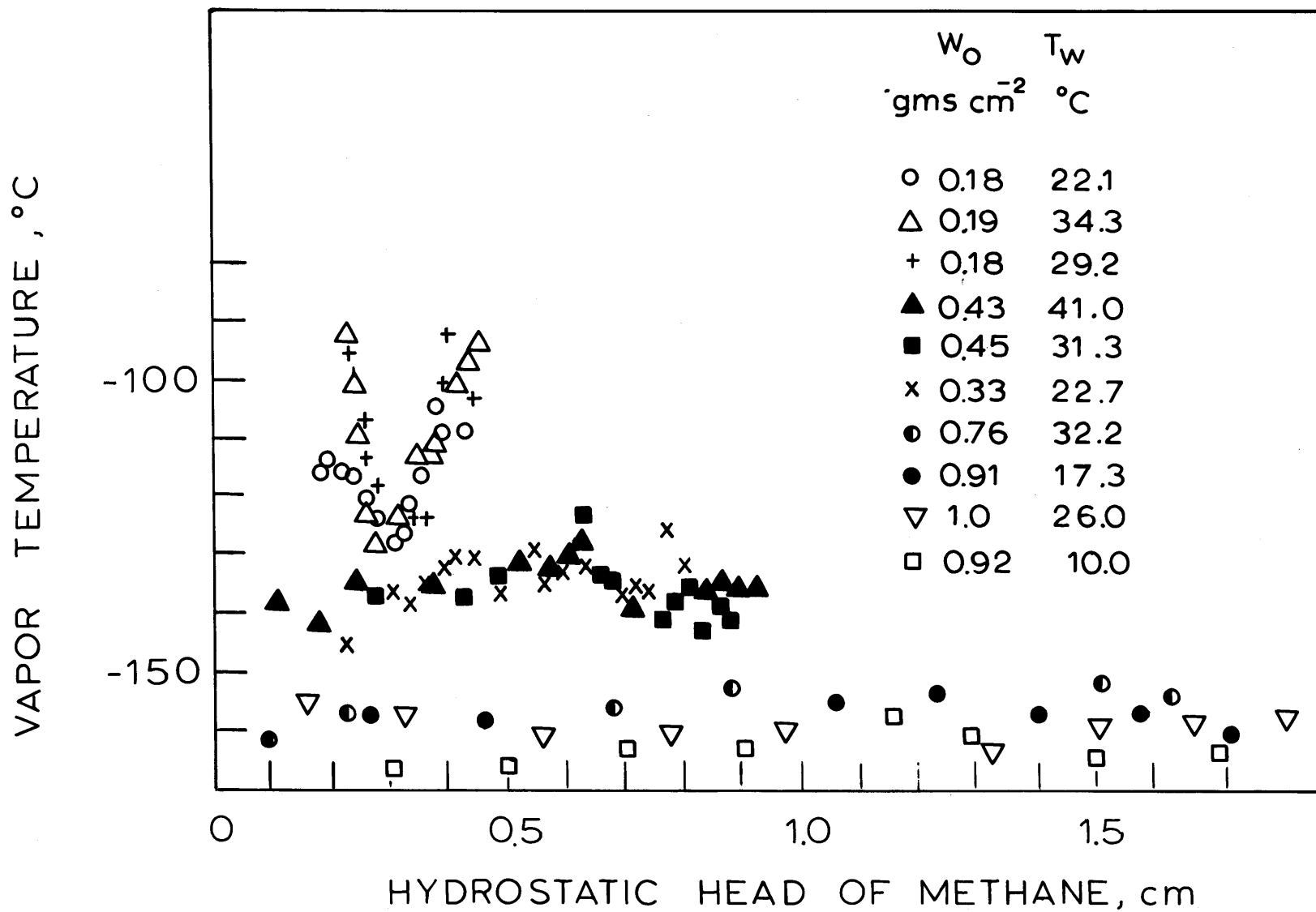


FIG. 4 VAPOR TEMPERATURES ABOVE BOILING POOLS OF METHANE (99.98%)

and for methane-rich LNG; some results are shown in Figure 5. Relative to the boiling point of pure methane, little superheat was noted. Finally, for a richer LNG, some of the data are shown in Figure 6. The data at short times are similar to those shown in Figure 5; as the mixture enriches in the heavy components, the bulk cryogen temperature increases and this is reflected in a corresponding rise in vapor temperature.

In general, the vapor superheat for LNG is relatively small; for pure methane and for nitrogen, however, significant superheat is possible, especially for shallow depths and high initial water temperatures.

Quantity Spilled and Initial Water Temperatures

For all pure hydrocarbon liquids studied, no significant effect was noted on the boiling flux when the quantity of cryogen was varied. Figure 7 contains data taken for pure liquid methane where the amount poured varied from about 0.2 g/cm² (0.5 cm) to 1.0 g/cm² (2.4 cm). The heat flux values showed no discernable trends with quantity spilled. The band in Figure 7 also includes a wide range of initial water temperatures (8 to 53°C) and again, no significant effect of this variable could be ascertained. For LNG mixtures as well as liquid ethane, similar results were noted when the spill quantity was varied. However, in these latter cases, there was an influence of initial water temperature on the heat flux, i.e., the flux increased somewhat as the initial temperature decreased. In

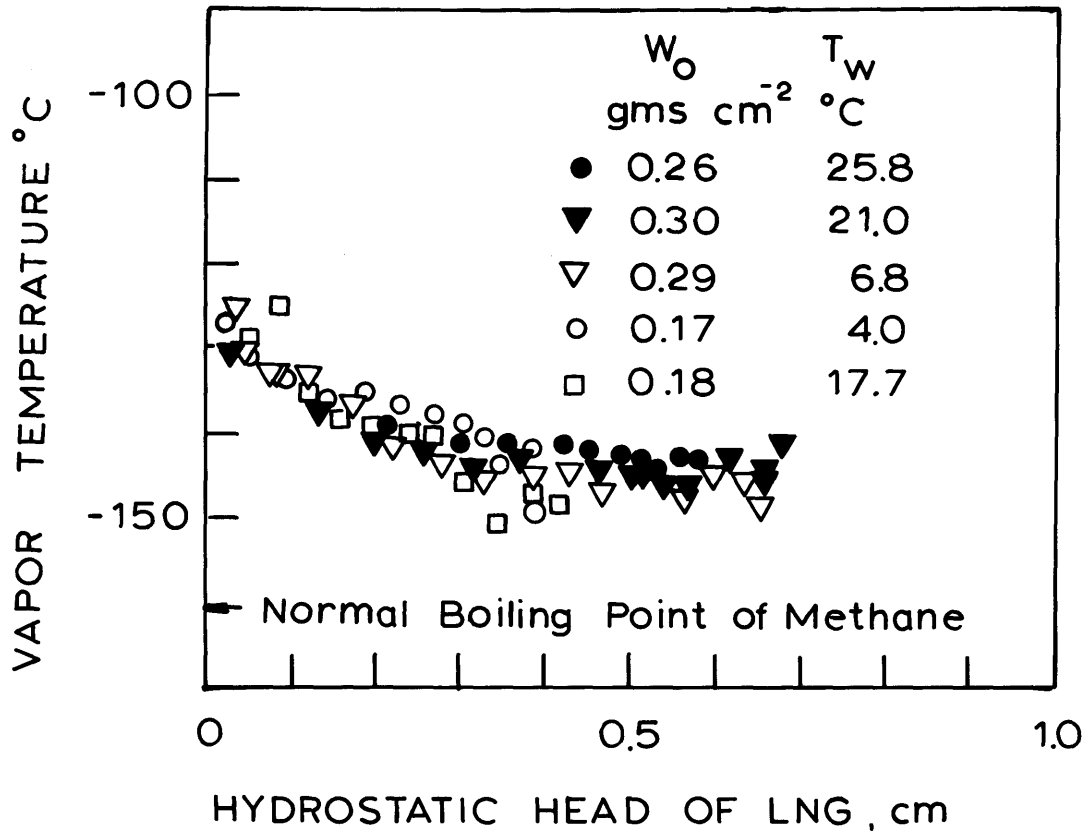


FIG. 5 VAPOR TEMPERATURES ABOVE BOILING POOLS OF COMMERCIAL METHANE (98.2% CH₄, 1.62% C₂H₆, 0.11% C₃H₈ PLUS TRACE BUTANES INITIALLY)

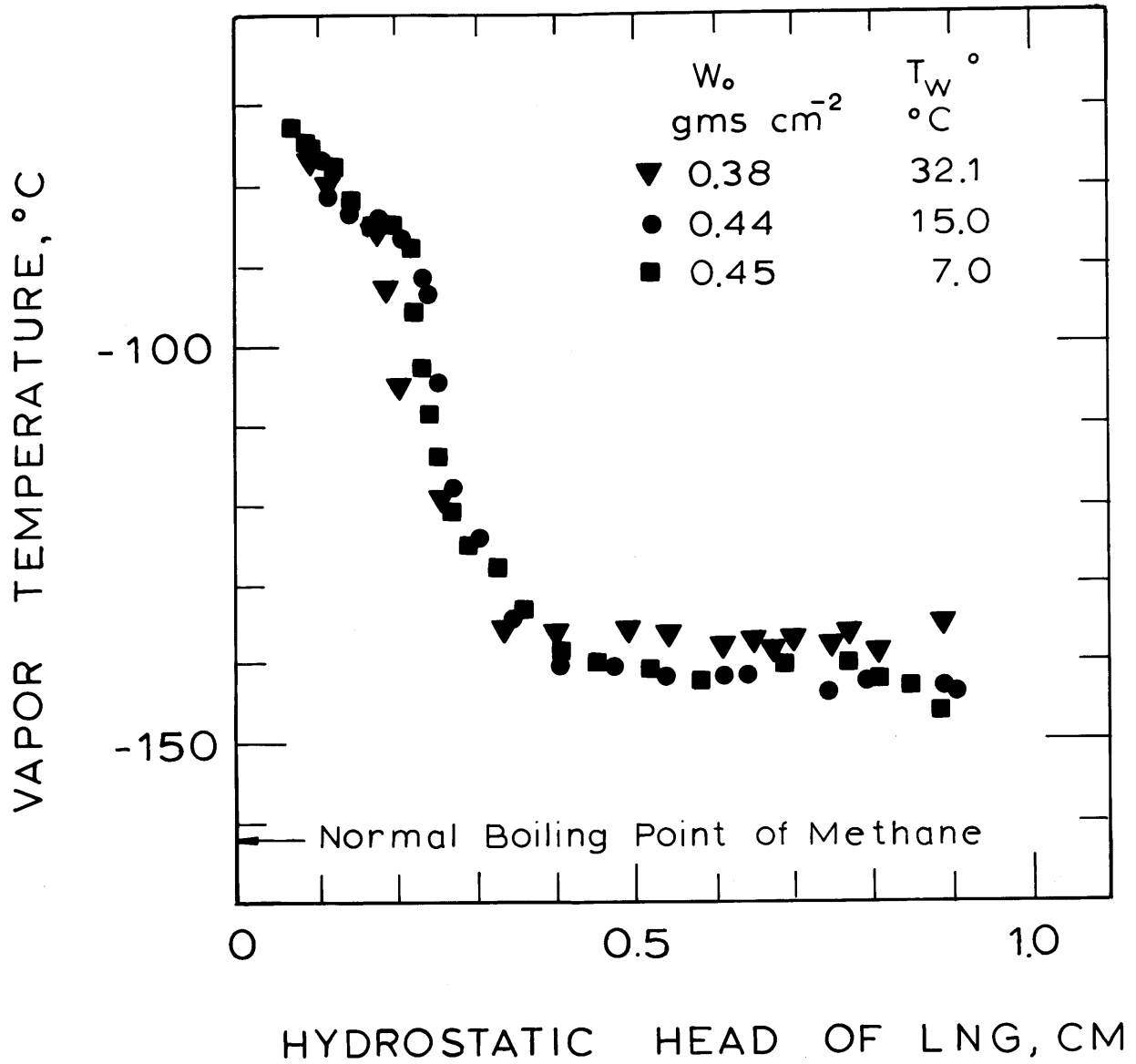


FIG.6 VAPOR TEMPERATURES ABOVE BOILING POOLS OF LIQUID NATURAL GAS (89.2% CH_4 , 8.2% C_2H_6 , 2% C_3H_8 AND TRACE BUTANES)

all cases, the heat flux increased with time. The data shown on Figure 7 are in disagreement with some earlier results of Boyle and Kneebone (1973) for liquid methane boiling on water. With water at 15°C, and after a 3 lb spill on a 9 ft² surface (0.38 cm) depth, they indicated a constant heat flux of about 16 kW/m² (5000 Btu/hr-ft²). Not only is their value considerably below those found in this work, but the time invariance is strange. Their depth of spill is quite low and it was found in this work that in such cases the vapor could be appreciably superheated. (The superheat contribution is included in the heat flux values shown on Figure 7. If we subtract this contribution, for tests where the initial head ≤ 0.5 cm, the heat flux would have been reduced by about 15%--still not enough to account for the difference.) In other experiments reported by Boyle and Kneebone, larger spills of methane did lead to a slight increase in heat flux with time.

Heat fluxes into liquid nitrogen boiling on water decreased with time and also, the heat flux increased significantly with the amount spilled. Initial heat fluxes were between 28 and 33 kW/m². The initial water temperature (<25°C) was, however, not an important variable.

Composition of Hydrocarbon Mixtures

Though the quantity of hydrocarbon spilled and the initial water temperatures were not particularly important variables in the boil-off experiments, the composition of the LNG was a very signifi-

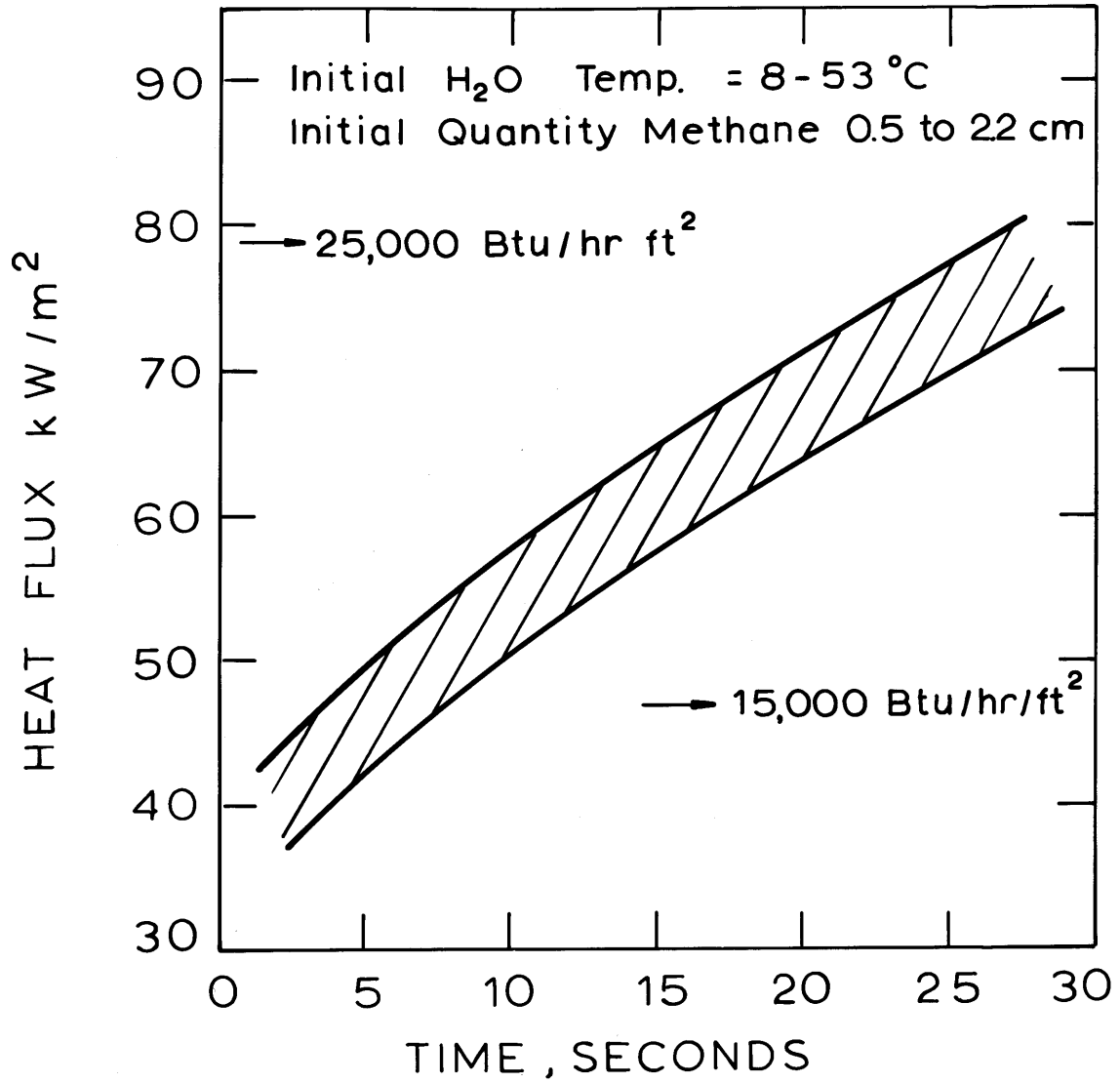


FIG.7 HEAT FLUXES BETWEEN WATER AND BOILING METHANE (99.98%)

cant variable. To illustrate, consider Figures 8 through 11. On each of these plots, the methane (99.98% pure) band of Figure 7 is shown. Also, the effects of adding small quantities of ethane, propane, and n-butane are illustrated. It is evident that even very small concentrations of hydrocarbons heavier than methane can affect the heat fluxes far out of proportion to their concentration. In Figure 11, two typical LNG curves are shown. From figures such as these, it is clearly meaningless to discuss LNG boiling rates on water without specifying the composition.

Water Temperatures

Thermocouples placed more than 5 mm below the surface usually did not record any large change in water temperature. However, occasional drops in temperature, with rapid recovery to almost the original values are noted. This is indicative of "thermals" (Turner 1973). On the other hand, thermocouples placed on the surface, or less than one mm below the surface, usually registered wild oscillations during an experiment (frequency $\sim 5-10$ cps, amplitude $\sim 5^\circ\text{C}$). For liquid nitrogen runs on water above about 10°C , the average surface temperature did not drop below 0°C except when very large quantities were poured. For pure liquid methane tests, the surface temperature did drop below 0°C during the runs when the initial water temperature was ambient or below. When hot water was used, the surface temperature decreased but seldom did it reach 0°C within the duration of a normal test. In contrast with LNG, the surface temperature dropped well below 0°C even though the

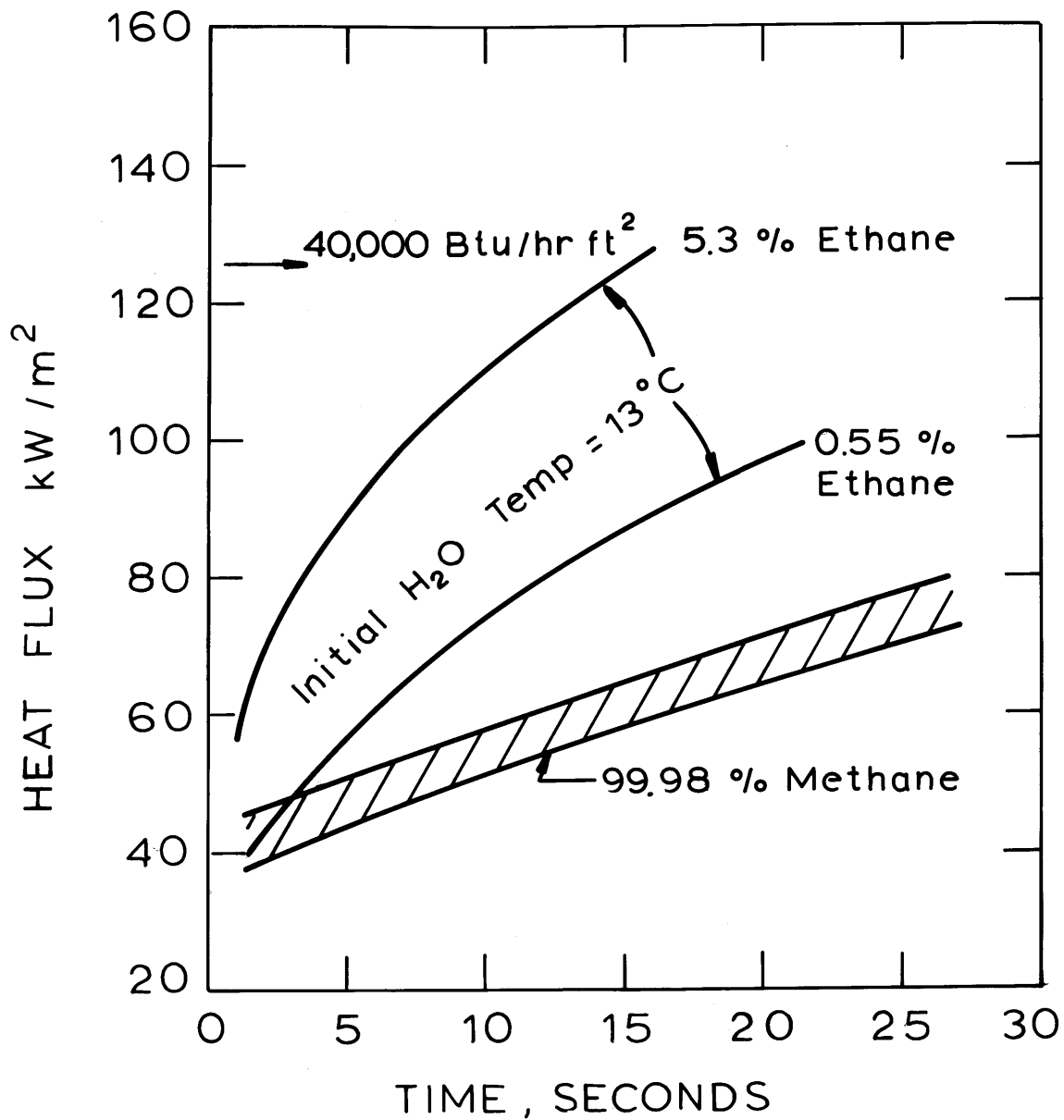


FIG. 8 HEAT FLUXES BETWEEN WATER AND BOILING METHANE-ETHANE BINARY MIXTURES

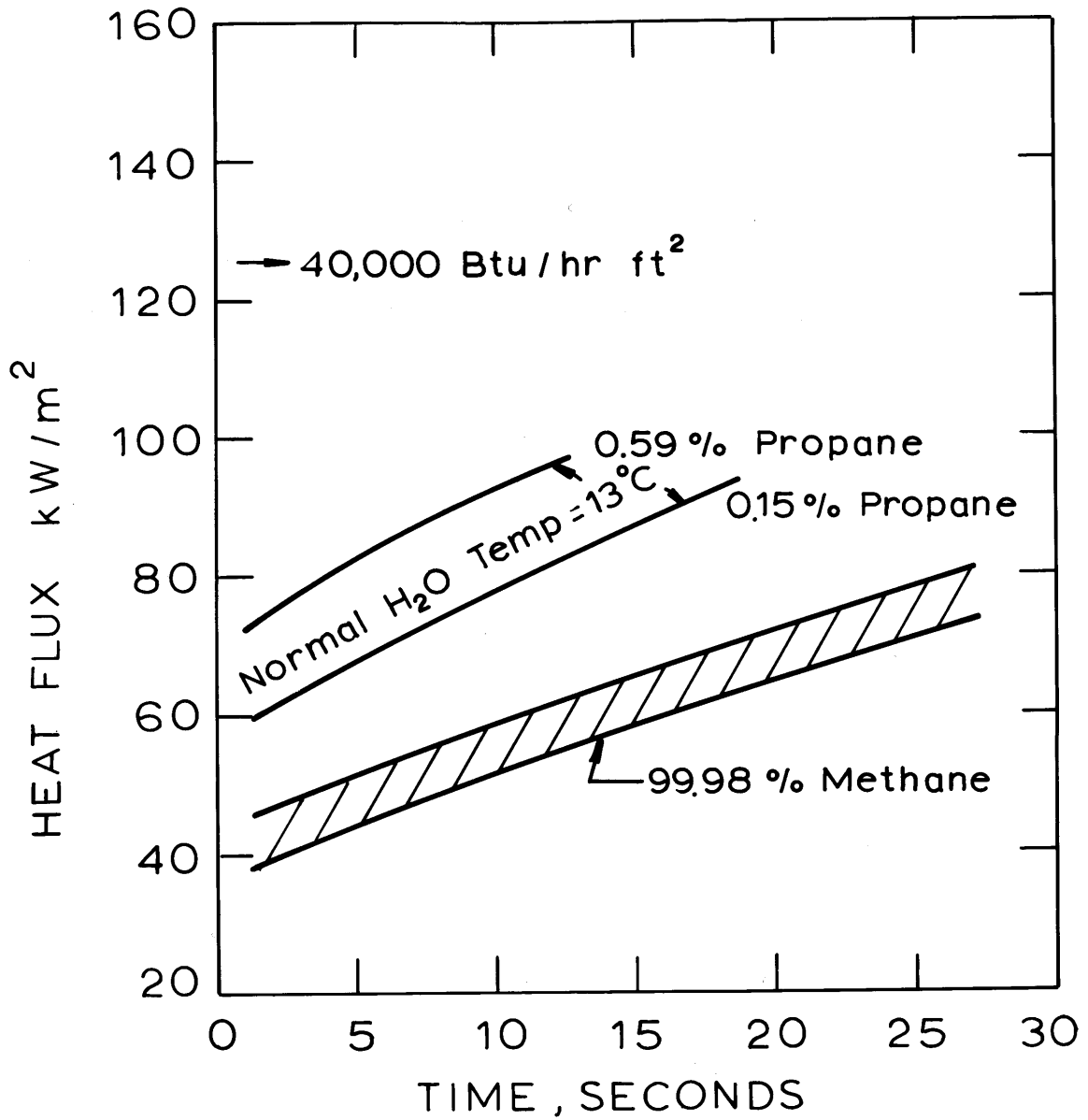


FIG. 9 HEAT FLUXES BETWEEN WATER AND BOILING METHANE-PROPANE BINARY MIXTURES

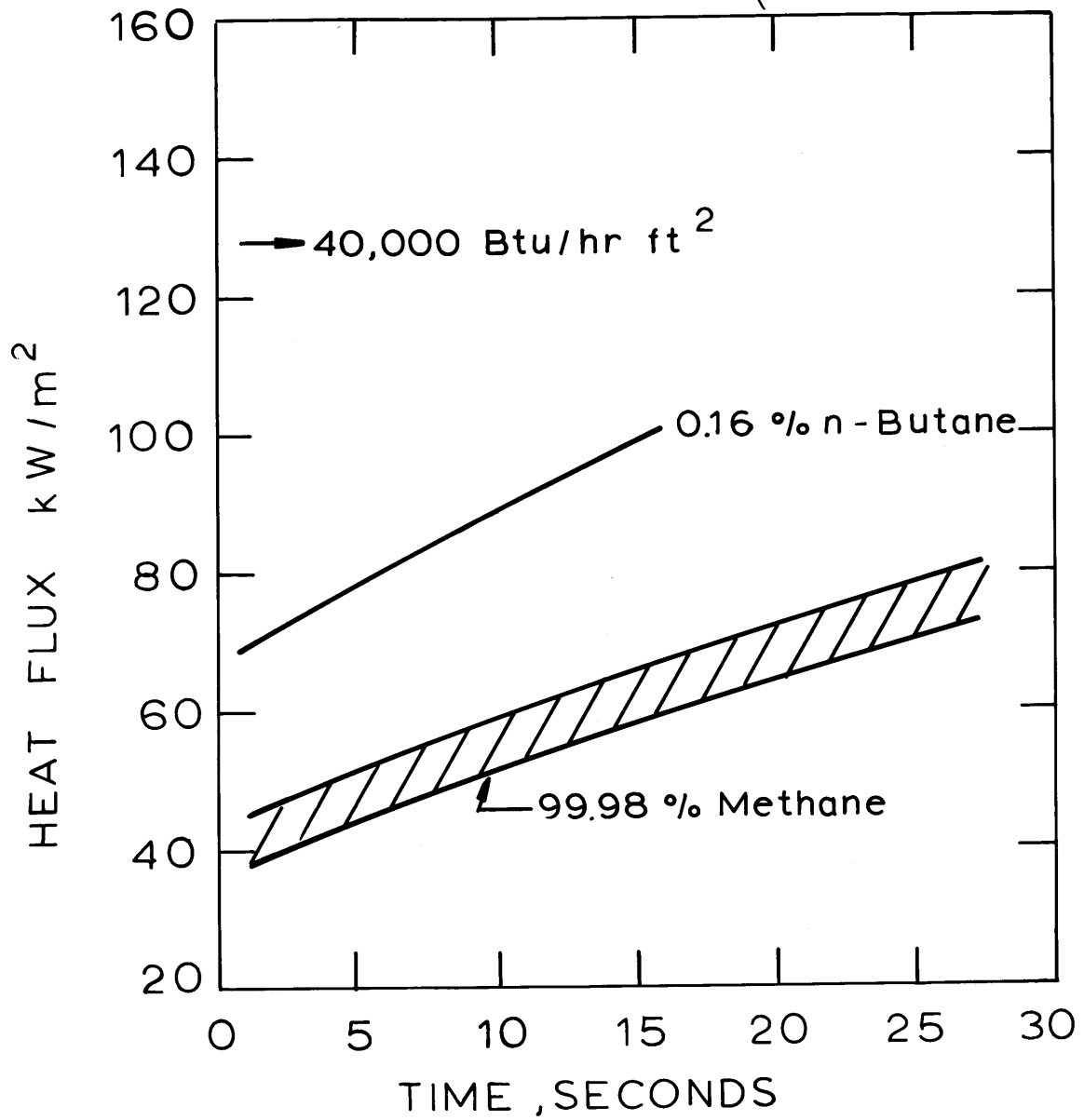


FIG. 10 HEAT FLUXES BETWEEN WATER AND BOILING METHANE-N-BUTANE BINARY MIXTURES

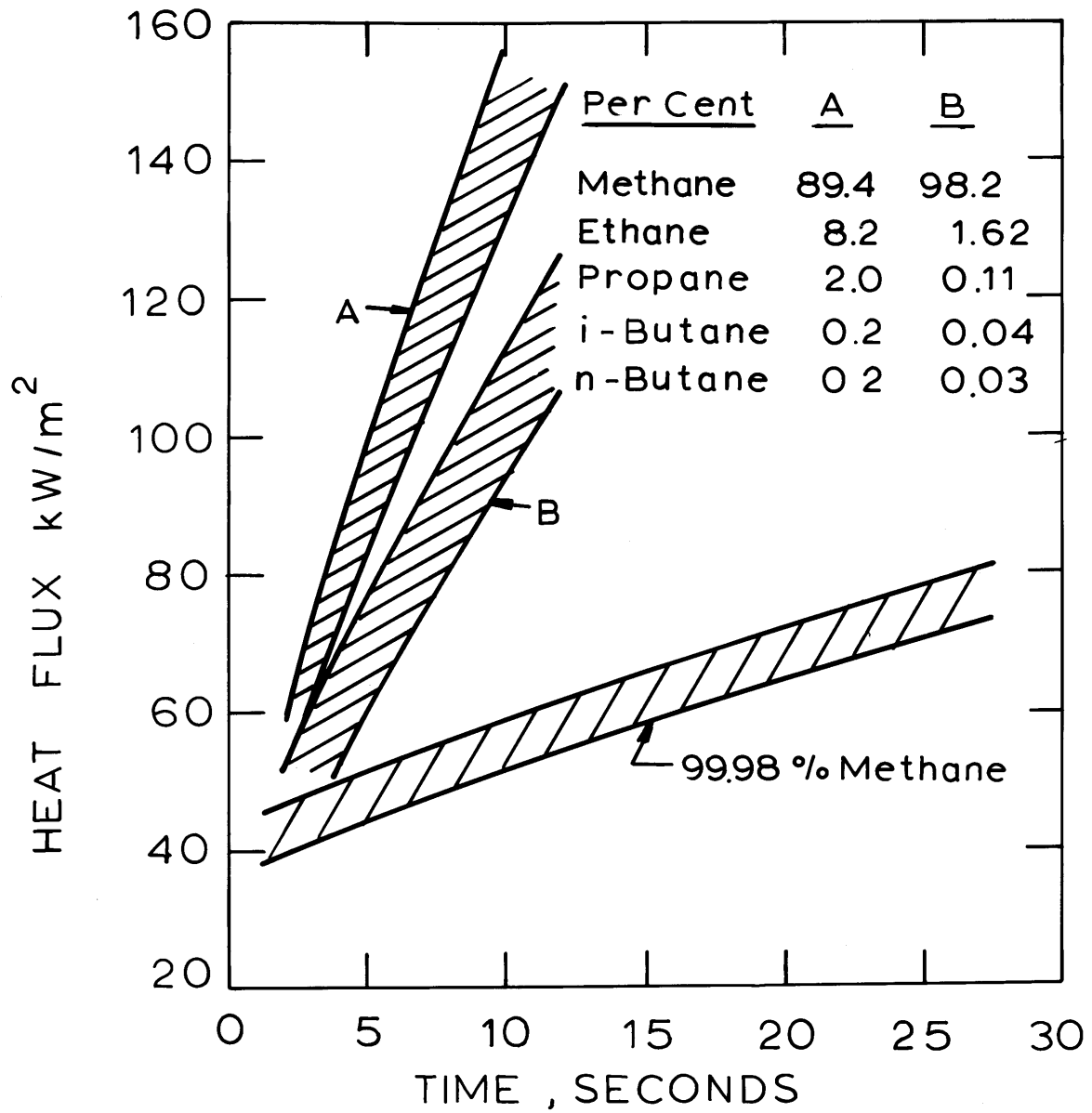


FIG. II HEAT FLUXES BETWEEN WATER AND BOILING ING

temperature 1 to 2 mm did not change appreciably. Pure ethane behaved in a manner similar to LNG.

The differences in water surface temperatures between the various cryogenics suggested that in the case of ethane and LNG, ice was rapidly formed at the surface. With methane, the evidence was conflicting and with liquid nitrogen, no ice was expected. Since a local water surface temperature was monitored by the thermocouple, some of the foregoing results could have been biased in that the thermocouple would read low temperatures when encapsulated by, or near a floating piece of ice, even though most of the surface had no ice present. The reverse situation, when ice is present but not sensed by the thermocouple, could also be true.

To investigate this point further, photographs of the interface were taken during a simulated boiling experiment. A special boiling vessel was employed that had an optically flat bottom as earlier described. The camera was placed beneath the vessel and focused on the interface.

Little or no ice was seen on the water surface for the first minute when nitrogen was spilled. Very small ice crystals did appear within the liquid nitrogen and it was assumed that these were entrapped solidified water from the fog that was generated. Bubble diameters ranged from 7.8 to 10.4 mm and it appeared as though film boiling was occurring. When pure methane was poured on water, most photographs appeared similar to those with nitrogen though the bubbles were larger (average 13.5 mm). Some small ice crystals may have been

formed on the surface but they were not easily seen. With pure ethane spills, thin ice wafers form within the first few seconds. In a short time, the surface is completely covered with ice; at this time, all fog over the vessel disappeared.

The most interesting photographs were those taken when LNG was poured on water. In contrast to any of the pure liquids, the surface was almost instantly covered with myriad small bubbles interspersed between a few large vapor bubbles. Such mixtures "foamed" during evaporation; a phenomenon also noted earlier by Burgess et al. (1970). The population density of the small bubbles decreased with time as the residual LNG enriched in the heavier components. Readily visible ice was formed when the initial water temperature was low, but it is only speculative whether much ice formed at the high temperatures. What appeared to be ice crystals in the photographs may only have been small gas bubbles. LNG is a "positive" mixture in that the more volatile component has a lower surface tension than the other components at a particular temperature, and foaming has been reported when positive organic mixtures were boiled (van Wijk et al, 1956; Hovestredijt, 1963).

1-5 DISCUSSION

The results obtained in this study indicate that the boiling rate of LNG on a water surface is extremely sensitive to composition. Even the addition of a few tenths of a percent ethane, propane, or butane to liquid methane can increase the boiling rate by 50% or more.

As a result of this sensitivity, it is not possible at the present time to predict in an a priori manner the boiling rate for a LNG of a given composition. In addition, it was clearly shown that vaporization rates of LNG, and even liquid methane, increase with time. The theory ordinarily employed to explain such rate increases involves the assumption that some ice very rapidly forms on the water surface. Nucleate boiling is initiated on the ice and the problem becomes one of conduction (within the ice) with continuous water-to-ice phase transformation. However, some doubt is raised as to the applicability of this theory. Photographs of the liquid-liquid interface do not indicate that an ice layer is instantaneously formed on the water surface except in the extreme case of liquid ethane spills. When LNG is spilled on water, there is unquestionably some ice formed (as noted in the photographs and water surface temperature measurements), but the ice is neither formed immediately on the water surface, nor is it a continuous layer when formed. It is suggested that small ice crystals may be mixed in the very top water layers and remelted; certainly there is photographic evidence to indicate significant micro-eddy activity in the upper layers.

The surprising observation that, for LNG spills, there is extensive small bubble formation may be an important clue in explaining the high LNG-water heat fluxes. The mechanism of production of these bubbles is not known. They may have been formed in a "nucleate boiling" type process soon after the liquids were contacted, i.e., when the volatile liquid experiences a step-change in temperature on direct

contact with water. Wehmeyer and Jackson (1972) experimentally found that a wire, subjected to a large step change in temperature while immersed in a liquid pool, produces discrete bubbles first. Then these bubbles coalesce to form a stable vapor film around the wire. Film boiling was not achieved instantaneously. It is suggested that, after a spill of a cryogenic liquid on water, discrete bubbles are also produced first while the liquids directly contacted each other. Film boiling is achieved when adjacent bubbles at the liquid-liquid interface coalesce. Furthermore, it is suggested that the bubbles formed in single component cryogenic liquids grow to relatively large sizes and coalesce readily to initiate film boiling. In mixtures, smaller bubbles are formed as a result of the hydrodynamic forces on each bubble in its early growth stage, and heat and mass diffusion control in the later or asymptotic stage (Scriven, 1959; van Strahlen, 1968). Moreover, these bubbles may not coalesce to initiate film boiling as readily as those in pure liquids due to temperature or concentration gradient-driven convective flows between bubbles, i.e., Marangoni effects (Saville, 1973; Blair and Quinn, 1969). Nevertheless, film boiling is ultimately achieved (probably after a few generations of small bubbles from the same site), and some of the insufficiently bouyant, small bubbles (seen in the photographs) are retained near the liquid-liquid interface within the cryogen.

The generation of these small bubbles is believed to lead to an enrichment of the less volatile, higher boiling point components

of the cryogen at its free surface near the water, i.e. at the interface. The consequence is that the temperature difference between the two liquids (which, without the enrichment would have indicated that stable film boiling occurred) is lowered and frequent, short duration liquid-liquid contact is encouraged. This is similar to what occurs in "Transition boiling" and high heat fluxes may be realized. (Rohsenow, 1970; Bankoff and Mehra, 1962). Even under conditions indicating that stable film boiling should occur, such momentary contacts may take place as photographically shown by Bradfield (1966).

If an area where the liquids momentarily touch is viewed as part of the interface between two semi-infinite bodies, at different temperatures, and with different transport and thermodynamic properties, the heat flux is given by (Carslaw and Jaeger, 1959)

$$q' = \frac{\theta k_1 \Delta T}{1 + \theta} \left(\frac{1}{\pi \alpha_1 t} \right)^{1/2} \quad (1-1)$$

and the total heat transfer per contact per unit area becomes

$$Q = \frac{2\theta k_1 \Delta T}{1 + \theta} \left(\frac{\tau_c}{\pi \alpha_1} \right)^{1/2} \quad (2-2)$$

where k_1 is the thermal conductivity of one of the liquids, α_1 is its thermal diffusivity, ΔT is the temperature difference across the inter-

face, τ_c is the contact time, and

$$\theta = \frac{k}{k_1} \left(\frac{\alpha_1}{\alpha_2} \right)^{1/2} \quad (1-3)$$

Subscript 2 refers to the second liquid.

Equation (1-1) indicates that the heat fluxes for short times may be extremely high. The instantaneous heat flux between the liquids, over the entire cross-section, is the sum of the contributions due to direct liquid-liquid contact at different sites (Equation (1-1) integrated over the total contact area), and the regular film boiling flux. The momentary contact area, A_c , frequency of contact, f , and the duration, τ_c , should depend on the magnitude of ΔT . The magnitude of these parameters increase as ΔT is lowered. With ΔT decreasing and τ_c and A_c increasing, the total heat flux may attain a maximum at a particular ΔT .

The system is, however, more complex than described above since more frequent and longer duration liquid-liquid contact also encourages the formation of ice and an attainment of nucleate boiling. Hence fluxes are further enhanced.

1-6 CONCLUSIONS AND RECOMMENDATIONS

1. The boiling rate of LNG on water is extraordinarily sensitive to the concentration of ethane and heavier constituents. Addition of 0.1 to 0.2% ethane, propane, or butane to pure methane can lead to increases in boiling rates of 50% or more.

2. The boiling rates of methane and LNG increases with time; liquid nitrogen behaves in an opposite manner.
3. The vapor evolved from boiling liquid nitrogen or pure methane is superheated; the degree of superheat increases as the amount spilled decreases or the initial water temperature increases. Little or no superheat was noted in vapors evolved from boiling LNG or pure ethane.
4. No significant trends were noted in the boil-off rates for hydrocarbons when the initial head was varied from 0.5 to 2.2 cm and the initial water temperature from 8 to 50°C, except for LNG where lower water temperatures enhanced the vaporization rate.
5. For short duration spills (less than one minute), little change is noted in the water temperature 5 mm or more below the surface. The surface temperature for liquid nitrogen remains above 0°C while in LNG and liquid ethane experiments, the surface temperature dropped below 0°C especially when the initial water temperature was low.
6. Ice formed very rapidly on the water surface in liquid ethane spills, Ice was also found in LNG spills but less readily than with ethane. No ice was formed at the water surface in liquid nitrogen tests.
7. In LNG spills, very small bubbles formed at the water-LNG interface. This phenomenon is credited with the higher heat fluxes observed for LNG compared to pure methane or nitrogen.

There is still a great deal to be learned about the boil-

ing mechanism when cryogenic hydrocarbon mixtures boil on water. In continuing research, the processes of small bubble formation, ice nucleation and growth, and flows within the water, especially near the interface should be investigated. Knowledge on these events will provide the basis for predicting the boil-off rates when cryogenic liquids contact water.

CHAPTER 2

INTRODUCTION

2.1 GENERAL FORMAT OF THESIS

2.2 LITERATURE ON BOILING AT LIQUID-LIQUID INTERFACES (2 IMMISCIBLE PHASES)

- a. Water and liquid hydrocarbons
- b. Mercury and other liquids
- c. Boiling of cryogenes on water
- d. Summary: liquid-liquid boiling studies

2.3 PRINCIPAL EVENTS INFLUENCING LIQUID-LIQUID BOILING

2.3.1 POOL BOILING HEAT TRANSFER

- a. Convective boiling
- b. Nucleate boiling
- c. Transition boiling
- d. Film boiling
- e. The influence of surface variables on boiling
- f. Boiling of single phase liquid mixtures

2.3.2 MECHANISMS OF ICE FORMATION AT A WATER SURFACE

- a. Frazil ice
- b. Hydrates

2.3.3 CONVECTIVE MOTIONS (IN HEAT SOURCE)

2.4 A COMPARISON OF SOLID-LIQUID AND LIQUID-LIQUID BOILING

2.5 OBJECTIVES OF THE PRESENT INVESTIGATION

2.1 GENERAL

Boiling heat transfer to liquids is a complex process during which a vapor phase is continuously generated. A comprehensive description of the process involves a large number of parameters such as the heating surface characteristics and the thermodynamic and transport properties of the liquid. As a result, no completely satisfactory, generalized descriptive equations nor correlations combining all pertinent variables are yet available. Considerable progress, however, has been achieved in formulating a physical picture with the aid of high speed photography and well-instrumented experiments.

In most studies, a solid heating surface has been used; the geometrical surface form has, however, varied widely, i.e., plates, wires and tubes have all been employed. Boiling from a solid immersed in a pool of liquid at its saturation temperature is called pool boiling.

In the present investigation, boiling heat transfer has been studied between water (initially liquid) and less-dense, immiscible, volatile cryogenic liquids.

The primary motivation for this study stems from the fact that many cryogenic liquids are shipped at atmospheric pressure in insulated tankers. Liquefied petroleum gas (LPG), liquefied natural gas (LNG), ammonia and chlorine are some common examples. The hazards associated with accidental spills on water are a cause for concern as the flammable and/or toxic liquids are vaporized and dispersed downwind. An evaluation of the possible dangers subsequent to a spill,

especially near highly populated areas and in congested harbors, require a knowledge of the source rate of vapor generation.

Thus, in addition to the many variables found to influence the boiling process on solid surfaces, several new ones must be included. Convection currents in the heat source liquid (water) modify the surface and subsurface temperature profiles; liquid-to-solid phase transformations (hydrates or ice production) are now possible with concomitant energy effects at the surface; and characteristics peculiar to mobile surfaces that lack microscopic irregularities or nucleation sites for bubble generation may be exhibited.

Format of Thesis

The remainder at this chapter includes a discussion of the few exploratory studies on liquid-liquid boiling, a literature review on some of the identifiable individual events which may act in concert during liquid-liquid boiling, and the statement of the principal objectives of this study.

Chapter 3 contains a description of the photographic study of the interfaces between the liquids in the boiling process. The apparatus, techniques and pictures of the interface are presented and described.

The fourth chapter deals with the more quantitative aspect of the study. Boil-off rates of the cryogenic liquids, and temperatures in the vapor departing the pool and in the water are presented, after the apparatus and procedures have been described.

In Chapter 5, the experimental results are discussed.

Chapter 6 contains the conclusions drawn from the present work, and recommendations are made to aid in formulating continuing research programs.

2.2 LITERATURE ON BOILING AT LIQUID-LIQUID INTERFACES OF IMMISCIBLE LIQUIDS

a. Water and Hydrocarbon Liquids

The first reported study on boiling heat transfer between liquids was made almost inadvertently by Jakob and Fritz (1931) in a study of the influence of the texture of the heating surface on the formation of steam bubbles. Their procedure in one set of tests was to coat the heating element with a thin layer of oil before immersing it into a pool of water. It was found that few bubbles were generated at the heating surface. The vapor cavities which did develop into bubbles were brimmed-hat shaped, and were spread out over the oily surface. These bubbles were apparently stable against buoyancy forces and they grew to large sizes (over 8.5 mm diameter) until eventually they pinched off. Jakob (1949) observed correctly that a superheating of the vapors would be expected, as most of the heat transfer occurred directly into the low thermal conductivity vapor that resided for long times on the hot oily surface.

Bonilla and Eisenberg (1948) were the first to study, quantitatively, boiling heat transfer between immiscible liquids. Their experiments were steady-state and involved heating a pool of water

above which was a hydrocarbon liquid.

They employed two hydrocarbons: styrene and butadiene. Styrene has a specific gravity of 0.9 and boils at 145°C at atmospheric pressure. Butadiene, on the other hand, is a gas at room conditions (b.pt. -4°C). Thus, in their experiments with butadiene, they operated the equipment at 4 atm, a pressure at which butadiene boils at 37°C (water boils at 143.5°C at 4 atm pressure). Butadiene has a specific gravity of 0.62 at this temperature and pressure. The styrene-water system does not satisfy the conditions of this study in that the less dense liquid is also the less volatile. For this reason, this system will not be discussed further.

The cylindrical test vessel of Bonilla and Eisenberg's set-up for the butadiene-water experiments had a stainless steel wall, and a chromium-plated copper bottom, 7.6 cm diameter. The bottom plate was electrically heated, and the over-all set-up was maintained at steady-state by the application of a reflux condenser. In each run, water and butadiene were introduced into the vessel, always to a constant total height of 6.35 cm, but the relative amounts of each liquid input were varied. Thus, the height of water was a variable in the experiments.

The heat input into the water was plotted against the steady state temperature difference between the solid heating surface and the boiling temperature of butadiene, as shown in Figure 2-1. From these data, the depth of water (within the range of experiments and

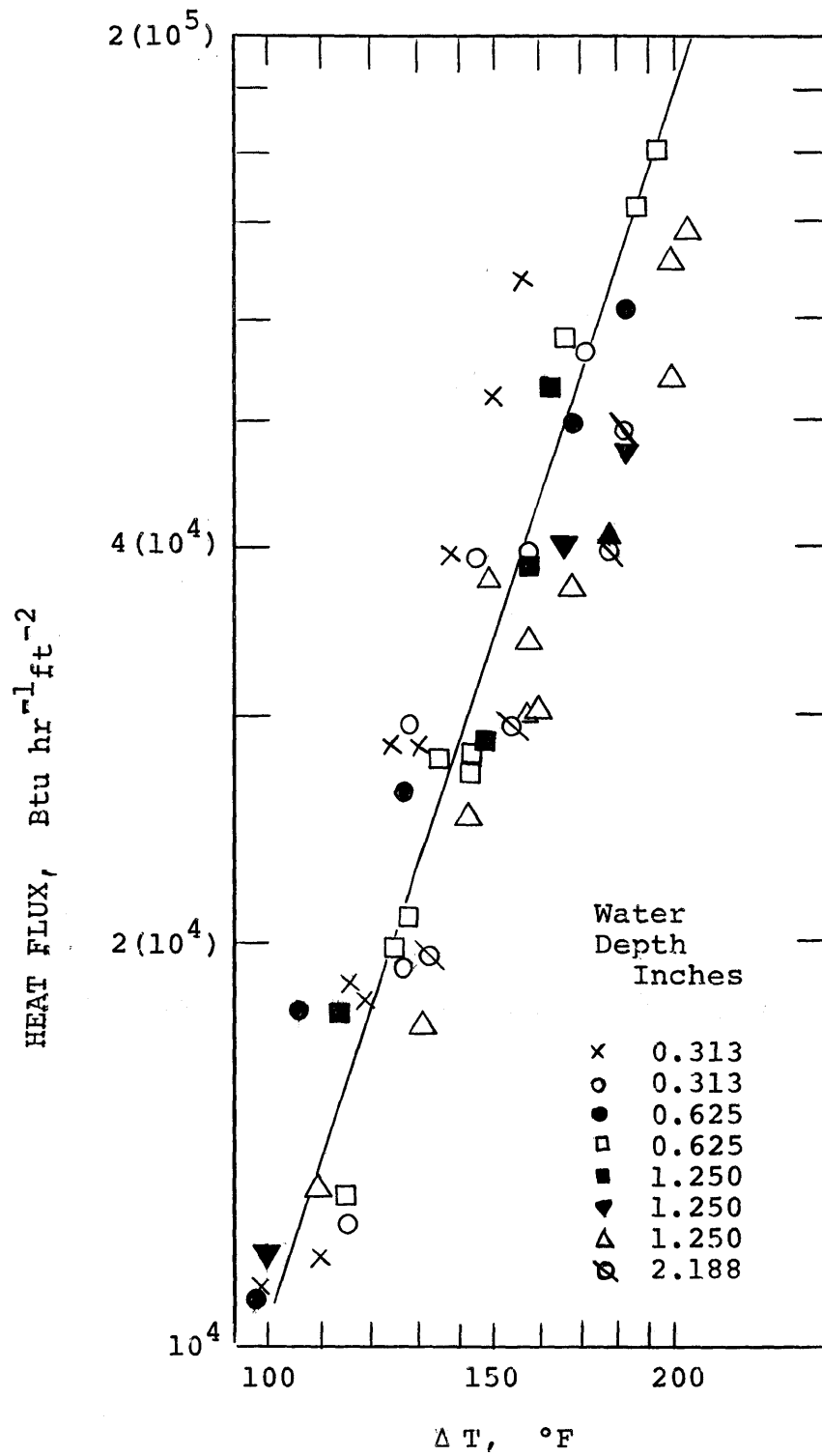


Fig. 2-1

Boiling Of Butadiene Water Mixtures
(Bonilla and Eisenberg, 1948)

scatter in data) was demonstrated to be an insignificant variable. Also, only convective flows were reportedly observed in the water for heating surface temperatures as high as 148°C (higher than the boiling temperature of water at 4 atm pressure). The butadiene layer, however, boiled vigorously.

It is not clear whether the butadiene vaporized in nucleate or film boiling under the experimental conditions. Nevertheless, it is apparent that the mechanism of heat transfer was more effective at the liquid-liquid interface than at the water-heating surface boundary.

Bragg and Westwater (1970) studied a method of enhancing the heat transfer to a liquid in film boiling. The method involved layering the boiling liquid with a more volatile, less dense and immiscible liquid, and noting the steady-state heat fluxes at prescribed heating surface temperatures.

They found that the presence of the volatile liquid caused subcooled boiling in the denser liquid. With the temperature of the heating surface unchanged, they observed lower temperatures in the denser liquid when there was the volatile liquid above it than otherwise. The depression of the bulk lower phase temperature was noted to increase as more volatile liquids were employed as the upper liquid. In their runs with n-hexane layered on water, the average bulk water temperature was 96.7°C, and the temperature measured 4.6 mm below the quiescent water level was 87.8°C. Since n-hexane

boils at 68.7°C, a thermal boundary layer must have existed in the water near the liquid-liquid interface.

b. Mercury and Low Conductivity Liquids

Data on boiling from mercury surfaces (in steady-state experiments) are presented in Figure 2-2.

Mercury is a liquid metal with a thermal conductivity of 159.2 W/m K (for water, the value is 0.63 W/m K at 25°C). This liquid depends primarily on its conductive properties for energy transfer, and much less on convective motion. Moreover, it has a free, microscopically smooth surface. The heat transfer characteristics should, therefore, be intermediate between those for boiling on a conducting solid surface, and on an ordinary liquid such as water. This prediction has been borne out by the data, Figure 2-2, since the heat transfer coefficients for liquids boiling on solid surfaces range from $3(10^3)$ to 10^5 W/m² K (McAdams, 1954).

A large discrepancy, however, exist between the data presented by the different investigators even when they used identical liquid combinations. The discrepancy can only be attributed to the experimental techniques, varying liquid purity and cleanliness of the mercury surfaces. Which of the data approach the true pool boiling data on clean mercury cannot be established, although Novakovic et al. (1964) seem to have taken many precautions to employ clean liquids.

c. Pool Boiling of Cryogenics on Water

Three recent exploratory studies have been reported on the

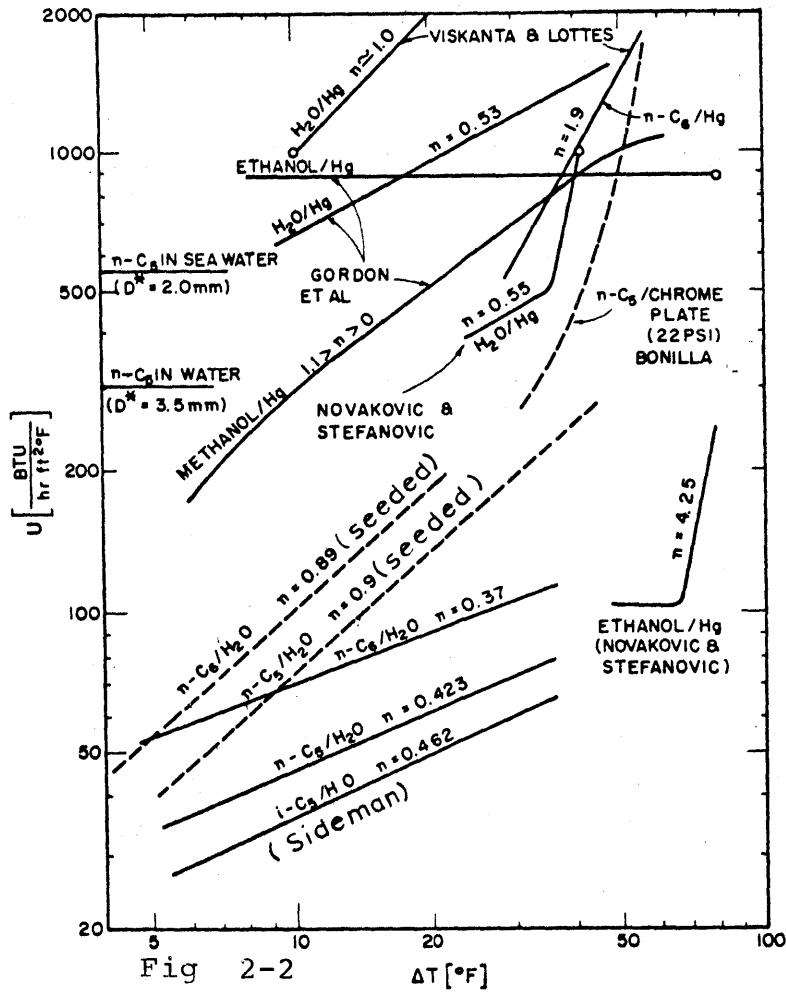


Fig 2-2
 Comparison of liquid - Liquid
 Boiling Systems (Sideman, 1966)

time-dependent vaporization rates of cryogenic liquids on confined and unheated water pools.

Burgess et al. (1970, 1972) issued reports on the hazards of accidental spillage of LNG (liquefied natural gas) in marine transportation. As a basis for studying the dispersion of vapor evolved from an evaporating LNG pool, they carried out some small-scale experiments to estimate the source rates of vapor generation.

Their experiments involved pouring liquid nitrogen, and LNG, on room temperature water contained in a test vessel mounted on a load cell. In the earlier experiments (1970), a glass aquarium, 30.5 cm by 61 cm was used as the test vessel. This was replaced with a styrene foam bucket (740 cm², cross-sectional area) in the later runs (1972).

The data consisted of determining the consecutive time intervals for losing 50g from the boiling pools, until the cryogen was completely boiled away. These gave the reported boiling rates summarized in Table 2-1. They found the boil-off rates of the liquids to be constant in the first 20 to 40 seconds of each run, and observed foaming with the LNG (none with the single component liquids). Ice was reported formed on water with the test cryogenic liquids, and, with LNG, it was formed quite readily.

An inspection of the two sets of data reveal a 20% difference in the ensemble average evaporation rates for identical systems. No explanations were offered for the discrepancy. Moreover, the maximum evaporation rates presented in the first report (presumably taken in

TABLE 2-1

Data of Burgess et al. (1970, 1972)

	System	Ensemble average evaporation rates, first 20 s g/cm ² s	Maximum evap, rates reported g/cm ² s
1970	LNG-Water (2.5 to 4cm)	0.018	0.03
	LNG-Ice	0.018	0.051
	LNG-Brine	0.018	0.025
	LN ₂ -Water	0.013	0.034
(minimum average rate for LN ₂ was 0.006)			
1972	LNG-Water	0.015	
	LNG-Aluminum foil	0.007	
	LN ₂ -Water	0.017	
	LN ₂ -Aluminum foil	0.013	
	LCH ₄ -Water (2.7 cm) (4.0 cm) (6.0 cm)	0.01 0.012 0.016	
1970	LNG contained 94.5% CH ₄ , 3.4% C ₂ H ₆ , 0.9% C ₃ H ₈ and 1.2 % higher hydrocarbons		
1972	LNG contained 92% CH ₄ , 6.3% C ₂ H ₆ , 0.1% C ₃ H ₈ plus nitrogen, oxygen and carbon dioxide.		

Numbers in parentheses were the heights of cryogen charged.
The aluminum foil covered a pool of water.

the first interval of their measurements) were as much as 200% higher than the (ensemble) average values. The smallest average (20s) evaporation rates for liquid nitrogen on water was 100% lower than the overall average value (for similar runs). The data, furthermore, indicate that the amounts of LNG proved did not influence its evaporation rates, but the reverse was true for methane. Thin aluminum sheets covering the water pools were, moreover, found to reduce the evaporation rates of nitrogen to a much lesser extent than for LNG.

Approximate heat fluxes in each system, calculated from the data, were between $2.5 (10^4)$ and $3.5 (10^4)$ W/m^2 for nitrogen on water or aluminum foils; $8(10^4)$ to $12(10^4)$ for LNG on water, and about $4(10^4)$ W/m^2 on aluminum foil; and $5(10^4)$ to $11(10^4)$ W/m^2 for methane charges between 2.5 and 6 cm deep.

It is not clear how the results might be completely interpreted as several important pieces of information, such as the amounts of cryogenic liquid charged (especially liquid nitrogen), the extent of splashing and conditions in the vapor departing, were not provided. However, it is apparent that the heat transfer to methane and LNG were much higher than to nitrogen. Furthermore, an aluminum foil separating water from the cryogenics influenced nitrogen less than LNG. These two pieces of information suggest that specific interactions between water and the hydrocarbon liquids might account for the enhanced fluxes. The observation that ice formed more readily with LNG than with nitrogen supports this view. Moreover, the fact that

the compositions of the hydrocarbons could be significant was demonstrated by the different boil-off characteristics of methane and LNG on water.

Experiments of Nakanishi and Reid (1971) were similar to those of Burgess et al., but they employed a glass Dewar as the test vessel. Boil-off rates were in the same order of magnitude. They observed that the presence of trace quantities of higher hydrocarbon such as pentane or n-hexane in liquid methane caused much higher boil-off rates to be achieved.

The third study, Boyle and Kneebone (1973), involved boiling LNG on confined salt water pools. The variables of their experiments included the LNG composition, the quantity charged, and the initial water temperature.

In each run, the cryogenic liquid was poured on water contained in an 1.04 m or an 2.18 m I.D. vessel balanced on three load cells; and the combined signal output by the load cells were continuously recorded on analog devices as the residual weights of the boiling liquid versus time. Slopes were manually taken off such curves to yield the boil-off rates.

Typical of their results is Figure 2-3 in which the effects of variations in initial water temperature was being studied. At the maxima, about 650g of the 2270g LNG reported poured (on the 2.18m diameter vessel) was indicated to remain above the water pool. The maxima, they stated, corresponded to the time when each continuous

boiling pool disintegrated into spheroids which floated freely and moved randomly on the water surface, i.e. the cryogen pool depth was 1.8 mm at the time of degeneration. An integration under the curves should then yield about 1620g. Such an integration, however, gave values between 1135g and 1400g. Thus, between 10 and 25% of the cryogenic liquid input was not accounted for. If 1.8 mm of the liquid were the minimum height required to form a continuous pool, then in a number of the reported runs, the water surfaces were only partially covered at all times. Since the covered areas were unknown, the corresponding data may be questioned and caution used when drawing inferences from these data. Moreover, because of the large surface areas used and the small volume of cryogens layered, the spreading of the cryogens should probably have been considered in the initial periods of each run. This was not done.

The general trends of the results, however, were that the LNG boil-off rates increased with; time; increasing quantities of cryogen poured; decreasing molar ratio of methane in LNG; and, decreasing water temperatures. Some of these trends, especially the time functions, are in disagreement with Burgess et al.'s order of magnitude experiments.

The highest boil-off rate reported was $0.02 \text{ g/cm}^2 - \text{s}$, which corresponds to a latent heat flux of 10^5 W/m^2 (a value in the range reported previously). They also found that a boiling cryogenic liquid carried off in its vapor, as much as 8% of its initial weight

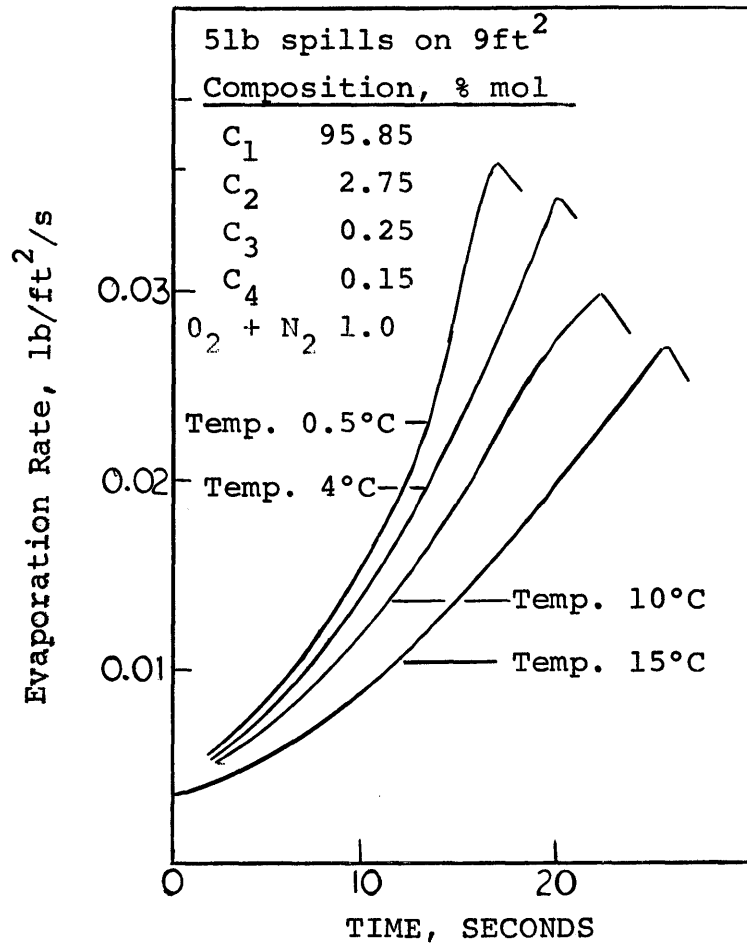


Fig. 2-3

The Effect of Water Temperature
on LNG Evaporation Rate

[reproduced from Boyle and Kneebone, 1973]

of water. This was attributed to an atomization process; the high velocities of vapors in the film between two liquids caused water entrainment. This mechanism presumes the boiling process to cause the generation of capillary waves on the water surface.

d. Summary: Liquid-Liquid Boiling Studies

The observations and deductions from the foregoing can be summarized as follows:

1. Bubbles disengaged at liquid-liquid interfaces, especially clean ones, have large diameters.
2. Heat fluxes to a liquid boiling on the surface of another liquid are proportional to the temperature differences between the heating surface and the boiling liquid, in steady state experiments.
3. Boundary layers may exist near the interface of liquids whose bulk are well mixed. This is true in spite of the fact that the interface is 'free'.
4. Boiling heat transfer rates from mercury to normal liquids, e.g., hydrocarbons, are intermediate to those between water or metallic solid surfaces and the boiling liquid.
5. Liquid nitrogen boils-off on water at much lower heat transfer rates than LNG, a cryogenic mixture of hydrocarbons. Both liquid to vapor and liquid to solid transformations occurred with cryogen-water systems.

The apparent heat fluxes to nitrogen were independent of the heating surface properties.

2.3 PRINCIPAL EVENTS INFLUENCING LIQUID-LIQUID BOILING

As indicated by the title, this section contains reviews of the literature on events which have been studied in other systems, and which occur simultaneously during boiling at the interface of two superposed liquids. Apart from the boiling phenomena itself, natural convective flows in the denser heat source liquid and solid formation at the interface are occurrences which should be examined. An understanding of these events will facilitate a proper interpretation and analyses of the results obtained during the boiling of cryogenes on water.

A. Pool Boiling Heat Transfer

Evaporation in the bulk of a liquid leading to formation and release of bubbles is termed boiling. Ordinarily, all that is required to initiate and sustain the process is to provide intimate contact with a medium whose temperature exceeds the local saturation temperature of the liquid.

Extensive review of the knowledge on boiling have been presented by Mc Adams (1954), Jakob (1949), Berenson (1960) and Rohsenow (1971). Continuing research has succeeded in establishing the existence of four distinct boiling regimes, after the pioneering efforts of Nukiyama (1934). These are separated according to the temperature

difference between the boiling liquid and the heated surface. In a typical water boiling curve Figure 2-4 fluxes are plotted against the temperature difference across the heat transfer interface, ΔT . The four regimes can be identified from the figure, and transition from one regime to another is either marked by sharp slope change or by a maximum/minimum point in the curve. The functional names of these regions are the convective, nucleate, transition and film boiling regimes. Sketches of the physical appearance while operating in each of the regimes are presented in Figure 2-5.

a. Convective Heat Transfer

With very small values of ΔT , for example, at point a (Figure 2-4), heat is transferred across the interface of the heating element by conduction. The liquid layer adjacent to the heated surface become hotter and less dense than the bulk liquid, and buoyancy forces cause circulation currents to develop in the liquid, as shown in Figure 2-5a. Liquid evaporation occurs only at the free surface and no bubbles are formed in the bulk. This region of low heat fluxes and free circulating flows is known as the convective heat transfer regime. A discussion on heat flux enhancements with convective flows over the conduction only heat transfer process will be presented subsequently.

b. Nucleate Boiling

As ΔT is increased, most of the heat is still conducted

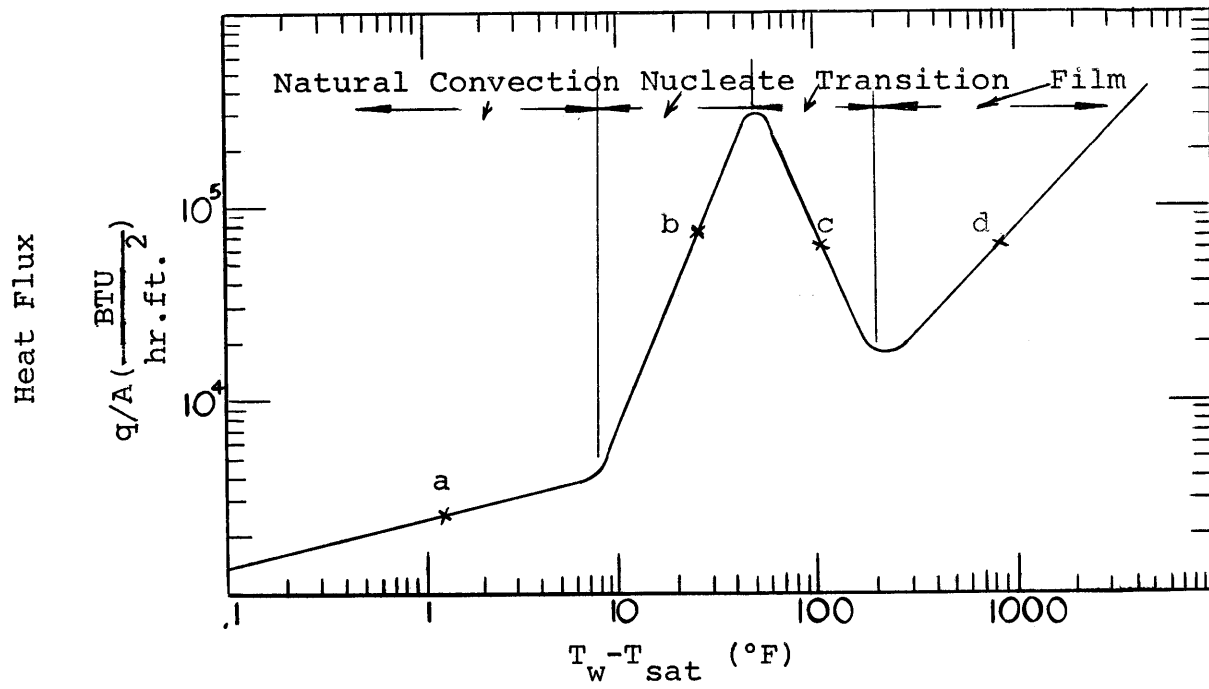


Fig. 2-4

Characteristics Boiling Curve For Water at 1 Atm

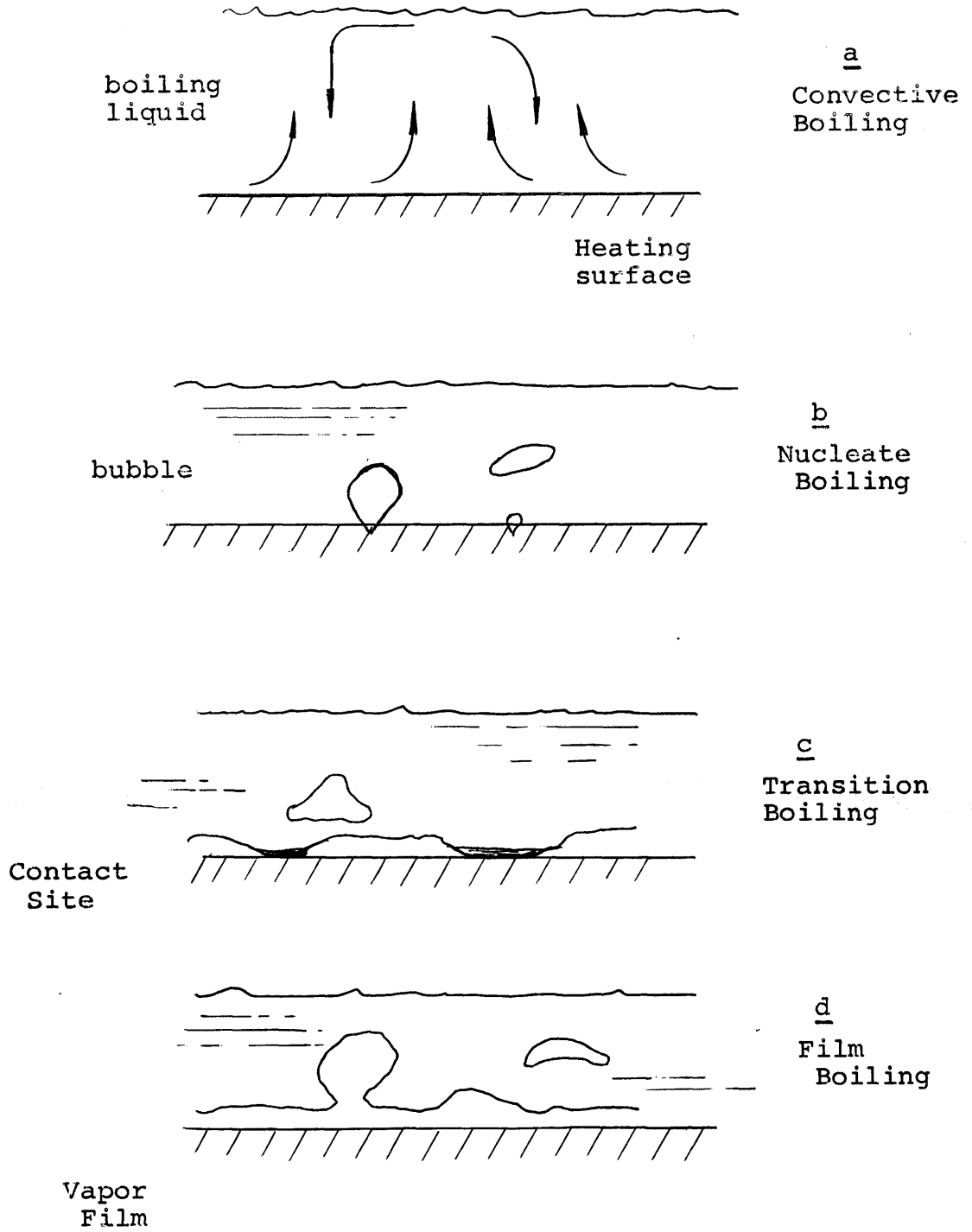


Fig. 2-5

The Regimes Of Boiling

directly into the liquid, but bubbles now begin to nucleate and grow at preferred sites on the heating surface, especially at microcavities in which vapor pre-exists on a solid surface (Jakob, 1949; Rohsenow 1971). The boiling process at point b (Figure 2-4) might appear as shown in Figure 2-5b. A major portion of the temperature difference between the heating surface and bulk liquid occurs in a very thin layer adjacent to the heating surface. This was experimentally confirmed by Marcus and Dropkin (1965).

The growth and release of the bubbles, and their movements through the liquid effect a vigorous agitation of the bulk and this prevents the liquid from being superheated much above its saturation boiling point. It has also been observed that the number of preferred sites, the frequency of bubble release from an active site and the heat flux increase as the bulk liquid-heating surface temperature difference is increased.

The range of ΔT over which the foregoing is observed, is called the nucleate boiling regime. As high heat fluxes accompany nucleate boiling, most industrial equipment is operated in this region of moderate ΔT s.

Rohsenow (1952), Forster and Zuber (1955), Kutateladze (1963), amongst others, have proposed partially-generalized correlations which relate heat fluxes and fluid physical properties to the bubble characteristics. Rohsenow's correlation is given in Equation (2-1).

$$\frac{C_L (T_w - T_s)}{\Delta H_v} = K \left[\frac{Q'/A}{\mu_L \Delta H_v} \left(\frac{\sigma}{g(\rho_L - \rho_v)} \right)^{1/2} \right]^a \left[\frac{C_L \mu_L}{K_L} \right]^b \quad (2-1)$$

This predictive expression relates the heat fluxes, Q'/A , to the heating surface-boiling liquid temperature difference, $T_w - T_s$, and the liquid properties. Rohsenow (1971) suggested the parameter values (based on his experiments) be 0.33 for a , $b=1$ for water and 1.7 for other liquids, and $K=0.013$ ($\pm 20\%$). The values of these parameters change when the characteristics of the heating surface are altered.

c. Transition Boiling

The rate of bubble generation in the nucleate regime, and the accompanying heat flux, continues to increase until a certain ΔT is reached. At this point, the frequency of bubble evolution and the number of active sites become very large that adjacent bubbles merge. The bulk liquid touches the heating surface only intermittently and at random locations. In experiments in which ΔT is an independent variable, a new region called the transition boiling regime has been attained. Point c (Figure 2-4) might indicate the heat flux for boiling with the configuration in Figure 2-5c. The pictures of Santangelo and Westwater (1955) clearly supports the proposed transition boiling configuration. As shown in Figure 2-4, the heat flux now decreases with increasing temperature, a fact first established by Drew and Mueller (1937).

Berenson (1960, 1961) presented a correlation for the heat

transfer coefficient, based on hydrodynamic stability analysis, at the upper bound of the transition regime (which also corresponds to the Leidenfrost point for film boiling). The correlation is

$$h = a \left[\frac{k_v^3 \Delta H_{v,v} (\rho_L - \rho_v)}{\mu_v \Delta T} \left(\frac{g (\rho_L - \rho_v)}{\sigma} \right)^{1/2} \right]^b \quad (2-2)$$

The parameter b has a value of $1/4$. This was established by a summation of the expressions defining the forces acting on a bubble during growth. In this case, the pressure, buoyancy and surface tension forces were considered. Coefficient a is related to the bubble sizes when detached; and its value obtained experimentally. The value of a provided by Berenson was 0.425. All the physical properties applied in the equation are determined at the conditions in the vapor film.

The two parameter expression fails to take the heating surface characteristic into account, and hence its applicability in the transition boiling regime is limited to a narrow ΔT range at the upper bound of the regime. Factors influencing bubble growth, such as contamination, will be expected to influence the values of parameter a .

d. Film Boiling

At high ΔT , e.g., at d in Figure 2-5, the liquid becomes separated from the surface by a film of its own vapor. Figure 2-5d

is a sketch of the probable instantaneous configuration. The vapor generated at the boiling liquid undersurface, as a result of heat conduction across the vapor film, causes nodes to develop. Some of these become pinched-off and are released as bubbles. Again, the pictures of Santangelo and Westwater (1955) display this boiling process clearly.

This region of unbounded upper ΔT (Figure 2-4) is called the film boiling regime. The correlation of Berenson (1961), Equation (2-2), is most often applied in this regime for which they are also valid. However, as stated earlier, parameter a must take a value appropriate to the mean bubble diameters detached from the vaporization zone.

As can be anticipated, many interfacial properties influence the shape and positions of the boiling curve shown in Figure 2-4. Amongst these are the heating surface texture and liquid properties. A brief review of the effects these factors on boiling, pertinent to the present study, is presented in the following.

e. The Influence of Surface Variables on Boiling

The degree of polish of a boiling surface, and the presence of contaminants, have been noted to cause significant shifts in the location of the boiling curves in the nucleate and transition boiling regimes. The first controlled experiments to establish this fact were performed by Corty and Foust (1955). Typical effects of surface cleanliness and roughness, obtained by Berenson (1960), are presented

in Figures 2-6 and 2-7.

In Figure 2-6, the effect of surface cleanliness is primarily exhibited in the transition boiling regime. The heat flux to a contaminated surface, at a given ΔT , is much higher than on a clean surface. Moreover, the minimum film boiling temperature, the Leidenfrost point, has been shifted to a higher ΔT . An explanation of these observations is not immediately obvious.

If Figure 2-7 is examined instead, it is observed both the nucleate and transition regimes are very dependent on the texture of the heating surface. Increased smoothness causes the nucleate boiling curves to be shifted to higher ΔT s. The film boiling regime is, however, not affected. A logical explanation is to relate the shifts to the relative ease of bubble generation at each of the surfaces. Mirror-finished surfaces have the least number of nucleating sites for bubble generation, hence, they allow one to attain the highest superheats in the bulk liquid.

In Figure 2-6, it can be seen that, although the shift in the nucleate regime is not appreciable, the direction of shift suggests that the presence of contaminants, on the initially rough surfaces, has the same effects as if the surface were polished and the number of active bubble sites reduced. The shift in the transition regime is, therefore, consistent with observations in Figure 2-7, but the extent of shift is much larger. It is, however, not clear why the Leidenfrost point should be delayed to higher ΔT s.

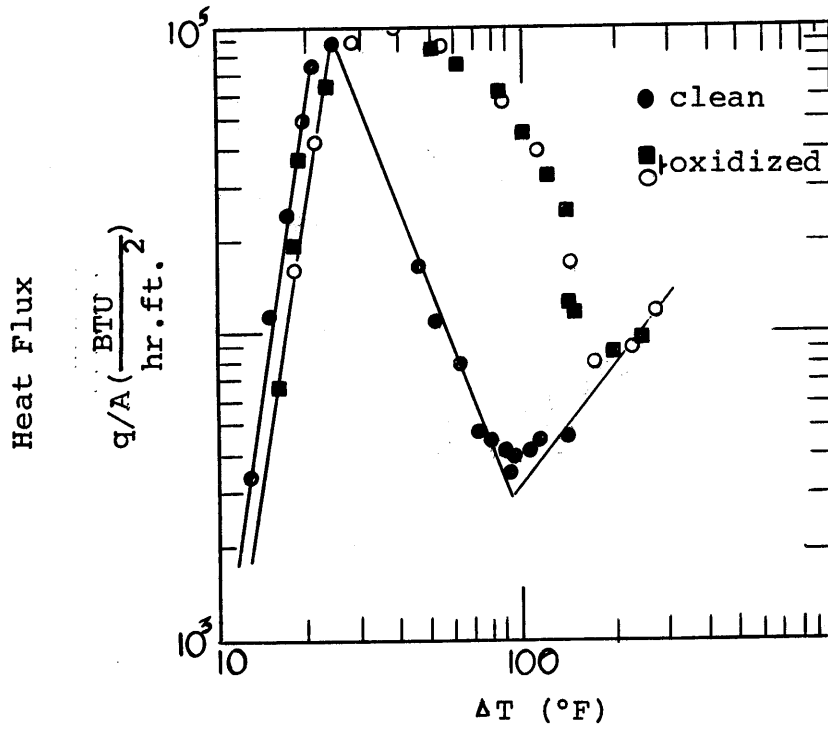


Fig. 2-6 Copper Pentane Test Results: Effect of Surface Cleanliness (Berenson, 1960)

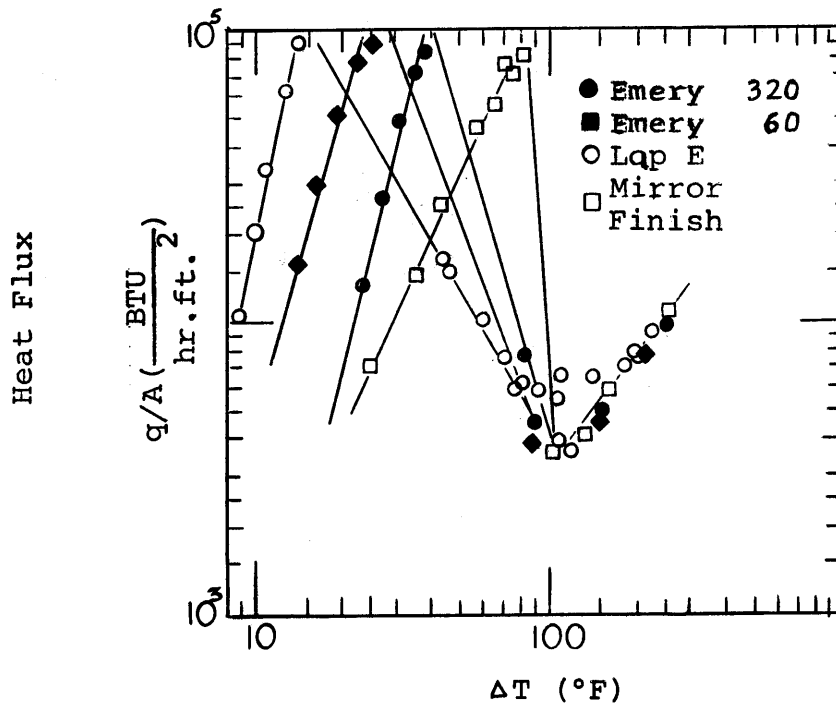


Fig. 2-7 Copper Pentane Test Results: Effect of Roughness (Berenson, 1960)

Berenson (1960) observed, also, that different solid materials, with the same treatments of the surfaces, exhibited shifts in the nucleate and transition regimes. This must be attributed to the physical properties of the surfaces and the fabrication processes.

f. Boiling of Single Phase Liquid Mixtures

So far in this section, it has been implicit that only single component liquids were being boiled. The present studies, however, include the boiling of single phase volatile liquid mixtures whose components have different relative volatilities.

The available literature is primarily on binary mixtures, and most investigators operated in the convective and nucleate boiling regimes. Typical boiling curves for miscible mixtures of liquids are presented in Figures 2-8 and 2-9 .

Vos and van Strahlen (1956) and van Wijk et al. (1956) presented data on heat flux versus heating surface-boiling liquid temperature differences for methyl ethyl ketone-water systems. The results, reproduced in Figure 2-8 , are for convective and nucleate boiling, up to the peak flux marking the start of the transition boiling region.

The first and most obvious fact in the figure is that the peak flux into the mixture containing 4.2% by weight methyl ethyl ketone, the more volatile of the liquid components, (b.pt. 79.6°C), is more than 120% higher than for pure water, and 450% higher than for the pure ketone! The mixture with 88.5% by weight ketone (an

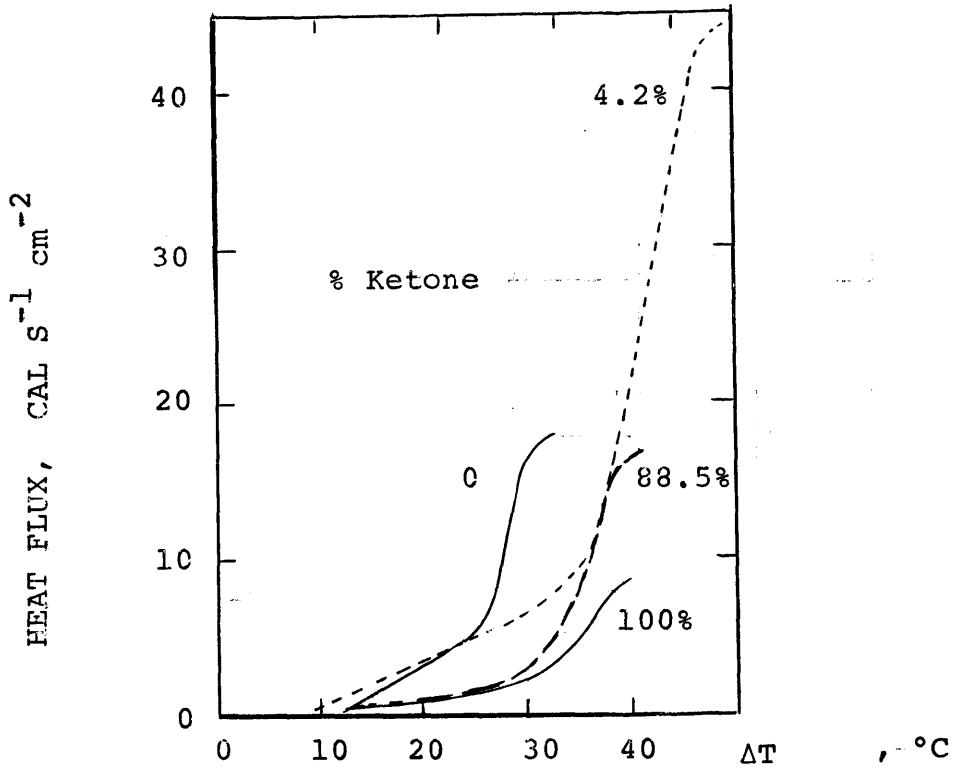


Fig. 2-8

Nucleate Boiling Of A Mixture Of Methylethyl-Ketone And Water At Atmospheric Pressure. (van Wijk, et al., 1956)

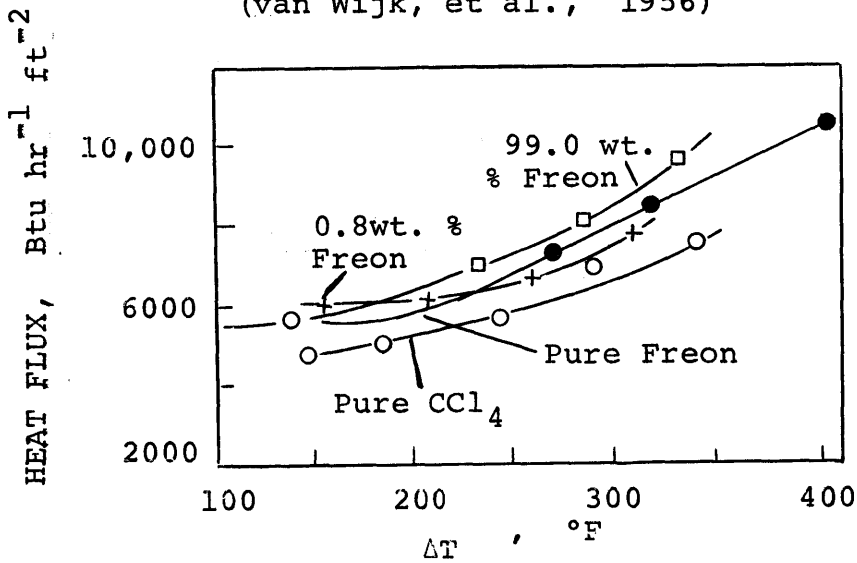


Fig. 2-9

Film-Boiling Curves For Mixtures of CCl₄ And Freon-113 On A Horizontal Plate At Atmospheric Pressure. (Kautzy and Westwater, 1967)

azeotropic mixture) exhibited convective boiling characteristics closer to that of pure ketone. At a higher ΔT ($\sim 30^\circ\text{C}$), in the nucleate boiling regime, the curves separate. The ΔT at the peak fluxes were almost the same, but the heat flux to the mixture was 130% higher than that to pure ketone.

In addition, van Wijk et al. (1956) and van Strahlen (1967, 1968) observed that the bubbles released in the 4.2% ketone mixture were smaller than those for the 88.5% ketone mixture and the pure liquids.

An attempt may be made to relate the observed pattern to the sites of the bubbles produced. (Mechanisms describing the function, and growth, of bubbles, in liquid mixtures, have been presented by van Wijk et al. (1956), Hovestredt (1963), van Strahlen (1967, 1968). These will not be reviewed here.) If the bubble sizes in mixtures are smaller than in pure liquids, and the frequency of release of bubbles from each active site is only slightly dependent on the sizes, as suggested by the pictures of van Strahlen (1968), then in nucleate boiling, the boiling curves of mixtures would be expected to be shifted to high ΔT s; higher than for the pure liquids. This should be true because the volumetric rate of vapor production has been decreased. (A decrease in vapor generation is also observed when a heating surface is polished, although this is attributed to a reduction in active sites rather than the bubble sizes). This is, however, not noted in Figure 2-8. The ΔT at which the small bubbles

merge at the heating surface (on-set of transition boiling) should be higher than with the bigger bubbles produced in pure liquids. It is not clear, however, why the fluxes should be higher in mixtures.

Figure 2-9 contains the data of Kautzy and Westwater (1967) for mixtures in the film boiling regime. Again it is apparent that small quantities of the more volatile component, in this case Freon 113 (1,1,2 - trichloro ethane, b.pt. 47.6 C at 1 atm.) in carbon tetrachloride (b.pt. 76.8 C at 1 atm.), caused the carbon tetrachloride to achieve heat fluxes up to 20% higher than the pure CCl_4 . The increase in heat fluxes to Freon 113 with 1% by weight CCl_4 was less, only about 10%.

The important observation here is that heat flux enhancements to mixtures in film boiling are much less than in the convective and nucleate regimes. No data are available in the transition regions and the influence of mixture compositions on the Leidenfrost point are not known.

2.3.2 MECHANISMS OF ICE FORMATION AT A WATER SURFACE

The saturation boiling temperatures of the volatile liquids layered on water in the present investigation are much lower than 0°C. Any ice formation would be expected, therefore, to originate at the water surface.

Most of the available literature on ice nucleation and growth has been on homogeneous and heterogeneous nucleation of ice in the bulk of liquids, especially in form of drops. These studies have

succeeded in determining the degree of cooling below 0°C that water can be exposed to before spontaneous ice formation occurs. Typical of the results was the data of Biggs (1953) and Langham and Mason (1958) reproduced in Figure 2-10 for homogeneous and heterogeneous nucleation in the bulk of water.

The mechanisms of ice formation and growth at water surfaces are essentially of two types; leading to the formation of frazil ice and hydrates.

a. Frazil Ice

Frazil ice consist of thin, free floating rounded discs of transparent ice, which on coalescing, followed by regelation, can form large ice masses in cold flowing streams.

The formation of frazil ice on water seldom requires that the water be cooled below -1°C . This was noted by Schaefer (1950) and Arakawa (1954, 1955). This subcooling is much less than the 20 to 40°C below zero required for nucleation in bulk water with cold flowing water. Schaefer noted that rarely more than 0.01°C supercooling was required for frazil ice to form and grow on the surface, as long as the ambient air was at temperatures considerably below 0°C ($< -10^{\circ}\text{C}$). The surface of the water must also be seeded with particles of ice. Other solid particles, such as dust, might also be suitable seeds. Furthermore, he reported that the thickness of the discs were between 25 and 100 μm for crystals to 5 mm diameter.

Arakawa (1954), working with stationary cooled shallow

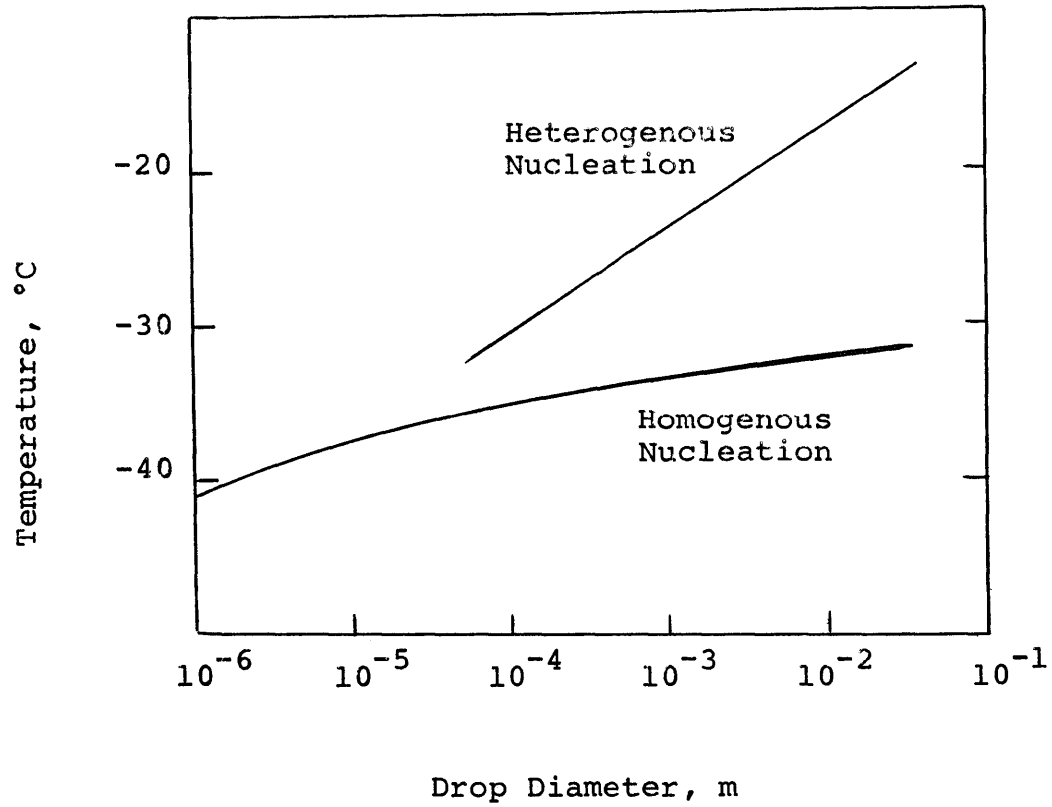


Fig. 2-10

Homogenous Nucleation of Ice in Water
(Mason, 1958)

dishes of water, observed the same discs on water whose bulk temperature was between 0.1 and 1°C. Moreover, the discs lost their circular profile at diameters between 2 and 3 mm to become six-sided stellar dendritic crystals.

The mechanism of frazil ice formation might be as follows. Water at temperatures higher than -1°C will not nucleate ice, even in the presence of solids in suspension in the water, as suggested in Figure 2-10. The free surface of water exposed to much colder ambient air, however, becomes cooled to low temperatures within a small boundary layer. The density inversion of water makes the attained temperature gradient stable, modified but not destroyed by convection currents in the underlying liquid.

The introduction of a seed within the boundary layer zone provides low energy sites where the growth process can start (heterogeneous nucleation). Ice particles, with the proper surface energies and growth planes with therefore be the most effective seeds. The thickness of the ice discs will be determined by the thickness of the cooled boundary layer and lateral growth of ice along the surface will be fastest; growth in the zone of maximum supercool.

b. Hydrates

Hydrates are members of the class of clathrates, inclusion compounds in which a molecule of one substance is caged in a correctly-sized cavity created by rigid arrangements of molecules of a substrate; with no chemical bonding established between the sub-

stances.

Low molecular weight hydrocarbons and inert gases are known to form hydrates with water. These are solids which resemble ice or wet snow in appearance. They float on water and show densities of 0.88 to 0.9 g/cm³. Detailed studies on hydrates here established the conditions under which they form (Hammerschmidt, 1934; Deaton and Frost, 1946, a and b; Katz et al., 1959). The lattice structures have also been established (Saito et al., 1964, 1965).

The principal conditions of formation are that liquid water must be present in contact with the gas of interest, (or at least, the gas must be saturated with water vapor), at high pressures and ordinary temperatures. The hydrate forming conditions are presented in Figure 2-11 for paraffin hydrocarbons. Katz (1959) also presented data to show that mixtures of the hydrocarbon gases form hydrates on water conditions intermediate to that required by the pure components.

As is apparent from Figure 2-11, the pressure at which hydrates are formed decreases with decreasing temperatures. No data are available below 0°C, but it can be hypothesized that, at sufficiently low temperatures, hydrates would form at 1 atm. with methane etc. in the presence of water.

The mechanism for hydrate formation is not understood, but it is obvious that subcooling of the water-gas mixtures below 0°C is not necessary. The low solubility of hydrocarbons in water, and hydrate generation in a gas supersaturated with water initiated at solid surfaces, suggest that the process is a surface phenomena

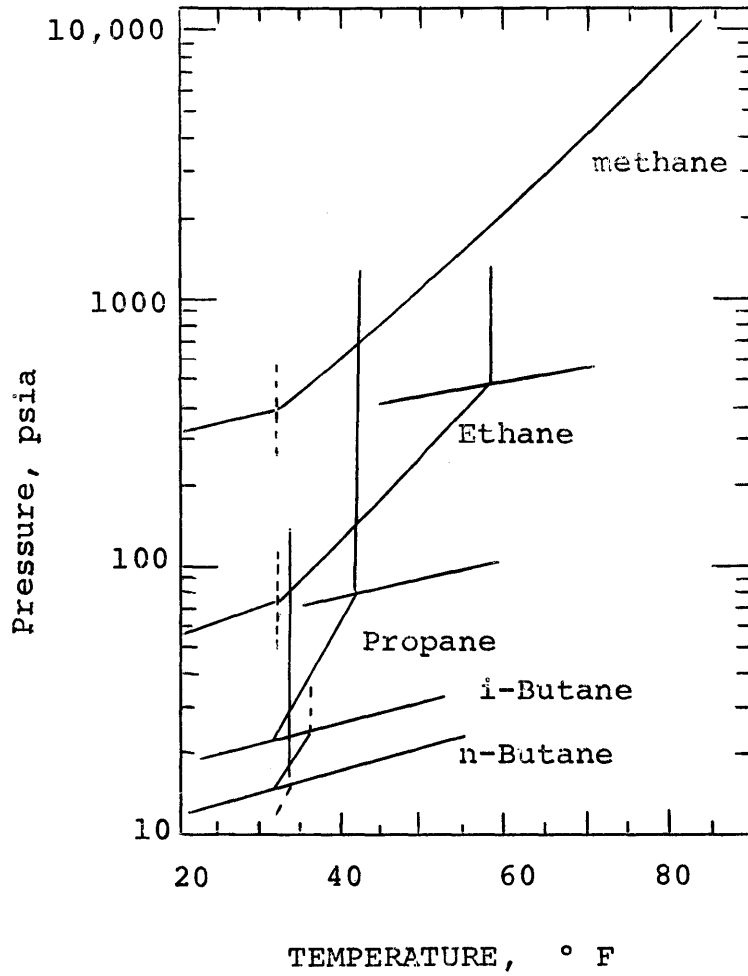


Fig. 2-11
 Hydrate-Forming Conditions For
 Paraffin Hydrocarbons
 (Katz et al., 1959)

and not a bulk water process.

2.3.3 CONVECTIVE MOTIONS (IN HEAT SOURCE)

It is the expressed purpose this thesis to study the transient boiling of a liquid on another liquid. For this reason, it is appropriate to examine the literature on heat transfer to a confined body of liquid cooled from above, or the corollary system of a fluid heated from beneath. One of the observed effects is the development of free convective motion in the liquid bulk. This motion is observed both in the boiling liquid and in the heat source liquid, i.e., water, in the present study.

The literature on free convection is large and the reader is referred to Chandrasekhar (1961) and Turner (1973) for excellent reviews.

The parameter generally used to describe the driving forces for convective flows is the Rayleigh number, Ra, after Lord Rayleigh (1916). This parameter is the product of two dimensionless groups defined below.

$$\text{Prandtl number } \alpha \frac{\text{momentum diffusivity}}{\text{thermal diffusivity}}$$

$$\text{Pr} = \frac{C_p \mu}{k} = \frac{\nu}{\alpha}$$

$$\text{Grashof number } \alpha \frac{\text{inertia forces} \times \text{bouyancy forces}}{(\text{viscous forces})^2}$$

$$\text{Gr} = \frac{g \rho \Delta T D^3}{\nu^2}$$

$$Ra = Gr \cdot Pr$$

Convective motion in a fluid can lead to significant enhancement of heat transfer rates. This is illustrated with the experimental data (Silverston, 1958) presented in Figure 2.12. The plot shows the dimensionless heat transfer coefficient, $Nu (= hD/k)$, against the Rayleigh number. Heat transfer across a stagnant fluid layer confined between two horizontal rigid conducting plates occurs by conduction for Ra less than 1800, thus the Nusselt number is unity up to this point. As the temperature difference across the plate or the plate separation is increased, or a less viscous and/or more thermal conducting fluid is substituted, the Rayleigh number become increased, and the fluid starts to move when Ra exceeds the critical value of 1760. As is apparent from the plot, heat fluxes are much enhanced when the confined fluid is in convective motion. The dimensionless transfer coefficient is doubled its 'conduction regime' value at an Ra of 5000.

Variations in the heat transfer system, such as a liquid body bounded by one rigid surface and one free surface or by two free surfaces, have the effect of lowering the Ra at which convective motions start (Chandrasekhar, 1961, Berg et al., 1966).

The water pool, upon which liquid cryogenics were boiled in this study, is a liquid layer cooled from above and subject to recirculating currents which will enhance the fluxes to the boiling liquid in two ways. First, the warmer water in the bulk is used to

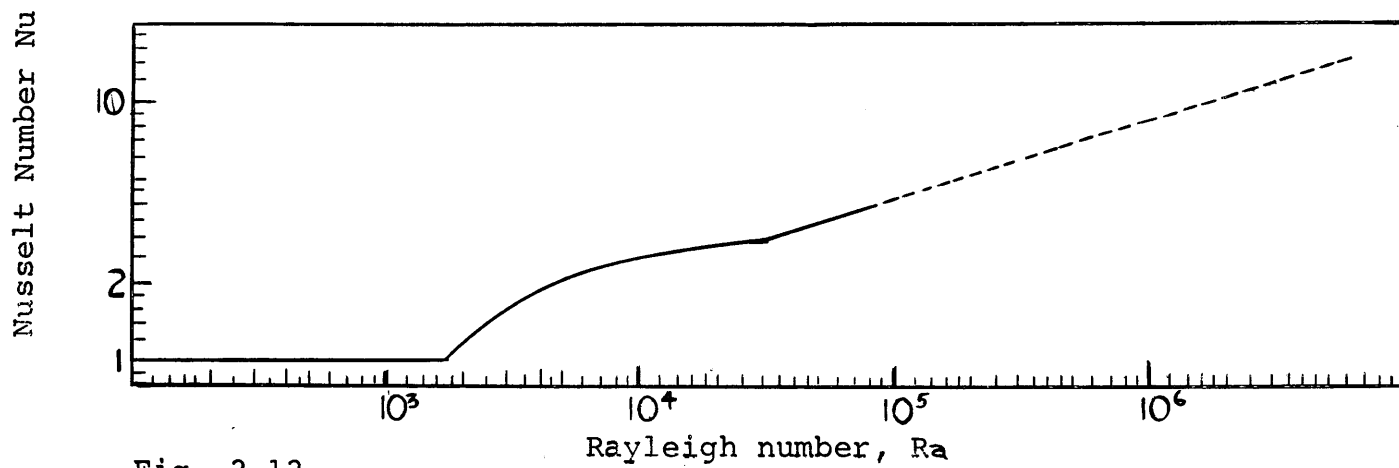


Fig. 2-12

Heat Transfer Enhancement With Convective Fluid Flows Between
Two Horizontal Rigid Plates. [Reproduced from Chandrasekhar, 1961]

replace the cooled surface layers, thereby assisting in maintaining a large temperature driving force for boiling. The second effect is that any ice nuclei and embryos formed on the water surface will be recirculated into the bulk where they are melted, and the heat flux is further increased.

The convective motion may not be altogether 'free'. The rapid growth and release of bubbles from the boiling cryogens with cause waves on the water surface. Secondary recirculations in the water will then result, and higher effective Ra become achieved. Longuet-Higgins (1953, 1960) and Phillips (1969) discussed these wave-induced motions.

2.4 A COMPARISON OF SOLID-LIQUID AND LIQUID-LIQUID BOILING

The primary differences between the phenomena of liquids boiling on solids and the boiling of cryogens on water, as carried out in this thesis, are two fold: operating conditions and properties of material.

Operating Conditions

Most boiling processes are controlled operations. Prescribed heat fluxes or heating surface temperatures are imposed on the fluid (liquid at moderate conditions) under test. Thus, the systems can be operated at fixed conditions and at steady state. This has been the technique used to determine the boiling curves. Because of the external control, a wide range of variables can be studied.

The cryogens used here were at their normal boiling temperatures at the start of the runs. These temperatures were considerably lower than that of water, and consequently energy for boiling was withdrawn from the essentially semi-infinite water pools. In the attempt to model spills on a large expanse of deep water, no external heat was supplied to the water to keep the operations at steady state.

Properties of Material

The second main difference pertain to the properties of the heating surface. Solids are highly conducting, and they do possess a surface microstructure. Gases are usually trapped in the micro-cavities, and these enhance bubble generation at low heating surface-bulk liquid temperature differences.

Liquids are devoid of these cavities, but they might contain dissolved gases. Moreover, except for mercury, normal liquids are poorly conducting, hence, rates of heat transfers would be low. In contact with colder fluids, normal liquid surfaces might, therefore, cool down sufficiently to start and maintain the growth of a solid phase; a process which is exothermic and could enhance the fluxes.

2.5 OBJECTIVES OF THE PRESENT INVESTIGATION

The objects of this study were two-fold.

1. To conduct a careful, detailed and accurate experimental study of vaporization rates of cryogenic liquids (nitrogen and the low molecular weight hydrocarbons) on confined pools of water. The effect of initial water tem-

perature, quantity of cryogen charged, and the cryogen composition were to be established. The conditions in the vapor evolved and in the heat source liquid were to be monitored continuously. Collectively, the data should permit accurate evaluation of the heat fluxes between two superposed liquids.

2. To investigate, photographically, the mechanisms of the heat transfer process and associated phenomena.

CHAPTER 3

A PHOTOGRAPHIC STUDY OF LIQUID-LIQUID BOILING INTERFACES3.1 INTRODUCTION

In later chapters of this thesis, quantitative data are presented that indicate experimental boiling heat fluxes for cryogenic liquids boiling on a water surface. In the present chapter, a more qualitative study is described.

Photographs were taken of the actual interface between the boiling cryogenic liquid and water. The pictures obtained provided valuable information relating to ice formation, liquid turbulence and bubble sizes. The variation in bubble size distributions between pure liquid methane and LNG was particularly pronounced.

3.2 EXPERIMENTAL

For all experiments, the liquid cryogen was boiled on glass or water surfaces. The boiling vessel was 14.5 cm in diameter and was constructed with an optically-flat bottom. Photographs were taken with a Nikkormat camera from below (see Figure 3.1). This camera was equipped with a 50 mm, f1.4 Nikon lens. Extension tubes permitted close-up images of the interface to be obtained. Illumination was from two 500W G.E. photoflood lamps whose color temperature was 3200K. Infra-red radiation from the lamps was attenuated by interposing parallel glass plates (1 cm apart), through which cold water was slowly flowed, between the lamps and the test vessel.



Room 14-0551
77 Massachusetts Avenue
Cambridge, MA 02139
Ph: 617.253.2800
Email: docs@mit.edu
<http://libraries.mit.edu/docs>

DISCLAIMER

**Page has been omitted due to a pagination error
by the author.**

(p.77)

In each run, the cryogenic liquid was introduced into the vessel which contained a 3 to 5 cm depth of water. (In a few experiments, no water was used to allow a comparison between the boiling phenomena on solid and water surfaces.) The photographs were taken every 2 to 3 seconds with exposure times of 1 millisecond. The 'depth of field' across the interface was less than 2 cm at the widest aperture of the lens (f1.4). The intensity of light entering the camera at this aperture was controlled by the rotation of two polarizing filters placed perpendicular to the light path into the camera opening.

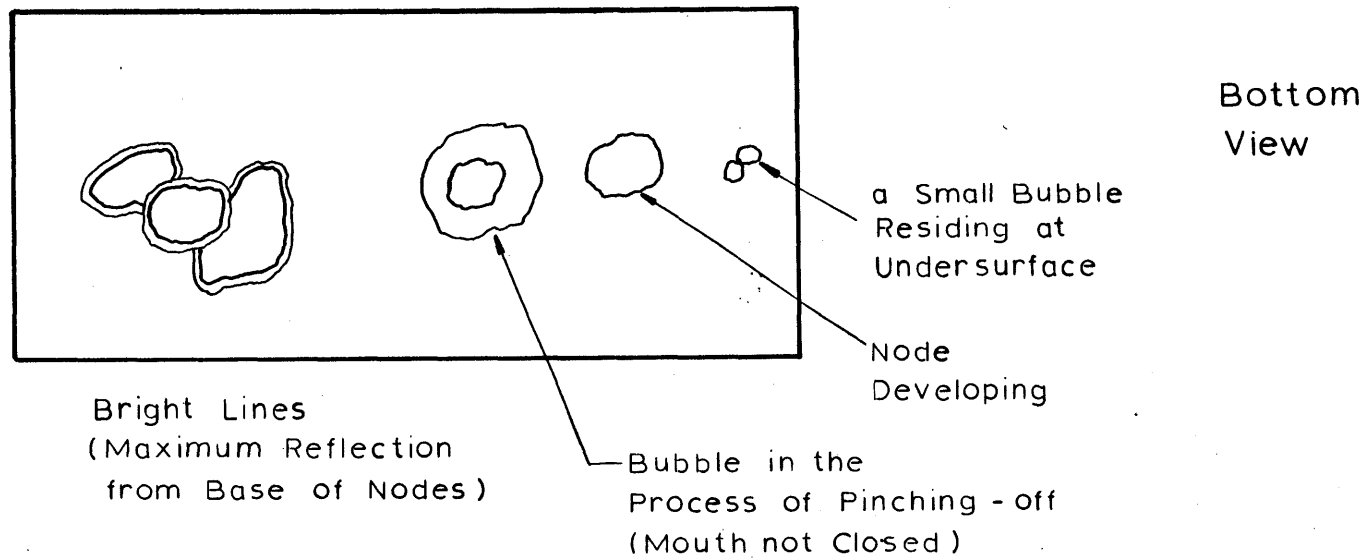
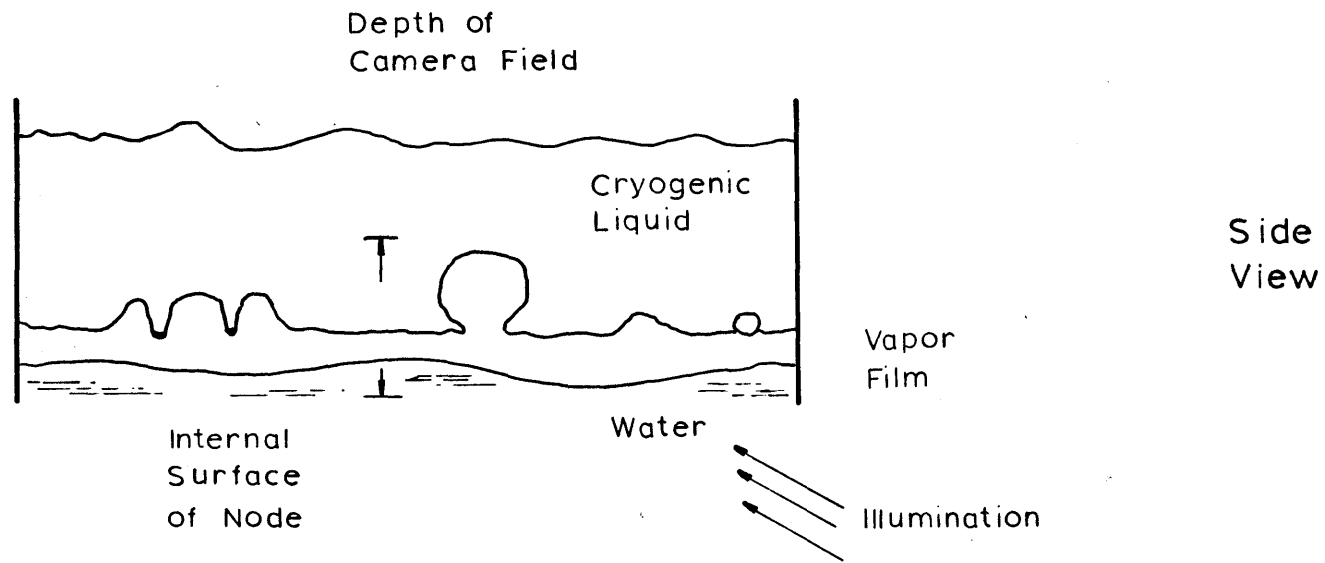
For the close-up pictures, extension tubes were employed to achieve a reproduction ratio of 0.5, and the area viewed was about 4.8 to 7.1 cm.

3.3 RESULTS

A few selected time-sequenced, long-range and close-up images of the cryogen-water (glass) interface are presented in Figures 3-2 to 3-10. The close-up pictures are full-sized unless noted otherwise.

The cryogens used were liquid nitrogen, methane (99.85% and 99.98% pure), ethane (99.84%) and LNG (98.2% CH₄, 1.62% C₂H₆, 0.112% C₃H₈, 0.043% iC₄H₁₀ and 0.03% nC₄H₁₀).

The features of the interface can be interpreted in terms of the proximity of the boiling liquid lower free surface to the heating surface. The sketches below show the significant structures believed to be obtained in both the side and bottom views. (The bottom views are presented in the pictures.)



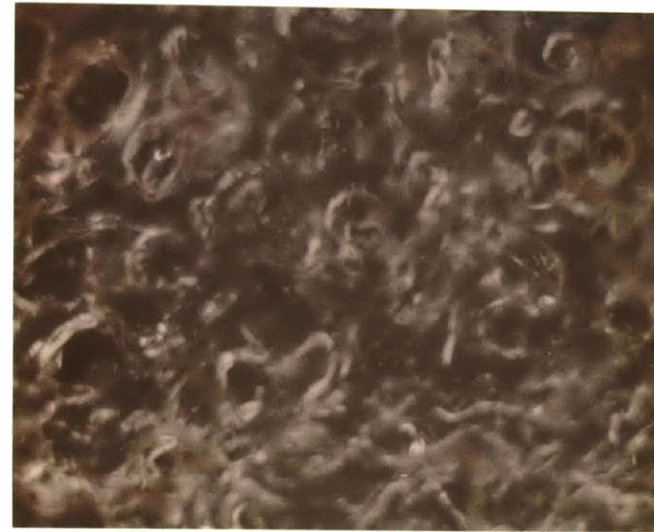
Sketch of the Significant Features of the Photographs

In Figure 3-2, three photographs of liquid nitrogen boiling on glass (no water was present) are presented. In (1) and (2), the gross pictures are shown whereas in (3) a close-up image is presented. The glass was originally at 24°C but it was cooled down rapidly. Based on the time required for frost to form on the outside of the glass, the room temperature and relative humidity, and the conductivity of the glass, it was possible to estimate the glass temperature at the interface with the boiling nitrogen. In pictures (2) and (3), taken 5 seconds after liquid nitrogen was input, the boiling ΔT had decreased to 150°C from an original value of 220°C.

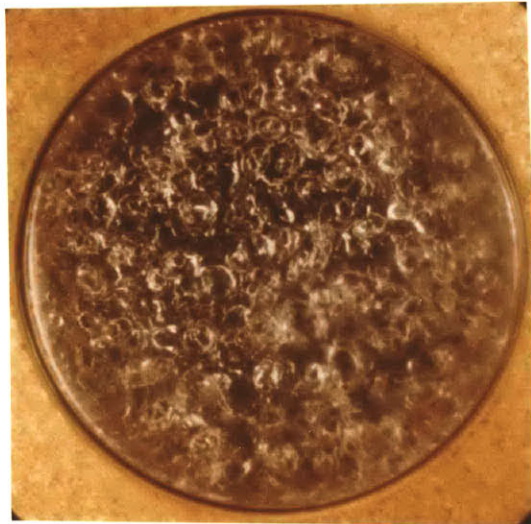
The pictures reveal a highly irregular pattern. As discussed previously, these patterns can be interpreted in terms of the position and shape of the liquid nitrogen interface. It is believed that the lighter areas and curves indicate where liquid nitrogen touches or comes very close to the glass surface. The circular areas shown in (3) presumably represent vapor bubbles in the process of formation and, if so, a technique for obtaining the approximate sizes of vapor bubbles leaving the lower free surface of the cryogenic liquid has been provided. The sizes varied from 4.5 to 9.6 mm with an average about 7 mm. These values represent the analysis of many photographs and are strictly valid only for short times after the start of the experiment. At longer times, when the glass was quite cold, the bubble size dropped significantly. Prior to this bubble size decrease, there was an audible 'fizzling' sound with an increase in vapor generation



(1) $t = 1\text{ s}$ $\Delta T = 220^\circ\text{C}$



(3) $t = 5\text{ s}$ $\Delta T = 150^\circ\text{C}$
x 1.5



(2) $t = 5\text{ s}$ $\Delta T = 152^\circ\text{C}$

Figure 3-2 Views of Liquid Nitrogen - Glass Interface as Seen from the Underside During the Film Boiling of Nitrogen (6. pt. -196 C). Frost is just Starting to Form on the Outside of the Glass in (2); the Room Temperature was 24°C and Relative Humidity was 40 % Vessel Diameter is 14.5 cms.

rate and a visible spray of small liquid nitrogen droplets. Presumably such an event indicated a transition from film to nucleate boiling.

Figure 3-3. Liquid nitrogen is shown boiling on water. Comparing this figure with Figure 3.2, it is clearly seen that there is an opaque white fog between the water and nitrogen surface. (If the fog were only above the nitrogen pool, it would not be visible in the photographs; also the bottom of the glass vessel never reached the dew point temperature.) At 8 seconds, and more pronounced at 20 seconds, clear ice is seen to be forming on the periphery of the vessel. At longer times, this ice grows radially inward and eventually the entire surface is covered. The formation of this clear ice is accelerated as the original water temperature decreases. Finally, close inspection of the photographs will show outlines of vapor bubbles disengaging from the interface. As the surface water temperature remained above 0°C (except at the periphery where ice formed), boiling most probably occurred in the film boiling regime.

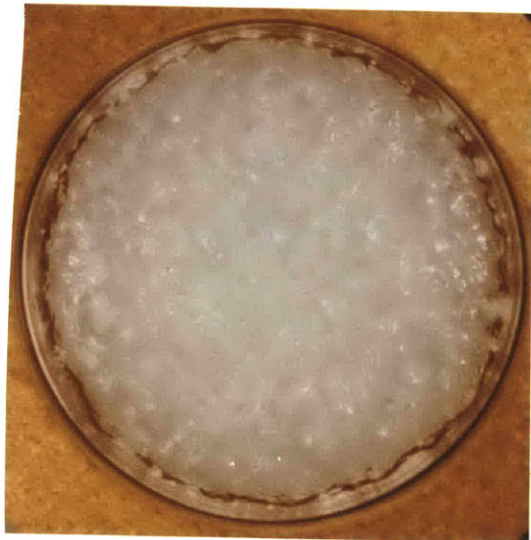
Figure 3-4. The close-up time-sequenced set of photographs shown in Figure 3-4 are for the same experiments as described above in Figure 3-3, i.e., for liquefied nitrogen boiling on water. These pictures were taken of the interface near the center of the vessel far removed from the clear periphery ice. The principal value of these pictures is to allow the vapor bubble sizes to be estimated. In fact, the bubble sizes are not greatly different from those found for nitro-



15



85



t = 20 s

Figure 3.3 Saturated Liquid Nitrogen (b. pt. -196 C) Film Boiling on a Water Surface Vessel Diameter Was 14.5 cms and the Water Was at 24 C at $t=0$

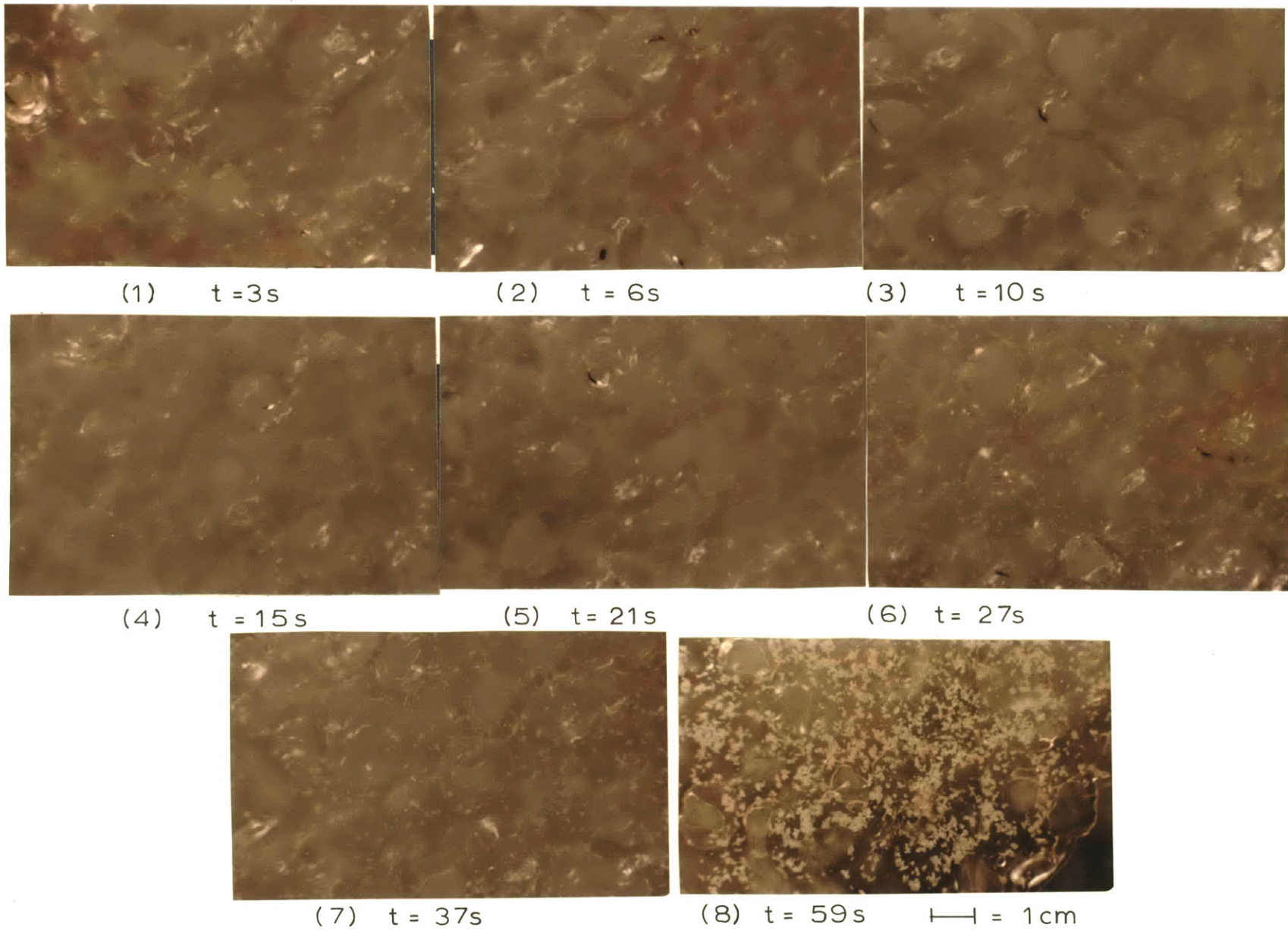
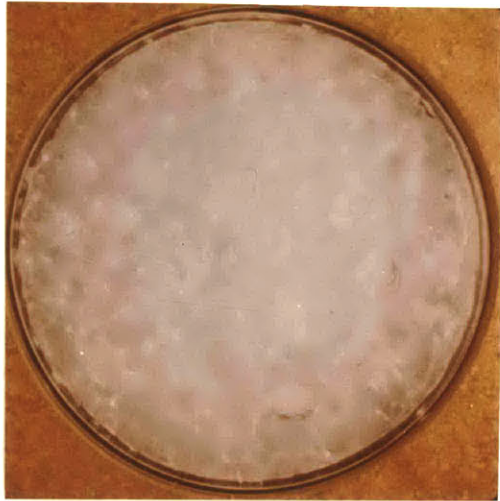


Figure 3-4 Close up Time Sequenced Images of a Liquid Nitrogen Water Interface During the Film Boiling of Nitrogen (b. pt. -196°C) as Viewed from Beneath. Temperature of Water at $t=0$ was 24°C .

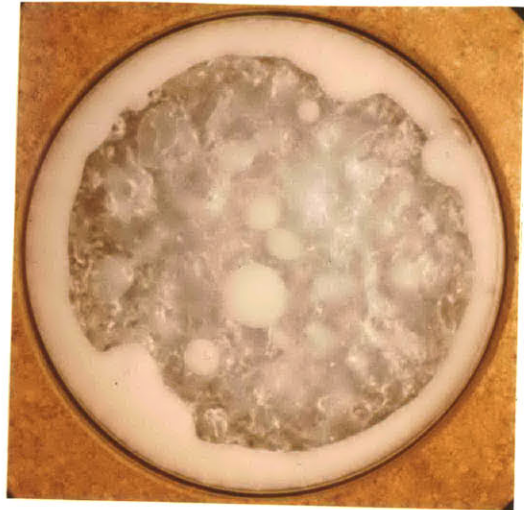
gen boiling on warm glass. The size range was from 7.8 to 10.4 mm (average of 8.7 mm); these diameters are slightly larger than those noted for the water-free boiling system. Another interesting feature of Figure 3-4 is the slow development of white spots which, by 59 seconds, are very clearly visible. These are believed to be small water-ice crystals entrained in the liquid nitrogen. Though only a conjecture, it appears reasonable to explain the appearance of these ice crystals by the transport and subsequent condensation of water vapor from the water surface to the colder nitrogen. It does not seem probable that they result from liquid water droplets entrained within the nitrogen (and frozen), as no evidence of significant wave action of the water surface was observed.

The mechanism noted above would also suggest that such entrained ice crystals would be found with all cryogenic liquids boiling on water. The facts are, however, that much fewer crystals are formed with liquefied methane and LNG. The reason for this difference is not clear. In any case, the water vapor transport mechanism may constitute an important element of the total heat transfer.

Figure 3-5. In these photographs, liquid methane (99.85%) with traces of ethane was poured on an 18°C water surface. The observed phenomenon is significantly different from the liquid nitrogen case (Figure 3-3). Peripheral ice forms much more readily and it is quite opaque. Ice also forms quite easily on the free water surface. Fog appears at the cryogen-water interface early in the run but the



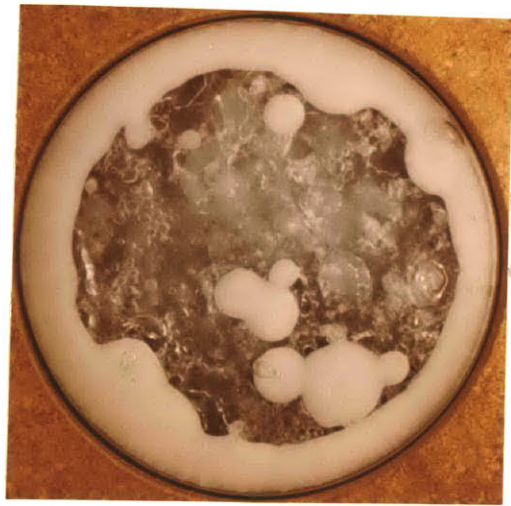
(1) $t = 5 \text{ s}$



(3) $t = 27 \text{ s}$



(2) $t = 9 \text{ s}$



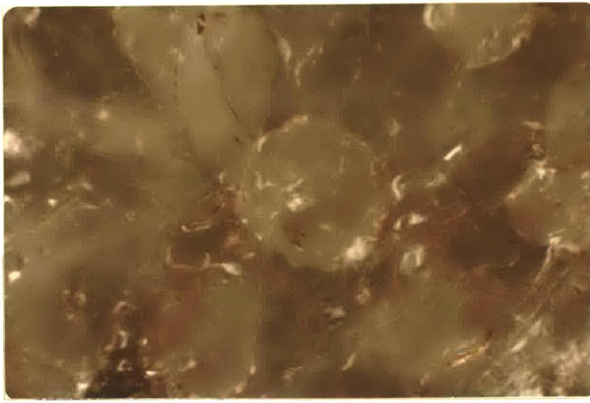
(4) $t = 32 \text{ s}$

Figure 3.5 Liquid Methane's Interface with Water During the Film Boiling of Methane (b.pt. $-161.5 \text{ }^\circ\text{C}$); the View is as Seen from Beneath. Liquid Methane Composition at $t=0$ was 99.85 % CH_4 and 0.15 % C_2H_6 . The Water was Initially at $18 \text{ }^\circ\text{C}$ and the Vessel Diameter is 14.5 cms.

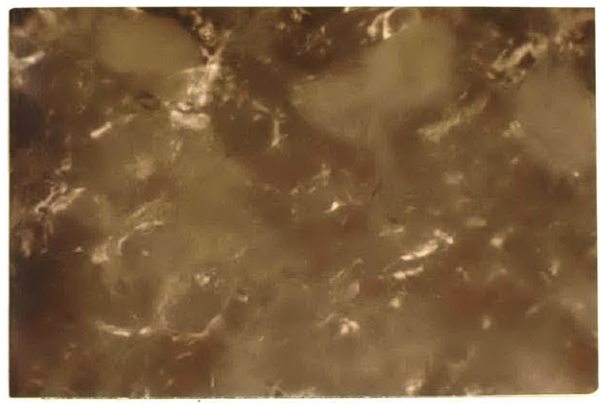
amount steadily decreases with time and after about 30 seconds, the fog has almost disappeared. The opacity of the ice is due to the occlusion of small gas bubbles though the reason why these should form is not at all clear.

Figure 3-6. These close-up photographs are from experiments similar to those described in Figure 3-5 though the methane was very pure (99.98%) and the water temperature was slightly higher (24°C rather than 18°C). A few important observations can be made from these photographs and many others taken in similar runs. Few, if any, small ice crystals were found in the liquid methane though fog is quite evident. The bubble sizes were larger than those noted earlier for liquid nitrogen (10 to 18 mm; average diameter of 13.5 mm). Ice formation rates in the center of the vessel are sensitive to the initial water temperature and percent ethane. The lower the temperature or the higher the ethane content, the more readily ice is formed on the water surface. The first conclusion is, perhaps, somewhat obvious; the second is not. As will be seen later, the presence of heavy hydrocarbons affects the rate of ice formation (and heat flux) in a very significant manner. In simple terms, the more the heavy hydrocarbon present, the more easily ice is formed and the higher the heat flux.

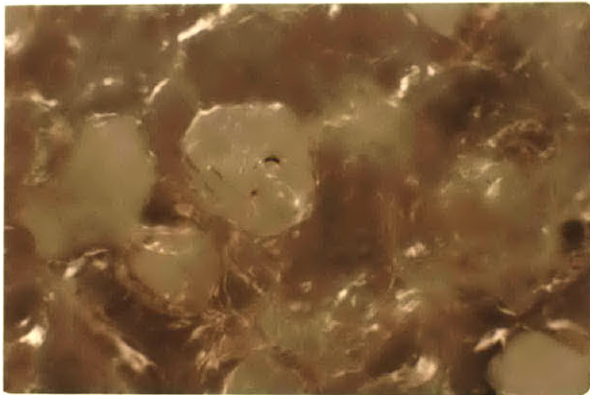
Figures 3-7 and 3-8. The photographs shown illustrate the surface between boiling ethane and water. The most significant point to be noted is the extraordinary rapidity with which the ice crystals



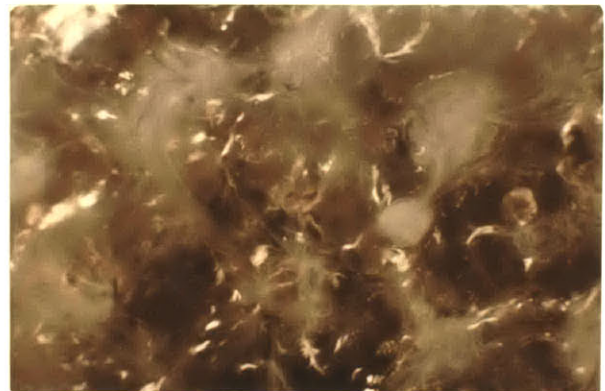
(1) 2 s



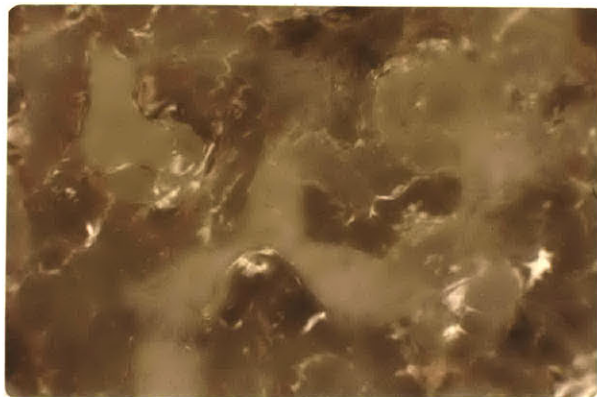
(4) 16 s



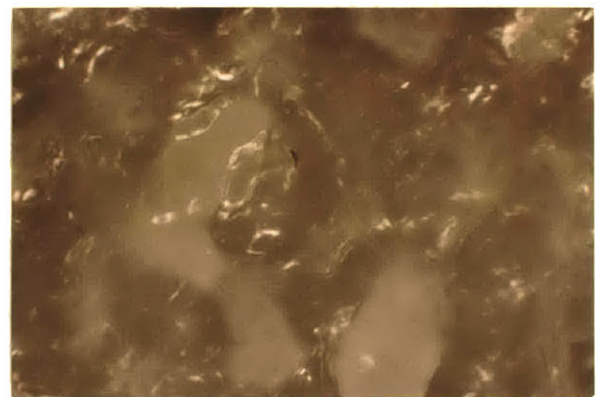
(2) 5 s



(5) 22 s

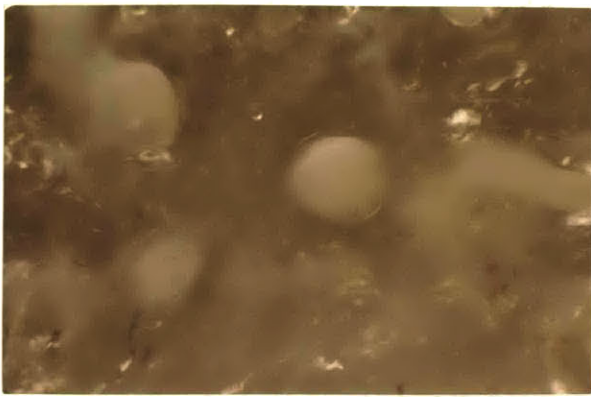


(3) 10 s

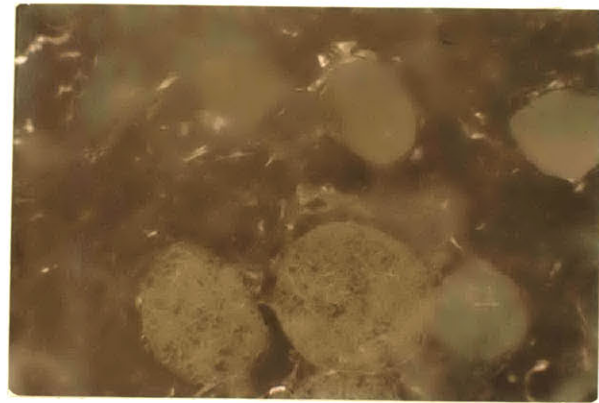


(6) 28 s

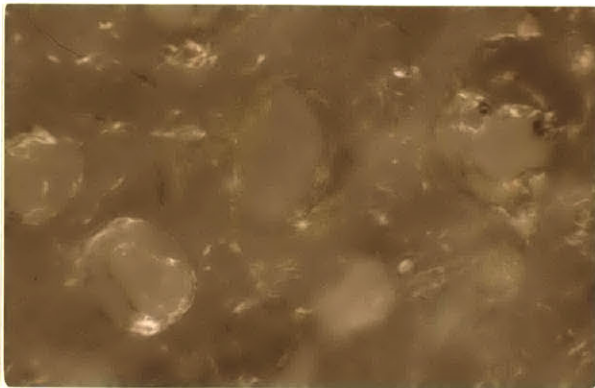
Figure 3-6 Close-up Time Sequenced Pictures of the Interface Between Liquid Methane and Water as Seen from Beneath. The Initial Water Temperature was 24°C , and Methane was 99.98 % Pure (b. pt. -161.5°C)



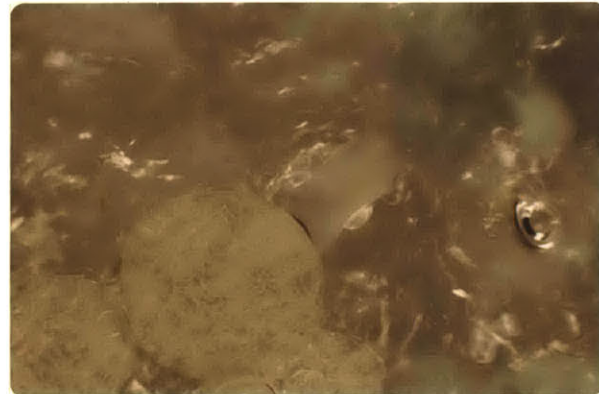
(1) 2s



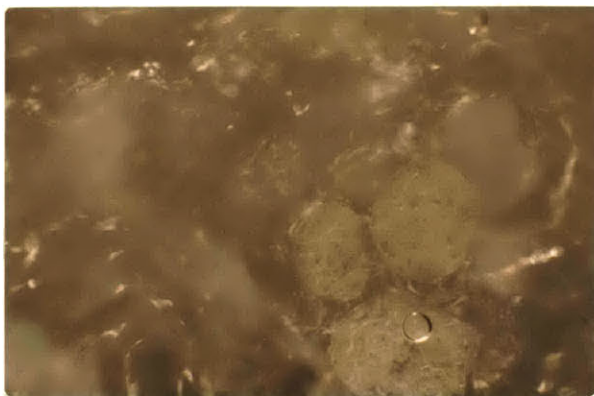
(4) 14 s



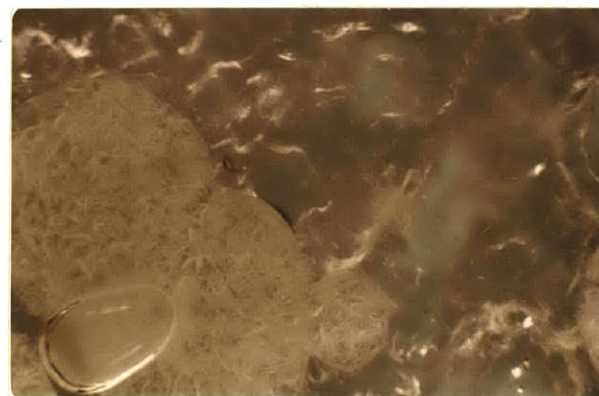
(2) 8s



(5) 17 s

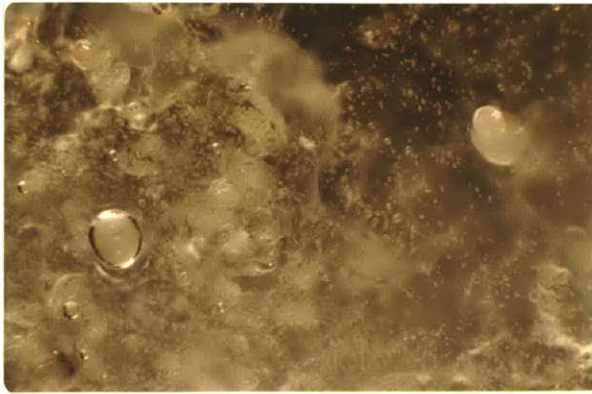


(3) 12 s

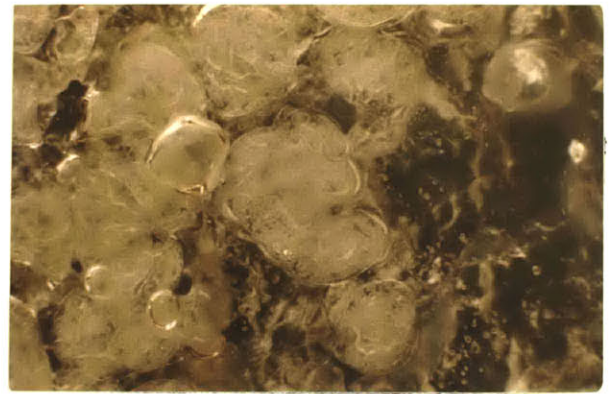


(6) 20 s

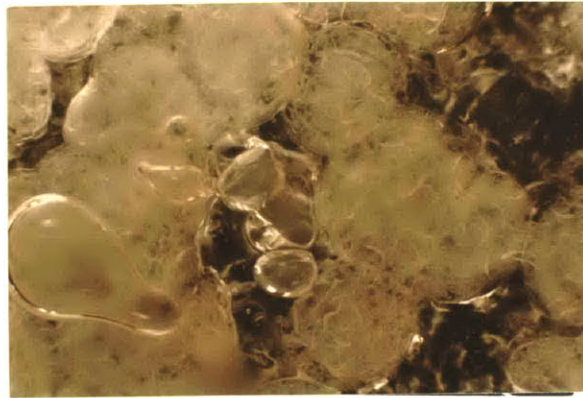
Figure 3-7 The Interface of Liquid Ethane and Water During the Boiling of the Former, as Viewed from Beneath. The Initial Water Temperature was 28°C and the Ethane Contained 0.16 % n-Butane at $t = 0$.



(1) 3s



(2) 5s



(3) 9s

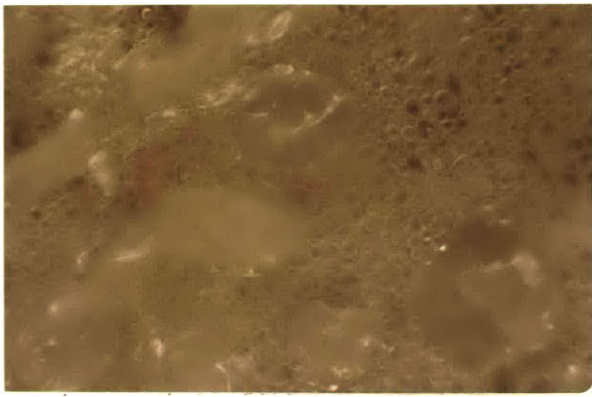
Figure 3-8 The Interface of Liquid Ethane (b.pt. -88.6°C) and Water During the Boiling of the Former on Water Initially at 18°C . The Ethane Contained 0.16 % n-Butane at $t = 0$

form and coalesce at the water surface. In the first second or so, fog is noted and vapor bubbles form. Soon thereafter large ice patches are evident and, if a single ice platelet is followed, growth is noted in the lateral direction (~ 0.1 to 0.14 cm/s). Platelets of different diameters (1 to 2.5 cm) withdrawn from the water surface during some runs measured between 500 and 1000 μm in thickness, with no correlations found between the diameter and thickness. It is obvious in the ethane experiments that the water surface is rapidly cooled to below 0°C . The ice formed is opaque (almost translucent) and cracked. Undoubtedly such a surface enhances nucleate boiling and heat fluxes. In many respects the formation of these thin ice platelets resembles those observed by Schaefer (1950) on flowing, slightly supercooled water ($\sim 0.1^\circ\text{C}$) in contact with -13°C air, and Arakawa (1954). Such platelets were termed frazil ice.

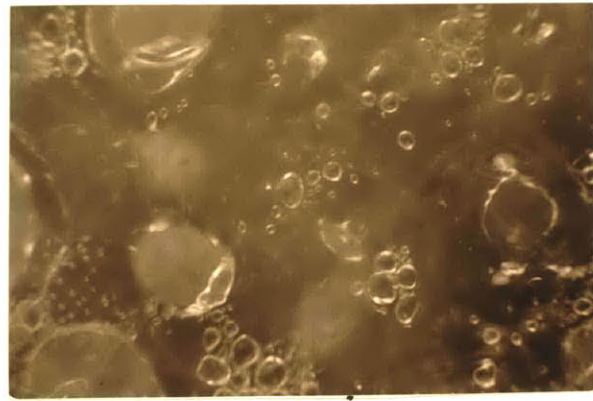
Figures 3-9 and 3-10. In these figures, typical photographs of the interface between boiling LNG and water are presented. The LNG composition at the start of the tests was

CH_4		98.2%
C_2H_6		1.6%
C_3H_8		0.1%
i C_4H_{10}	\sim	0.04%
n C_4H_{10}	\sim	0.03%

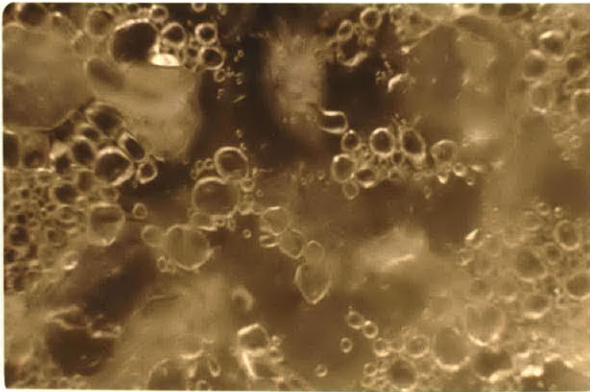
The photographs show an unusual phenomenon not noted in any of the



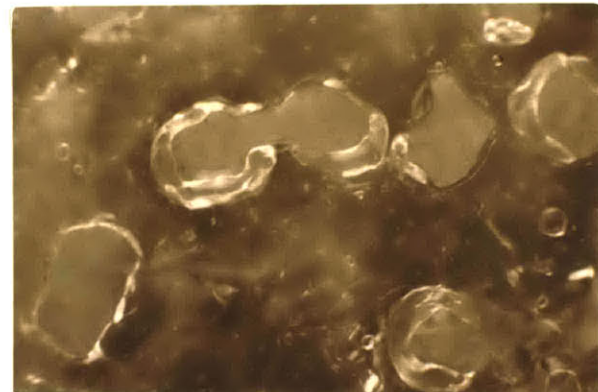
(1) 2 s



(4) 12



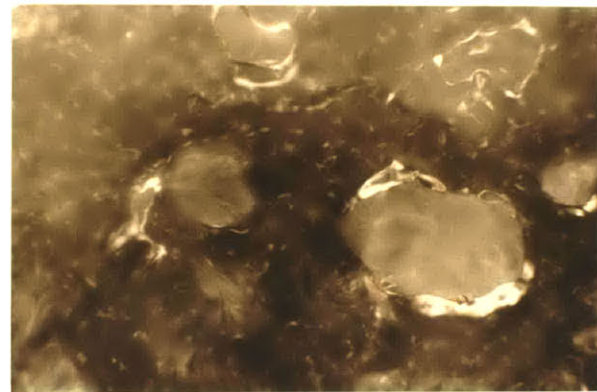
(2) 5 s



(5) 16 s

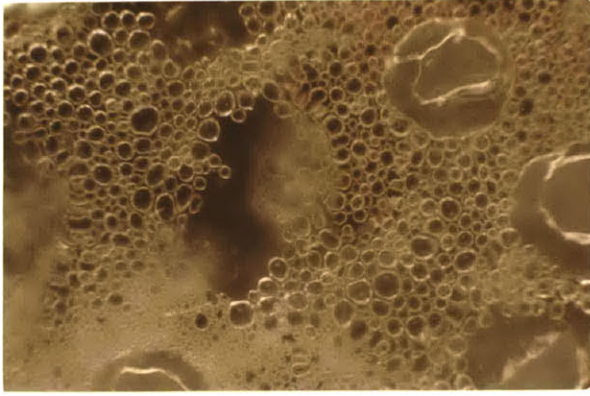


(3) 9 s

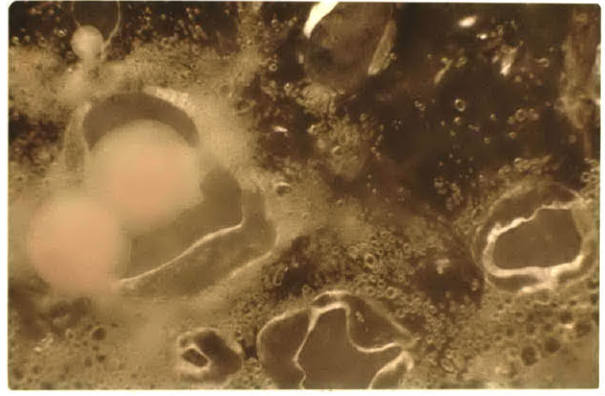


(6) 20 s

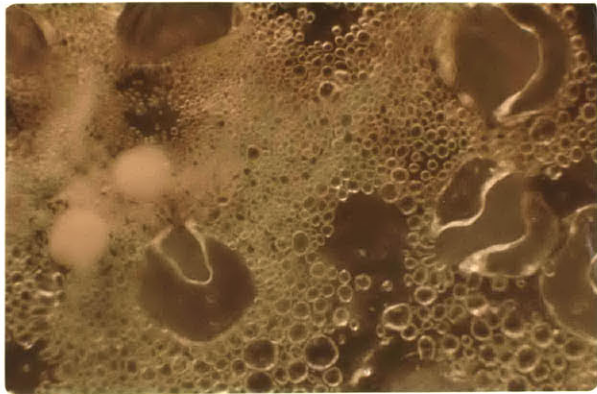
Figure 3-9 Close-up Time Sequenced Bottom Views of the Interface of Lean Liquid Natural Gas (LNG) with Water Initially at 32 °C. The LNG Contained 98.2 % CH_4 , 1.62 % C_2H_6 , 0.112 % C_3H_8 , 0.043 % $i\text{C}_4\text{H}_{10}$ and 0.03 % $n\text{C}_4\text{H}_{10}$ at $t = 0$



(1) 2 s



(3) 9 s



(2) 5 s

Figure 3-10 Close-up Time - Sequenced Bottom Views of the Interface of LNG with Water Initially at 18 °C. The LNG Contained 98.2 % CH_4 , 1.62 % C_2H_6 , 0.112 % C_3H_8 , 0.043 % C_4H_{10} and 0.03 % $n\text{C}_4\text{H}_{10}$ at $t=0$

previous pictures of pure boiling cryogenic liquids. Almost instantaneously after the initial contact of the LNG with water, a very large number of small, clear gas bubbles (< 6 mm diameter) are seen. Large vapor bubbles are fewer in number, but those that do form were about 1.35 cm diameter (the same as for pure methane). Some fog is evident but it is only pronounced within the large gas bubbles. It appears that the small bubbles reside in the cryogenic liquid (Figure 3-12), held to the cryogen lower free surface by surface tension forces. (On plate (2), Figure 3-9, top center, it would seem that one small bubble has just broken and is feeding a large growing bubble node.). It is believed that these small bubbles, produced only at the beginning of the runs with the LNG, coalesce to sizes large enough for buoyancy forces to disengage them into the bulk cryogen. Consequently, the population of the small bubbles decays rapidly. Few small bubbles are visible in Figure 3-9(5), 16 seconds into the run. The small bubbles are probably responsible for the extensive foams observed above boiling positive liquid mixtures such as LNG (i.e., those mixtures in which the most volatile component has a surface tension lower than other components. In Figure 3-11, surface tension data for ethane and other higher alkanes have been extrapolated to -161.5°C (the b.pt. of CH_4) for comparison purposes.) Burgess et al. (1970) earlier observed foaming above boiling LNG pools, van Wijk and van Strahlen (1956) and Hovestreijsdt (1963) also reported that they observed foams above boiling positive liquid mixtures. The origin of

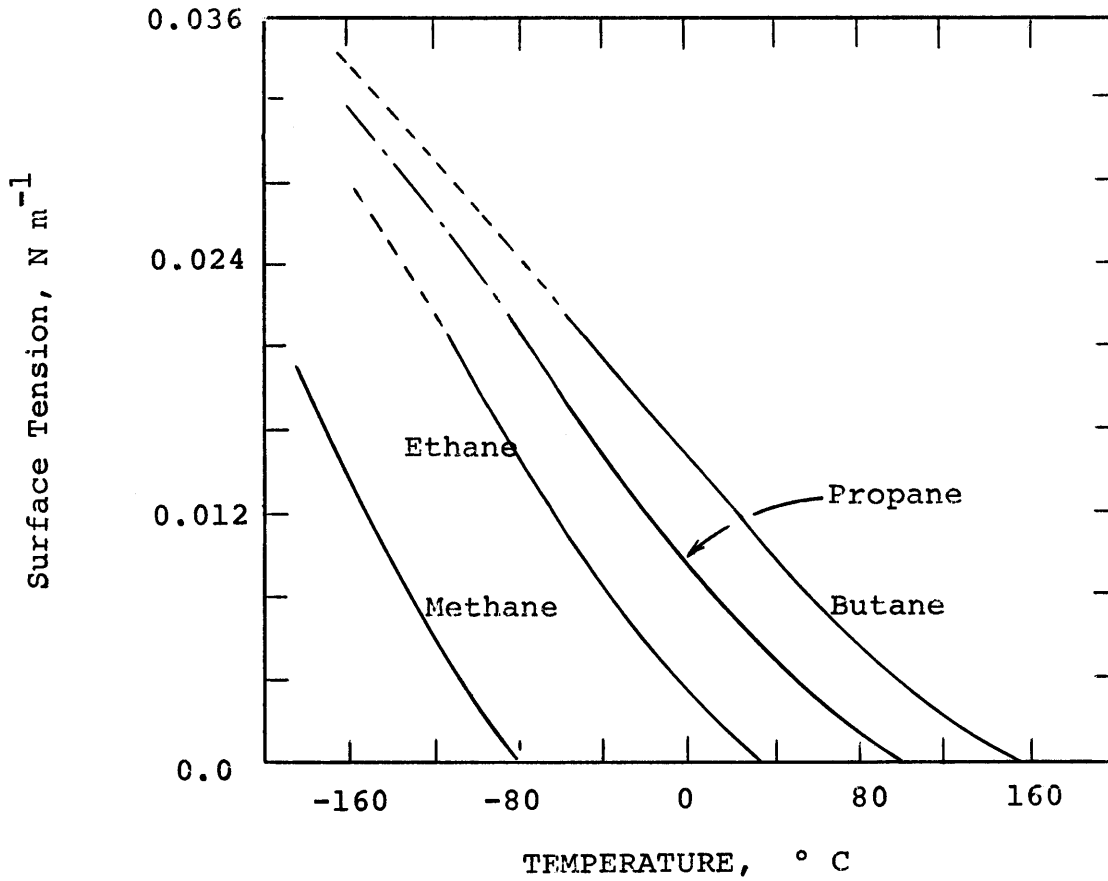
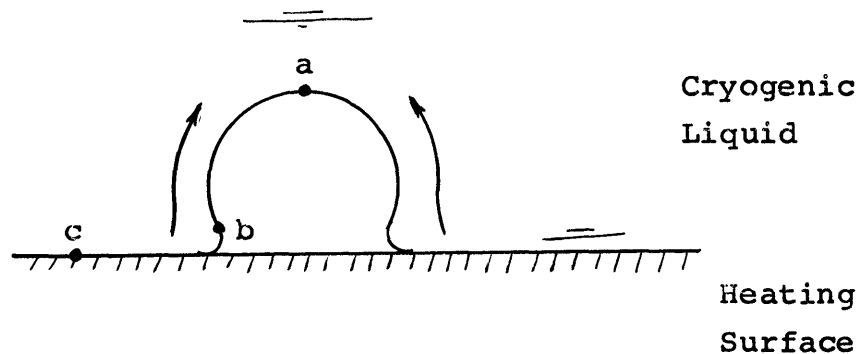


Fig. 3 - 11

Surface Tension vs. Temperature For
Cryogenic Hydrocarbon Liquids (Gallant,
1968)

the small bubbles is not exactly understood, but it may be related to the activities as soon as a cryogenic liquid mixture is contacted with a hot surface, water in the present studies. The first vapors produced from a typical LNG, probably by heterogeneous nucleation at the cryogen-heating medium interface, will be almost pure methane. The depletion of this volatile component at the liquid wall surrounding the vapor causes a concentration gradient to exist, both between the bubble surface and bulk liquid, and along the bubble walls, i.e., the concentration of methane at a is less than at b which, in turn, is less than at c (Figure 3-12). The latter implies that a surface tension gradient should exist at the wall, and surface tension induced liquid motion (Marangoni effect) should occur from site b to site a, in the sketch below. An upward drag force is, therefore, exerted on the bubble.

Fig. 3.12



Thus acting on the bubble are buoyancy, inertia and drag forces

(assisting bubble growth) and surface tension (resisting deformation). The relative magnitude of these forces determine whether the bubbles will grow to big sizes and be detached into the bulk cryogen, form small bubbles which may be retained near the interface, or revert to a flat surface. In a rapidly growing bubble, the effective bubble wall surface tension increased with time. It is postulated here that small bubbles become pinched-off (to minimize surface area) when the effective surface tension force overtakes the net growth assisting force and the bubble shape is similar to, or more developed than shown in the sketch. Moreover, if the pinching-off process is sufficiently rapid, and the buoyancy force on the bubble formed is low, surface tension will stabilize the bubble at the interface.

This model is in effect a combination of the bubble growth slowing-down process proposed by van Wijk and van Strahlen (1956), and the Marangoni effect proposed by Hovest Reidjt (1963).

The events, just described, occur rapidly, before the cryogen is separated from the heating surface (water) by a vapor film (and fog), as plate (1) Figure 3-9 suggests. With high ΔT across the liquids, no new small bubbles are believed generated after this initial period, unless where the liquids touch again. Another mechanism can be postulated that as soon as the liquids contact, the cold liquid becomes superheated in a zone next to the interface. Then homogeneous nucleation of small bubbles takes place within this layer or zone. This is fine, except that it implies that small bub-

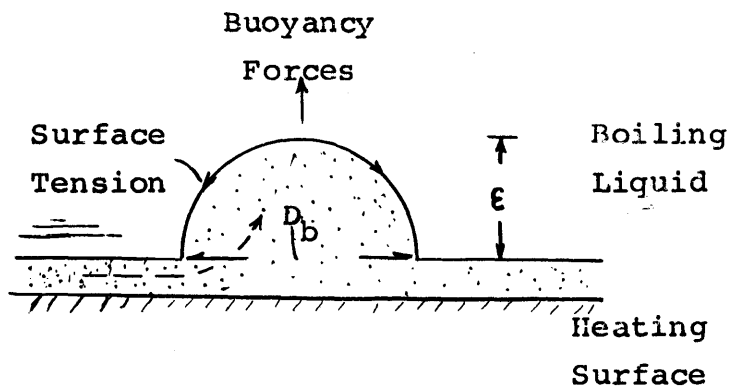
bles should be generated within pure methane as well as in LNG contacted with water. The small bubbles, however, were not obtained with pure cryogenic liquids, as show in Figures 3-2 to 3-8.

Ice is quickly formed by LNG on the cooler water, as is obvious from the opaque circular ice floes in Figure 3-10. In the warmer water, it appears that very small ice crystals may be seen, Figure 3-9, (4), (5) and (6), though if these are such crystals they are moving so rapidly that they are not clearly resolved (they leave streaks) in a 1 millisecond exposure.

3.4 CORRELATION FOR BUBBLE DIAMETERS

A model of a bubble node in static equilibrium, as shown below, is subjected to two primary forces; buoyancy and the surface tension forces.

Model of Bubble in Film Boiling



The force balance equation is given by

$$V_b g (\rho_L - \rho_V) = \pi D_b \sigma \quad (3-1)$$

where the node volume, V_b , can be related to the diameter, D_b ,

with the expression, experimentally established by Borishansky (1959), i.e.,

$$\text{node height, } \quad \epsilon = 0.68 D_b \quad (3-2)$$

Equation 3-1 then becomes

$$D_b = \phi \sqrt{\frac{\sigma}{g(\rho_L - \rho_V)}} \quad (3-3)$$

where ϕ is 2.8.

In the boiling processes of this study, however, bubbles were observed to grow so rapidly that additional forces, such as inertia, pressure and drag forces, should be taken into account in any analysis. Since the data for quantizing some of these forces are unavailable, the prefactor, ϕ , (Equation 3-3) has been computed from experimental data and is presented in Table 3-1.

The average value of ϕ for the cryogenic hydrocarbon liquids is 7.7. Hence, the bubble sizes are correlated with the following expression

$$D_b = 7.7 \left[\frac{\sigma}{g(\rho_L - \rho_V)} \right]^{1/2} \quad (3-4)$$

(Equation 3-4) is strictly valid for the experimental conditions of this study. It is conceivable, though, that the range of application may be broader.) As shown in the table, the prefactors obtained here are larger than presented by Berenson (1961) for boiling hydro-

TABLE 3-1

VALUES OF THE PREFACTOR ϕ (EQUATION 3-3) FOR DIFFERENT SYSTEMS

<u>System</u>	<u>$\phi \pm 10\%$</u>
Liquid nitrogen - glass	7.0
Liquid nitrogen - water	8.12
Liquid methane (99.98%) - water	7.6
Liquid ethane (99.85%) - water	7.78
n-Pentane - ; Carbon tetrachloride - metallic surfaces (Berenson, 1961)	4.7
Static equilibrium	2.8

carbons near the Leidenfrost point. This is consistent with the fact that larger bubbles are observed in this study than reported by him. The high values of ϕ are also evidence of the departure from the static equilibrium situation. The final expression will be employed in the heat flux correlations in Chapter 5.

3.5 SUMMARY

The observations made in the photographic study can be listed as follows:

1. Fog was observed produced in the vapor film between the cryogenes in this study and water. The fog intensity was highest in the growing bubbles.
2. The type of ice formed and the rate of nucleation and growth differed for all the cryogenes. Nitrogen formed clear ice slowly, methane and LNG produced opaque white ice which occluded tiny bubbles on low temperature water ($< 15^{\circ}\text{C}$), and ethane produced translucent ice platelets (frazil ice).
3. LNG produced very small vapor bubbles (0.2 to 4 mm diameter) immediately it was contacted with water, the heating medium. Thereafter, only big bubbles (~ 1.35 cm) were produced. The same bubble size was observed with pure methane and ethane boiling on water.

CHAPTER 4

BOIL-OFF RATES OF CRYOGENIC LIQUIDS ON WATER4.1 INTRODUCTION

Most experimental studies dealing with boiling liquids employ a hot solid surface and, in so far as possible, attempts are made to maintain steady-state conditions when measuring heat fluxes or temperatures. In the present study, by its very definition, all measured variables are time-variant and, in addition, the heat source is a poorly characterized liquid which may even undergo a phase change during the experiment. Thus, to study the boiling rate of cryogenic liquids on water, rather elaborate and specialized instrumentation is required. Moreover, facilities must be available to compile and store the extensive data collected in any test. Each of the present experiments lasted one minute or less, hence, an observer was necessarily limited in what measurements could be made manually.

The details of the experimental apparatus are described below. Briefly, however, each test was begun by pouring the cryogenic liquid on a quiescent water surface within a well-insulated container. The cryogen boiled vigorously, and the amount vaporized was monitored by a load-cell while liquid and gas temperatures were simultaneously recorded. When the cryogen had completely boiled away, the water was stirred (and any ice dissolved) and a final mix-up temperature measured.

4.2 APPARATUS

The apparatus components are shown schematically in Figures 4-1 and 4-2. The equipment consisted of a boiling vessel and associated thermocouples, a top-loading balance that generated an electrical signal proportional to the load, and recorders.

The boiling vessel, shown in greater detail in Figure 4-1, was a triple-walled container, 9.92 cm I.D. and 17.8 cm deep. Its innermost wall was fabricated out of 127 μm scratch-free cellulose acetate sheets with very smooth surfaces. The 'lining' was separated from the adjacent acrylic wall by an air gap, $400 \pm 40 \mu\text{m}$ wide. This separation was achieved by the use of rigid highly porous polyurethane foam pieces, $400 \pm 20 \mu\text{m}$ thick, 1 cm wide and 17.8 cm long, spaced longitudinally, 3 to 4 cm apart, around the perimeter of the acetate walls. Any air flow that could develop within this gap would be laminar and stable*, thus heat transfer across the gap is by conduction only.

The bottom of the inner wall was also constructed from 127 μm cellulose acetate sheet and was suspended on insulating air pockets trapped as bubbles in thin polyethylene films. Further details are to be found in Appendix B.

* $Ra = 1.95$ for the most severe conditions attainable in the experiments, i.e., a ΔT of 220K across the gap.



Room 14-0551
77 Massachusetts Avenue
Cambridge, MA 02139
Ph: 617.253.2800
Email: docs@mit.edu
<http://libraries.mit.edu/docs>

DISCLAIMER

**Page has been omitted due to a pagination error
by the author.**

(Pages 104-105)

About two centimeters inside the open end of the vessel, was inserted an acrylic double cone, 7.6 cm in diameter, below which was hung the vapor-temperature thermocouple tree. This cone was suspended free of the boiling vessel, and served the dual purposes of controlling the flow of cryogenic liquid during the fast, initial pour, and preventing ambient air from entering the vessel during the course of a run. A more complete description is presented in Appendix B.

The cryogen delivery arrangement consisted of a Dewar pivoted on a fixed horizontal rod. A line was attached to base of the Dewar, and this was passed over a caster. Rapid discharge of the Dewar content was accomplished by pulling sharply on the taut wire. As much as 100 cm^3 of liquid was discharged within 0.5s.

The copper-constantan thermocouples, fabricated out of $25.4 \text{ }\mu\text{m}$ wires, were of two configurations. The vapor temperature thermocouples were heat-stationed (with more than 10 cm lengths of wire on either side of the junction) and suspended in a web-like arrangement with cotton threads looped on prong-shaped Teflon supports. A plan view of the structure as well as heat leak calculations are presented in Appendix B. Errors in each thermocouple reading did not exceed 0.5°C .

The second configuration was for measuring temperatures in the water. The very thin thermocouple wires were not easily held at fixed locations, therefore, they were encased in ceramic insulation and supported in $360 \text{ }\mu\text{m}$ stainless steel sheaths. The

junctions, together with 2 mm - to - 2 cm lengths of the bare heat-stationed thermocouple wires were, however, exposed to water. Again, details are provided in Appendix B.

The boiling vessel was located on a fast-response force-compensating Mettler balance, described in detail in Appendix B. This in turn was situated on a vibration-absorbing cork platform.

The signals from the balance and thermocouples were fed to both Sanborn recorders to reproduce the analog outputs, and to a Hewlett-Packard data acquisition system. In the latter, the signals were digitalized and stored on paper tape at a pre-set data sampling frequency. (These devices are described in Appendix B.)

The hydrocarbon compositions were determined by gas chromatography. Two G.C. units were employed: a Hewlett-Packard unit, Model 700, equipped with porapak-Q resin-beads columns and a thermal conductivity detector; and, an Elmer-Perkin 900 G.C. with Durapak C8 polyaromatic-resin columns, and a flame ionization detector.

G.C. gas samples with the same compositions as the liquids under test were obtained with a special sampling device. This consisted of an evacuated 150 cm^3 glass bottle with a stainless steel cannula sealed-in at one end. To withdraw a cryogenic liquid sample, the cannula was dipped into the cryogen and allowed to cool to the temperature of the liquid. Opening of the valve between the cannula and the glass compartment caused some of the liquid to be injected into the evacuated space. The space is then re-evacuated in a flushing

process. This sequence was repeated twice before the final sample was taken for G.C. analysis. The procedures and equipment are further described in Appendix B.

4.3 METHOD:PROCEDURE

The sequence of steps followed in a typical run commenced with the test vessel located on the load cell, and partially filled with filtered distilled water at the desired temperature. The initial water depth was varied between 5 and 6 cm. The junction of the thermocouple nearest the water surface was then adjusted with a clean glass hood such that the bead junction just touched the water under-surface. It was sufficiently free to 'ride' with the water surface, when an oscillatory disturbance was applied. This bead, 56 μm diameter, essentially monitored a local water surface temperature. The level of the other thermocouples, deeper in the water, were measured with respect to the quiescent free water surface with a cathetometer.

The vapor thermocouple 'tree' and fluid directing double cone was rigidly suspended above the water with the thermocouple 'webs' maintained as parallel to the water surface as possible. The distance of each web to the water surface was then measured with the cathetometer.

A predetermined but approximate volume of the test cryogen was then charged into the pivoted cryogen-discharge Dewar. A precaution taken, especially with mixtures, involved precooling the Dewar to

temperatures equal to or slightly lower than the bubble points of the test liquid. This minimized any change in the liquid composition before and during discharge on to the water. The sample for G.C. analysis was withdrawn from this Dewar shortly before its content is discharged on to water.

The recorders were next activated with the digital data logger set to scan and record the signals from six sources, i.e., from the load cell and five thermocouples in the fluids, and the time, once every second. The two Sanborn recorders, each with a response time of 7 ms, were employed to record the analog signals from two thermocouples in water, and two in the vapor evolved.

The spill was made as quickly as possible. The impact force was broken by the double-cone as it directed the liquid flow toward the walls. The angle of impact was such that the initial reaction on the balance was minimal (less than 2% overshoot) and the balance quickly stabilized. Moreover, the cryogen flowed down the vessel walls on to the water 3 to 6 cms below, and splashing was avoided.

During the tests, intermittent observations of the liquid-liquid interface, and the mean level of the upper surface of the boiling liquid were made. These permitted determination of the vapor hold-up in the boiling liquid, since the residual weight of the liquid at the times of observation (and thus the hydrostatic liquid head) was recorded on the data logger.

At the end of each run, the vessel was stirred to dissolve any ice formed and the final mixing-cup water temperature measured. When the ice could not be completely melted within 60s, the final temperature was not recorded.

Design of Experiments

The principal independent variables studied were:

1. Initial water temperature
2. Amount of cryogenic liquid spilled
3. The chemical composition of the cryogen.

A list of the experiments performed, and the corresponding values of the variables noted above are presented in Appendix F, and Table 5-1.

4.4 PRELIMINARY EXPERIMENTS

These experiments were exploratory and designed primarily to improve the apparatus and techniques.

The first observation made was that only statistical average measurements could be obtained. In Figure 4-3, we show a typical analog output of the temperature measured by three thermocouples for a liquid methane-water test. The average amplitude of the methane vapor temperature fluctuations was about 5°C. The amplitudes were lower and the frequencies higher for temperatures measured in water, Figure 4-3-b, and the average departure from the mean was normally within 2°C. Temperatures measured 1 cm below the surface, Figure 4-3-c,

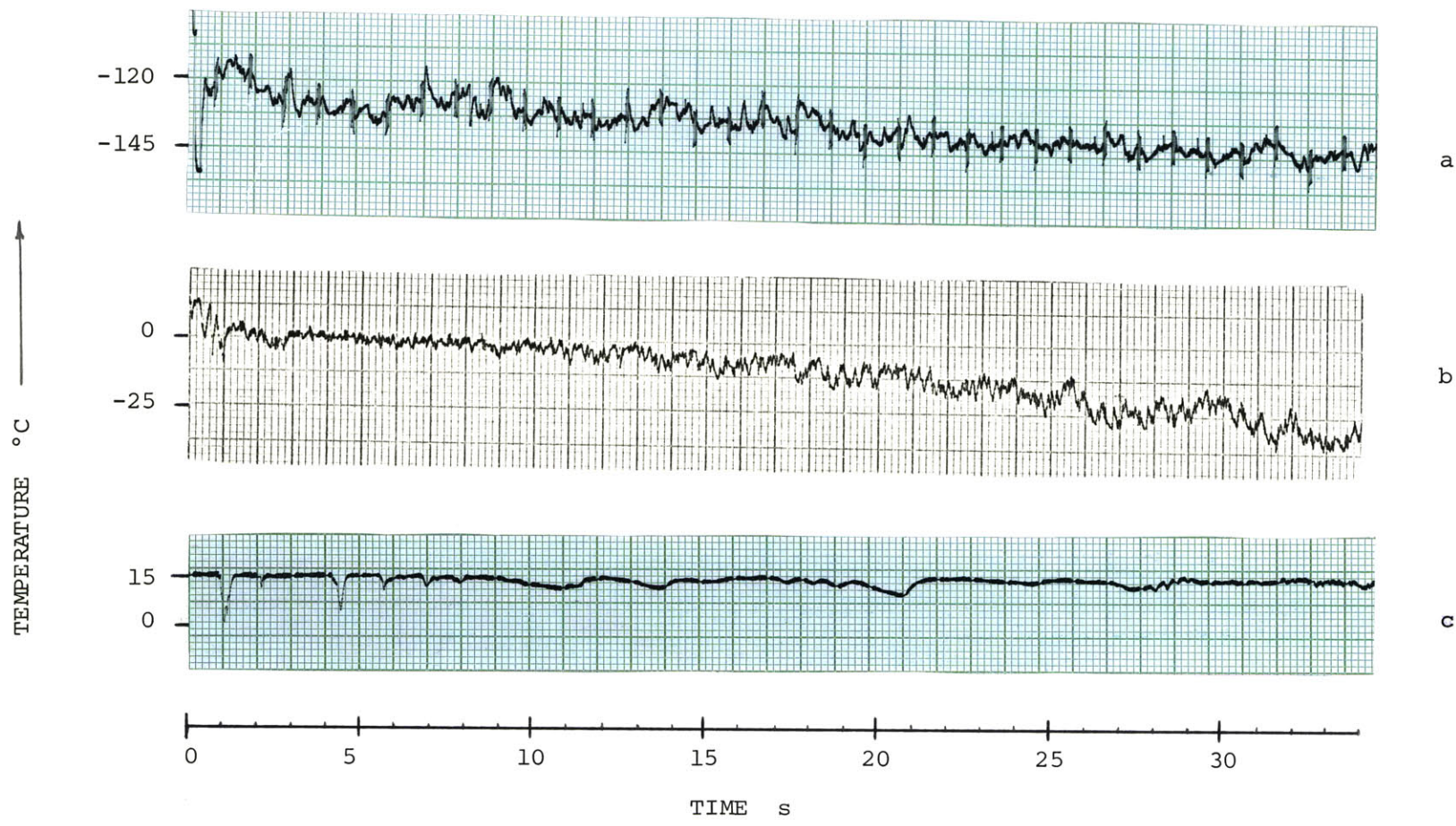


FIG 4-3 TYPICAL TEMPERATURES MEASURED BY THE SANBORN RECORDERS (Run 214)

- a. Methane Vapor (Time marks are superimposed)
- b. Water Temperature at Free Surface
- c. Water Temperature 1.0 cm Below Surface

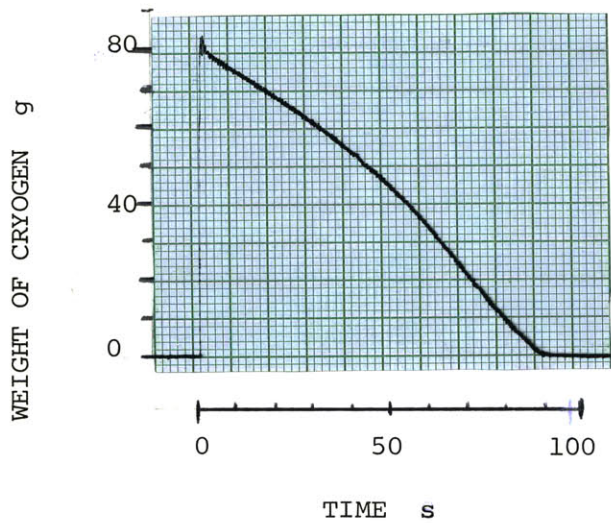
did not show rapid fluctuations.

Typical weight-time curves of boiling cryogenic liquids are shown in Figure 4-4. The boil-off rates of methane (A) typified those of other alkane cryogenic hydrocarbon liquids (single component or mixtures) in that the evaporation rates increased with time. For liquid nitrogen (B) boil-off rates decreased with time.

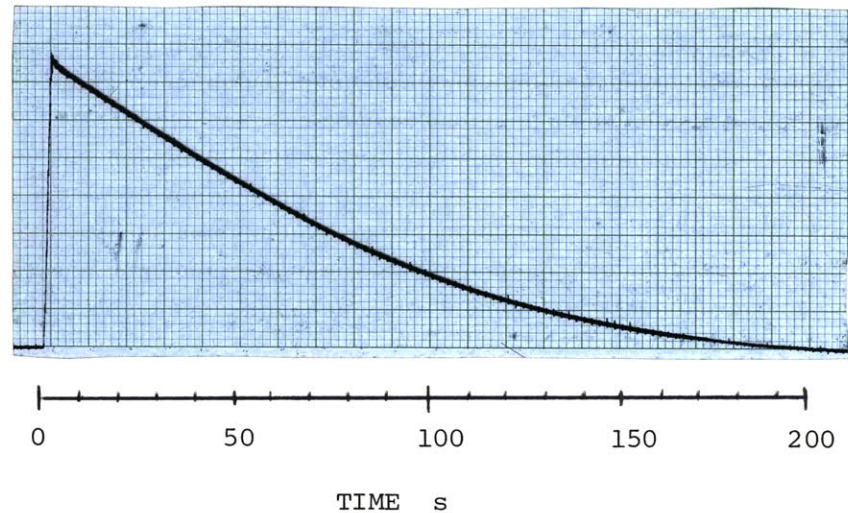
Of considerable interest were the transient temperatures attained at the smooth surface of an initially uniform-temperature, semi-infinite liquid pool upon which a volatile liquid was boiling. Knowledge of such temperatures would permit the definition of an appropriate ΔT for use in comparing heat transfer rates with those measured on solid surfaces.

Thus, temperature profiles were measured in glycerol (containing 0.5% water), a liquid with a high viscosity (180 Ns/m^2 at 13°C and $4.5 (10^4) \text{ Ns/m}^2$ at -41°C), low thermal conductivity ($2.9 (10^{-3}) \text{ W/cm-K}$ at 0°C), and low supercooling temperature (a viscous liquid to rigid glass transformation occurs between -70 and -110°C). Ethane and n-butane were boiled on the surface. (The transient temperatures at the free surface and in the bulk of a pool of mercury on which liquid nitrogen boiled were also measured.)

The temperatures at different distances below the surface of glycerol are presented in Figures 4-5 and 4-6 as functions of time. From these curves, at any given instant, the temperature profiles in the glycerol were determined by plotting the temperatures versus the



A



B

FIG 4-4 TYPICAL WEIGHT-TIME CURVES FOR LIQUID METHANE (A) AND LIQUID NITROGEN (B) BOILING ON WATER

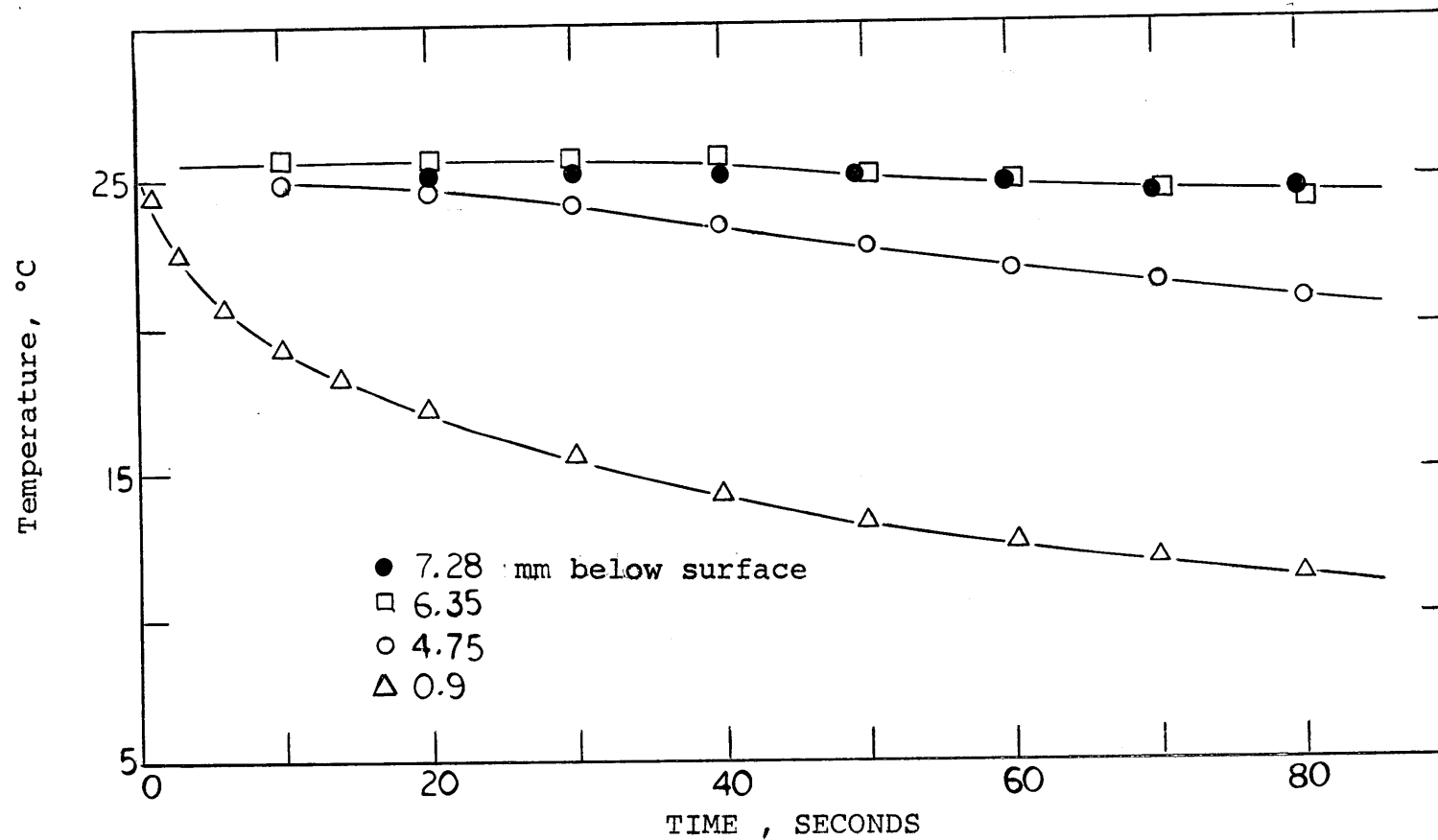
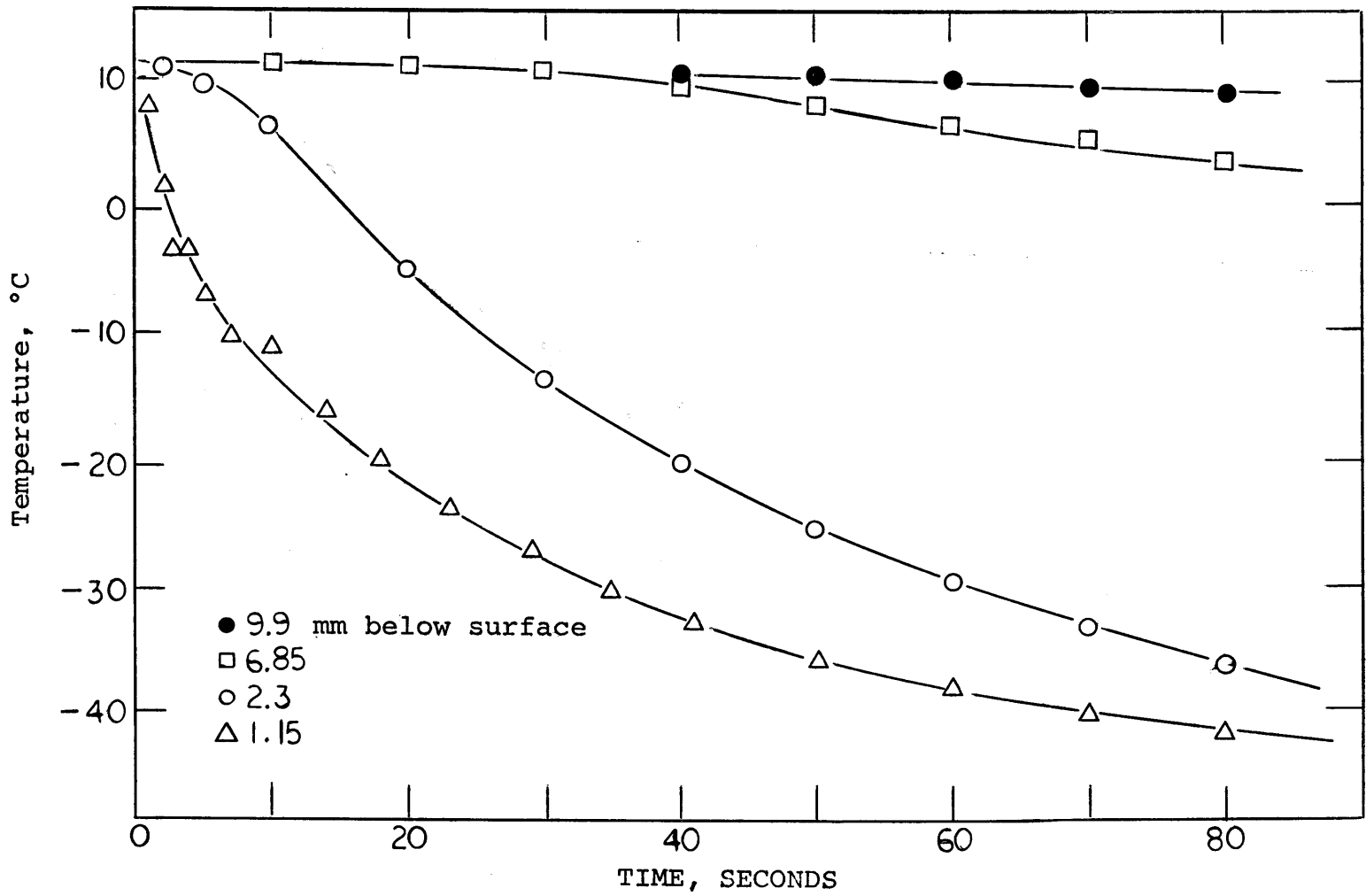


Fig. 4-5

Temperatures At Different Levels In Glycerol During n-Butane Boil - Off.
 (Run 21). [Temperature of n-Butane = 0.65°C]



115

Fig. 4-6

Temperatures At Different Levels In Glycerol During Ethane Boil - Off.
 (Run 24) $T_{\text{ethane}} = -88.6 \text{ }^\circ\text{C}$

distance below the interface. The profiles generated are presented in Figures 4-7 and 4-9 (for the boiling of n-butane and ethane on glycerol, respectively). Extrapolation of each of these curves to zero distance would indicate the glycerol-surface temperature. Thus, the free surface temperatures can be approximated as a function of time. The extrapolated values have been plotted in Figures 4-8 and 4-10. The data indicate an initial rapid drop in surface temperature.

The energy balance equation for heat conduction into a semi-infinite slab is given by

$$\frac{\delta \phi}{\delta t} = \alpha \frac{\delta^2 \phi}{\delta z^2} \quad (4-1)$$

where

$$\alpha = \frac{k}{\rho c_p} \quad \text{and} \quad \phi = \frac{T - T_0}{T_1 - T_0}$$

The initial temperature, every where in the slab, equals T_0 . If the surface temperature is suddenly changed to and maintained at T_1 (i.e. no surface resistance), the solution to Equation (4-1) is (Carslaw and Jaeger, 1959).

$$\phi = \text{erfc} \left(\sqrt{4\alpha t} \frac{z}{2} \right) \quad (4-2)$$

If the boundary conditions were convective, but with a constant surface conductance, h , and the ambient fluid temperature T_i were known, the solution is (Schneider, 1955).

$$\phi = \text{erfc}(X) - e^{\beta(2X + \beta)} \text{erfc}(X + \beta) \quad (4-3)$$

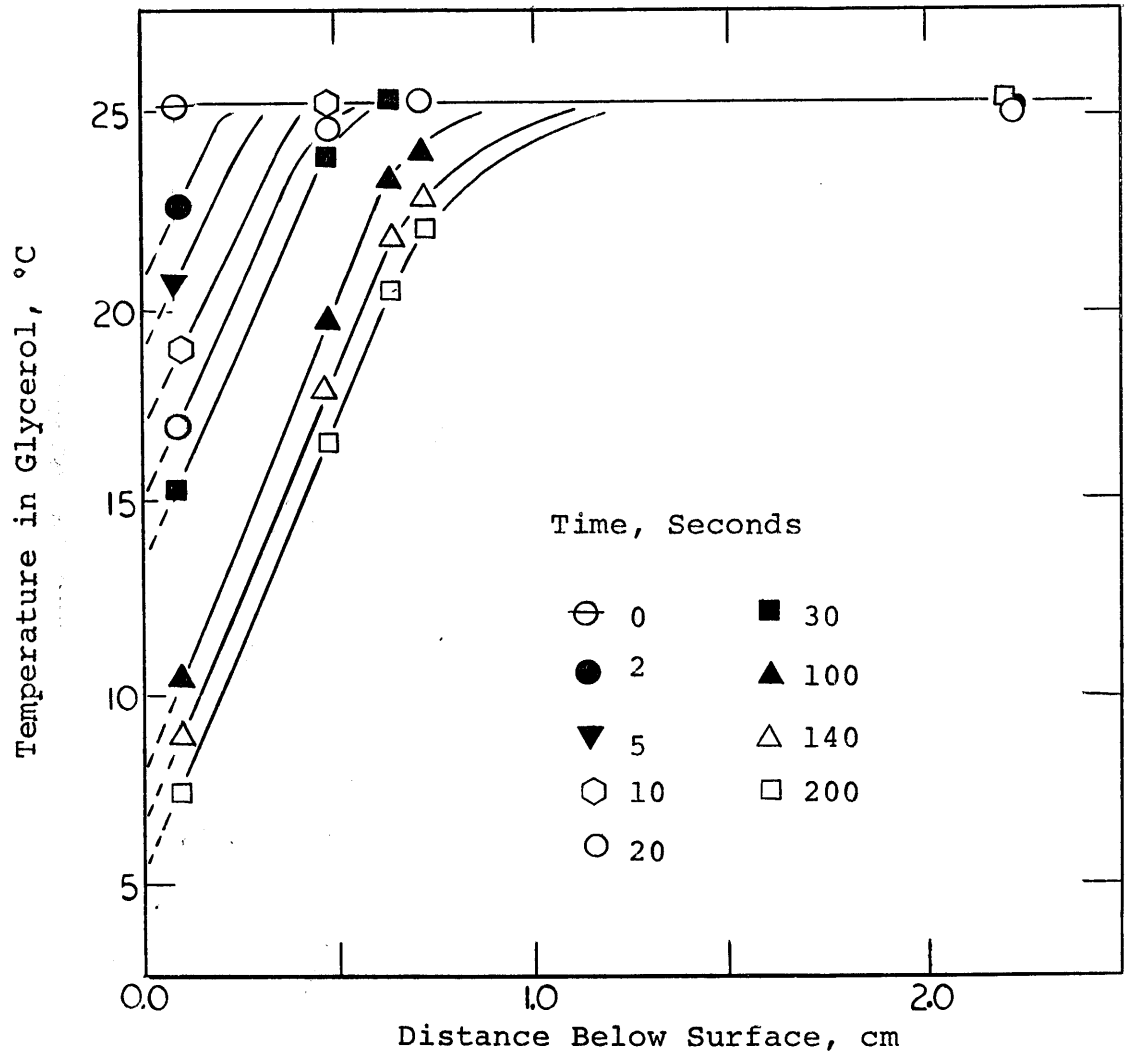


Fig. 4-7

Temperature Profiles in Glycerol Above Which
n-Butane Boiled - Off. (Run 21)

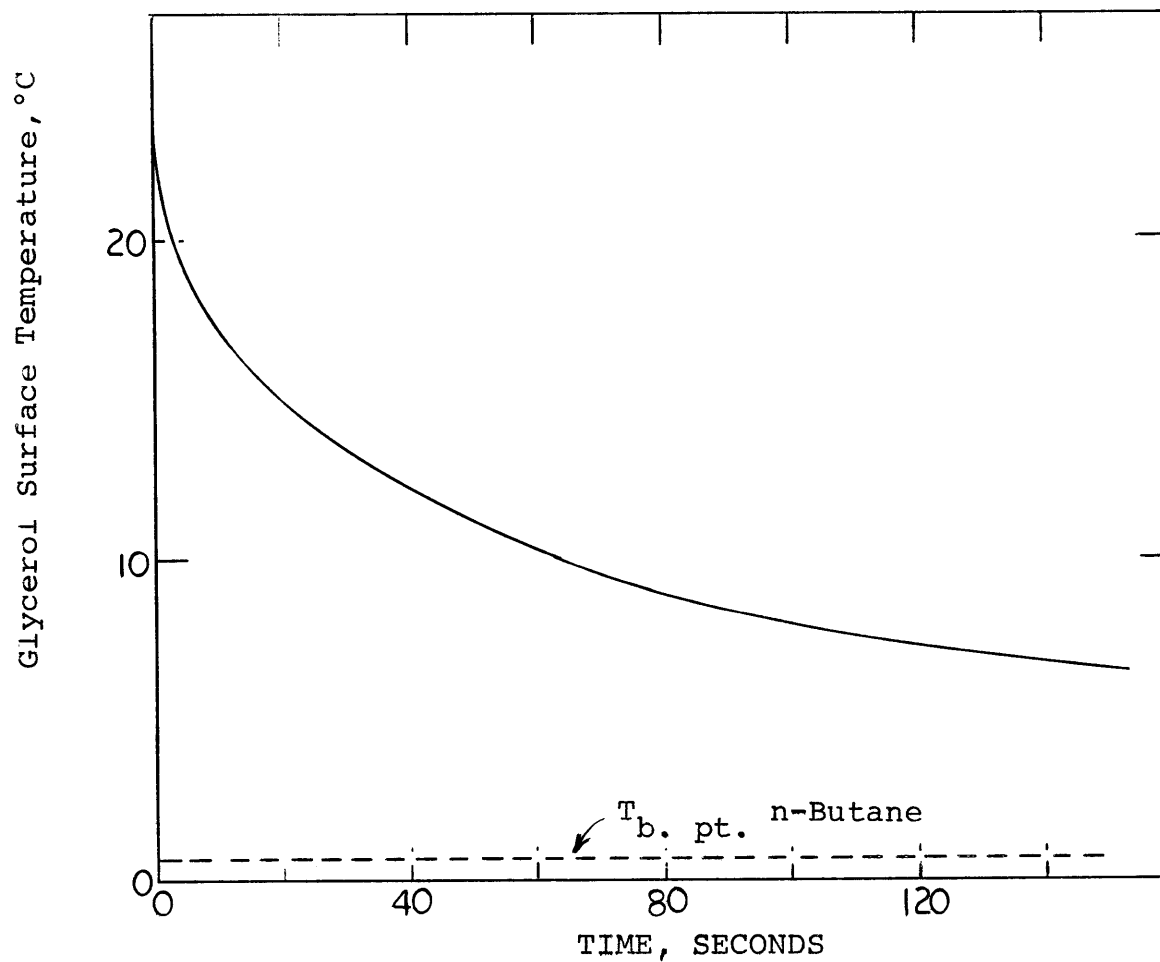


Fig. 4-8

Glycerol Surface Temperatures During n-Butane
Boil - Off (Run 21)

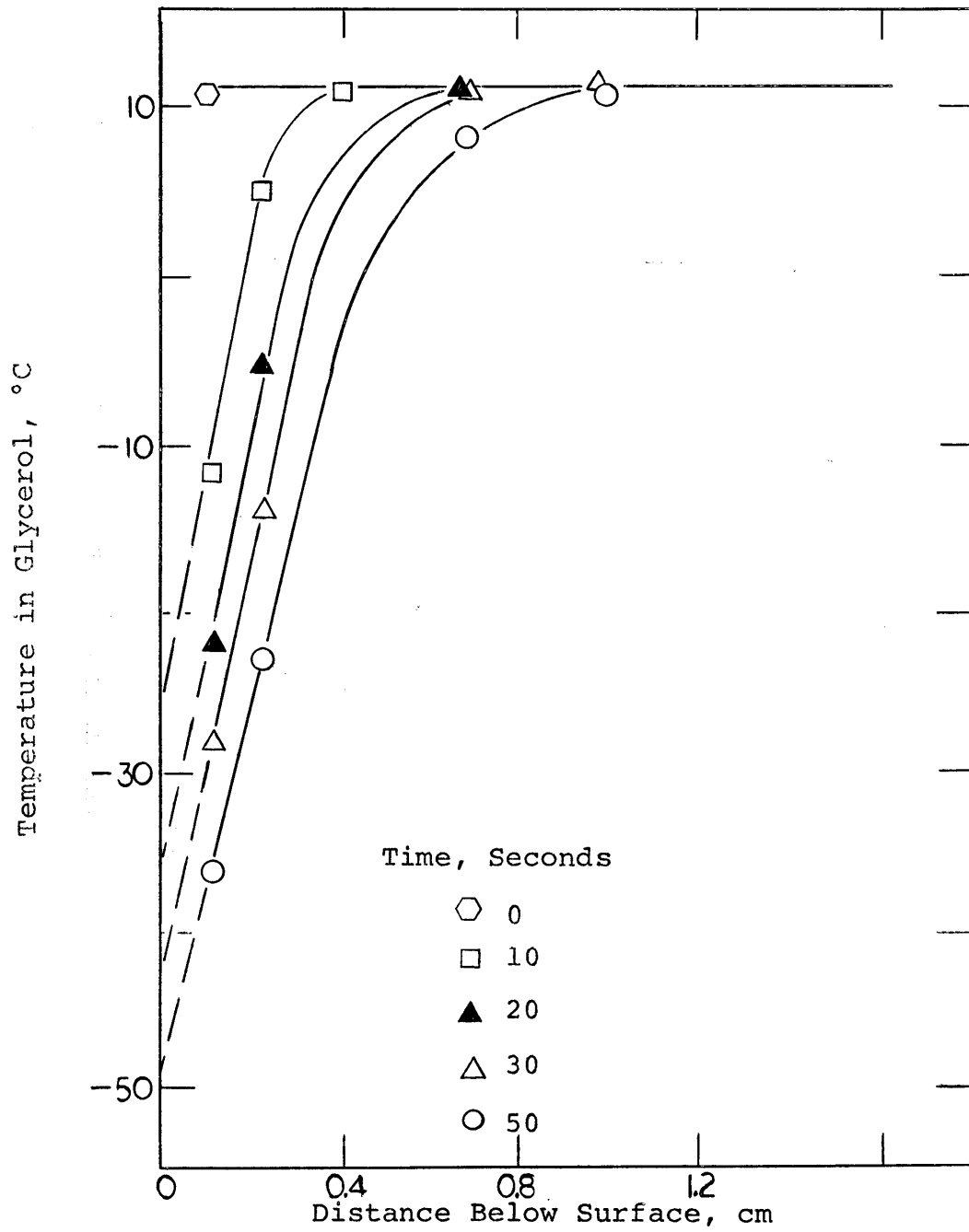


Fig. 4-9

Temperature Profiles In Glycerol Above Which Ethane Boiled - Off. (Run 24)

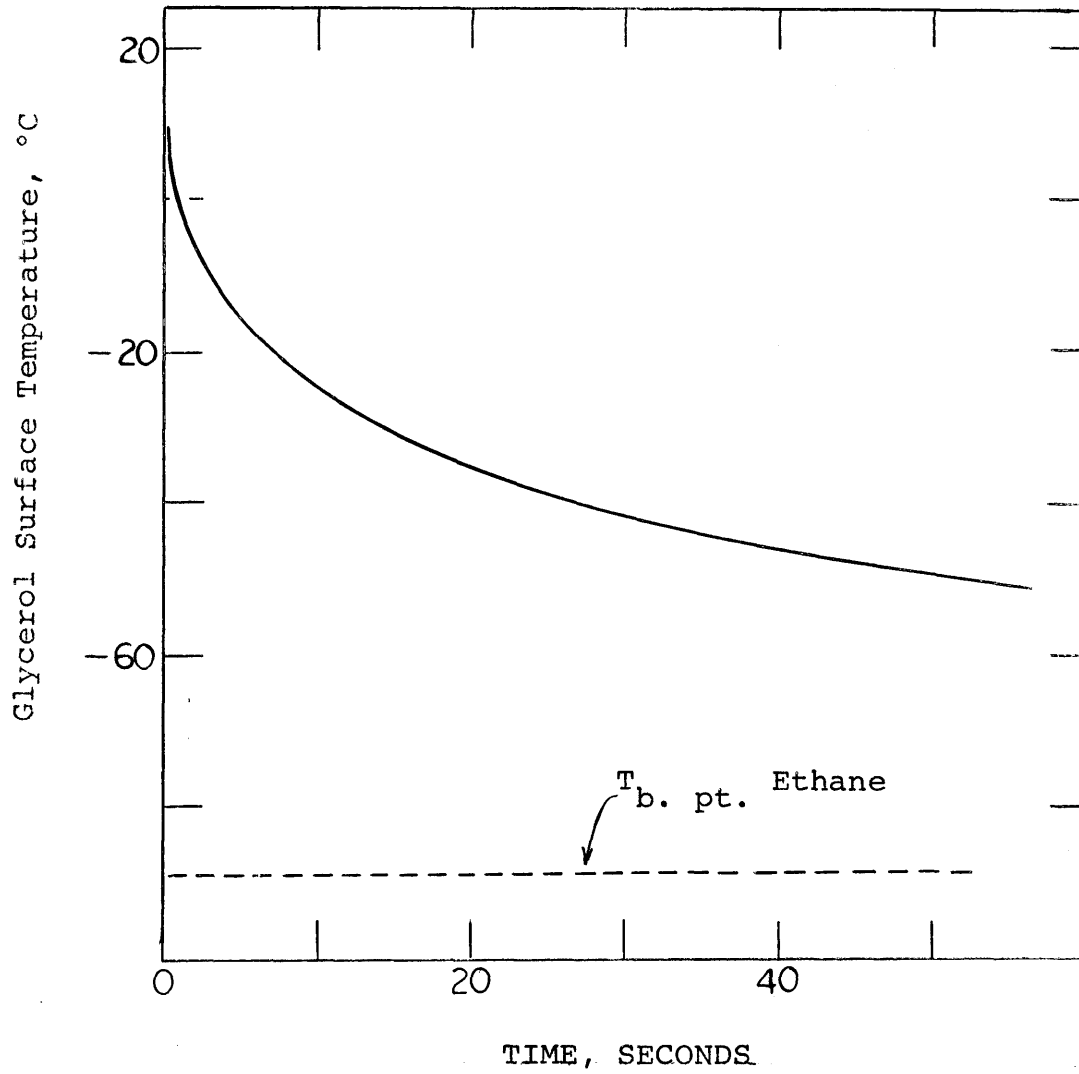


Fig. 4-10

Glycerol Surface Temperatures During Ethane
Boil - Off (Run 24)

$$\text{where } X = \frac{z}{\sqrt{4\alpha t}}$$

$$\text{and } \beta = \frac{h\sqrt{\alpha t}}{R}$$

The slab surface temperature (at $z=0$) is obtained from Equation (4-3) as:

$$\phi_s = 1 - e^{\beta^2} \operatorname{erfc}(\beta) \quad (4-4)$$

In solid-liquid boiling studies, h has been found to be a function of the temperature difference across the boiling interface, i.e. $T_i - T_s$ or ΔT_s . Furthermore, it is shown in Figures 4-8 and 4-10 that ΔT_s is a function of time in the present studies. Hence, the surface temperature cannot be described with Equation 4-4 in which a constant h has been assumed. It is logical, however, to seek a relation between ϕ_s , $\sqrt{\alpha t}$ and the temperature difference between the boiling liquid and the bulk of the heat source, $T_i - T_o$ (or ΔT).

The general correlations chosen is

$$\phi_s = A(\Delta T)^a (\sqrt{\alpha t}/\gamma)^b \quad (4-5)$$

where

$$\gamma = \frac{\sigma}{g(\rho_L - \rho_V)} \text{ is a characteristic}$$

boiling liquid property used to non-dimensionalize the time. The parameters have been evaluated from experimental data plotted in Figure 4-11. The final correlation is

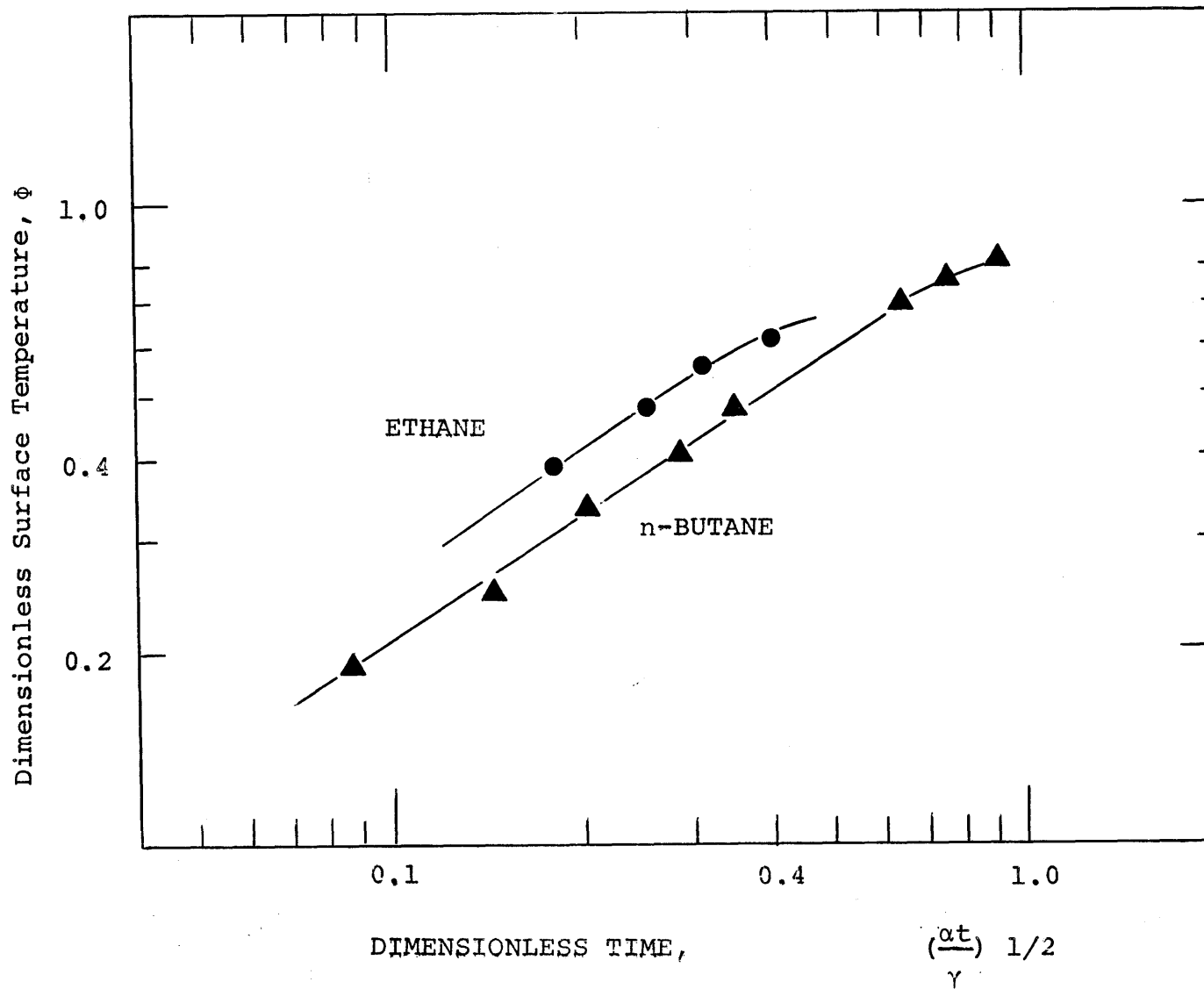


Fig. 4-11

The Dimensionless Glycerol Surface Temperature, ϕ , As A Function of Time

$$\frac{T_s - T_o}{T_i - T_o} = \phi_s = 0.568 (\Delta T)^{0.15} \left(\frac{\alpha t}{\gamma}\right)^{0.326} \quad (4-6)$$

surface
temperature

dimensionless
time

This expression applies, with $\pm 5\%$, to both n-butane and ethane boiling on glycerol for $0 \leq \phi_s \leq 0.7$.

Equation (4-6) and the data indicate that the interface between the superposed liquids has a time-dependent temperature. This is contrary to that predicted by a 2-slab conduction model, i.e., when two semi-infinite bodies at different temperatures are brought in contact. The latter model predicts that

$$\phi_s = \frac{k_1 \sqrt{\alpha_2}}{k_1 \sqrt{\alpha_2} + k_2 \sqrt{\alpha_1}}$$

4.5 RESULTS

As noted earlier, three independent variables were studied and their effect on the boiling flux determined. These variables were cryogen quantity spilled, initial water temperature, and the type of cryogen.

A. EFFECT OF QUANTITY SPILLED

For all hydrocarbons studied, no effect was noted on the boiling flux with the quantity of cryogenic liquid spilled. As shown in Figures 4-14, 4-15, and 4-16, the quantity of cryogen boiled away as a function of time was essentially independent of W_o , the original amount spilled (expressed as g/cm^2).

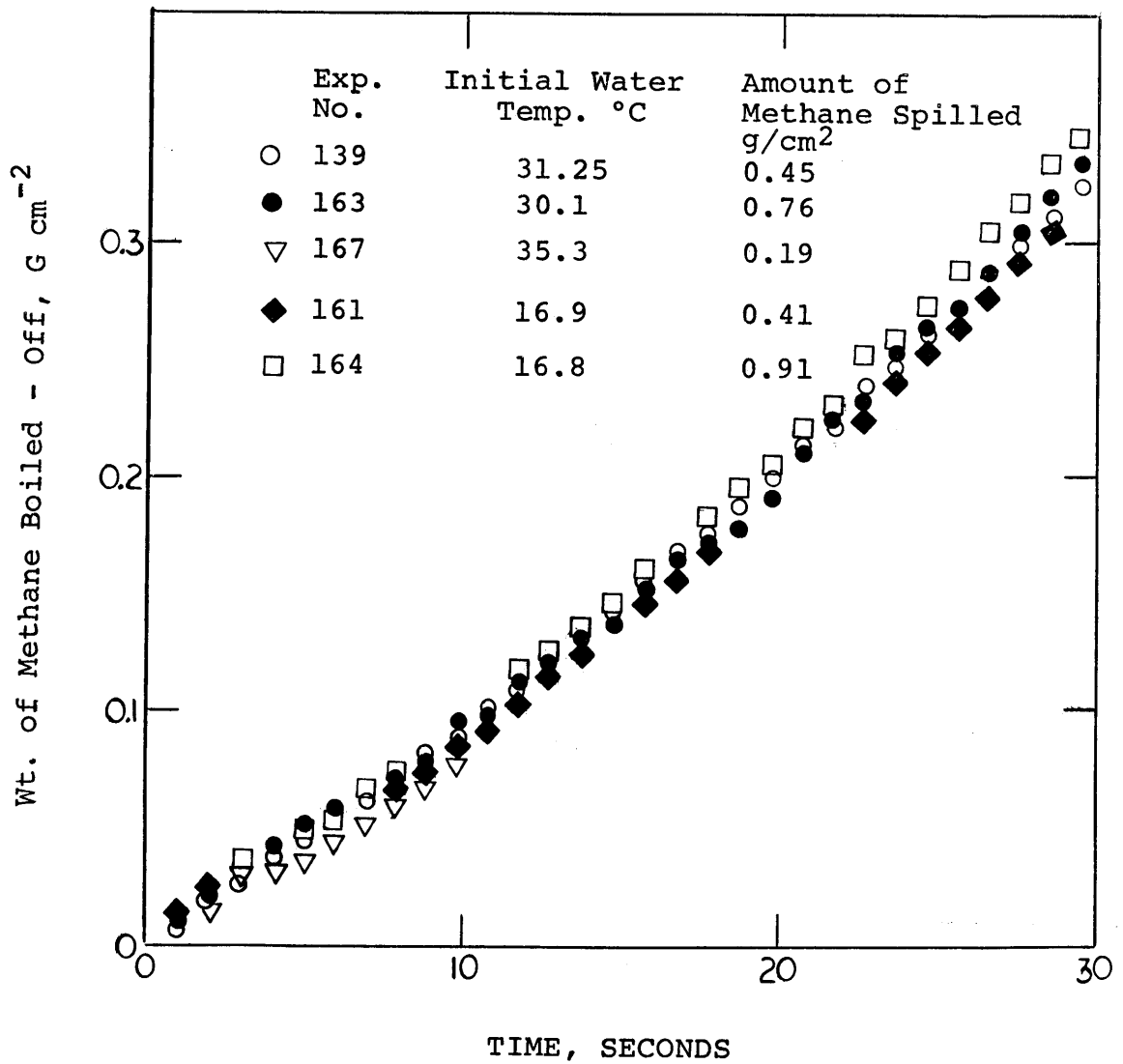


Fig. 4-14

The Effect of Quantity Spilled on Boil - Off Rates of Methane (99.98%)

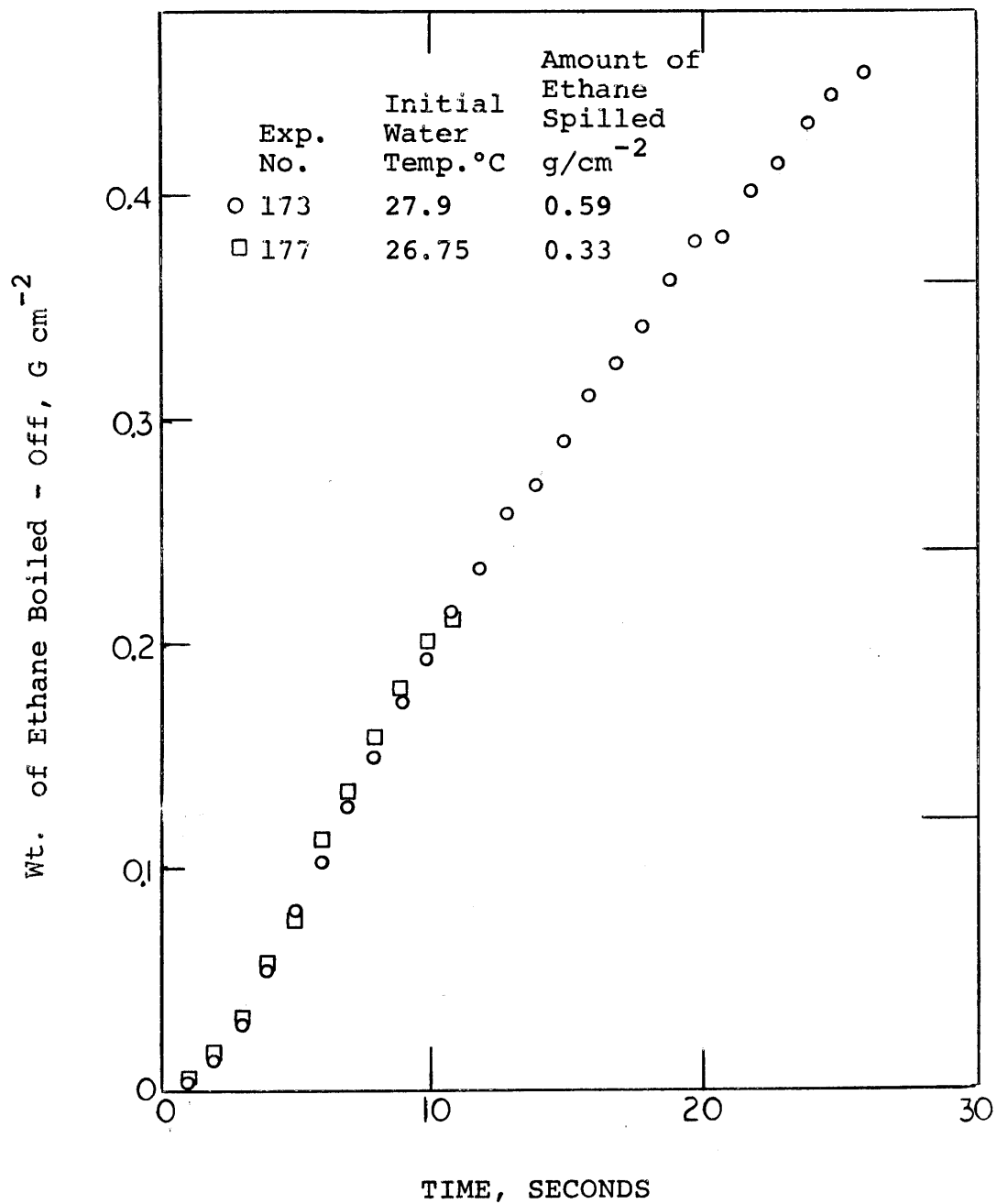


Fig. 4-15

The Effect of Quantity Spilled on the Boil - Off Rates of Ethane

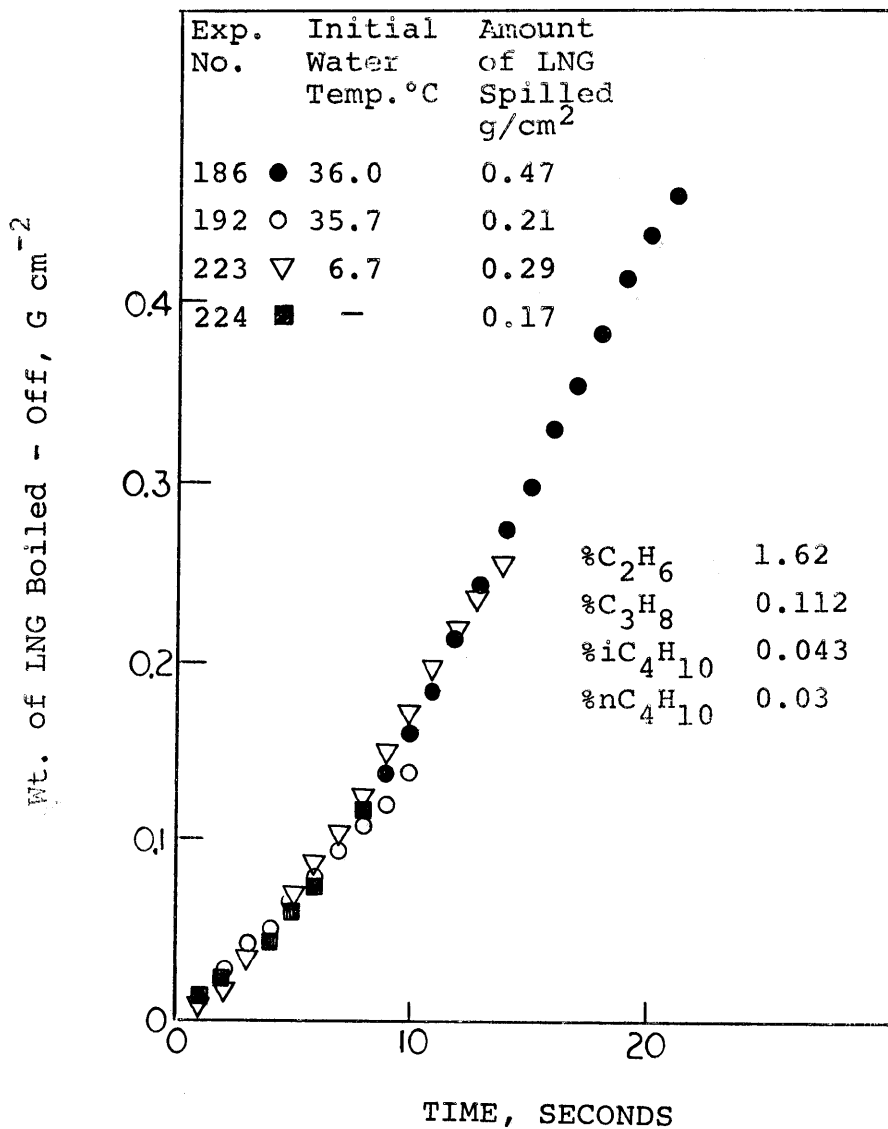


Fig. 4-16

The Effect of Quantity Spilled on the Boil - Off Rates of LNG.

For nitrogen spills, however, a significant change in the rate of boiling resulted when the quantity was varied. This is clearly seen in Figure 4-17. The more spilled, the more rapid the rate of boil-off --- though the increase is not quite proportional to the increase in the quantity spilled.

B. EFFECT OF INITIAL WATER TEMPERATURE

Since the water surface temperature would be expected to vary during a test, it is perhaps most meaningful to compare only the effect of water temperature on the initial boil-off rates. However, as a mitigating effect, the relatively small variations in water temperature, relative to the large temperature difference between the cryogen and water, may be unimportant in the boil-off process. Such seems to be the case for liquid nitrogen on water as shown in Figure 4-18. As noted earlier in Section A, there is an effect of the quantity of nitrogen spilled, but clearly there is little or no effect of initial water temperature. Similar conclusions can be drawn for pure methane (99.98%) as illustrated in Figure 4-19; in the tests shown, the initial water temperature was varied from about 10 to 52°C.

In ethane spills on water at different temperatures, the boil-off rate versus time curves are unusual as indicated in Figure 4-20. Clearly the initial vaporization rates are less for hot water. As shown in Chapter 3, the interface photographs for ethane spills indicated that ice was formed quite rapidly, especially when the initial water temperature were low. It is probable that the separation of

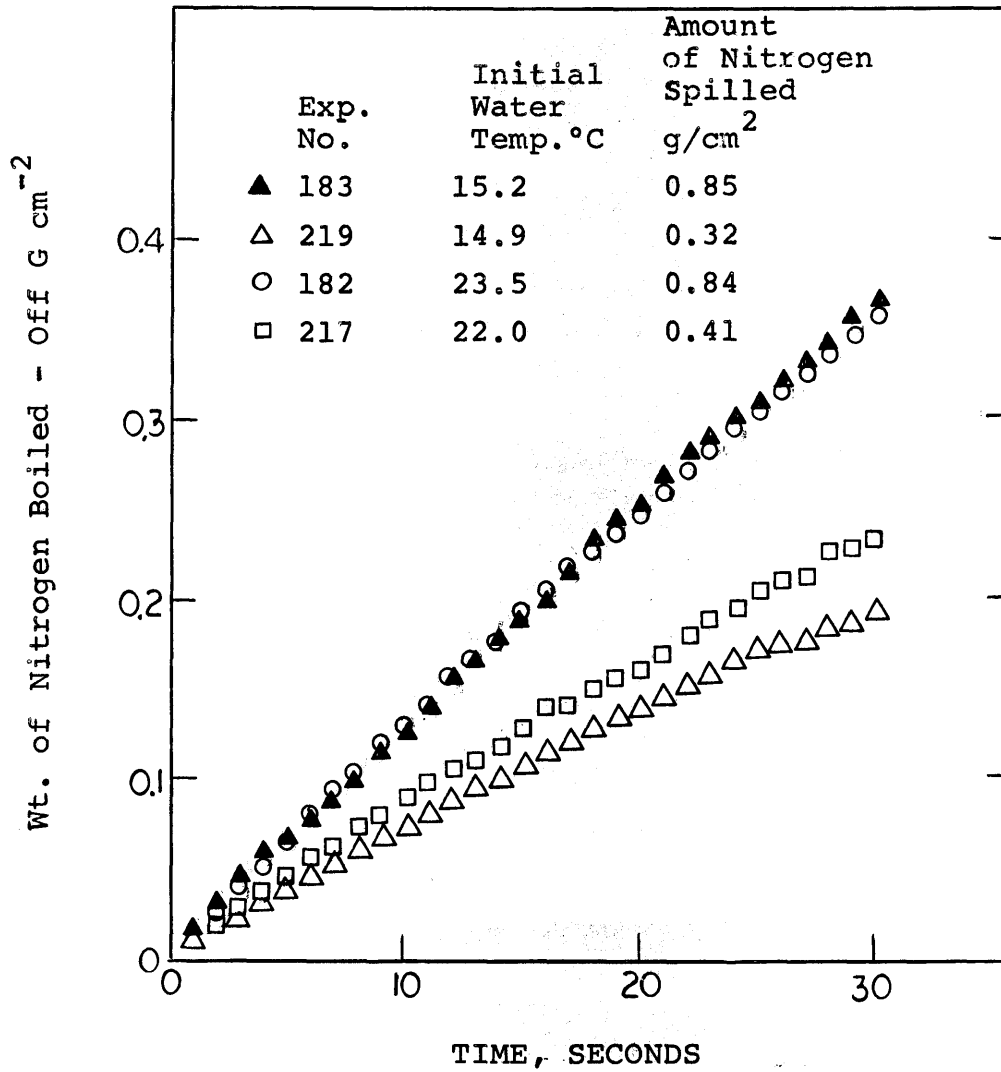


Fig. 4-17

The Effect of Quantity Spilled on the Boil - Off Rates of Nitrogen

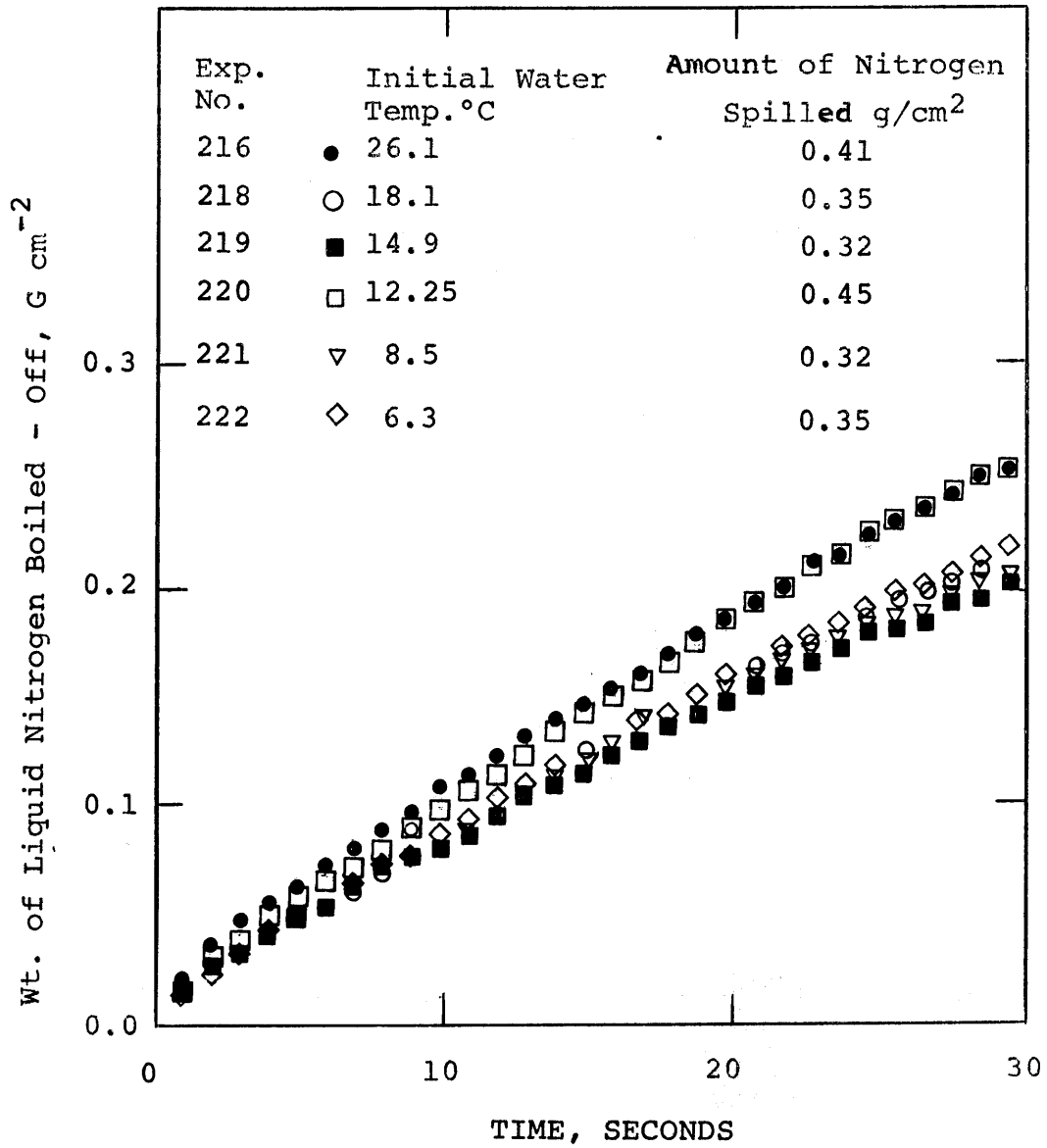


Fig. 4-18

The Effect of Initial Water Temperature on the Boil - Off Rate of Liquid Nitrogen

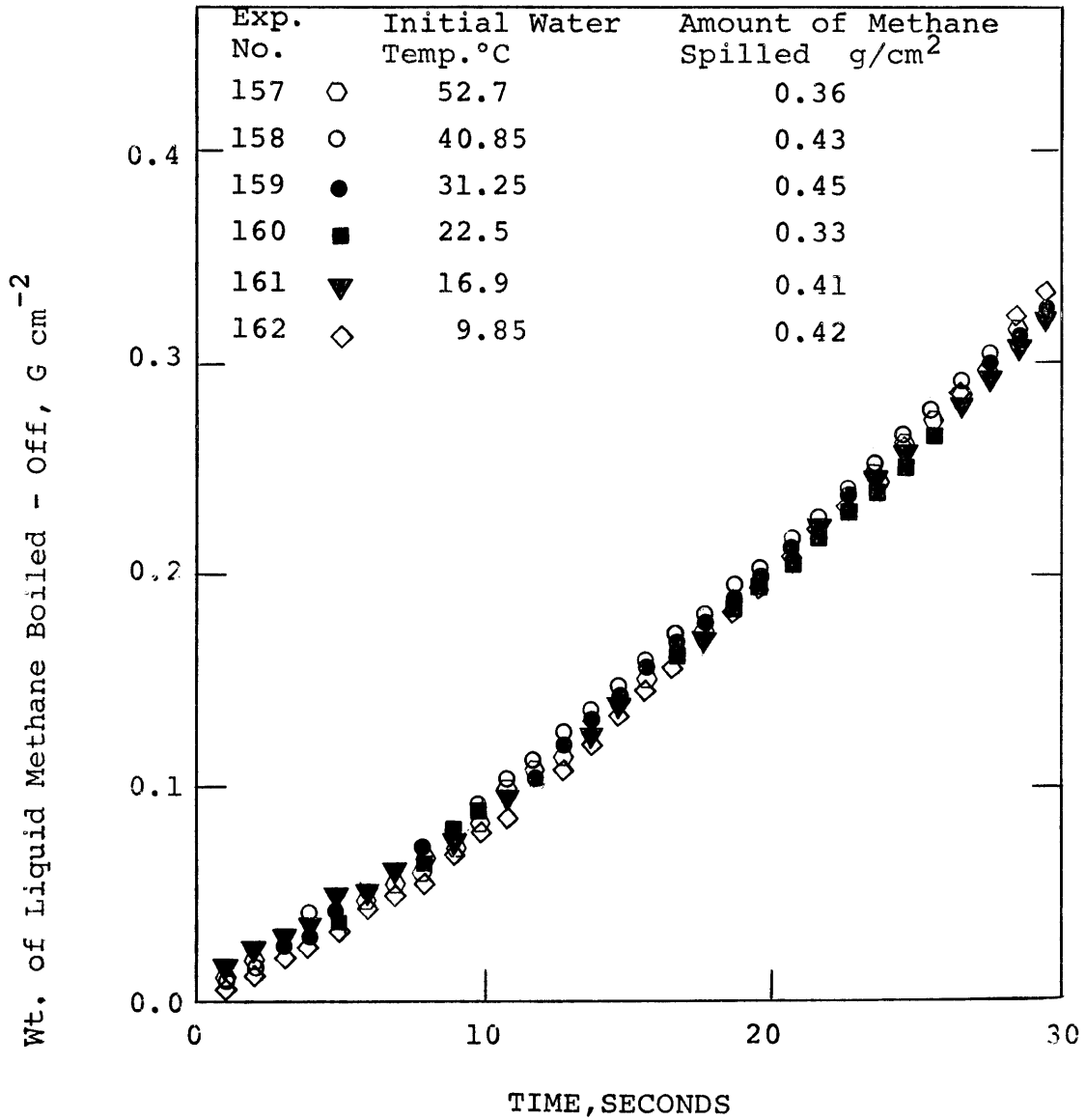


Fig. 4-19

The Effect of Initial Water Temperature on the Boil - Off Rate of Methane (99.98%)

the curves in Figure 4-20 reflects the fact that ice forms less rapidly on hot water; and thus, the shift from film to nucleate boiling is delayed. In fact, by shifting the time scales slightly for each run (i.e. add a constant time to each run, with the constant increasing as the initial water temperatures are lowered), all the curves may be made superimposed over a relatively long time. See Figure 4-21.

The effect of water temperatures on the vaporization rates of cryogenic hydrocarbon liquid mixtures are presented in Figures 4-22 and 4-23. Binary-mixture boil-off rates are presented in Figure 4-22. Except for the experiment with 5°C - water with a high boil-off rate, the initial water temperature does not influence the rate of evaporation for water temperatures less than 27°C.

Lean 5-component mixtures, Figure 4-23, show minor variations in boil-off rates as the initial water temperature was changed. The vaporization rates were slightly less on higher temperature waters. Heavier hydrocarbon mixtures also show very mild effects of water temperature similar to the lean mixture, as shown in Figure 4-24. A superposition of Figures 4-23 and 4-24, however, shows that the boil-off rates of the heavier mixture was higher. This composition effect is examined as follows:

C. EFFECT OF CRYOGEN COMPOSITION

Binary Mixtures

For methane-ethane binary mixtures (no heavier hydrocarbons),

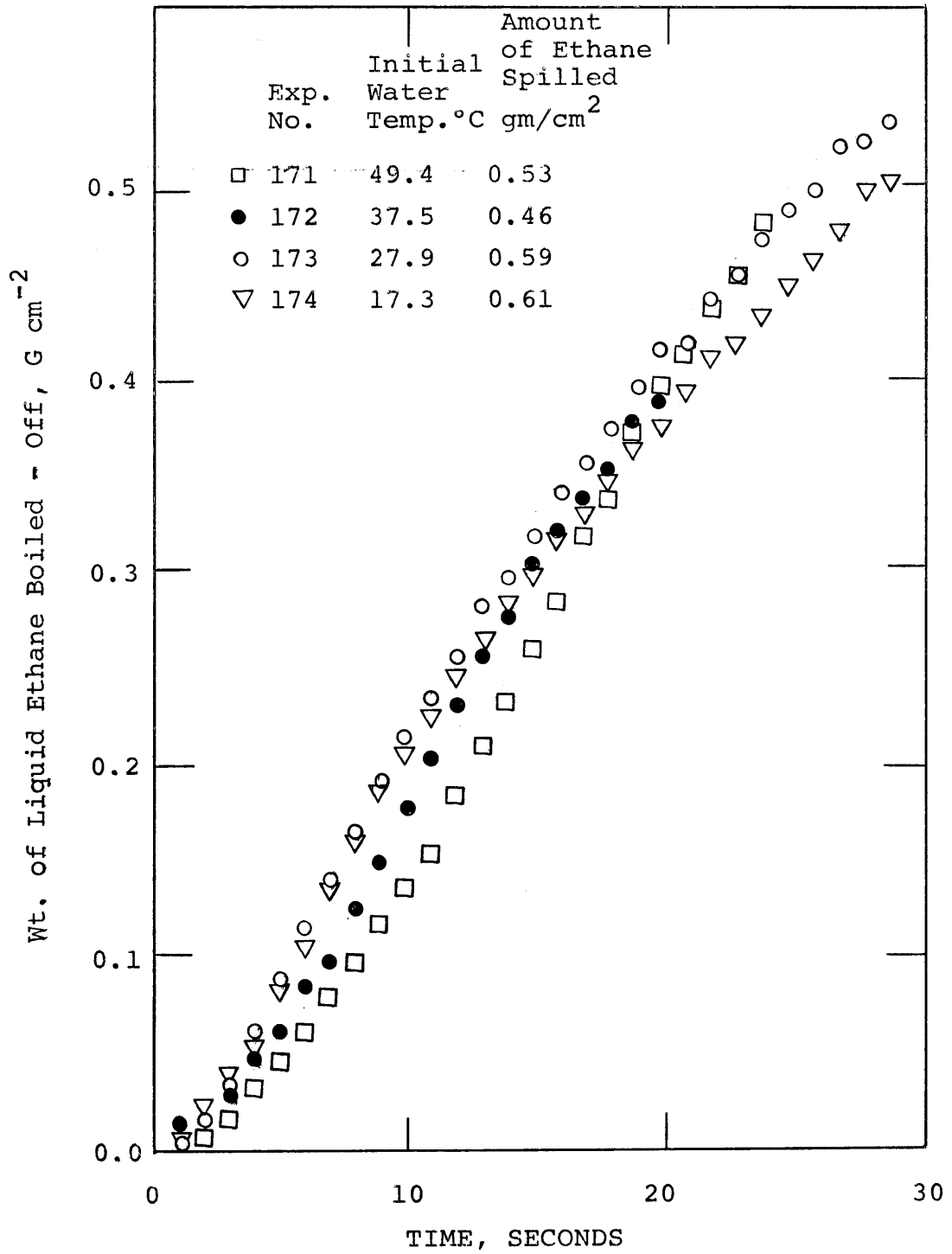


Fig. 4-20

The Effect of Initial Water Temperature on Boil - Off Rates of Liquid Ethane (99.84%)

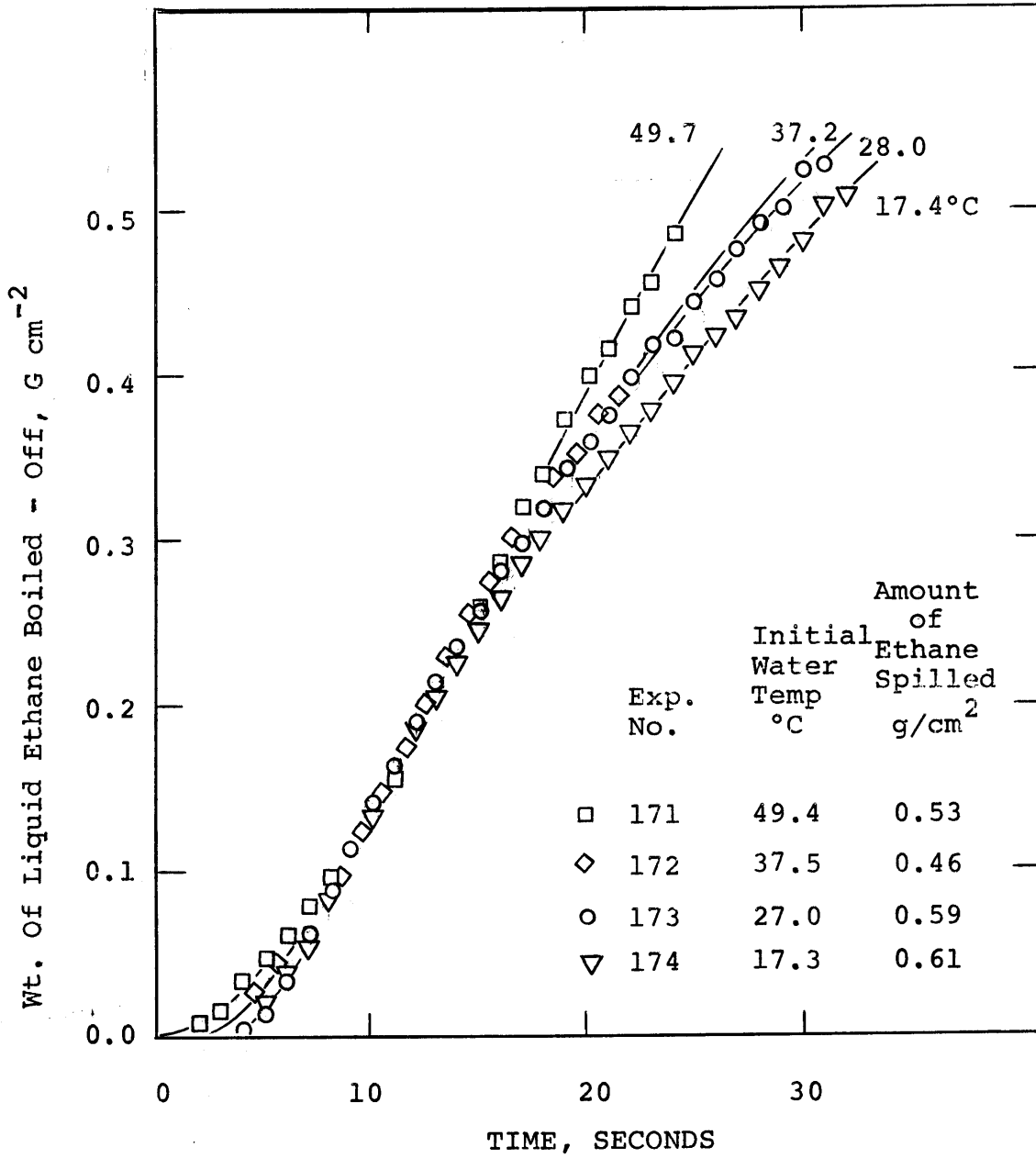


Fig. 4-21

Liquid Ethane (99.86%) Boiling on Water. (The same plots as in Fig. 4-20 with the starting points shifted right for all runs but #171).

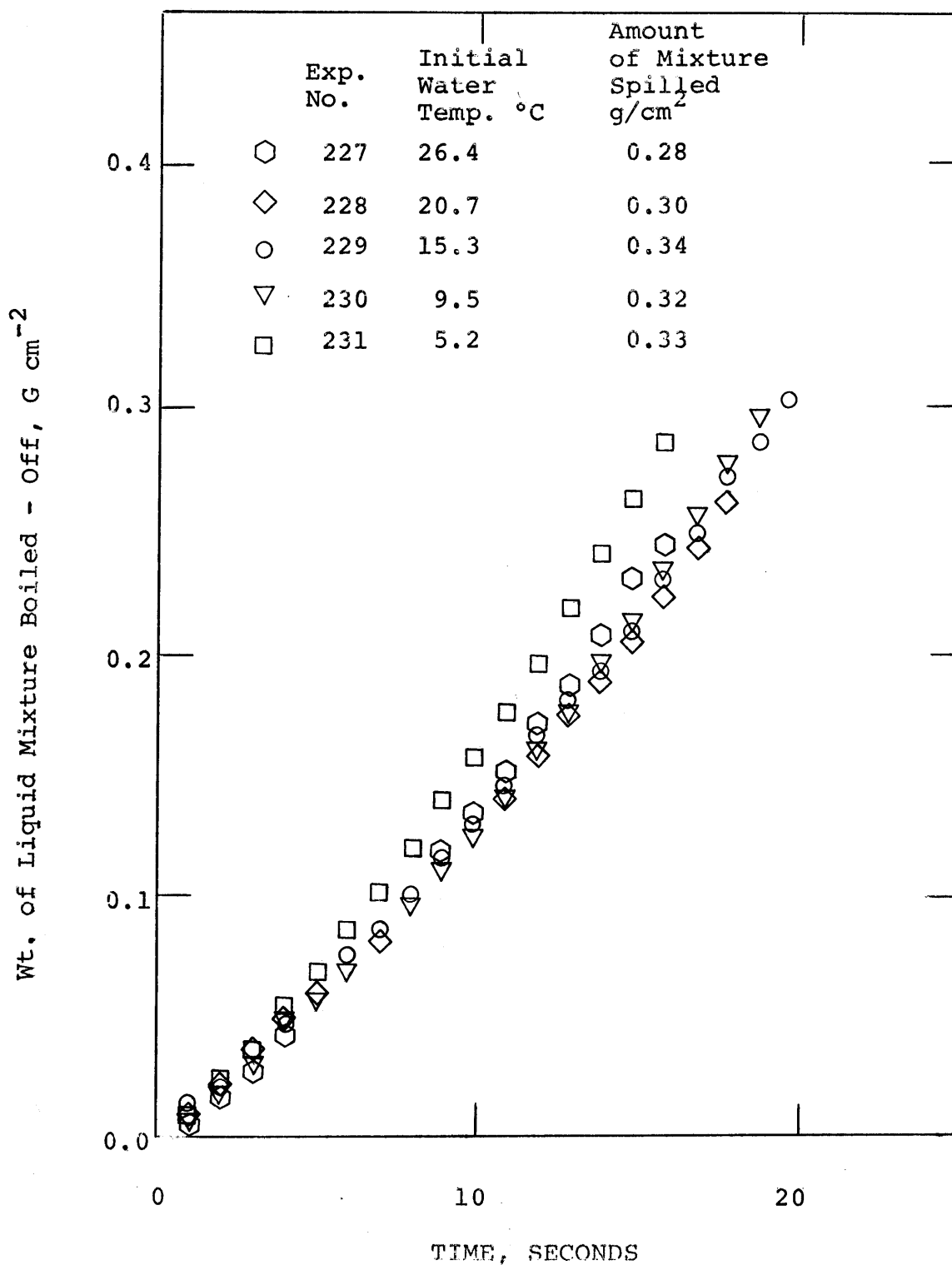


Fig. 4-22

The Effect of Initial Water Temperature
on Boil - Off Rates of Mixtures (98% CH₄,
2% C₂H₆)

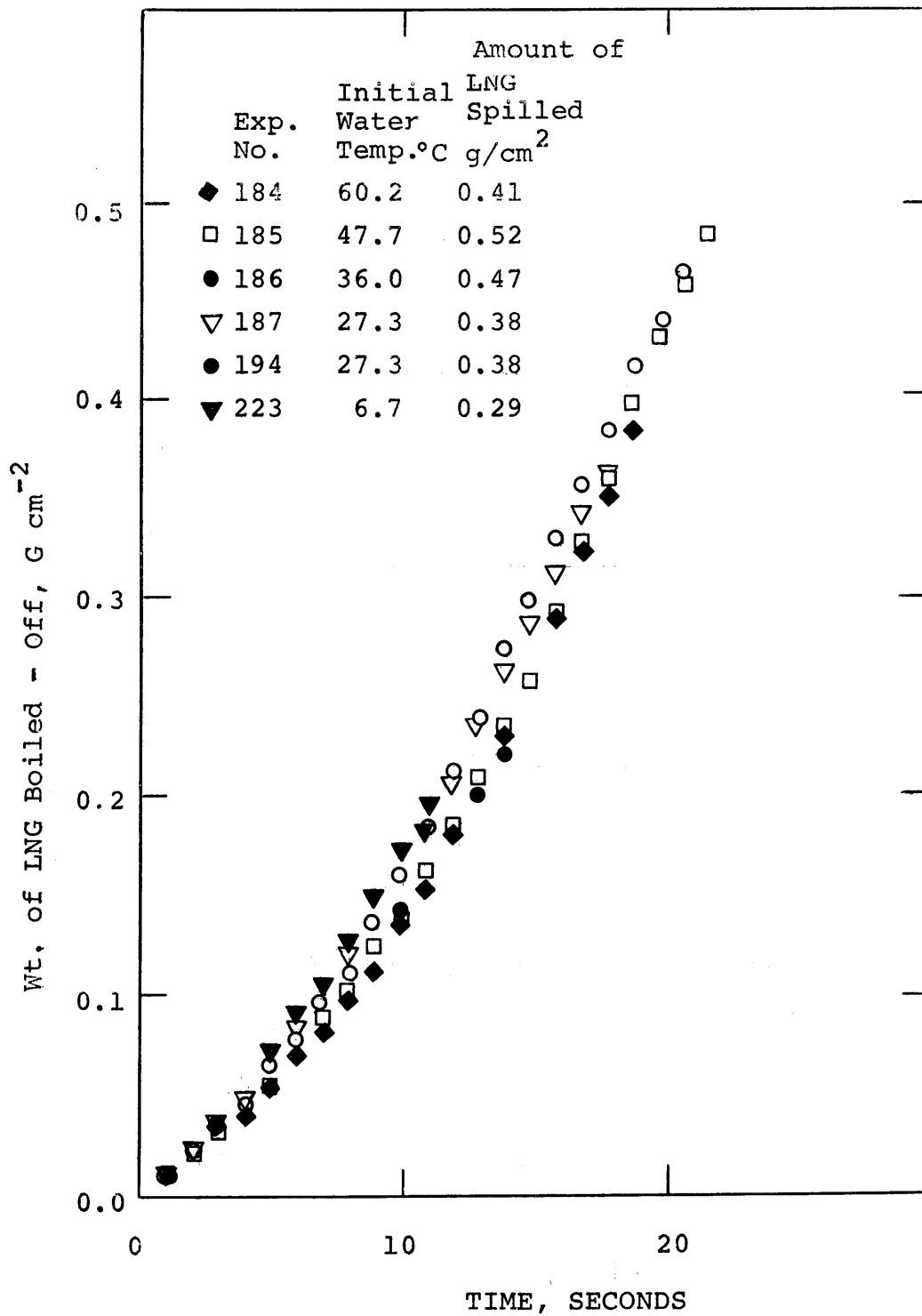


Fig. 4-23

The Effect of Initial Water Temperature on Boil - Off Rates of LNG (98.2% CH₄, 1.62% C₂H₆, 0.11% C₃H₈ and trace butanes)

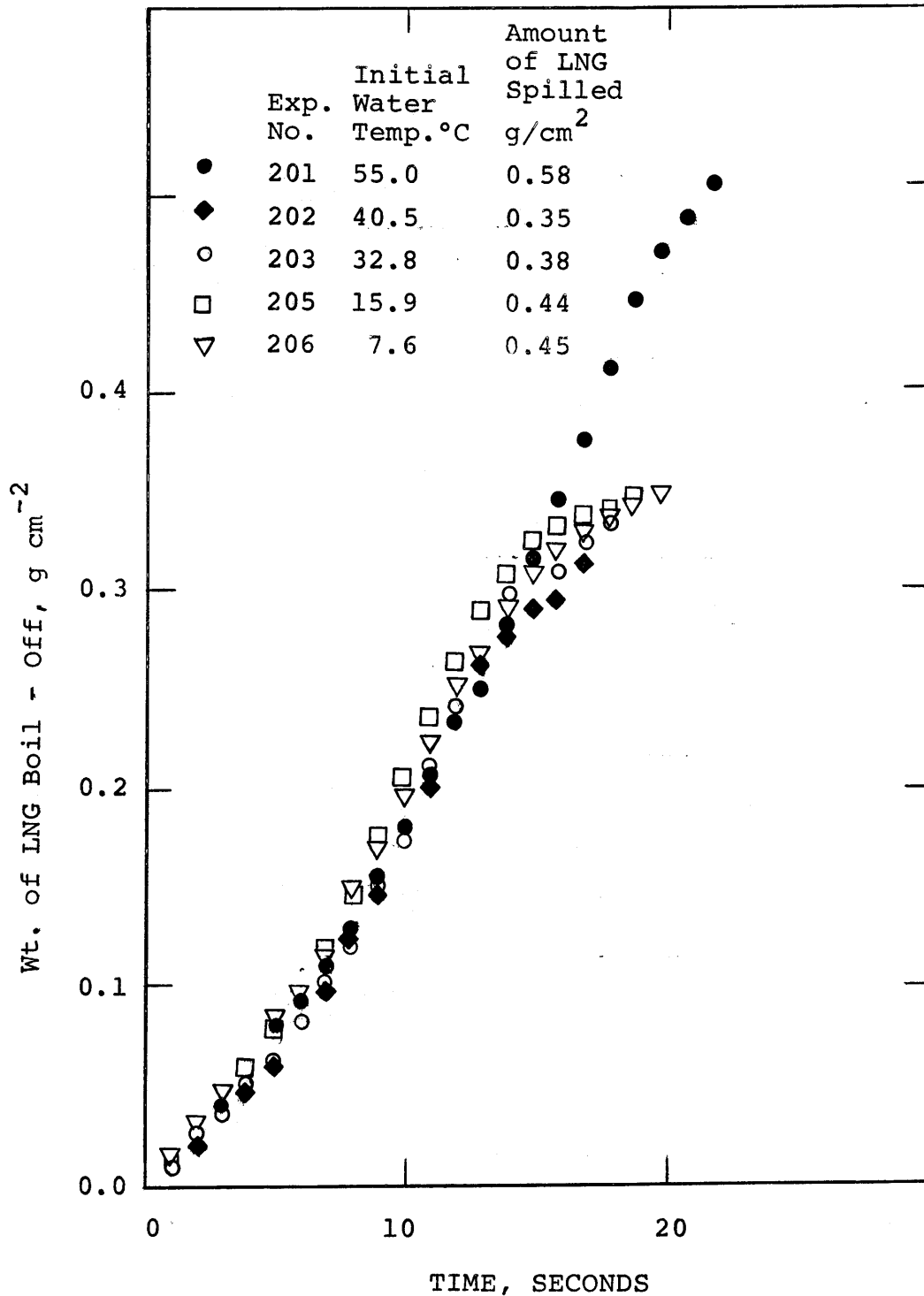


Fig. 4-24

The Effect of Initial Water Temperature on Boil - Off Rate of LNG (89.2% CH₄, 8.2 % C₂H₆, 2 % C₃H₈ plus trace butanes)

the boil-off versus time curves exhibit an unusual trend. This may be seen on Figure 4-25 . The results from seven runs are shown. In most the runs, the initial temperature of water and the quantity spilled were held reasonably constant. (Also, as indicated earlier, variations in these parameters have a small, if not negligible, effect on the boil-off process.)

Liquid ethane boils most rapidly, and methane the least. Mixtures do not show any simple behavior. A very small amount of ethane in methane increases the boiling rate far out of proportion to the amount added. With only about 5% ethane present, the boiling rate is close to (although less than) that of pure ethane. Increasing the ethane content above this level actually leads to a drop in boil-off rate. In Figure 4-26 , the total amount of liquid boiled-off in the first 10 seconds is shown for various mixtures.

The same odd effect is noted (Chapter 5) if the actual boiling flux, W/m^2 , were plotted instead of g/cm^2 since the latent heat of vaporization per gram (ΔH_v) is almost constant for methane-ethane mixtures. ΔH_v for pure methane is 510.2 J/g, and 489.7 J/g for ethane at the saturation boiling temperatures. For a 20% ethane - 80% methane cryogenic liquid mixture, ΔH_v is about 506.6 J/g.

The data for the binary mixture of methane and propane boiling on water are presented in Figure 4-27. Similar to the methane-ethane runs, traces of propane in methane cause large enhancements in boil-off rates. With 0.15 mole percent propane present, an increase of

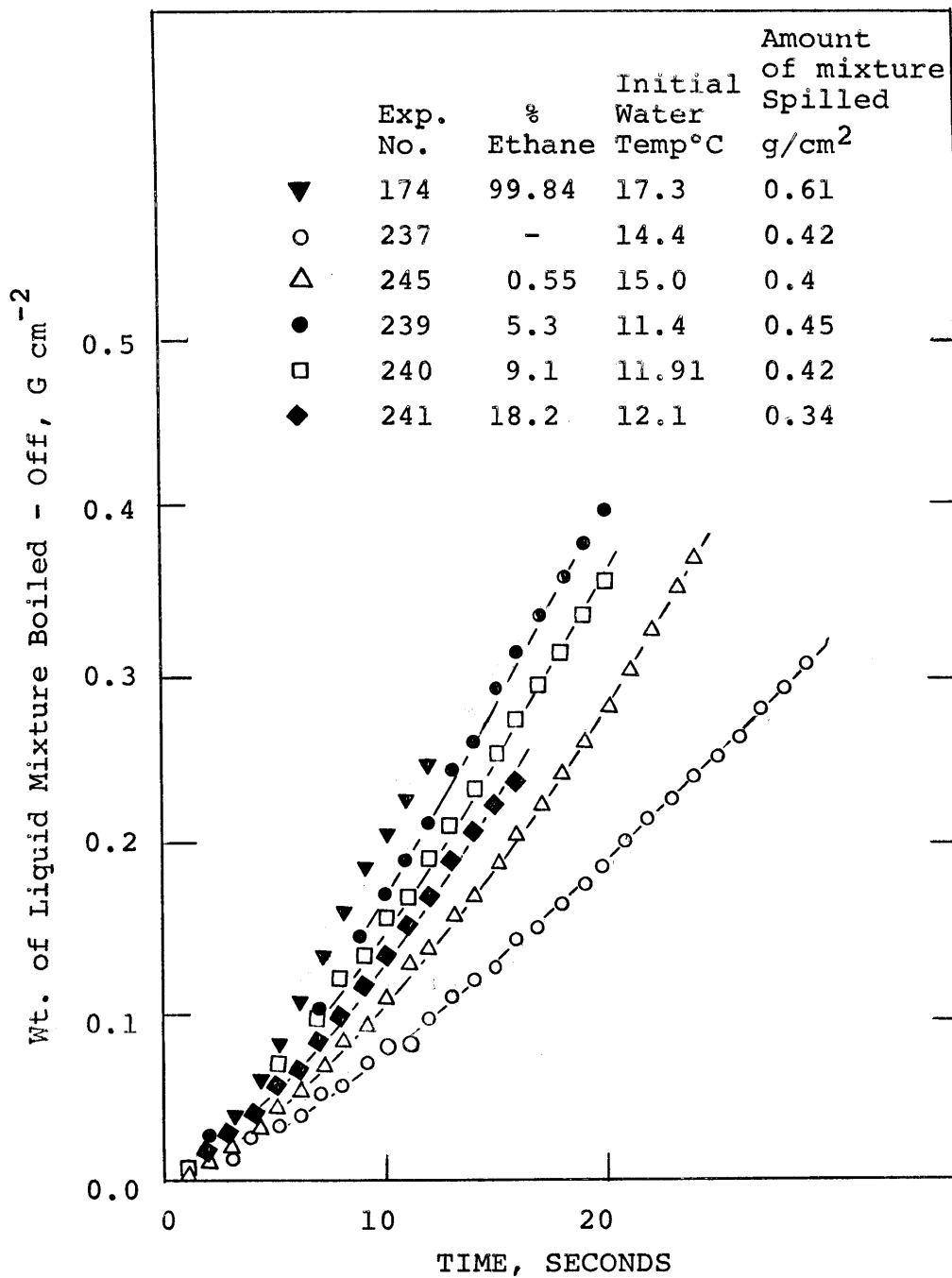


Fig. 4-25

The Effect of Variations in Liquid Composition on Boiling Rates of Binary Methane/Ethane Mixtures.

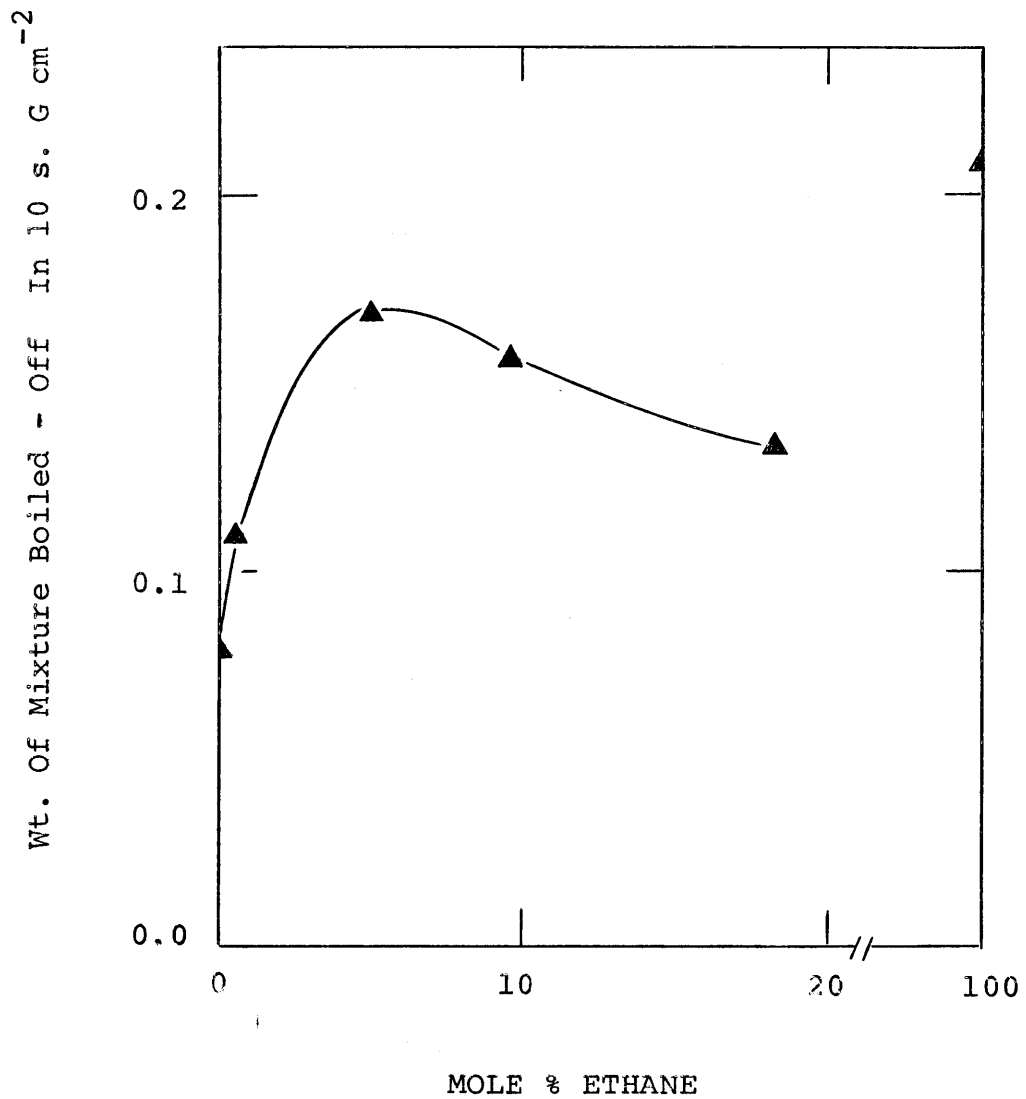


Fig. 4 - 26

The Total Amount of Cryogenic Binary Mixture of Methane And Ethane Boiled - Off In The First 10 Seconds As A Function Of % Ethane.

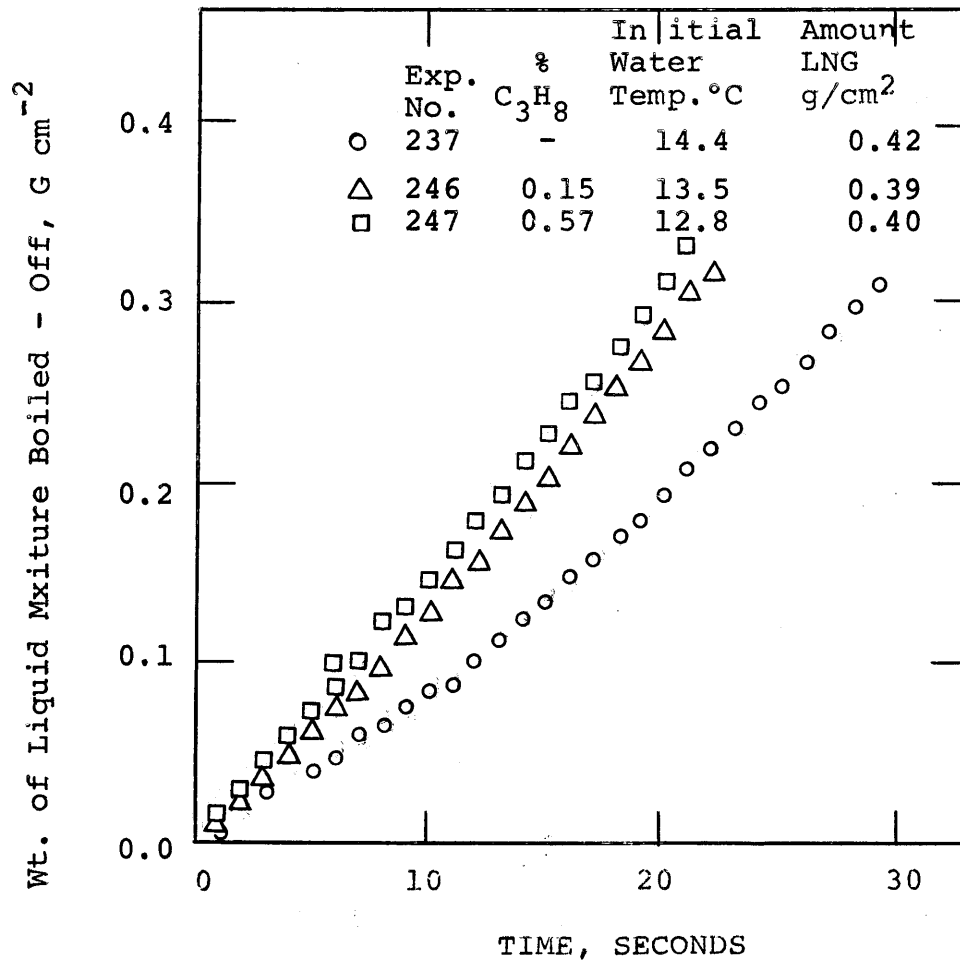


Fig. 4-27

The Effect of Composition on Boil-Off Rates of Binary Methane/Propane Cryogenic Liquid Mixtures.

about 50% was noted in the boil-off rate.

The enhancement was 75-100% when the amount of propane was increased to 0.57%. The experiments were performed with initial water temperatures between 12 and 15°C, and with $0.7 \pm 0.02 \text{ g/cm}^2$ cryogenic liquid charged.

D. COMPARISON OF THE EFFECTS OF ADDITIVES

The effects of the addition of ethane, propane and n-butane on the boil-off rates of methane are examined in Figures 4-28 to 4-30. In Figure 4-28, boil-off rate enhancements by adding about 0.55% ethane or propane are indicated. The curves show that propane is considerably more effective at that concentration level and the operating conditions (initial water temperatures $\sim 14 \pm 2^\circ\text{C}$ and $0.4 \pm 0.02 \text{ g/cm}^2$ cryogen charged).

At much higher concentration levels and a higher initial water temperature range, Figure 4-29, the reverse was exhibited, although the data for ethane and propane mixture with methane were not significantly different. This observation is consistent with the fact that a maximum occurs when boil-off rates are plotted against percent additive, as shown in Figure 4-26 .

In Figure 4-30, the effects of trace quantities of propane and n-butane are compared. Again the higher member of the homologous series was more effective in enhancing the boil-off rates of methane.

5-Component Liquid Mixtures on Water

Data on the vaporization rates of five-component cryogenic

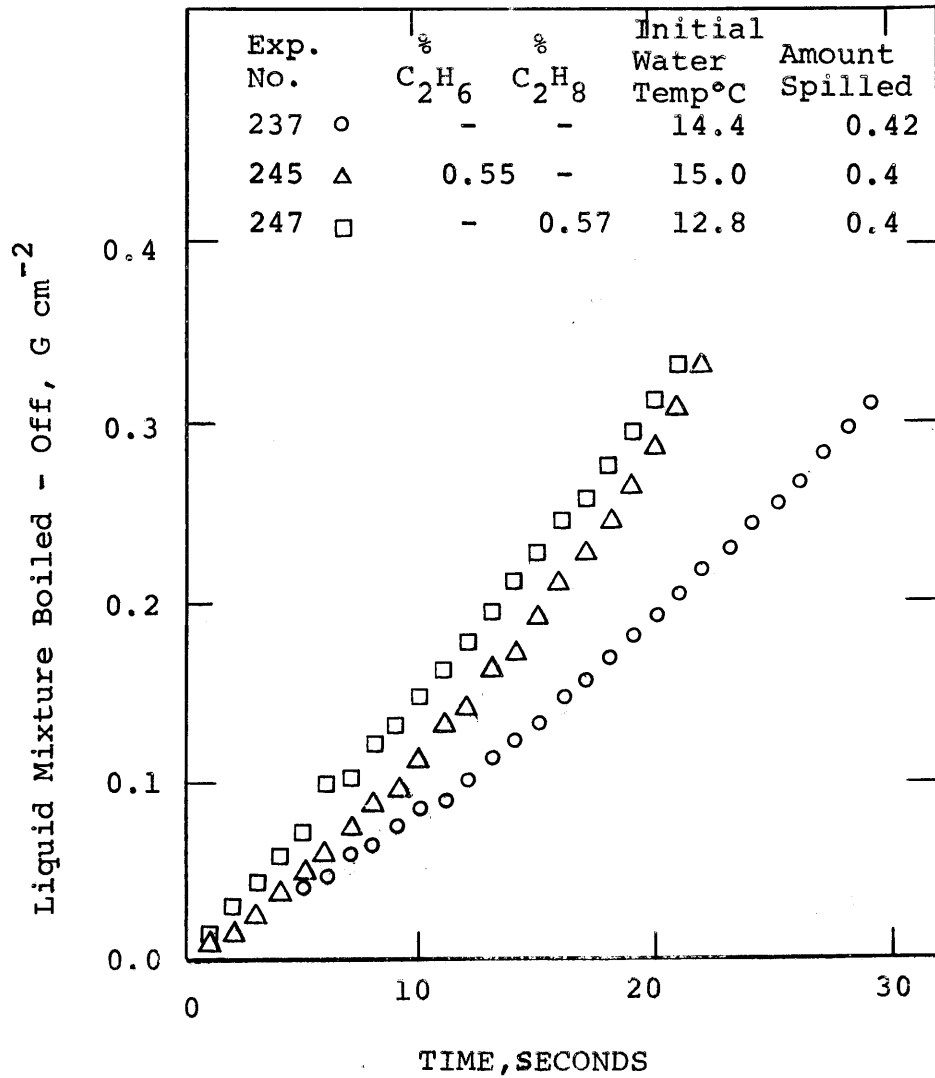


Fig. 4-28

The Effects of Trace Quantities of Ethane and Propane on Boil - Off Rates of Methane

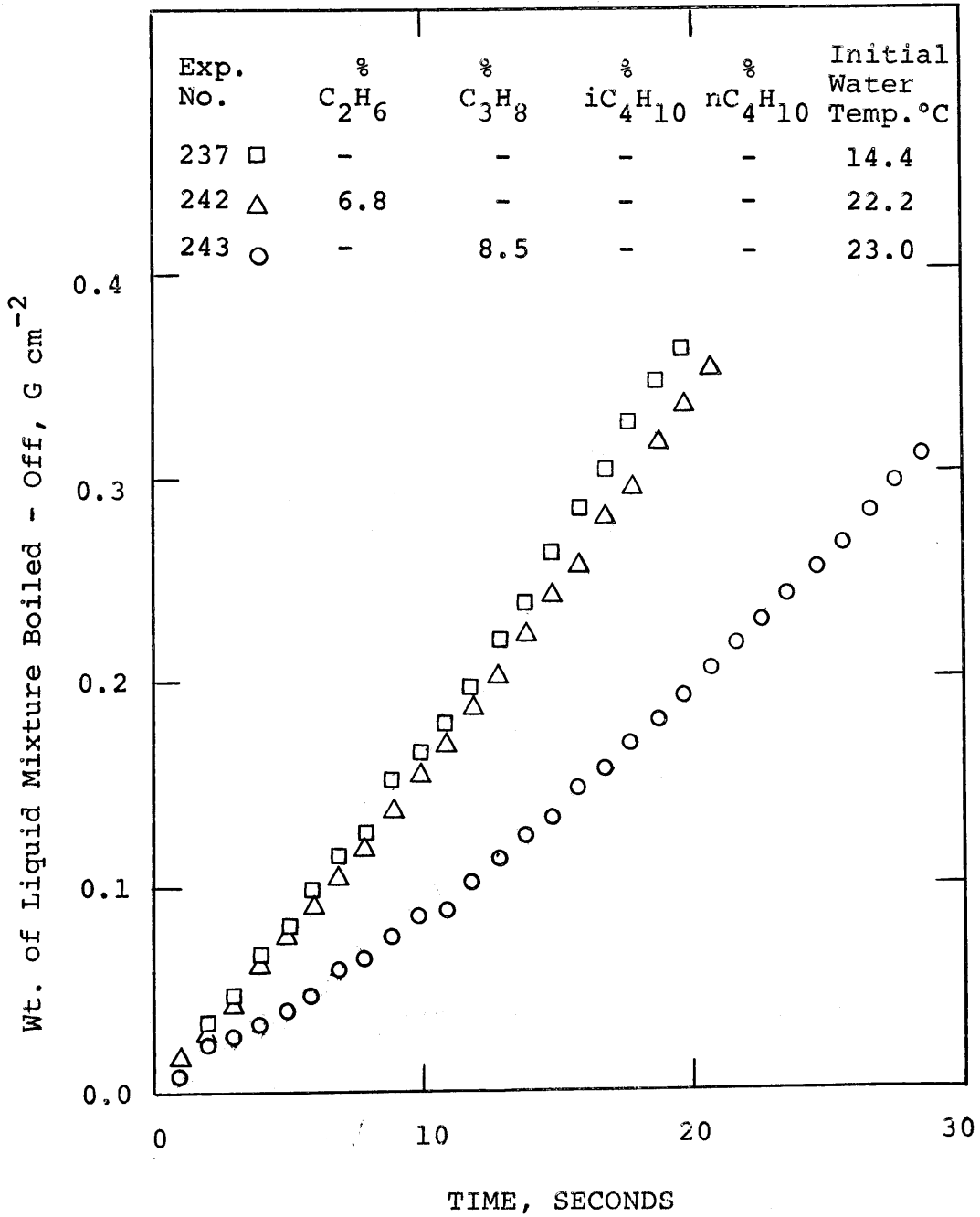


Fig. 4-29

The Effect of Variations in Liquid Composition on Boiling Rates of Binary Mixtures ($0.42 \pm g.cm^2$ Liquid Spilled)

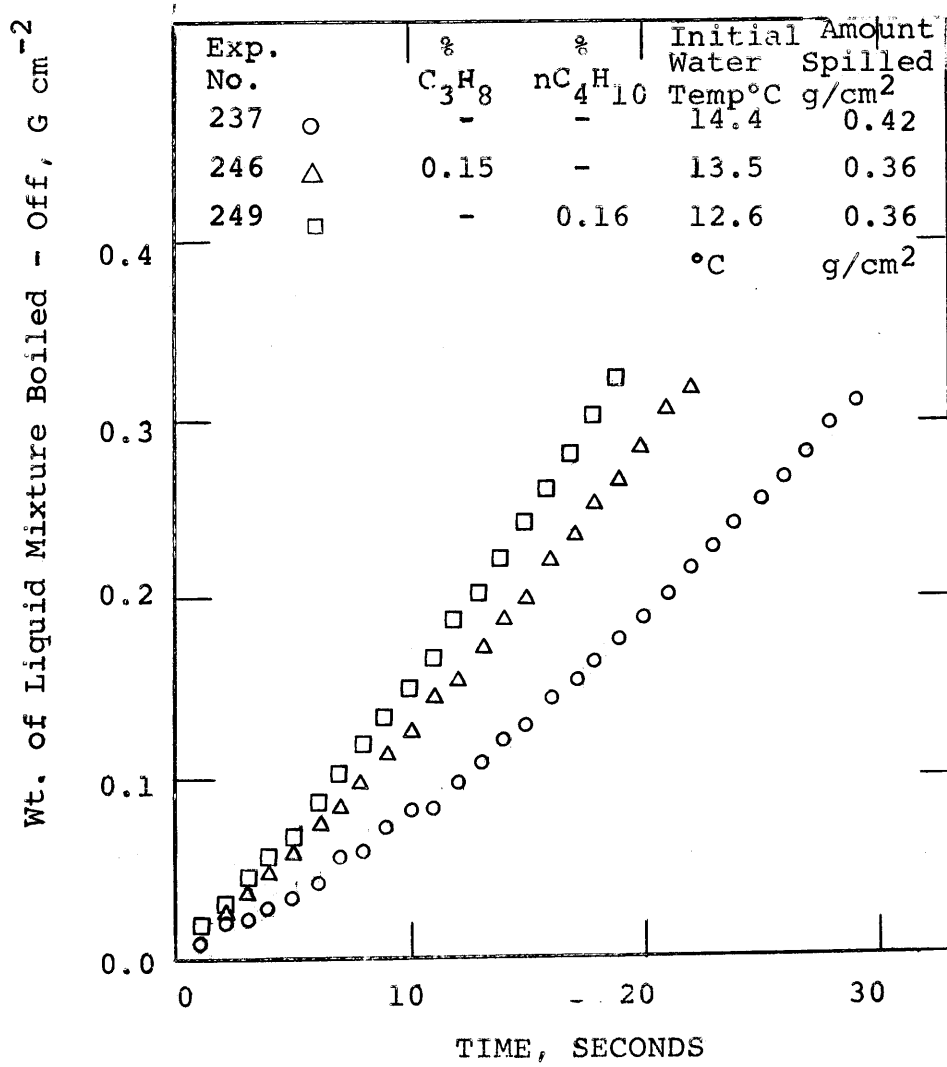


Fig. 4-30

The Effects of Trace Quantities of Propane and n-Butane on Boil - Off Rates of Methane

liquid mixtures are presented in Figure 4-31. The amounts of cryogen charged were 0.44 ± 0.06 g/cm² and the initial water temperatures, in each of the runs, ranged between 15 and 33°C.

With the compositions employed, the vaporization rates of the cryogenic liquids increased as the mole fraction of methane decreased. A comparison of runs 205 and 244 which have approximately the same mole fraction of ethane suggest that the additives act in parallel, i.e., each component, at least partially, influences the boil-off rates independent of other components. Run 244 exhibited an 80-100% enhancement in boil-off rates over run 205. The observation is further reinforced by the fact that the liquid mixture in run 207 has a higher percent ethane (14.6%), and a higher total fraction of ethane plus propane (17.6%) than in run 244 (8.6% ethane and 6.9% propane), yet the boil-off rates of run 207 was about 25% less than that of run 244. Nevertheless, it is clearly seen that the first small quantities of additives to methane caused the maximum enhancements per unit weight. (Compare runs 161, 187 and 205). A comparison of the boil-off of pure methane, runs 161 and 237, with the 5-component liquid of run 244 show an enhancement of 240% in boiling rates after 10s into each run!

E. VAPOR TEMPERATURES

It is normally assumed that vapor evolved from boiling liquids is at the saturation temperature. This is often a poor approximation for cryogenic liquids boiling on water. As described in Section 4-2,

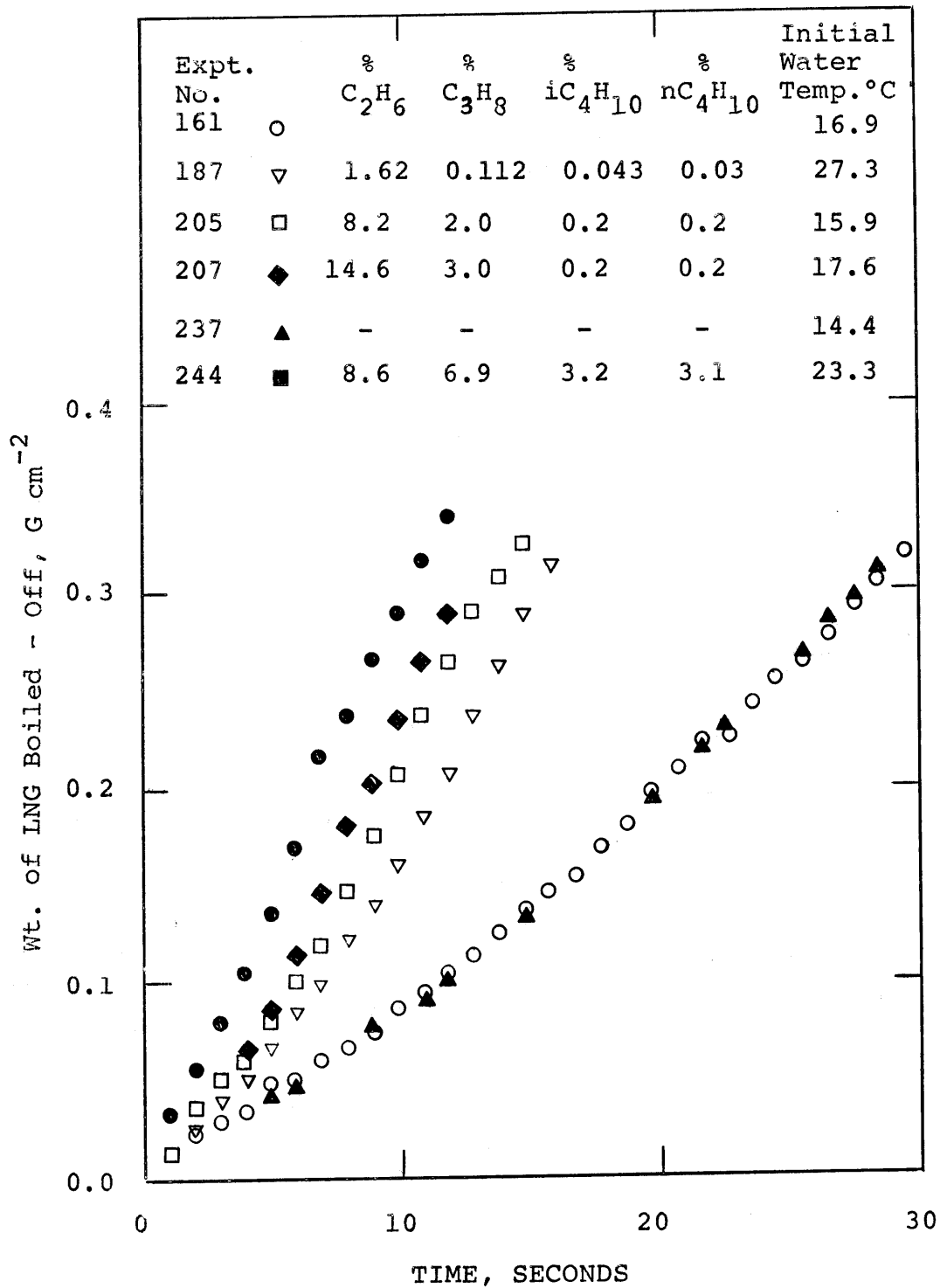


Fig. 4-31

The Effect of Variations in Liquid Composition on Boiling Rates of LNG (Liquid Spilled $0.42 \pm 0.05 \text{ g/cm}^2$)

(and Appendix B), considerable care was taken to heat-station several thermocouples, and exclude warm ambient air in the vapor space above the boiling pools. The outputs of the thermocouples showed no significant axial or radial temperature gradients. Thus, the space-mean average is used to characterize the vapor temperature.

Nitrogen vapor temperatures are shown in Figure 4-32. Since liquid nitrogen boils at -196°C (at 1 atm. pressure), it is quite obvious that the vapor evolved from nitrogen boiling on water is significantly above this temperature for all runs shown. The abscissa represents the depth of liquid nitrogen (uncorrected for vapor bubble expansion, or vapor hold-up), thus, as time increases, the curves are traced from right to left.

As the quantity of nitrogen spilled increases, the vapor temperature drops; also, the higher the initial water temperature the higher the vapor temperature. An odd, but reproducible, phenomenon occurs when the quantity spilled is low. The vapor temperature curve appears to go through a minimum*.

When pure liquid methane boiled on water, the vapor temperatures were quite sensitive to the quantity spilled as indicated in Figure 4-33. When the amount was equal to about one g/cm^2 , the recorded vapor superheat was essentially zero. With lesser quantities,

*The warm air above the water, prior to the spill of the cryogen, is estimated to be completely swept out of the test vessel (treated like a backmix reactor) within the first 0.5 seconds of each experiment. Hence, the phenomenon is real.

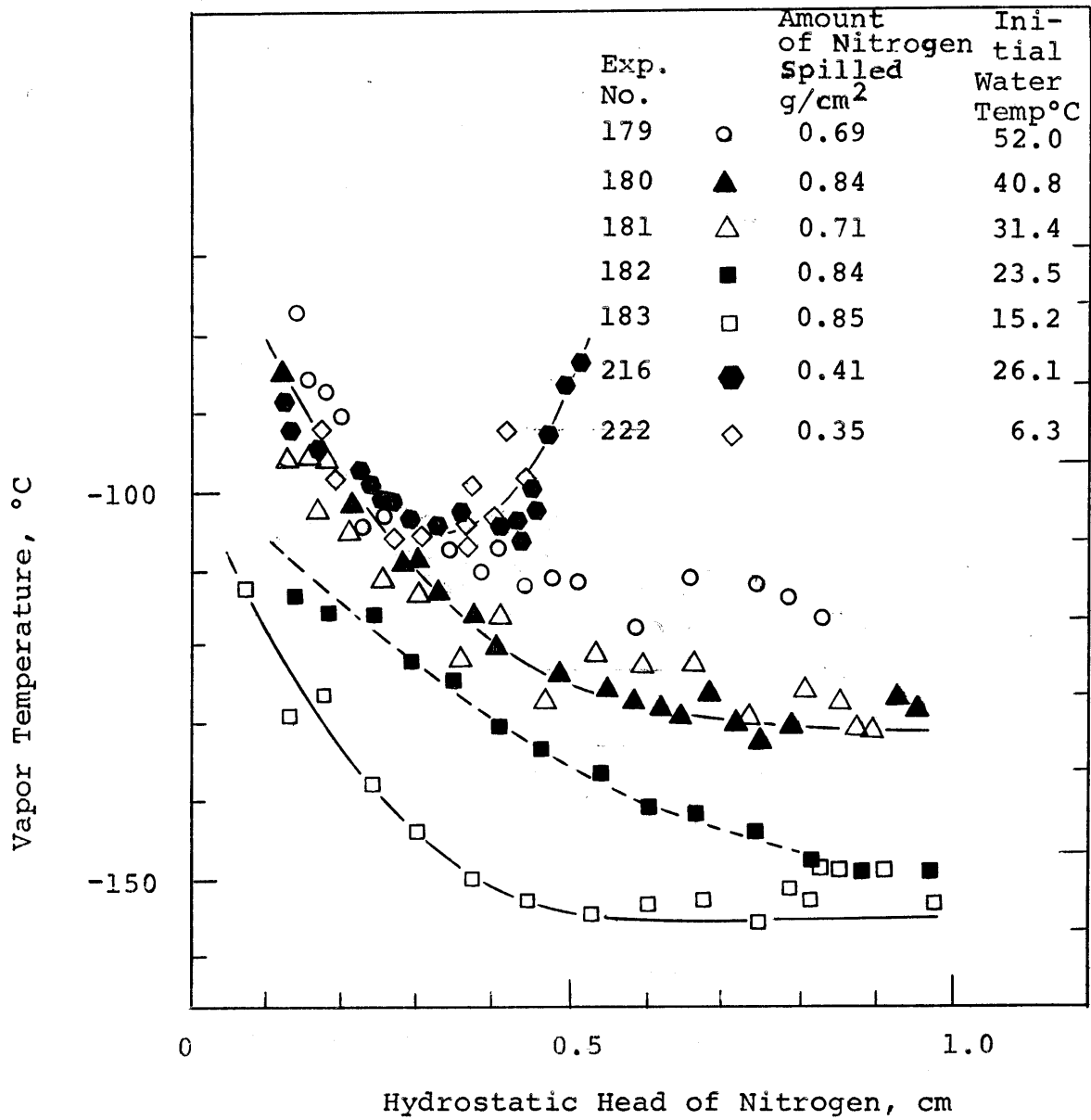


Fig. 4-32

Vapor Temperatures Above Boiling Pools
of Nitrogen

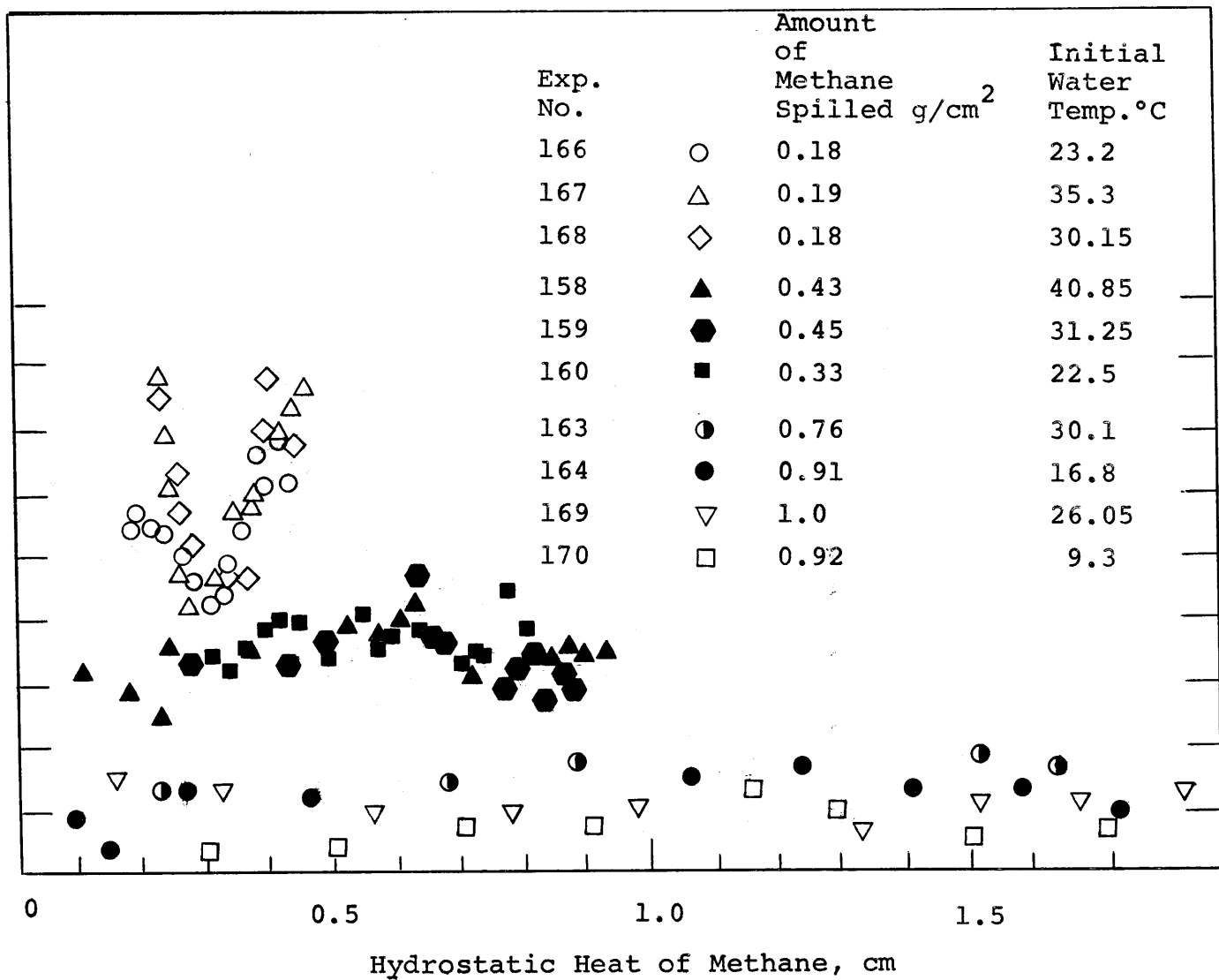


Fig. 4-33

Vapor Temperatures Above Boiling Pools of Methane (99.98%)

larger superheats were measured and again, as for liquid nitrogen, for very small spills, there is a clear indication of a minimum vapor temperature. The hydrostatic head at the minimum, 2.8 mm, is 1 mm higher than indicated by Boyle and Kneebone (1973) as the point of pool disintegration into discrete puddles. Pool break-up might explain the small spills, but no similar increase in vapor temperature was noted for the larger spills.

With liquid ethane spills, essentially no superheated vapor was noted except for the small spills. See Figure 4-34. With lean LNG, the vapor superheat was again low, except for small spills on hot water, as shown in Figures 4-35, 4-36 and 4-37. This was not unexpected since photographs of the liquid interface (See Chapter 3) revealed many small bubbles which form foams above the boiling cryogenics.

With heavier LNG, Figure 4-38, the initial vapor temperatures were comparable to those of lean LNG (See Figure 4-36). However, the vapor temperature rose sharply after more than 50% of the cryogenic liquid spilled had vaporized. This is consistent with the fact that, as the boiling progressed, the very volatile methane vaporizes first, and the residual liquid becomes richer in higher boiling components. The almost discontinuous change in slope with about 75% (by volume) of the liquid boiled-off, (Figure 4-38), indicates that ethane was then the component primarily vaporized.

F. TEMPERATURES IN THE WATER

Temperatures in the water were measured with thermocouples

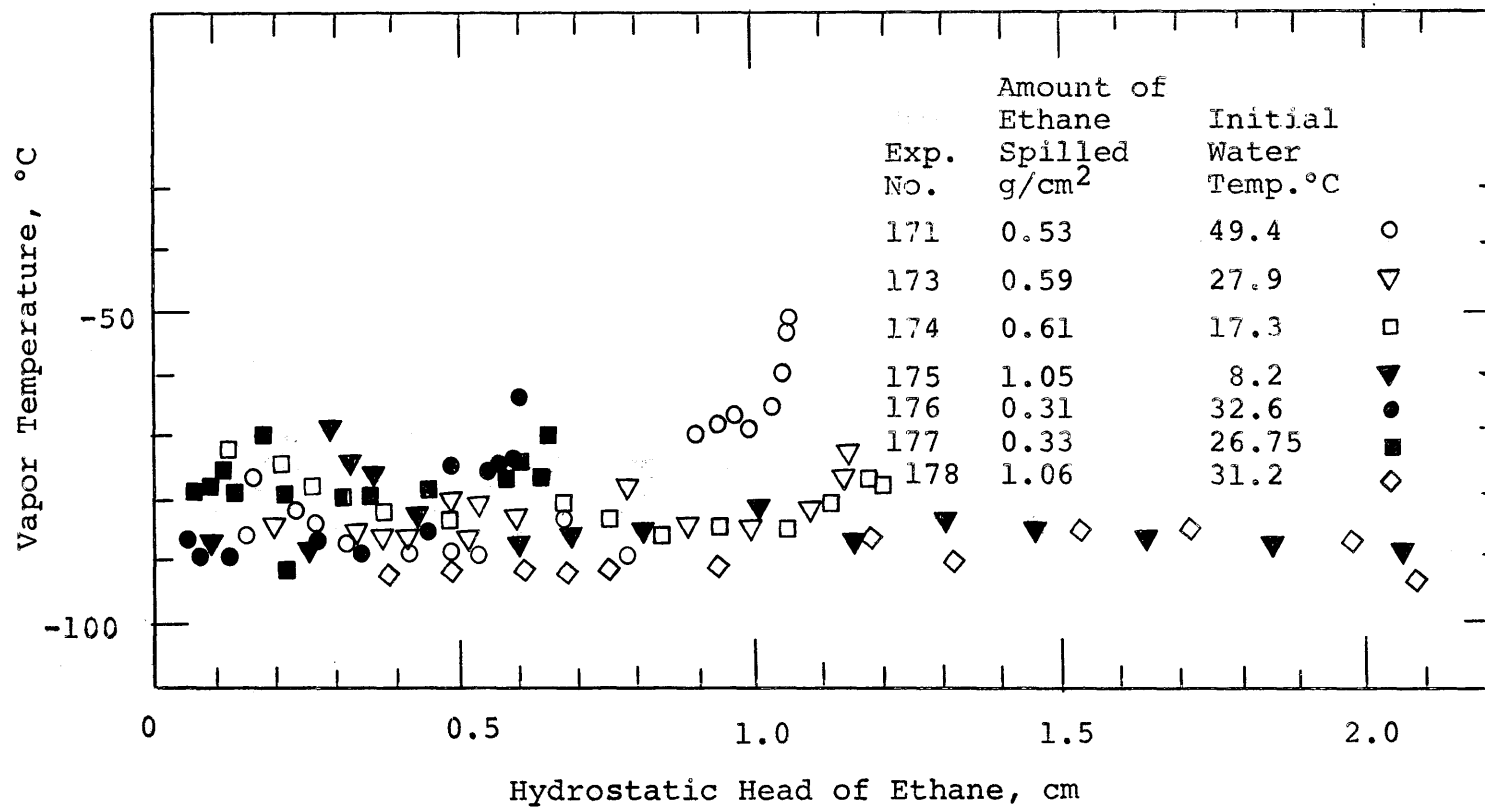


Fig. 4-34

Vapor Temperatures Above Boiling Pools of Ethane (99.84%)

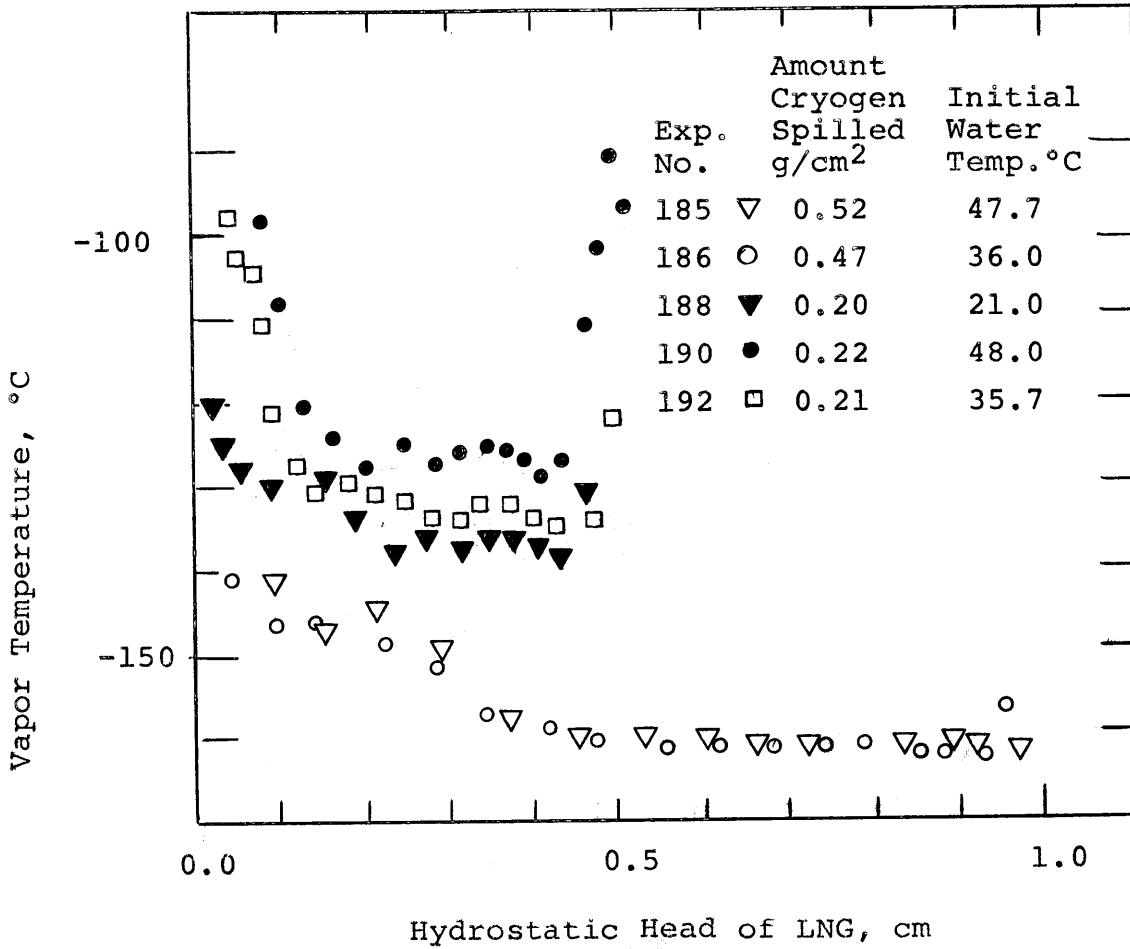


Fig. 4-35

Vapor Temperatures Above Boiling Pools of LNG (98.2% CH₄, 1.62% C₂H₂, 0.11% C₈H₈ plus trace butanes)

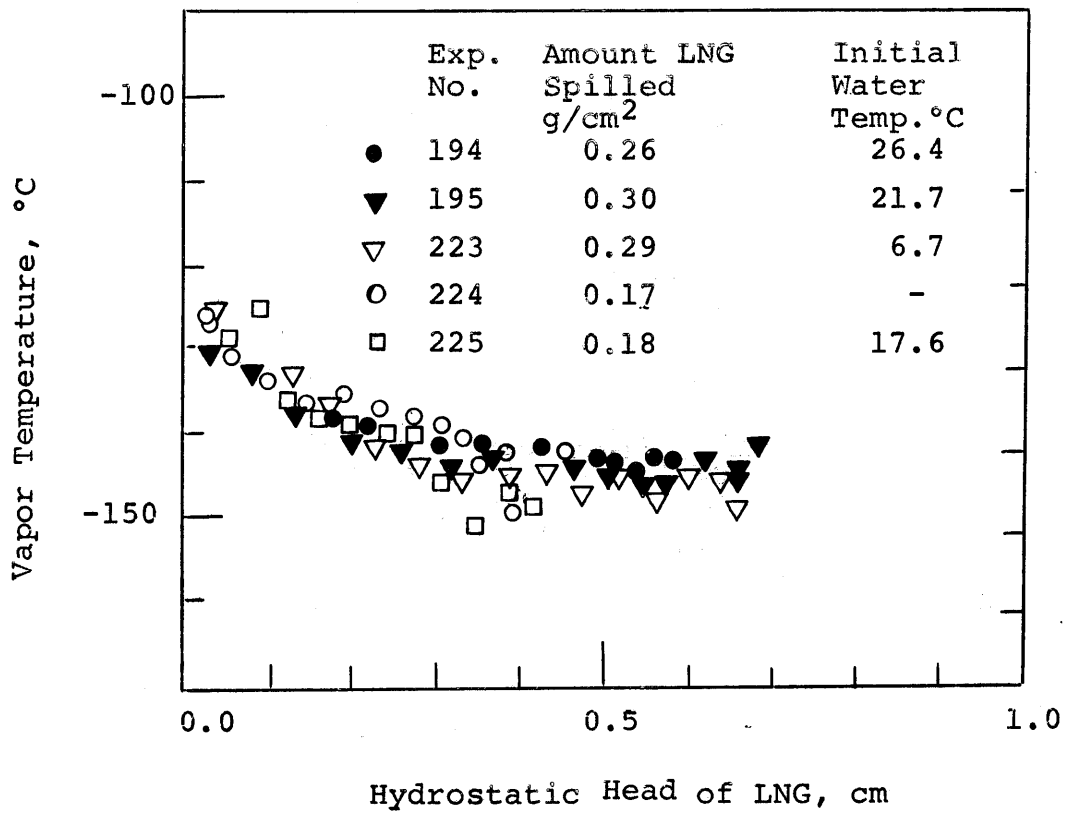


Fig. 4-36

Vapor Temperatures Above Boiling Pools of LNG (98.2% CH₄, 1.62% C₂H₆, 0.11% C₂H₆ plus trace butanes)

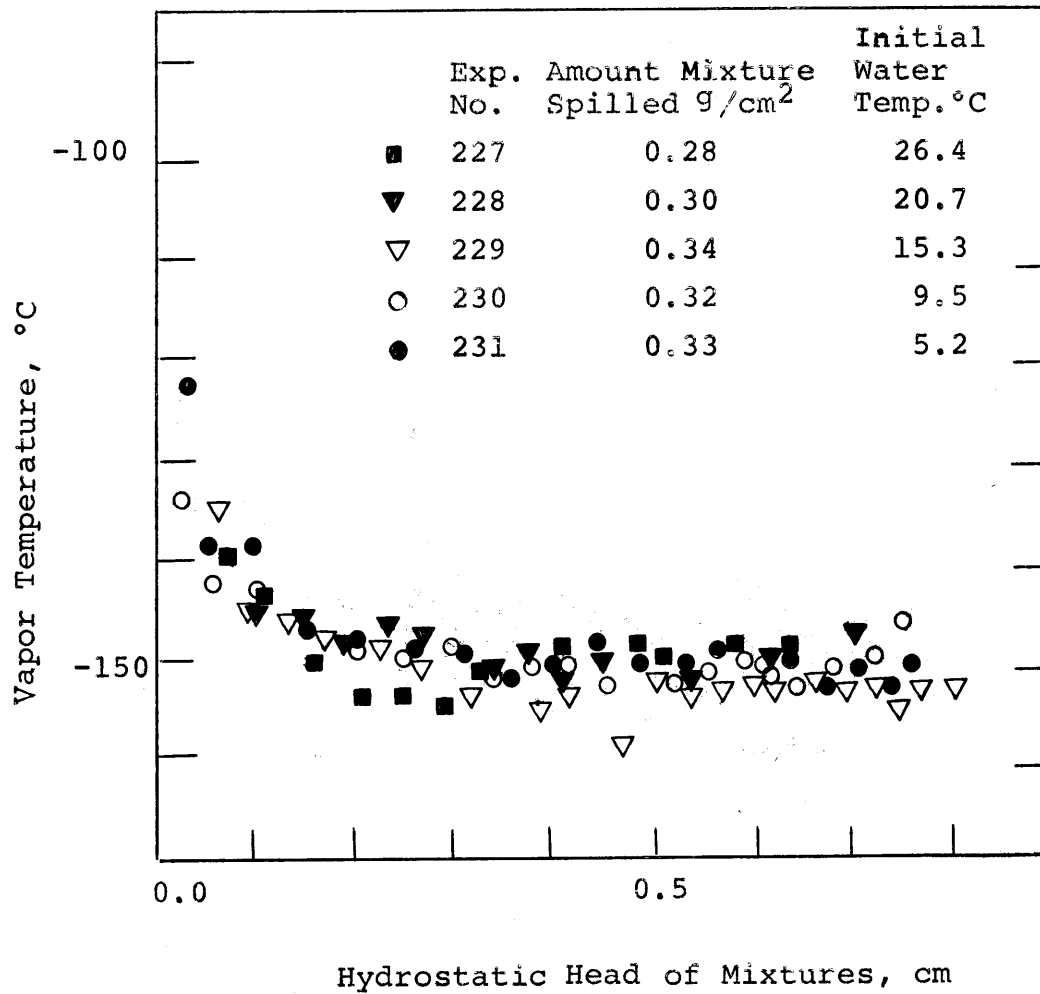


Fig. 4-37

Vapor Temperatures Above Boiling Pools of Binary Mixtures (98% CH_4 , 2% C_2H_6)

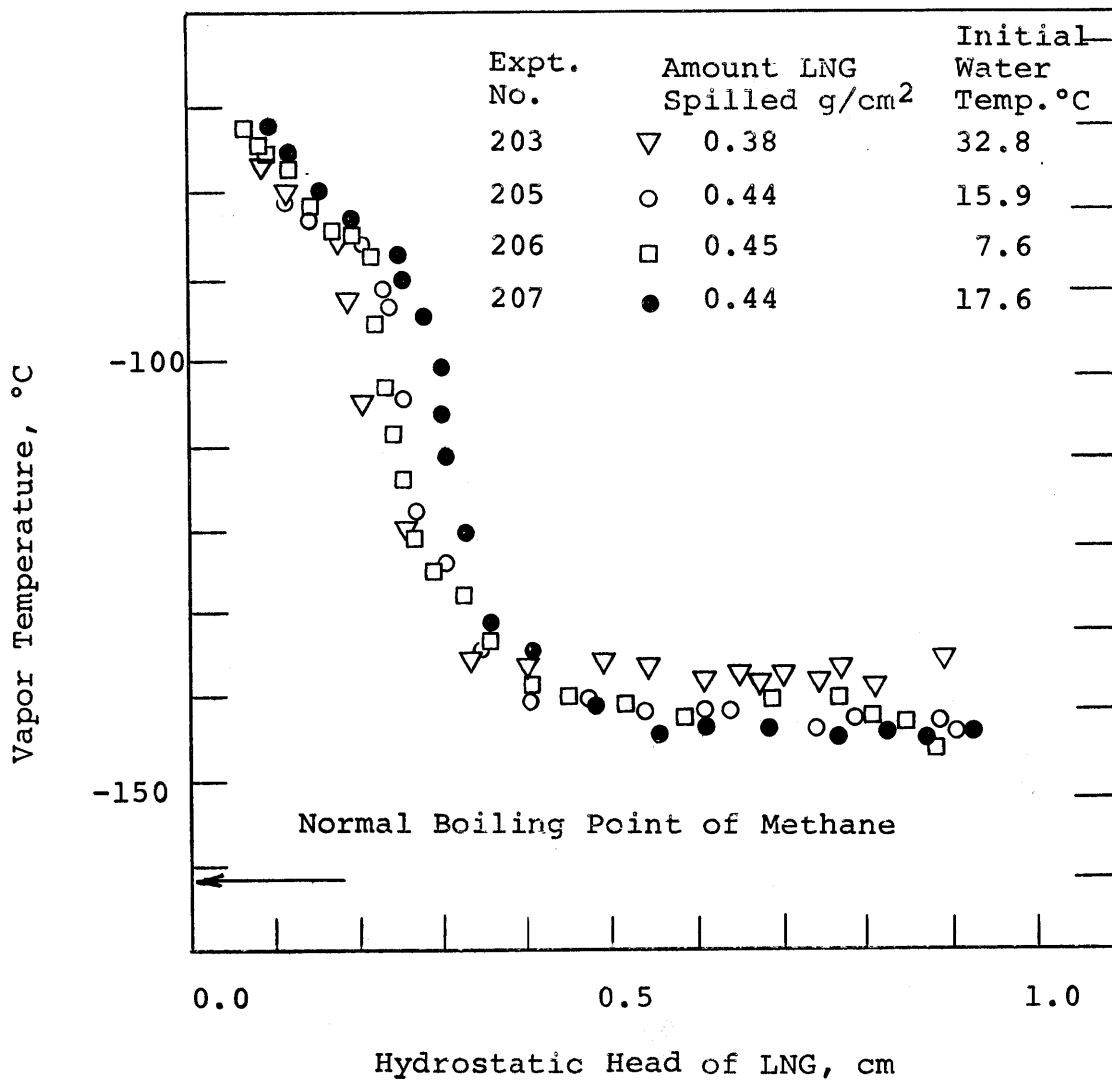


Fig. 4-38

Vapor Temperatures Above Boiling Pools of LNG (89.4% CH₄, 8.2% C₂H₆, 2% C₃H₈ plus trace butanes for all except #207 - 82% CH₄, 14.6% C₂H₆, 3% C₃H₈)

inserted into the test vessel from beneath, (See Section 4-2), and the signals were recorded on the Sanborn recorders as well as the data logger.

A few analog outputs are presented in Figures 4-39 to 4-41, as these clearly demonstrate the rapid temperature fluctuations in the neighborhood of each thermocouple junction.

Figure 4-39-1 is a typical water surface temperature pattern measured with a thermocouple whose junction rode with the water surface, while liquid nitrogen boiled was boiling over water. This pattern endured for most of each run, with the average thermocouple reading averaging about 5°C , 10 to 20 seconds into each run. Figure 4-39-2 indicates the output recorded by a junction 0.5 mm below the quiescent level of the water during liquid nitrogen boil-off. One millimeter down into the water, and with colder water (6.4°C initially), the fluctuation are further decreased and a steady decrease in temperature was observed.

Figure 4-40 and 4-41 show similar outputs while methane and LNG boiled respectively on water.

The boiling of LNG, Figure 4-41, show a characteristic different from single-component liquid runs. With a lean LNG (Figure 4-41-1) on hot water (55°C), the thermocouple at the surface registered severe oscillations in temperature. On lowering the water temperature and increasing the concentration of ethane and propane in the LNG, Figure 4-41-2, the oscillations are dampered considerably

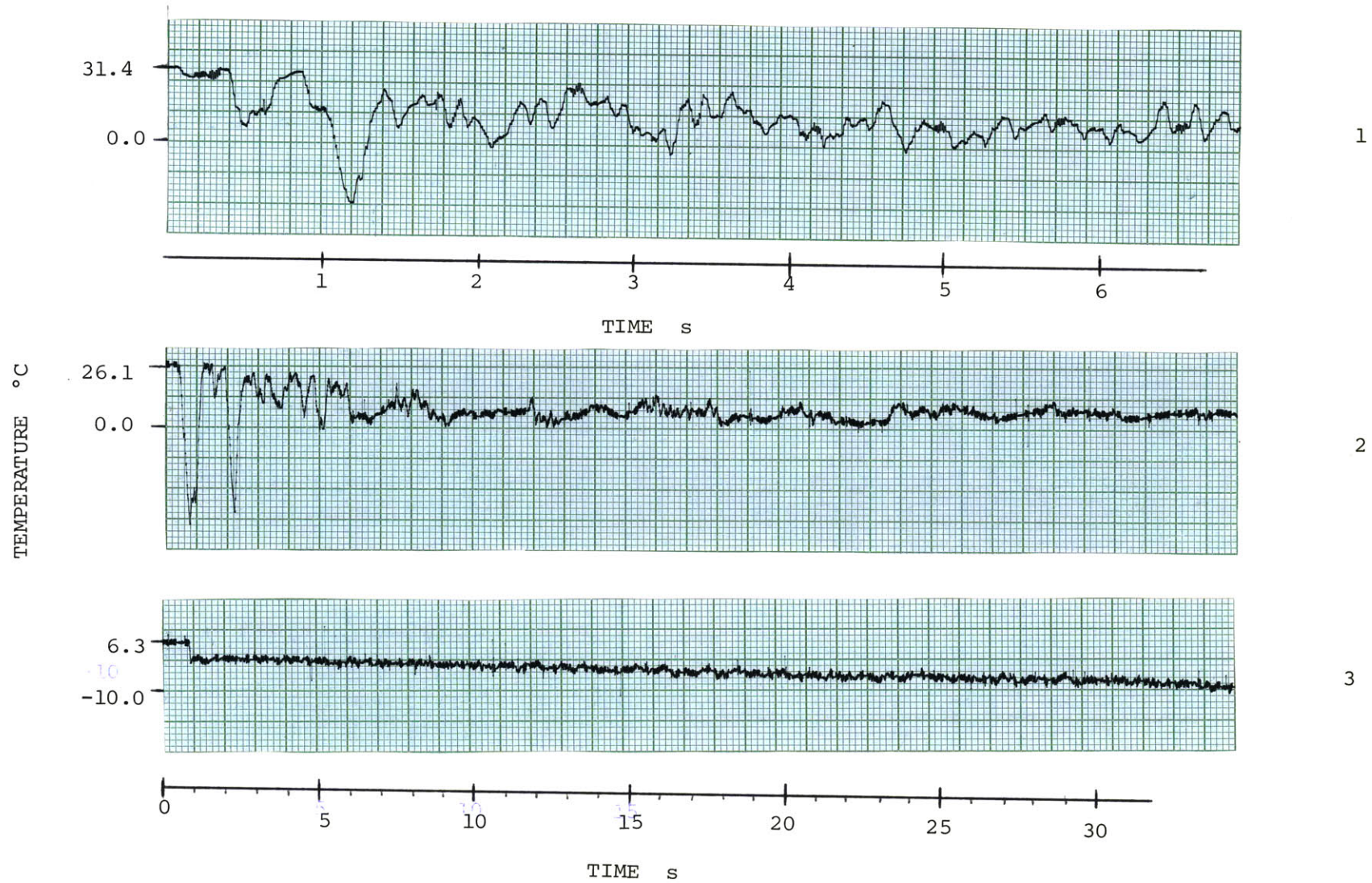


FIG. 4-39 TEMPERATURE FLUCTUATIONS IN WATER ON WHICH LIQUID NITROGEN BOILED

1. $T_w(\text{initial}) = 31.4^\circ\text{C}$, $z = 0.0$ mm (at the surface) (181)
2. $T_w(\text{initial}) = 26.1^\circ\text{C}$, $z = 0.5$ mm (below surface) (216)
3. $T_w(\text{initial}) = 6.3^\circ\text{C}$, $z = 1.0$ mm (below surface) (222)

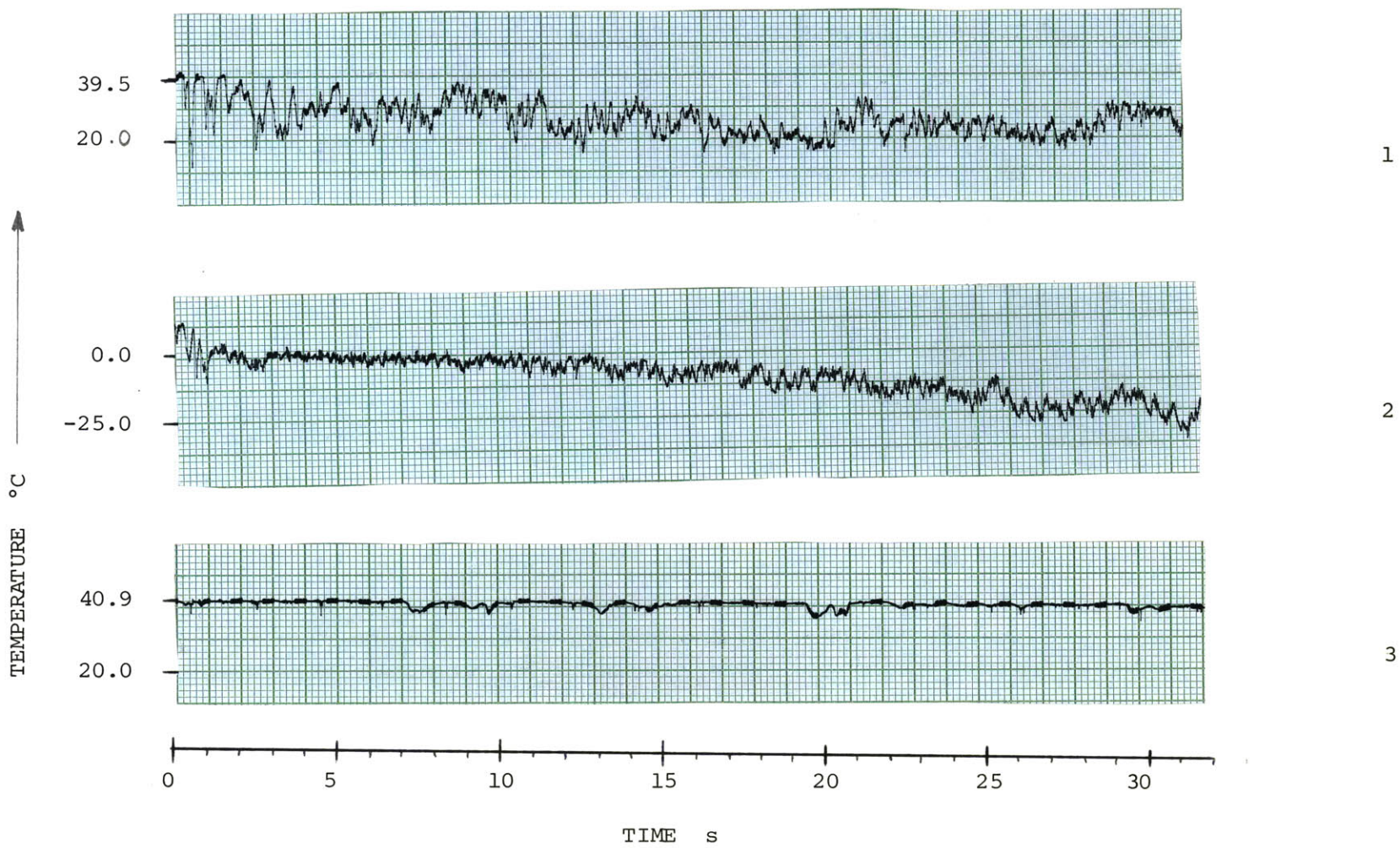


FIG. 4-40 TEMPERATURE FLUCTUATIONS IN WATER ON WHICH LIQUID METHANE (99.98%) BOILED

1. $T_w(\text{initial}) = 39.5^\circ\text{C}$, $z = 0.0$ (at the surface) (211)
2. $T_w(\text{initial}) = 15.0^\circ\text{C}$, $z = 0.0$ (at the surface) (214)
3. $T_w(\text{initial}) = 40.85^\circ\text{C}$, $z = 6.0$ mm (below surface) (158)

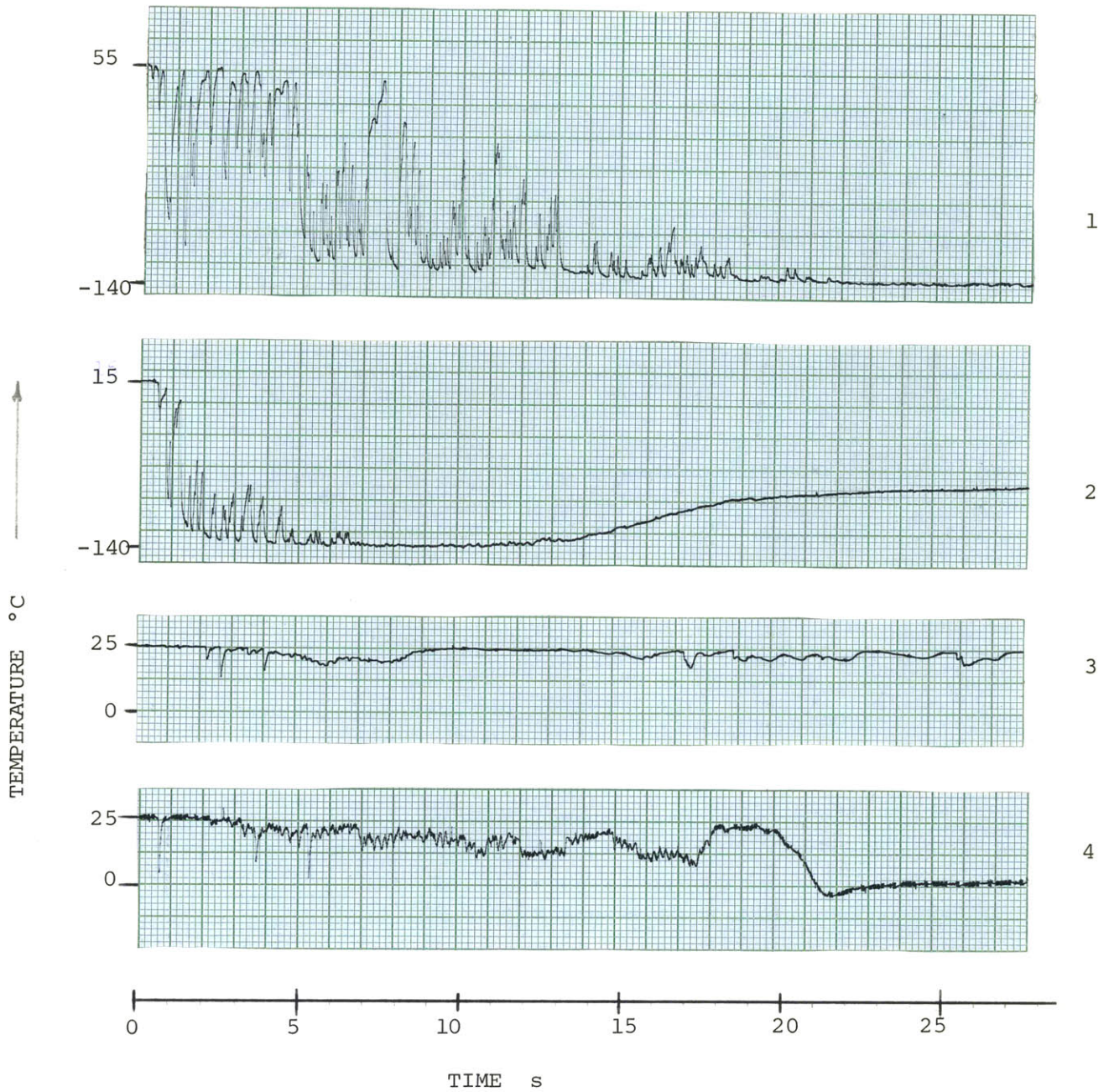


FIG 4-41 TEMPERATURE FLUCTUATIONS IN WATER ON WHICH LIQUID NATURAL GAS BOILED

1. T (initial) = 55.0°C, $z = 0.0$ mm (at surface) (197)
2. T_w (initial) = 15.9°C, $z = 0.0$ mm (at surface) (205)
3. T_w (initial) = 25.4°C, $z = 1.8$ mm (below surface) (208)
4. T_w (initial) = 27.5°C, $z = 1.4$ mm (below surface) (232)

and a low surface temperature is quickly achieved.

Temperatures measured about 1.8 mm below the water surface in run 208, Figure 4-41-3, indicated only minor disturbances when LNG with 82.0% methane boiled over-head. The disturbance was, however, more pronounced when a two-component LNG mixture boiled on the water, as shown in Figure 4-41-4.

In runs with pure ethane, water (ice) surface temperatures of $-84 \pm 5^{\circ}\text{C}$ were always recorded within 5 seconds of contacting ethane with water (initial temperatures $< 60^{\circ}\text{C}$).

4.6 SUMMARY OF RESULTS

The results of the boil-off rate study can be summarized as follows:

1. The initial water temperature has little or no effect on the vaporization rates of cryogenic liquids.
2. Cryogenic hydrocarbon liquid boil-off rates are independent of the amount of liquid spilled. Vaporization rates of liquid nitrogen, however, is significantly influenced by the amount of nitrogen spilled.
3. Trace quantities of higher alkanes (ethane, propane and the butanes) added to liquid methane significantly enhance the boil-off rates of the latter.
4. The vapors departing pools of cryogenics film boiling on warm surfaces are superheated, although the degree of superheat measured depends on the amount of liquid cryogen in the pools.

5. While liquid nitrogen and pure methane boiled away, the mean water-surface temperature was maintained above 0°C. Ethane- and LNG-water interfaces, however, indicate very low temperatures; as measured by ice-encapsulated surface-thermocouple beads.

CHAPTER 5

DISCUSSION OF RESULTS

- 5-1 INTRODUCTION
- 5-2 MODELS OF THE BOILING PROCESS
- 5-3 HEAT FLUXES ACROSS WATER-CRYOGEN INTERFACES
- 5-4 DISCUSSIONS
- 5-5 COMPARISON OF RESULTS WITH PREVIOUS WORK

5-1 INTRODUCTION

The results of the study are examined in this chapter. First, mathematical models of the boiling processes are introduced. These models are primarily on the formation of small bubbles in nucleate boiling, and on film boiling. Next, the fluxes evaluated from the foregoing data are presented. In the discussion that follows, the data are analyzed, and the various photographic observations, together with the models are employed to elucidate the general phenomena of liquid-liquid boiling.

Finally, the results are compared with previous work on the boiling of cryogenics on water and, the differences and similarities are emphasized.

5-2 MODELS OF THE BOILING PROCESS

The events after a cryogenic liquid is spilled on water may be as described in the following.

Although the temperature difference between the liquids (separated) is large, usually much larger than the minimum ΔT for film boiling, it is believed that the liquids directly contact each other (at least partially) after layering. That is, film boiling is not instantaneously initiated in the system. Wehmeyer and Jackson (1972) obtained data that illustrate this fact. They noted that a wire, heated to $900-1100^{\circ}\text{C} \pm 20^{\circ}\text{C}$ in $145 \mu\text{s}$ while immersed in water, initially formed discrete bubbles as in nucleate boiling. Stable film boiling was not attained until after 1 ms.

Furthermore, Bradfield (1966) photographically showed that boiling liquid-heating surface contacts may be obtained in stable film boiling, i.e. even after the bodies were separated by a vapor layer. His pictures show a vaporizing water drop intermittently touching a heated mirror-smooth chromium plate when a ΔT of $\sim 240^\circ\text{C}$ existed between the drop and the plate.

In the present problem, the superposed liquids approximate two semi-infinite fluid bodies at different temperatures suddenly brought together. Heat is conducted across the interface and temperature profiles may develop within the bodies. The interface instantaneously attains a temperature, T_i , estimated with (Eckert and Drake, 1973): #

$$\frac{T_i - T_{10}}{T_{20} - T_{10}} = \frac{k_1 \sqrt{\alpha_2}}{k_1 \sqrt{\alpha_2} + k_2 \sqrt{\alpha_1}} \quad (5-1)$$

where T_{10} and T_{20} are the bulk liquid temperatures, k_1 the thermal conductivity and α , the thermal diffusivity of the liquids.* The conduction temperature profiles in the bodies are given by

$$\frac{T_1(x,t) - T_{10}}{T_{20} - T_{10}} = \frac{1}{1 + \theta} (1 + \theta \operatorname{erf} \eta_1) \quad (5-2)$$

and

$$\frac{T_2(x,t) - T_{10}}{T_{20} - T_{10}} = \frac{1}{1 + \theta} (1 - \operatorname{erf} |\eta_2|) \quad (5-3)$$

where

$$\theta = \frac{k_2}{k_1} \left(\frac{\alpha_1}{\alpha_2} \right)^{1/2}$$

*For water initially at 40°C and liquid nitrogen at -196°C , T_i is approximately -15.5°C . # see footnote next page.

$$\text{and } \eta_i = \frac{x}{\sqrt{(4\alpha_i t)}} \quad , \quad x = 0 \text{ at interface}$$

$$(i= 1,2) \quad \eta_1 > 0$$

$$\eta_2 < 0$$

The heat flux

$$q' = \frac{\theta}{1 + \theta} \frac{k_1 (T_{20} - T_{10})}{\sqrt{\pi\alpha_1 t}} \quad (5-4)$$

is very large for short times.

Soon after contacting, bubbles begin to form at the interface, especially on dust particles initially present on the water. If the nucleated bubbles are many and near each other, they may merge and film boiling results.

It should perhaps be stressed that the total time from liquid-liquid contact to film boiling may be extremely short, possibly of the order of 1 ms as obtained by Wehmeyer and Jackson (1972).

The photographs presented in Chapter 3 show that very many small bubbles were produced when cryogenic mixtures contacted water. No such small bubbles were noted for single-component liquids. This may be tentatively explained if the bubbles produced on initial contact (between the liquids) were bigger in pure cryogenic liquids than in mixtures. Sufficiently big bubbles are bouyant and not retained near the liquid-liquid interface. The pictures also reveal a fog at the cryogenic liquid mixture-water interface (and it usually obscured the small bubbles). Moreover, the bubble population density decreased with time. Both of these factors suggest that, with mixtures, film boiling was the heat transfer mode between the liquids after the small

footnote. It is more convenient in the analysis to ignore the interfacial temperature modifications by convective flows. Hence,

bubbles were formed initially. As will be described later, much higher heat fluxes were obtained with mixtures than with single component liquids at comparable saturation boiling temperatures.

It is believed that the small bubbles provide the clue to interpreting the enhanced heat fluxes. Bubble sizes may be important. In sections 5-2-1 to 5-2-3, the existing equations (in the literature) on the growth rates of bubbles are briefly surveyed, and the reasons why bubbles formed in mixtures are smaller than those in single-component liquids are explored. Then concentration profiles at the wall of a single bubble growing under isothermal conditions in a mixture are sought. The concentration boundary layer thickness may indicate the maximum inter-bubble spacing for adjacent bubbles to coalesce. For separations larger than the maximum, convective flows could be maintained between the bubbles to keep them separated. Thus the onset of film boiling is delayed. (A hypothesis on how production of the small bubbles result in large heat fluxes is presented in section 5-4.)

In section 5-2-4, the existing theories on heat transfer during film boiling are reviewed. Modifications are proposed for the correlation introduced by Berenson (1960, 1961) on film boiling for comparison with the present work.

5-2-1 BUBBLE GROWTH THEORIES

Existing theories deal primarily with the spherically symmetric growth of a single bubble in an infinite body of a liquid at rest. It is generally recognized that a bubble grows in three stages:

 equation 5-1 is preferred to equation 4-16. Besides, equation 4-16 may not be applicable when water (which is less viscous than glycerol and hence capable of more convective motion) is used.

1. The inception or formation of an embryo (a process thermodynamically defined).
2. An early growth of the embryo. (This is a dynamic process controlled by the pressure forces, surface tension and inertia of the liquid.)
3. A late or asymptotic growth stage which is diffusion controlled. The supply of latent heat of evaporation by conduction and convection from the liquid bulk to the expanding bubble walls limit the bubble growth rates. Diffusion of material is also important in liquid mixtures.

Only the latter two stages are of interest in the present^e work.
k

Survey of Literature

Equations describing the growth of a single spherical bubble has been formulated by Plesset and Zwick (1945), Scriven (1959) and Skinner (1963) among others. Solutions to the equations have, however, been sought mostly for the asymptotic growth stage. The available solutions agree very well with the experimental data of Dergarabedian (1953, 1960) and van Strahlen (1967, 1968).

The pertinent equations and boundary conditions describing the growth of a single bubble are presented in the complete forms in Table 5-1. Equations 5-7 and 5-9 are employed only when liquid mixtures are involved.

The complete set of equations has not been solved, but solutions exist when simplifying assumptions are made, especially in

TABLE 5-1*

BUBBLE GROWTH EQUATIONS

A. Equation of motion (Scriven, 1959, 1962)

$$RR'' + \left(2 - \frac{\varepsilon}{2}\right) R'^2 + 4v\frac{R'}{R} = \frac{P(R) - P_\alpha}{\varepsilon\rho_L} \quad (5-5)$$

where $P(R) = P_b - \frac{2}{R} \left(\sigma + 2K\frac{R'}{R}\right)$ (5-5a)

B. Energy equation (no sources)

$$\frac{\delta T}{\delta t} = \alpha \left(\frac{\delta^2 T}{\delta r^2} + \frac{2}{r} \frac{\delta T}{\delta r} \right) - \frac{\varepsilon R' R^2}{r^2} \frac{\delta T}{\delta r} \quad (5-6)$$

C. Material balance on the more volatile component of a binary mixture (no chemical reaction)

$$\frac{\delta x_A}{\delta t} = D_{AB} \left(\frac{\delta^2 x_A}{\delta r^2} + \frac{2}{r} \frac{\delta x_A}{\delta r} \right) - \frac{\varepsilon R' R^2}{r^2} \frac{\delta x_A}{\delta r} \quad (5-7)$$

Equations (5-5) to (5-7) must satisfy the following boundary conditions:

$$4\pi R^2 k \frac{\delta T(R, t)}{\delta r} \Big|_{r=R} = \sum_i \Delta H_{v_i} \frac{dm_i}{dt} + \Delta H_{\text{mixing}} \frac{dm}{dt} + \frac{\delta(mC_p T)}{\delta t} \quad (5-8)$$

where $m = 4/3\pi R^3 \rho_V$

and $m_i = y_i m$ (y_i is mass fraction of component i inside the bubble)

$$-4\pi R^2 \rho_L D \left. \frac{\delta x_A}{\delta r} \right|_{r=R} = x_A \frac{dm_B}{dt} - x_B \frac{dm_A}{dt} \quad (5-9)$$

(x_A or x_B is the mass fraction of component A or B in the liquid)

Other conditions include the initial bubble size and the bulk fluid temperatures and concentrations.

the asymptotic growth regime. Most solutions (e.g. Plesset and Zwick, 1954) assume the existence of a thermal or concentration boundary layer around a growing bubble, negligible viscous effects, zero bubble translational velocity, no temperature or concentration gradients within the bubble, negligible compressibility effects due to rapid growth, and thermal equilibrium between the bubble contents and surrounding wall. Moreover, a bubble is assumed to grow as a result of (and controlled by) heat and/or mass transfer from the surrounding superheated liquid, across the growing boundary layer.

Single-Component Liquids

Bošnjakovic (1930) derived the equation for growth of a bubble as:

$$k \frac{\delta T(R, t)}{\delta r} = \rho_v \Delta H_v R' \quad (5-10)$$

where the temperature profile is assumed to be the same as obtained in transient heat conduction into a semi-infinite body, with a constant temperature (different from the bulk) suddenly imposed upon the plane boundary. (This eliminates the necessity of solving Equation (5-6).) Equation (5-10) means simply that the heat conducted from the bulk liquid to the bubble boundary (which is at the liquid's boiling point) is entirely applied for vaporization and, therefore, bubble growth. For the semi-infinite body (Carslaw and Jaeger, 1959):

$$\left. \frac{\delta T}{\delta z} \right|_{z=0} = \frac{\Delta T}{\sqrt{\pi \alpha t}} \quad (5-11)$$

Hence, if the bubble curvature is neglected,

$$\frac{\delta T(R, t)}{\delta z} = \frac{\Delta T}{\sqrt{\pi \alpha t}} \quad (5-12)$$

and the bubble radius is given by

$$R(t) = \left[\frac{2k\Delta T}{\Delta H_V \rho_V (\pi \alpha)^{1/2}} \right] t^{1/2} \quad (5-13)$$

i.e. the bubble radius $R(t)$, ($= Kt^{1/2}$), is proportional to $t^{1/2}$.

Plesset and Zwick (1952, 1954) presented a more comprehensive, but still approximate, solution based on a perturbation technique. Lagrangian transformations of the equations of motion and thermal diffusion were carried out. The zeroth-order solution of the unsteady state temperature profiles (Equation (5-6), after transformation) was employed to estimate the term $\frac{P(R) - P_\alpha}{\epsilon \rho_L}$ in Equation (5-5) (equilibrium was always assumed between the bubble walls and the vapor within the bubble, and the surface dilational viscosity* term was not considered). The leading term of the asymptotic solution of Equation (5-5) gave

*The significance of this term was pointed out in subsequent studies by Scriven (1960, 1962).

$$R(t) \approx \sqrt{3} \left[\frac{2k\Delta T}{\Delta H_V \rho_V (\pi\alpha)^{1/2}} \right] t^{1/2} \quad (5-14)$$

This equation is different from Equation (5-13) only by the constant $\sqrt{3}$.

Forster and Zuber (1954) derived another approximate solution by considering the walls of the expanding bubble to constitute a spherical heat sink. The bubble wall temperatures (always equal that of the vapor) were obtained as a time-variable by an integration of the Green's function. The derivation of the bubble wall temperature-time relation implicitly involved the concept of discontinuous bubble growth. The final solution for the late or asymptotic growth stage was given by:

$$R(t) \approx \frac{\pi}{2} \left[\frac{2k\Delta T}{\Delta H_V \rho_V (\pi\alpha)^{1/2}} \right] t^{1/2} \quad (5-15)$$

The early growth of the bubble from a critical embryo radius R_0 , requires that a thermal or kinetic impulse be present. If a constant local heat flux, Q' is supplied for the short early growth duration, and the hydrodynamic forces on the bubble growth are neglected, the early growth rate is given by

$$R(t) \approx \frac{1}{\sqrt{2}} \left[\frac{\sigma Q'}{\rho_L^2 C_p R_0 \Delta T} \right]^{1/2} t^{3/2} \quad (5-16)$$

$$\text{or} \quad \approx \frac{1}{2} \left[\frac{\rho_v \Delta H_v Q'}{2 C_p T_{bpt}} \right]^{1/2} t^{3/2} \quad (5-17)$$

R_0 is the initial stable-equilibrium bubble radius, and the Clausius-Clapeyron equation has been applied to obtain Equation (5-17) from (5-16). It is seen from Equation (5-17) that the early growth rate estimated from Forster and Zuber's analysis is independent of the superheat in the liquid.

Scriven (1959) presented exact solutions for the asymptotic growth stage based on a similarity analysis of the boundary value problem. His final expression, for a moderate superheating of the liquid ($\Delta T \geq 0.25^\circ\text{C}$), is identical with the zero-order solution of Plesset and Zwick (1954), Equation (5-14).

It should be noted from the foregoing that the asymptotic solutions to the equations in Table 5-1, as derived by Plesset and Zwick (1954), Forster and Zuber (1954) and Scriven (1959), differ only by a multiplier ($\sqrt{3}$ or $\pi/2$) from Equation (5-13) more simply derived by Bošnjakovic (1930).

Bubble Growth in Liquid Mixtures

The rate of growth of a single bubble in a pure liquid (uniformly superheated) is controlled, in the asymptotic stage, by heat fluxes towards the bubble walls. In mixtures, both mass flux of the mixture components and heat fluxes are important. The more volatile component is rapidly and continuously depleted from the boundary as

the bubble expands, and a concentration profile develops within the liquid adjacent to the wall.

Van Wijk, Vos and van Strahlen (1956) proposed that the early growth of a bubble occurs discontinuously by flash vaporization in the superheated liquid mixture. At the end of this growth stage, both thermal and concentration equilibrium exist between the bubble wall and vapor within. The final bubble wall temperature, T_b , (the same as the dew temperature of the vapor), is less than the temperature of the superheated bulk, T_α , but higher than the saturation boiling point of the mixture, $T_{bp_{mix}}$. The difference, $T_\alpha - T_b$, is the superheat available for further bubble growth in the asymptotic stage. Van Wijk et al. pointed out that, for a binary mixture, $T_\alpha - T_b$ attains a minimum (or $T_b - T_{bp_{mix}}$, a maximum) particular at a low concentration of the more volatile component. Hence, they suggest that the subsequent bubble growth rates will be a minimum at this concentration. The corollary is that, after a specified asymptotic bubble growth period, the bubbles with the highest T_b at the start of the late growth stage will also have the smallest diameters. The radii of the bubbles formed at the end of flash vaporization was implicitly assumed constant, or even zero. ρ Scriven (1959) was first to quantitatively describe bubble growth in mixtures. Considering the asymptotic growth state to be controlled by the combination of heat and mass transfer, he showed that an exact similarity solution can be found for a binary mixture with constant initial temperature and composition. He presented a solution valid for moderate superheats

as: $R(t) = 2\beta(\alpha t)^{1/2}$ (5-18)

where

$$\beta = \left(\frac{3}{\pi} \right)^{1/2} \left(\frac{\Delta T}{\frac{\rho_V}{\rho_L} \left(\frac{\Delta H_V}{C_{PL}} - \left[(m_A \rho_L - C_{A\alpha}) \left(\frac{\alpha}{D_{AB}} \right)^{1/2} \right] \left| \frac{\delta C_A}{\delta T} \right|_P \right)} \right)$$

$$\left. \frac{\delta C_A}{\delta T} \right|_P \approx \frac{-C_{A\alpha} \Delta H_{VA} [M_B C_{A\alpha} + (\rho_L - C_{A\alpha}) M_A]}{\rho_L R T_{sat}^2} \left[\frac{1 + \alpha \ell}{1 - \alpha} \right]$$

$$\alpha = \gamma_B P_B / \gamma_A P_A \quad (\text{relative volatility})$$

and $\ell = \left\langle \Delta H_{VB} (\rho_L - C_{A\alpha}) \right\rangle / \Delta H_{VA} C_{A\alpha}$

(γ_A or γ_B is activity coefficient)

For water-ethylene glycol mixtures, he showed that β attains a minimum with about 5% by weight of water present in the bulk liquid, i.e. $C_{A\alpha} = 0.05$. At this composition, water is rapidly depleted from the bubble boundary, while at the same time, the wall temperature has been sufficiently depressed below the bulk liquid's and vaporization of the glycol occurs relatively more slowly. Again, the initial bubble diameter was taken to be zero.

Bubble growth rates in mixtures are further slowed down in the asymptotic stage if the bubbles are crowded, and inter-bubble spacing is of the order of the concentration boundary layer thickness. The experiments of Luborsky (1957) on the growth of a large population of spherical iron crystallites in mercury (a liquid-solid system) show

that the spheres grew at rates given by:

$$\frac{dR}{dt} \propto (1 - P^{1/3}) \quad (P \text{ is volume fraction of iron crystallites})$$

and $R^{4.4} \propto t$

These represent considerably slower growth rates than predicted for single bubbles (Scriven, 1959). It is not an unexpected growth rate since the concentration driving force decreases as material was depleted from the interstices between adjacent crystallites. The exact relation obtained may only have been predicted, however, if the lattice distribution of the growing spherical bodies is provided.

Van Strahlen (1968, pt II) showed a similar effect of the depletion of a mixture component on the growth rates of swarms of bubbles.

5-2-2 SURFACE TENSION EFFECTS ON BUBBLE GROWTH

The theories presented in Section 5-2-1 were on the asymptotic stage of the growth of single bubbles within slightly superheated liquids. The diameter of the bubbles at the start of this stage of growth were assumed small, sometimes negligible. However, the photographs presented by van Strahlen (1968) may be interpreted to suggest that this is not the case. Bubbles which grew on a heated horizontal wire ($T_{\text{wire}} \sim T_L + 20^\circ\text{C}$) immersed in slightly superheated boiling liquids, i.e., liquids at temperatures 0.2 to 1°C above the boiling point, attained large diameters in very short times after inception. About 50 to 80% of the bubble diameters at 10 ms after formation appear to have been realized within the first 0.2 ms. This is a period which includes the early growth stage during which forces on the bubbles primarily control the growth rates.

Furthermore, bubble diameters, after this initial rapid growth, were smaller in 'positive' liquid mixtures than in pure liquids, e.g., the Ketone-water mixtures used by van Strahlen (1968, pt II). The small bubble sizes have generally been attributed to heat/mass transfer rate limitations at the bubble walls. The assumption of diffusion control is the basis for the solutions presented earlier. The analysis of Plesset and Zwick (1954) included an examination of the regimes at which the dynamics or heat transfer effects are predominant. In the paper, they treated variations in liquid surface tension as negligible.

In this section, a simple tentative analysis is presented on the effects of surface tension variations on the growth rates of a single bubble. Any effects should be primarily exhibited in the early growth periods of dynamic control in the real situation. An increase in surface tension forces at a growing bubble boundary would have the effect of slowing down the growth rate, in addition to the heat/mass transfer rate limiting effects. Time-dependent surface tension may be realized for a bubble growing in a 'positive' mixture, such as LNG.*

Here, only the equation of motion and the appropriate forces are considered. The bubble is assumed to be spherical and located in an inviscid fluid. Compressibility effects are neglected. Neither the diffusion of material or energy is allowed to limit the growth of the bubble.

The pertinent growth equation is:

$$RR'' + \frac{3}{2} R'^2 = \frac{P(R) - P_\alpha}{\rho_L} \quad (5-19)$$

where

$$P(R) - P_\alpha = P_b - P_\alpha - \frac{2\sigma(X_A)}{R}$$

*e.g., for a binary methane-ethane mixture, the effective surface tension, σ , could be as high as 0.028 N/m, i.e., σ for ethane (Figure 3-11) is extrapolated to -161.5°C .

i.e., the term $2K\frac{R'}{R}$ in Equation (5-5a) has been neglected, and σ is a function of composition.

The problem may be further simplified if the bubble growth is assumed to be isothermal and the other mixture components non-volatile. These assumptions appear to be approximate for cryogenic hydrocarbon mixtures. As shown in Figure 5-1, the saturation temperatures of LNG slowly decreased with methane fraction until the mixture contained less than 40 mole % methane. Moreover, at $T = -160^\circ\text{C}$, the vapor pressure of ethane, the next most volatile alkane, is only 1 mm Hg.

Equation (5-19) becomes on substituting for $P(R) - P_\alpha$

$$RR'' + \frac{3}{2} R'^2 + \frac{2\sigma(X_A)}{\rho_L R} = \frac{\Delta P}{\rho} \quad (5-20)$$

Two further assumptions are made to make Equation (5-20) tractable. The first is that ΔP acting counter to bubble growth is a constant.* The second is that the bubble wall instantaneously attains and maintains a constant surface concentration (not necessarily in equilibrium with the vapor). This is logical if one remembers that the bubble growth rate is much faster than the rate at which the vaporized component is replenished by convective and diffusion processes. Hence,

*Both this pressure difference and surface tension forces oppose the bubble growth which is initiated by an impulse. The impulse may be kinetic (inertia of the liquid) or thermal (Gibson, 1972). The bubble pressure is assumed constant and slightly less than the external value.

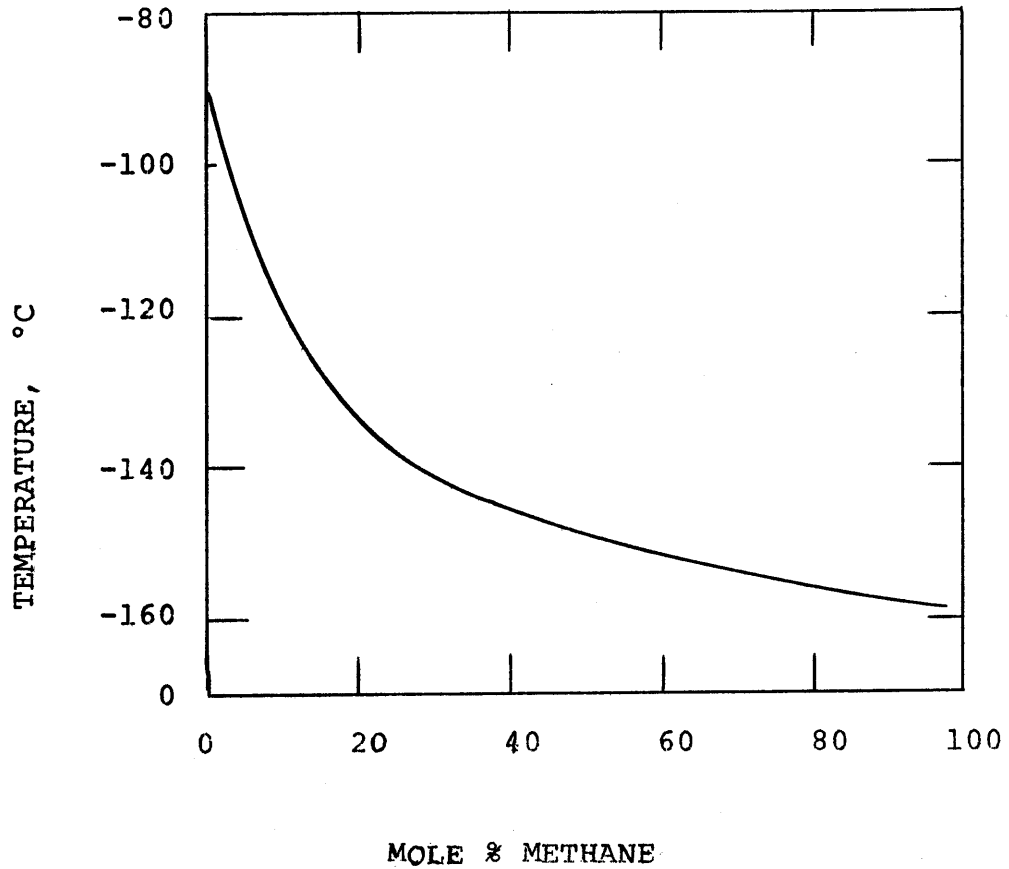


Fig. 5-1

Saturation Temperatures of LNG (primarily methane and ethane) As a Function of Composition.
(derived from the data of Enger and Hartman, 1972)

the lining of the bubble wall will contain essentially the non-volatiles. The flux of material, determined by the concentration gradient at the wall is, however, sufficiently high that the transport process is non-limiting. The assumption of a constant X_A is made to keep $\sigma(X_A)$ constant. (Note: $\sigma(X_A)$ depends on the mixture constituents, the ratios of these constituents, and temperature.)

For $P(R) - P_\alpha$ equals zero, a trivial solution is

$$R = \text{a constant}$$

i.e., $R' = R'' = 0$, and the bubble exists in stable equilibrium. In general,

$$R(t) = (K_1 t + K_2)^{2/5}$$

where K_1 and K_2 are constant.

For $\Delta P = 0$, i.e., only surface tension retards the bubble growth, Equation (5-20) can be integrated to give

$$R'^2 = \frac{2\sigma}{\rho_L} \left[\frac{R_f^2 - R^2}{R^3} \right] \quad (5-21)$$

where $R = R_f$ when $R' = 0$

For $\sigma = 0$, Equation (5-20) becomes the Rayleigh equation, and

$$R'^2 = - \frac{2}{3} \frac{\Delta P}{\rho_L} \left[\frac{R_f^3 - R^3}{R^3} \right] \quad (5-22)$$

The general first level integration of Equation (5-20) is approximately given by:

$$R'^2 = \frac{2\sigma}{\rho_L} \left[\frac{R_f^2 - R^2}{R^3} \right] - \frac{2}{3} \frac{\Delta P}{\rho_L} \left[\frac{R_f^3 - R^3}{R^3} \right] \quad (5-23)$$

where $R = R_f$ when $R' = 0$ at $t = \tau_f$. The implication of the condition is that the bubble growth stops at τ_f which marks the beginning of the asymptotic stage. This is not true. But a comparison of the bubble diameters during the early and asymptotic growth stages (van Strahlen, 1968; Fig. 9, 12, pt II) shows that the rates of growth differ considerably. Hence, $R' = 0$ at $t = \tau_f$ is a fair approximation for the boundary condition.

Equation (5-23) can be transformed with $\psi = R/R_f$ into

$$\psi'^2 = \gamma^+ \left[\frac{1 - \psi^2}{\psi^3} \right] + \phi \left[\frac{1 - \psi^3}{\psi^3} \right] \quad (5-24)$$

where

$$\gamma^+ = \frac{2\sigma}{\rho_L R_f^3} \quad \text{and} \quad \phi = - \frac{2}{3} \frac{\Delta P}{\rho_L R_f^2}$$

Equation (5-24) can be re-written as

$$\psi'^2 = \frac{\phi}{\psi^3} \left[(1 - \psi^2)\gamma^+ + (1 - \psi^3) \right] \quad (5-25)$$

where

$$\gamma = \frac{\gamma^+}{\phi} = - \frac{3\sigma}{\Delta P R_f}$$

This equation satisfies the conditions

$$\psi(0) = 0, \quad \psi(\tau_f) = 1 \quad \text{and} \quad \psi'(\tau_f) = 0$$

Hence,

$$-\phi^{1/2} t = \int_0^{\psi} \frac{\psi^{3/2} d\psi}{\left[(1-\psi^2)\gamma + (1-\psi^3) \right]^{1/2}} \quad (5-26)$$

The integral in Equation (5-26) has been evaluated and plotted in Figure 5-2 for 3 values of γ . The abscissa is negative since the plot actually shows the bubble history for a 'virtual' impulse* for growth. Calculations show that, for a given ΔP or $\phi^{1/2}$, the growth period (up to 0.99ψ max.) for $\gamma = 5$ is less than half that for $\gamma = 0$ (i.e., $\sigma = 0$, or R_f and ΔP infinitesimal).

It may therefore be concluded that if bubbles grow faster in pure liquids than in mixtures due to the smaller net growth retarding force and, as just shown above, the early growth duration decreases as the surface tension increases, much larger bubbles could be formed in pure liquids than in mixtures. Unfortunately, the values

*Both the surface tension forces and pressure act counter to this impulse.

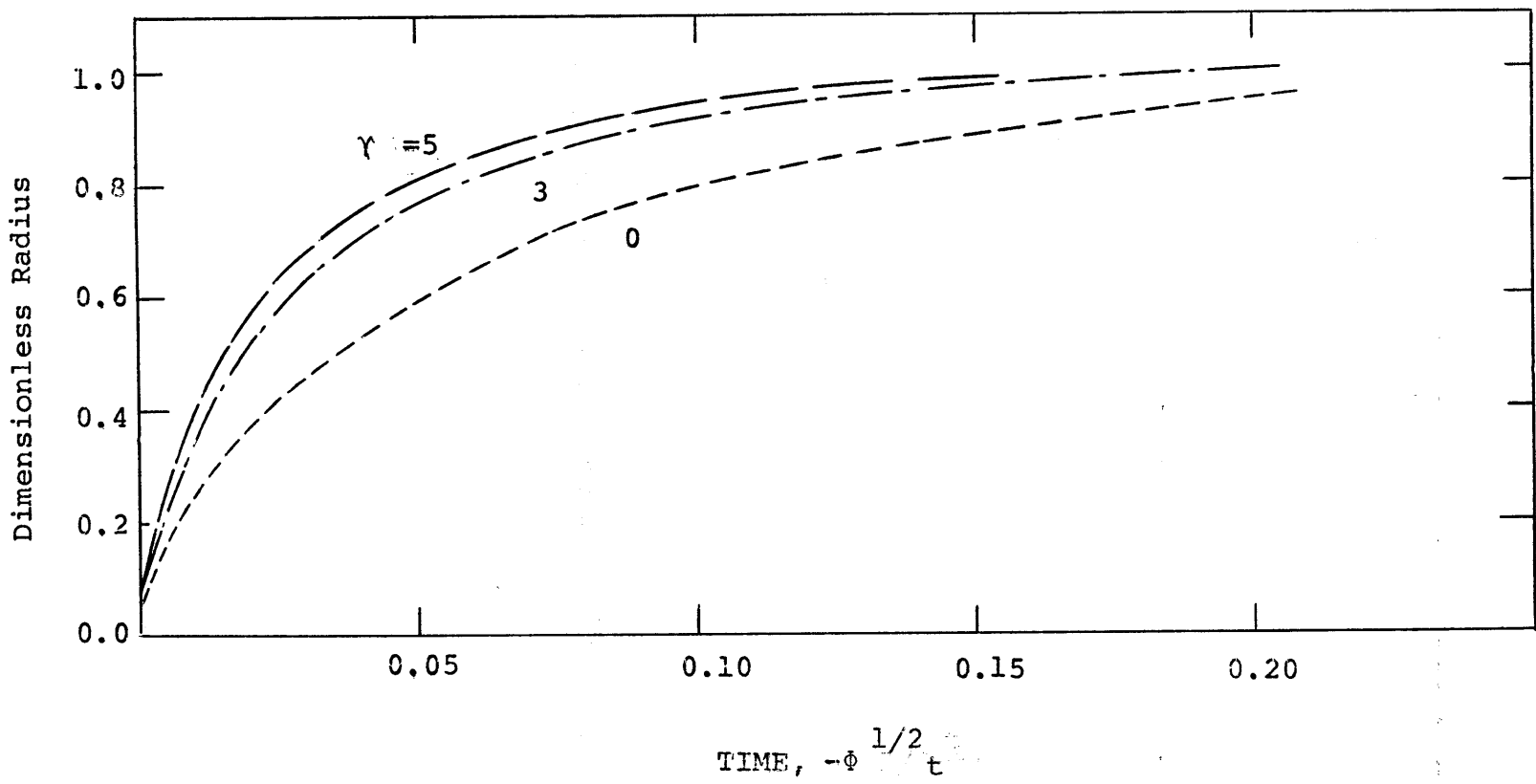


FIG. 5-2

Dimensionless Bubble Radius (R/R_f) vs. Time

of ΔP for boiling in saturated liquid mixtures are not available in the literature, so that the relative ratios of R_f (pure liquids: mixtures) cannot be compared. Photographic data on bubble radii in the early stages will also be helpful.

A more complete analysis of the growth of a bubble requires that a solution be found for the coupled dynamic and diffusive processes. Experimental data on transient concentration and temperature profiles, and surface tension at the bubble boundary are needed.

It should, perhaps, be noted here that the interpretation to some results presented by Roll and Myer (1964) on surface tension effects on bubble sizes is contrary to that predicted in the preceding. Their experiments involved adding surfactants to water and measuring bubble growth rates, and break-off volumes. They reported that bubble volumes decreased as the static surface tension of the liquid decreased. Bubble growth times were also reported reduced as the surface tension was lowered.

Surfactants are, however, known to accumulate at interfaces (Davies and Rideal, 1963). In the dynamic process of bubble growth, a surface dilational viscosity or elasticity effect should, therefore, become important, (Scriven, 1960). That is, the term $2K\frac{R'}{R}$ may be quite large in Equation (5-5a). Thus, the 'effective' surface tension would be larger than in the absence of the surfactants. If their interpretations are disregarded, it may be quite possible to estimate the dilational viscosity coefficient, K , from experiments similar to theirs and a complete solution to Equation (5-5).



Room 14-0551
77 Massachusetts Avenue
Cambridge, MA 02139
Ph: 617.253.2800
Email: docs@mit.edu
<http://libraries.mit.edu/docs>

DISCLAIMER

**Page has been omitted due to a pagination error
by the author.**

(p.186)

5-2-2. CONCENTRATION PROFILES AROUND A GROWING BUBBLE

The concentration profile at the wall of a bubble growing under isothermal conditions is described by Equation (5-7) subject to the boundary conditions that

$$\begin{aligned} x_A &= x_{AS} && \text{a constant at the bubble wall} \\ \text{and } x_A &= x_{A\alpha} && \text{far from the bubble} \end{aligned}$$

This problem is similar to that of solid-liquid phase changes analyzed by Chambré (1956). If the growth of a spherical bubble, within a constant temperature environment is described by

$$R(t) = 2\beta\sqrt{Dt} \quad (5-27)$$

i.e. an asymptotic stage growth rate, a similarity concentration profile within the surrounding fluid, for Schmidt number (ν/D) equal unity, is given by:

$$\frac{x - x_{A\alpha}}{x_{AS} - x_{A\alpha}} \approx \frac{4}{\sqrt{\pi}} \frac{\left(\frac{\rho_L}{\rho_V}\right) \beta^3 e^{\beta^2 \xi_\eta}}{\left[\frac{2}{\sqrt{\pi}} + \left(\frac{\rho_L}{\rho_V}\right) \beta^3 e^{\beta^2 \xi_\beta}\right] \Lambda} \quad (5-28)$$

where $\xi_\eta = \frac{2}{\sqrt{\pi}} \frac{e^{-\eta^2}}{\eta} - 2[1 - \text{erf}(\eta)]$

ξ_β is the same with β substituted for η

$$\Lambda \approx \frac{2}{\sqrt{\pi}} + \left(\frac{\rho_L}{\rho_V}\right) \beta^3 e^{\beta^2} \left(\frac{2}{\sqrt{\pi}} \left[\frac{e^{-\beta^2}}{\beta} - \frac{e^{-\eta^2}}{\eta} \right] - 2[\operatorname{erf}(\eta) - \operatorname{erf}(\beta)] \right)$$

$$\eta = \frac{r}{2\sqrt{D}\tau}$$

and r is distance within the liquid measured from the bubble centroid.

The appropriate expression is considerably more complex if Schmidt number ($Sc = \nu/D$) is not unity. This is the case for diffusion within liquids. The concentration profile is, in such cases, evaluated from

$$\frac{x - x_{A\alpha}}{x_{AS} - x_{A\alpha}} \approx 2(Sc) \frac{\rho_L}{\rho_V} \left(\frac{2}{\sqrt{\pi}}\right)^{2(Sc)} \beta^3 e^{(Sc)\beta^2} \int_{\eta}^{\alpha} \Omega^{(Sc)} \frac{dt}{t^2} \quad (5-29)$$

where

$$\Omega \approx e^{-t^2} \left[\frac{2}{\sqrt{\pi}} + \frac{\rho_L}{\rho_V} \beta^3 e^{\beta^2} \frac{2}{\sqrt{\pi}} \int_{\beta}^{\eta} \frac{e^{-s^2}}{s^2} ds \right]^{-2}$$

It can be shown from these expressions that the thickness of the concentration boundary layer is given approximately by:

$$\delta \approx \left(4 - 2\beta \frac{\rho_V}{\rho_L}\right) \sqrt{D}\tau \quad (5-30)$$

Hence δ may be extremely small if the growth times are very short or β large. For the early growth rate not described by $R(t) = 2\beta\sqrt{D}\tau$, attempts to arrive at solutions for the concentration profiles by quadrature may not yield useful results. With $R(t)$ known, the concentration profiles could, however, be determined by involved numerical techniques.

For estimation purposes, one may assume that Equation (5-30) is obeyed with

$$\frac{\rho_v \beta}{\rho_L} \ll 2$$

Therefore, one obtains

$$\delta \approx 4\sqrt{Dt} \quad (D \sim 10^{-5} \text{ cm}^2/\text{s} \text{ in liquids})$$

If the time for growth of each bubble is chosen (arbitrarily) to be 1 ms, one obtains that the concentration boundary layer thickness is given by

$$\delta \sim 4 \mu\text{m}$$

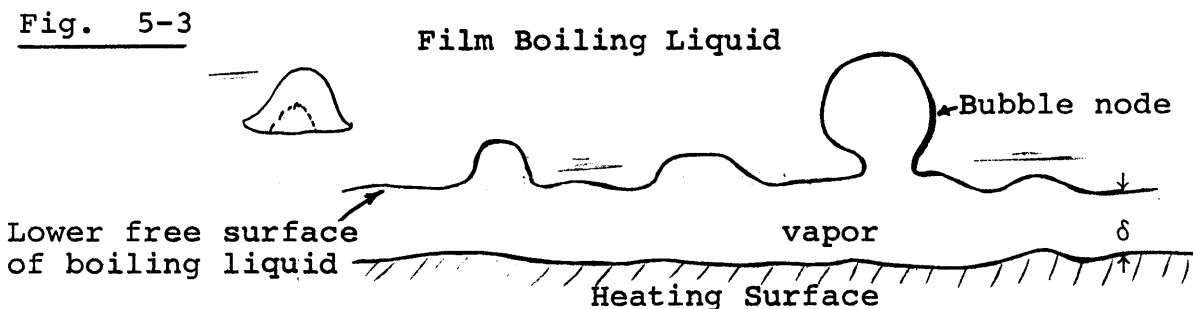
For bubbles formed on external surfaces, a concentration gradient may exist along the bubble wall due to the different life times of bubble surface segments. This gradient may cause convective flows in the neighborhood of the bubble.* The net effect is that bubbles separated by more than 4 μm may be prevented from coalescing by the liquid flow in the interstices. This is an extremely small separation distance.

*Such concentration induced flows were studied by Blair and Quinn (1969), Saville (1973) among others. The induced flows are commonly known as the "Marangoni" effect.

For bubbles formed at a cryogenic liquid mixture-water interface, a dense population of bubbles may, therefore, be required before film boiling is initiated. Such clusters can be seen in Figures 3-9 and 3-10. The generation of these bubbles most probably causes a local enrichment of the less volatile mixture component. To the enrichment process is attributed the high heat fluxes noted for mixtures. This point is further explained in section 5-4.

5-2-4 FILM BOILING THEORIES

As earlier indicated, film boiling appears to be a primary regime of heat transfer in the present work. The regime is characterized by a continuous vapor film which separates a boiling liquid from the heating surface when a high ΔT is applied (Figure 5-3).



Bromley (1950) presented the first correlation for stable film boiling. His geometry was a horizontal cylinder (diameter D) separated by a vapor film (thickness δ) from the boiling liquid. ($\delta/D \ll 1$) Heat was transferred across the film by conduction and radiation to evaporate the liquid. The vapor produced flowed under laminar condition

to the top of the cylinder where it formed bubbles. The problem solved, therefore, involved conduction, convection and radiative heat transfer. The final expression (after he solved the pertinent flow and energy equations) for an "effective" heat transfer coefficient is:

$$h = x \left[\frac{k_v^3 g \Delta H_v \rho_v (\rho_L - \rho_v)}{D \mu_v \Delta T} \right]^{1/4} \quad (5-31)$$

where x is 0.51 when the vapor-liquid boundary is assumed rigid, and 0.73 with no shear stress at the boundary. x was chosen to be 0.62 (the average).

This correlation was successfully shown to predict heat transfer rates from small tubes into liquid nitrogen, water, ethanol, benzene, carbon tetrachloride and diphenyl ether. The correlation should, however, fail when a wire whose diameter is of the same order of magnitude as the film thickness is used as heating element. This is because the assumed vapor flow in which heating surface curvature has been neglected is no longer satisfied (i.e., $\delta/D \sim 1$). When horizontal plates or large tubes are used, the problem also arises as to how D should be defined. The hydrodynamic instability theories subsequently developed on film boiling avoid these problems.

Taylor (1950) proved mathematically that the configuration in which the denser of two superposed fluids is above is dynamically unstable. A disturbance applied to this system will be continuously amplified. Bellman and Pennigton (1954) extended Taylor's analysis to include the effects of surface tension and viscosity. They found that

surface tension stabilizes the interface against the growth of disturbances with small wavelengths, and slows down the rate of growth of intermediate wavelength oscillations. Long waves are hardly affected. Viscosity retards the growth rates of all wave motions but the longest. Experiments by Lewis (1950), Allred and Blount (1954) and in more recent times have verified these instability analyses.

Chang (1956) and Zuber (1958) applied the stability analysis to film boiling. Zuber's approach involved an estimation the heat content of a bubble of typical diameter released from a plate or tube. The overall heat flux was obtained by multiplying the frequency of bubble production at a site, the inverse of the area associated with a bubble and the latent heat required to create the bubble. That is

$$\frac{q}{A} = \underbrace{\Delta H_v \rho_v \frac{4}{3} \pi \left(\frac{\lambda}{4}\right)^3}_{\text{bubble latent heat}} \underbrace{\frac{1}{\tau} \frac{2}{\lambda^2}}_{\substack{\text{inverse area of} \\ \text{bubble production} \\ \text{frequency}}} \quad (5-32)$$

where λ is the wavelength at the vapor-liquid interface, $\lambda/4$ is an approximate bubble radius, and τ is the period of bubble production from a site whose area is $\lambda^2/2$.

When the wavelength (at minimum film boiling) is given by its maximum value that can be completely stabilized by surface tension forces, i.e., according to Bellman and Pennigton (1954),

$$\lambda/2\pi = \left[\frac{\sigma}{g(\rho_L - \rho_V)} \right]^{1/2} \quad (5-33)$$

and the frequency of bubble release corresponds to the natural frequency of oscillation of the vapor-liquid boundary, i.e.,

$$\frac{1}{\tau} = \left[\frac{\sigma m^3}{\rho_L + \rho_V} \right]^{1/2} \quad (5-34)$$

where $m = 2\pi/\lambda$. Equation (5-32) becomes

$$\frac{q}{A} = \frac{\pi}{24} \Delta H_V \rho_V \left[\frac{\sigma g (\rho_L - \rho_V)}{(\rho_L + \rho_V)^2} \right]^{1/4} \quad (5-35)$$

Equation (5-35) does not include a ΔT , hence it may be valid only at the minimum film boiling point for which it was derived.

Variations of Equation (5-35) were also presented by Zuber.

Berenson (1960, 1961) combined parts of Zuber's concepts on hydrodynamic stability analysis and the conduction model of Bromley. He considered the vapor-liquid boundary near a horizontal heating plate to consist of stationary oscillations whose wavelenth correspond to that of the most unstable waves, i.e., the waves whose amplitude grow the fastest when a perturbation is applied to the boundary which was initially undisturbed. This critical wavelength was found by solving the general non-viscous equation of motion (Lamb, 1945) with an assumed first order perturbation equation

$$\eta = \eta_0 e^{-int} \cos mz \quad (5-36)$$

The solution (Milne-Thomson, 1956) is

$$\begin{aligned} m\rho_V(u_V - c)^2 \coth m\delta_V + m\rho_L(u_L - c)^2 \coth m\delta_L \\ = \sigma m^2 - g(\rho_L - \rho_V) \end{aligned} \quad (5-37)$$

where $c (= n/m)$ is the wave velocity. When both the vapor and liquid velocities (u_V and u_L) are neglected, and $m\delta_L$ and $m\delta_V$ are assumed large,* Equation (5-37) simplifies to

$$-in = \left[\frac{g(\rho_L - \rho_V)m}{\rho_L + \rho_V} - \frac{\sigma m^3}{\rho_L + \rho_V} \right]^{1/2} \quad (5-38)$$

The fastest growing wave corresponds to that with the largest growth constant, $-in$. Hence

$$n_c = \frac{2\pi}{\lambda_c} = \left[\frac{g(\rho_L - \rho_V)}{3\sigma} \right]^{1/2} \quad (5-39)$$

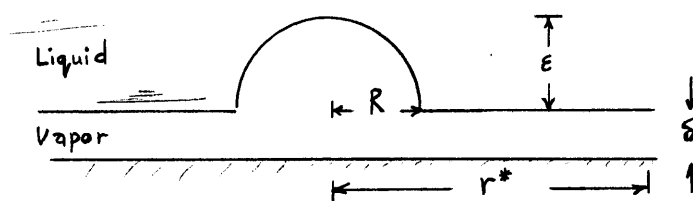
Similar to Zuber (1958), the area associated with each bubble is assumed equal $\lambda_c^2/2$, where λ_c is calculated from Equation (5-39). The equivalent boiling area associated with, and surrounding the base of each bubble is evaluated from

 *Since the vapor film thickness, δ_V , is $\sim 10^{-2}$ cm, it may not be immediately obvious why $m\delta_V$ can be assumed large. The wave profile (in 2-d) appears to be a trochoid with sharp crests (nodes) and flat troughs (antinodes). The vaporization process within the film supplies the vapor required for the expansion of a node. Furthermore, the average distance of the trough to the heating surface probably varies little, and, the growth of the node appears to be by a combination of an elastic

$$\pi r^*{}^2 = \lambda_c^2 / 2 \quad (5-40)$$

The model of a growing bubble is shown in sketch below.

An Idealized Growing Bubble Node



The next step involves the assumption that the bubble derives its vapor from an area equal $(\pi r^*{}^2 - \pi R^2)$ at the base of the node. Evaporation of the liquid occurs by conduction across the film and the vapor is convected, in laminar flow, into the crest. The problem hence becomes that of radial flow between two horizontal plates with one rigid, and one partially "free" boundary. When one solves the equation of motion, the necessary pressure gradient for flow can be estimated. The actual pressure difference is obtained by an integration of this gradient over, r , i.e., from r^* to R (see Berenson, 1961). R , the bubble radius was correlated, by using experimental data at the minimum film boiling temperature, with

$$R = 2.35 \left[\frac{\sigma}{g(\rho_L - \rho_V)} \right]^{1/2} \quad (5-41)$$

deformation (or pressure expansion as in a rubber balloon) primarily, and wave action from nearby bubbles. The expansion (growth) of a node will, therefore, depend upon the pressure within the film more than the film's thickness.

The same pressure difference is evaluated by considering the forces on the bubble. That is

$$P \Big|_{r^*} - P \Big|_R = \epsilon (\rho_L - \rho_V) g - \frac{2\sigma}{R} \quad (5-42)$$

Berenson assumed

$$\epsilon = 1.36R \quad (5-43)$$

When he equated the expressions for the pressure difference, he obtained the vapor film thickness to be

$$\delta = 1.4 \left[\frac{1.09\beta\mu_f k_v \Delta T}{\Delta H_v \rho_v g (\rho_L - \rho_V)} \sqrt{\frac{\sigma}{g(\rho_L - \rho_V)}} \right]^{1/4} \quad (5-44)$$

where β , the shear stress factor, equals 12 when the vapor-liquid boundary is assumed rigid, and 3 for no shear stress. By defining a heat transfer coefficient as

$$h = \bar{k}_v / \delta \quad (\bar{k}_v \text{ is average film thermal conductivity})$$

and assuming β approximately equals 8, he obtained

$$h = 0.425 \left[\frac{\bar{k}_v^3 \Delta H_v g \rho_v (\rho_L - \rho_V)}{\Delta T \mu_v \sqrt{\frac{\sigma}{g(\rho_L - \rho_V)}}} \right]^{1/4} \quad (5-45)$$

Near the minimum film boiling temperature, Berenson (1960) showed this correlation to agree with the data on boiling n-pentane and carbon tetrachloride within 10%. Other investigators (Clements and Clover, 1972) noted larger errors at temperatures much above the minimum film boiling temperature.

Berenson's derivation is limited in four primary respects. These are the expressions for bubble radius (Equation (5-41)), the area associated at any instant with a developing bubble, $\lambda_c^2/2$, the bubble height, ϵ , and the arbitrary choice of $\beta = 8$ for the shear stress factor. Small percentage deviations in any of these values result in significant changes in the values of the prefactor (= 0.425 in equation). A 20% reduction in the value of h results if, for instance, $\beta = 3$, i.e. the vapor-liquid boundary has zero shear stress.

Berenson (1960) measured the diameters of freely suspended bubbles in the boiling liquid. These were in the 6.0 to 8.5 mm range. It has been shown, however, that bubbles with diameters >2 mm become deformed when suspended in a liquid (Levich, 1962). It is thus quite probable that the reported bubble diameters were less than would have been measured at the base of the growing bubble. The correlation obtained in the present work with cryogenic fluids and techniques described in Chapter 3 is

$$R = 3.85 \sqrt{\frac{\sigma}{g(\rho_L - \rho_V)}} \quad (5-46)$$

The bubble patterns noted at the liquid-liquid interfaces

appear to be triangular rather than rectangular. It also appears that the inter-bubble spacing is in the order of a bubble diameter. The area then associated with a bubble is, approximately, $\sqrt{3}/2(\lambda_c^2)$ (where $\lambda_c = 4R$). This is about 73% higher than assumed by both Berenson (1960) and Zuber (1958).

The bubble height, ϵ , was reportedly correlated from the data of Borishansky (1959) (Berenson, 1960, 1961) with Equation (5-43). This relationship was, however, based on bubbles breaking-through evaporating liquid spheroids on a flat plate. Since spheroids, while film boiling, lose some of their vapor at the perimeter, it is apparent that the measured ϵ could be low. The correlation suggested from the interferometric study of Beer and Burow (1971) (pool boiling) is:

$$\epsilon = 1.76R \quad (5-47)$$

The fourth limitation has to do with the choice of $\beta = 8$. Studies on two-phase flows (Lock, 1951; Tong, 1965) show that when a vapor (or gas) flows over an initially stagnant liquid surface at a velocity U_v , the shear stress, τ_{ro} , is given by

$$\tau_{ro} = \frac{0.33\rho_v U_v^2}{Re^{1/2}} \quad (5-48)$$

Figure 2 of Lock's analysis shows that, even for moderate gas flows the shear stress at the water surface is high, i.e. the water hardly

moves (or Re is low). Hence in the formulation of Berenson (1960), β close to 12 should probably have been used.

When the corresponding adjustments were made, Equation (5-45) becomes

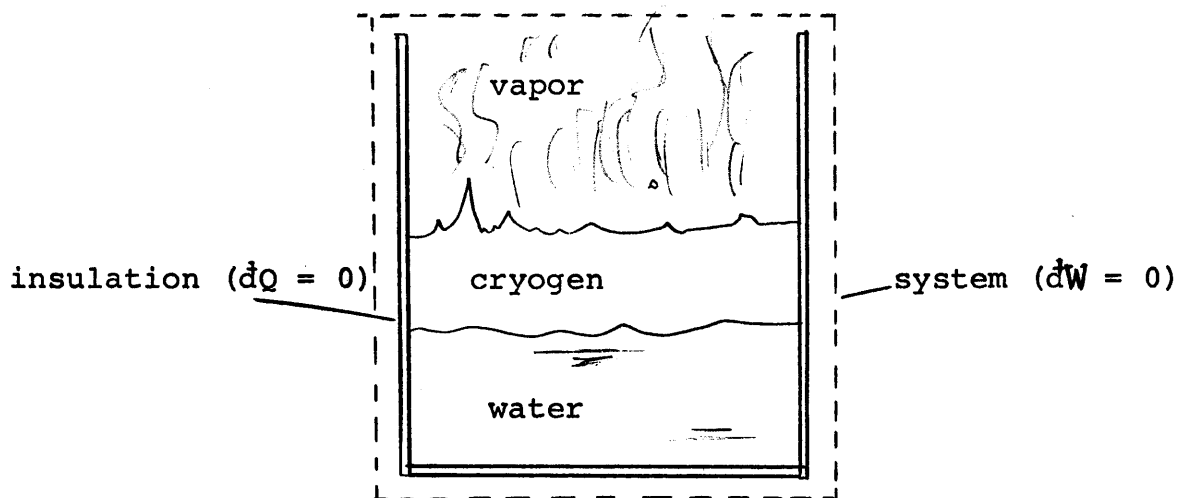
$$h = 0.5 \left[\frac{k_v^3 \Delta H_v g \rho_v (\rho_L - \rho_v)}{\Delta T \mu_v \sqrt{\frac{\sigma}{g(\rho_L - \rho_v)}}} \right]^{1/4} \quad (5-49)$$

The heat fluxes calculated with this expression are about 18% higher than Berenson's and closer to the experimental data in literature (e.g. Sauer and Ragsdell, 1971).

Most of the available correlations on film boiling are modifications and extensions of the theories of Bromley (1950), Zuber (1958) and Berenson (1960). These have been reviewed recently by Clements and Clover (1970, 1972). Expressions that best-fit data (Borishansky and Fokin, 1965; Ruzicka, 1959), and correlations based on dimensional analysis (Morozov, 1963) and equations of state (Clements and Clover, 1970, reference 183) have also been reported.

5-3 HEAT FLUXES ACROSS THE WATER-CRYOGEN INTERFACES

Boil-off data were obtained as mass vaporized as a function of time. These had to be converted to an energy flux. To carry out such computations, the thermodynamic system chosen was the boiling vessel as indicated in the sketch.



The general first law for a flow system is

$$d[m(U + KE + PE)]_{\text{system}} + [(H + zg + \frac{1}{2} u^2) dm]_{\text{flowing streams}} = \dot{Q} - \dot{W} \quad (5-51)$$

The system chosen is adiabatic ($\dot{Q} = 0$), rigid ($\dot{W} = 0$) and the kinetic and potential energies may be neglected. Equation (5-51) then becomes

$$d[mU]_{\text{system}} + H_{\text{out}} dm_{\text{out}} = 0 \quad (5-52)$$

The system contains three subsystems (water, cryogen and vapor), and the total energy is cumulative. Hence

$$mU_{\text{system}} = m_w U_w + m_L U_L + m_v U_v \quad (5-53)$$

total internal energy water cryo- genic liquid vapor

With the present system

$$m_v U_v \ll m_L U_L \quad \text{or} \quad m_w U_w$$

and $d(m_v U_v)$ is very small. Consequently,

$$mU_{\text{system}} \approx m_w U_w + m_L U_L \quad (5-54)$$

Since m_w is essentially constant

$$dm_{\text{out}} = -dm_L \quad (5-55)$$

On substituting Equations (5-54) and (5-55) into (5-52), and using the fact that the internal energy for liquids U , is approximately equal to the enthalpy, H , the following expression is obtained

$$m_w \frac{dH_w}{dt} = \left[\Delta H_{L-v} + C_{p_v} (T_v - T_{\text{sat}}) \right] \frac{dm_L}{dt} \quad (5-56) *$$

*See bottom of next page.

i.e., the energy withdrawn from the water evaporates the cryogenic liquid, and heats the vapor above the saturation temperature. This expression, therefore, gives the heat flux across the liquid-liquid interface. Both T_v and $m_L(t)$ were measured values and are presented in part in Table 5-1, and in full in Appendix F. Hence, heat transfer rates can be determined.

Two points about Equation (5-56) will be clarified before the calculated fluxes are presented. First, the vapor temperatures do not necessarily correspond to the maximum values in the system. The highest temperatures would be recorded at the liquid-liquid interface. During the ascent of the vapors, transported as bubbles in the cryogenic pool, some of the sensible heat is applied to vaporize more material. Consequently, although the term $(T_v - T_{sat})$ measured is less than $(T_v - T_{sat})_{\text{maximum}}$, the total amount of liquid vaporized is higher than that vaporized only at the liquid-liquid interface. The calculated flux is, therefore, the same as would have been obtained with the knowledge of the interfacial conditions.

*We will assume that ΔH_{L-v} is not a function of time, and it equals the value at the saturation boiling point. However, it can be shown (Denbigh, 1966) that:

$$\frac{d(\Delta H_{L-v})}{dT} \approx C_{p_v} - C_{p_L} \quad (= \Delta C_p)$$

The cryogenic liquids boiled here were only slightly superheated, if at all. Hence the assumption appears justified.

approximately, be established as a function of time, t . The reasons are that "thermals" were steadily generated in the water. (See Spangenberg and Rowland (1961) for photographic evidence.) Ice was also continuously formed in certain experiments. Under these circumstances, unless the entire temperature distribution and rate of phase changes (water to ice) in the water can be determined, $H_w(t)$ cannot be determined by considering the water alone. Hence only the overall heat balances were evaluated.

Presented in Table 5-1 are data which include the total enthalpy changes noted. The energy residual, A-B-C, was generally within 10% of the total flux. This should have been zero, however. The origin of most error lies in the measurement of the final mix-cup temperature of the water pool. This temperature was recorded after any ice formed was melted and the pool was well-mixed. An 0.6°C change in the water temperature, after each experiment, but before the mix-cup temperature could be measured is equivalent to an error of about 1 kJ in the calculated enthalpy change. With hot water, the mix-cup temperature was generally slightly lower than would have been were this temperature measured immediately at the end of boil-off. A-B-C is then positive. The reverse is noted for cold water when heat is gained from the surroundings during the mixing. The error could be large in this case as the extent of ice formed was larger as the water temperature was lowered. In fact, the final temperature of water was not measured if the ice could not be melted within a reasonable time (~ 60 s). The foregoing described results indicate

Secondly, the analysis assumes that no unvaporized liquid cryogen is carried out of the system. This loss can be obtained only if very small liquid droplets, (<100 μm diameter), are produced as the bubbles burst at the cryogen upper free surface. (See Day, 1964, 1967, and Blanchard, 1963.) Such sized droplets could be carried out by the cold cryogenic vapors.

It has, however, been photographically demonstrated, in Appendix C, that big bubbles, in the same size range noted in the photographs in Chapter 3, do not produce such small droplets. The drops (~ 0.6 mm), that are sometimes produced, fall back into the cryogen before they vaporized appreciably in the surrounding vapor. (See Appendix C for calculations on droplet vaporization.) The small bubbles observed in Figures 3-9 and 3-10 form foams above the boiling pools and do not burst until the sizes were significantly larger.

A quantitative check of the significance of liquid loss by atomization involves taking an energy balance over the entire system. An integration of Equation (5-56) over the experiment duration would show that, if the amount of liquid loss and heat exchange with the ambient were negligible, the rate of energy withdrawal from the water equals the sum of the latent heat of the cryogenic liquid and the sensible heat transported in the vapor times the vapor evolution rate.

However, the enthalpy of the water, $H_w(t)$, was known exactly at the start and end of the experiments, i.e., when the mix-cup temperatures and system weights were measured. Even though the water temperatures were being recorded continuously, H_w could not, even

that liquid loss by atomization is not significant in the present work.

Further evidence supporting the above conclusion is that the thermocouples in the vapor did not register very large amplitude oscillations. If atomization were significant, the vapor thermocouples (analog output) would be expected to read the cryogen saturation temperatures when droplets impinge on the thermocouple junctions at a sufficiently high frequency; or at least, the thermocouples will register short duration, but constant, temperatures lower than the mean value in vapors. This was very infrequently observed.

The method of evaluating dm_L/dt is presented in Appendix E. Briefly, it involves a least-square fitting of the residual weights of cryogen, $m_L(t)$, with a suitable polynomial regression equation. Derivatives of the expressions give a time-smoothed instantaneous boil-off rates, dm_L/dt .

The calculated heat fluxes are presented in Figures 5-4 to 5-12. As shown in Appendix D, maximum errors in the heat transfer rates due to heat leak from the surroundings is less than 2%.

EXPERIMENTAL DATA
AND HEAT FLUXES

TABLE 5-1
— . —

$$A = m_w c_{pw} (\bar{T}_w^o - \bar{T}_w^f)$$

$$B = m_L \Delta H_v$$

$$C = \int_0^{\theta_f} c_p (\bar{T}_v - \bar{T}_{set}) \frac{dm_L}{dt} dt$$

RUN	m_w^o Mass Water g	T_w^o Temp. Water Initially °C	m_L Mass Cryogen Spilled g	ξ Head of Cryogen Spilled cm	T_w^f Final Water Temperature °C	θ Time s	m_L Mass Cryogen g	\bar{T}_V Average Vapor Temp. °C	$\frac{1}{A'} \frac{dm_V}{d\theta}$ (m') mg/cm ² -s	$m' \Delta H_V$ kW/m ²	$m' C_P (T_V - T_{sat})$ kW/m ²	$dQ/d\theta$ kW/m ²	Δm_w mg/cm ²	A kJ	B kJ	C kJ	A-B-C kJ		
157	475.7	52.7	28.05	0.86	44.3	2	27.5	-75.5	7.0	35.7	10.3	46.0	29.4	16.7	14.3	2.1	0.3		
						4	26.5	-112.1	7.7	39.3	6.5	45.8							
						10	22.5	-117.0	9.6	49.0	7.3	56.3							
						20	14.0	-112.1	12.0	61.2	9.0	70.1							
						25	9.4	-126.0	19.1	65.2	11.6	76.8							
158	470.9	40.85	33.4	1.02	31.6	2	33.0	-109.3	8.5	43.4	7.6	51.0	12.5	18.2	17.0	1.2	0.0		
						5	30.3	-149.7	9.0	45.9	1.8	47.7							
						10	27.1	-136.5	9.9	50.5	4.2	54.3							
						15	23.1	-139.1	10.8	55.1	4.2	59.3							
						20	18.5	-132.4	11.7	59.7	5.8	65.5							
						25	14.1	-149.4	12.6	64.3	2.6	66.9							
159	468.7	31.25	34.75	1.07	22.5	2	34.3	-128.3	8.2	41.8	4.7	46.5	9.1	17.2	17.7	1.5	-2.0		
						4	32.8	-137.5	8.6	43.9	4.4	48.3							
						10	23.8	-141.4	9.96	50.8	4.2	55.0							
						12	27.0	-143.0	10.4	53.1	4.0	57.1							
						20	20.4	-123.3	12.2	62.2	9.5	71.7							
						30	10.8	-138.1	13.3	67.9	6.7	74.6							
160	468.1	22.5	25.6	0.78	15.8	2	25.1	-125.7	7.3	37.2	4.5	41.7	---	13.1	13.1	1.2	-1.2		
						5	23.3	-135.7	8.3	42.4	3.7	46.1							
						10	19.6	-141.3	9.7	49.3	3.4	52.7							
						19	12.5	-132.3	11.2	57.1	5.6	62.7							
162	465.6	9.85	32.5	1.0	1.5*	2	32.1	-132.3	5.65	28.8	2.8	31.6	1.3	16.3	16.6	1.2	-1.5		
						5	30.6	-138.8	7.2	36.7	2.8	39.5							
						10	27.3	-134.7	9.5	48.15	4.4	52.6							
						15	23.4	-138.5	11.4	58.2	4.5	62.7							
						20	18.6	-139.5	12.7	64.8	4.8	69.6							
						25	13.6	-141.3	13.6	69.1	4.7	73.8							
161	466.3	16.9	31.75	0.98	8.6*	2	30.7	-126.3	6.7	34.2	4.1	38.3	1.0	16.2	16.2	1.3	-1.3		
						7	27.8	-135.8	8.3	45.3	3.6	39.5							
						10	26.0	-134.8	9.1	46.5	4.2	50.7							

163	450.1	30.1	58.85	1.8	*	2	58.29	-136.4	9.17	46.8	3.95	50.7	11.6	---	30.0	1.25	---					
						5	55.70	-145.2	8.9	45.5	2.50	48.0										
						10	52.81	-154.3	9.04	46.1	1.12	47.1										
						15	48.97	-151.7	9.8	50.1	1.65	51.7										
						20	45.30	-149.8	11.2	57.1	2.25	59.3										
						30	34.28	-148.0	16.1	82.1	3.73	85.7										
165	448.3	27.8	17.45	.54	22.1	2	16.6	-105.8	7.4	37.8	7.08	44.9	---	10.7	8.9	1.6	0.2					
						5	15.15	-120.2	7.1	36.2	5.03	41.2										
						10	11.78	-128.0	8.9	45.5	5.13	50.6										
						15	8.49	-137.1	10.6	45.3	4.44	58.8										
166	445.3	23.2	14.0	.43	18.7	2	13.90	-109.0	5.74	29.3	5.17	34.5	4.0	8.4	7.14	1.22	0.0					
						5	12.19	-104.2	6.2	31.7	6.11	37.8										
						10	9.81	-128.1	5.86	29.9	3.36	33.3										
						15	7.49	-116.7	4.39	22.4	3.38	25.8										
167	429.0	35.3	14.66	.45	30.3	2	14.11	-96.9	6.87	35.1	7.61	42.7	---	9.0	7.5	1.45	0.1					
						5	12.17	-110.8	7.58	38.7	6.60	45.3										
						10	9.50	-132.4	6.58	33.5	3.29	36.8										
						15	7.21	-92.4	3.19	16.3	3.78	20.1										
169	---	26.05	77.96	2.40	*	2	76.81	-153.8	8.93	45.6	1.18	46.8	8.8	---	39.8	1.0	---					
						5	74.63	-155.0	8.86	45.2	.98	46.2										
						10	71.40	-152.8	9.09	46.4	1.36	47.8										
						15	68.05	-155.7	9.77	49.9	.97	50.6										
						20	63.97	-159.5	10.9	55.6	.37	56.0										
						30	54.1	-158.7	14.5	73.9	.69	74.6										
210	440	50.15	26.53	.81	41.5	2	26.10	-74.7	6.5	33.3	9.70	43.0	9.05	15.9	13.54	1.6	0.8					
						5	24.09	-102.4	8.08	41.2	8.19	49.4										
						10	20.67	-106.3	10.1	51.6	9.56	61.1										
						15	16.49	-109.0	11.4	58.4	10.3	68.7										
						20	12.23	-115.6	12.1	61.7	9.53	71.2										

METHANE

212	436.4	29.8	28.09	.86	21.2	2	27.46	-110.8	5.05	25.8	4.39	30.2	9.96	15.7	14.3	1.66	-0.26
						5	26.56	-124.7	6.65	33.9	4.20	38.1					
						10	23.19	-127.0	8.89	45.4	5.20	50.6					
						15	19.55	-132.4	10.6	54.2	5.29	59.5					
						20	15.27	-125.9	11.8	60.2	7.21	67.4					
213	435.6	22.0	28.54	.87	13.6	2	28.36	-130.3	7.41	37.8	3.96	41.8	1.42	15.32	14.55	1.25	-0.48
						5	26.42	-132.0	8.11	41.4	4.11	45.5					
						10	23.06	-132.7	9.30	47.5	4.60	52.1					
						15	19.06	-139.9	10.5	53.5	3.89	57.3					
						20	14.89	-139.5	11.7	59.6	4.42	64.0					
164	450.5	16.8	70.4	2.17	*	2	69.9	-152.8	7.46	38.1	1.1	39.2	---	---	35.9	1.0	---
						5	67.2	-151.3	8.3	42.4	1.45	43.85					
						10	64.2	-155.4	9.74	49.7	1.0	50.7					
						20	55.3	-156.1	12.6	64.3	1.2	65.5					
						25	51.1	-157.7	14.0	71.4	0.9	72.3					
						30	44.4	-157.3	15.4	78.6	1.1	79.7					
168	430.5	30.2	14.2	0.43	25.9	1	14.2	-102.8	5.55	28.3	5.6	33.9	9.7	7.75	7.25	1.2	-0.7
						2	13.7	-96.7	6.3	32.1	7.0	39.1					
						3	12.7	-92.1	6.83	34.8	8.1	42.9					
						5	12.0	-109.4	7.29	37.2	6.5	43.7					
						8	10.3	-126.0	6.81	34.7	4.1	38.8					
						10	9.2	-126.0	5.96	30.4	3.6	34.0					
170	438.8	9.3	71.1	2.19	*	2	70.1		12.4	63.3	0.0	63.3	---	---	36.3	0.0	---
						5	67.1		13.6	69.4	0.0	69.4					
						10	61.3	sat.	15.4	78.6	0.0	78.6					
						20	48.5		17.3	88.3	0.0	88.3					
						25	41.9		17.4	88.8	0.0	88.8					
						30	35.3		17.1	87.3	0.0	87.3					
211	445.5	39.5	34.14	1.05	29.8	1	34.1	-103.1	6.8	34.7	6.8	41.5	14.9	18.1	17.4	1.5	-0.8
						3	33.2	-111.1	7.54	38.5	6.5	45.0					
						6	31.1	-128.3	8.57	43.7	4.9	48.6					

METHANE

						12	26.7	-125.7	10.5	53.6	6.4	60.0						
						16	23.4	-128.7	11.7	59.7	6.6	66.3						
						21	18.6	-136.1	13.1	66.8	5.7	72.5						
214	443.6	15.0	29.5	0.9	6.7*	2	28.7	-135.4	5.4	27.6	2.4	30.0	11.0	15.4	15.1	1.0	-0.7	
						5	27.2	-134.4	7.3	37.2	3.4	40.6						
						10	24.1	-136.4	9.9	50.5	4.3	54.8						
						15	19.8	-140.2	11.7	59.7	4.3	64.0						
						20	15.1	-143.8	12.8	65.3	3.9	69.2						
						25	10.3	-145.9	13.1	66.8	3.5	70.3						
215	442.9	8.3	15.48	0.48	4.6*	2	15.3	-105.8	5.9	30.1	5.6	35.7	1.3	6.9	7.9	1.3	-2.3	
						3	14.6	-104.8	6.2	31.6	6.0	37.6						
						5	13.8	-106.6	6.9	35.2	6.5	41.7						
						8	12.0	-115.2	7.7	39.3	6.1	45.4						
						10	12.0	-115.2	7.7	39.3	6.1	45.4						
						14	8.2	-117.4	9.0	45.9	6.8	52.7						
237	453	14.4	32.2	1.0		2	31.4	-132.7	6.5	33.2	3.2	36.4	4.7	---	16.4	---	---	
						5	29.8	-134.7	7.5	38.3	3.5	41.8						
						10	26.5	-138.9	9.1	46.4	3.5	49.9						
						15	22.8	-142.0	10.6	54.1	3.5	57.6						
						20	18.5	-142.3	11.9	60.7	3.9	64.6						
						25	13.6	-144.8	13.1	66.9	3.4	70.6						
						30	8.4	-143.8	14.1	71.9	4.3	76.2						

*Ice was not completely melted when T_w^f was recorded

ETHANE (99.84%)

176	448.3	32.6	23.65	0.6	26.2	2	23.37	- 72.9	6.37	31.2	1.69	32.9	0.9	12.0	11.6	0.25	-0.1	
						4	21.69	- 75.4	19.2	94.2	4.25	98.5						
						6	17.67	- 84.6	27.2	133.2	1.72	134.9						
						8	13.3	- 88.3	30.3	148.4	0	148.4						
						10	8.59	- 88.3	28.4	139.2	0	139.2						

LIQUID ETHANE (99.84%)

						16	21.3	-137.8	10.7	54.4	4.4	58.8					
						20	17.9	-132.2	11.6	59.1	4.8	63.9					
						27	11.3	-142.0	12.9	66.0	4.3	70.3					
171	442.7	49.4	41.06	1.04	38.2	2	40.87	- 70.5	6.2	30.4	1.9	32.3	----	20.8	20.1	0.6	0.1
						5	38.56	- 68.8	12.3	60.3	4.2	64.5					
						7	36.50	- 63.0	20.5	100.4	9.0	109.4					
						10	32.15	- 85.6	26.3	128.8	0.7	129.5					
						15	23.25	- 87.2	27.3	133.7	0.3	134.0					
						20	12.42	- 68.0	26.7	130.8	9.4	140.2					
172	440.9	37.15	35.2	0.89	37.5	1	35.2	- 59.3	8.7	42.6	4.4	47.0	4.5	17.8	17.2	0.3	0.3
						3	33.6	- 61.6	10.8	52.9	5.1	58.0					
						5	31.75	- 74.0	15.0	73.5	3.8	77.3					
						10	23.9	- 79.8	25.7	125.8	3.9	129.8					
						12	19.7	- 86.6	26.3	128.8	0.9	129.7					
						15	14.0	- 87.4	26.2	128.3	0.5	128.8					
173	440.3	27.9	45.3	1.15	15.7	2	45.1	- 76.3	9.75	47.8	2.1	49.9	1.3	22.5	22.2	0.6	-0.3
						5	40.7	- 85.3	24.0	117.6	1.4	119.0					
						8	34.7	- 83.9	27.3	133.7	2.2	135.9					
						10	30.8	- 79.7	23.4	114.6	3.6	118.2					
						15	22.5	- 77.9	21.3	104.3	3.9	108.2					
						20	14.7	- 85.0	18.4	90.1	1.1	91.2					
174	439.5	17.3	47.05	1.19	6.2*	2	46.6	- 76.9	9.34	45.8	1.9	47.7	0	20.4	23.0	0.4	-3.0
						5	43.9	- 82.6	22.5	110.2	2.4	112.6					
						10	32.8	- 85.6	23.8	116.6	1.3	117.9					
						15	25.2	- 82.7	18.8	92.1	1.9	94.0					
						20	19.0	- 82.7	16.4	80.3	1.7	82.0					
						25	13.6	- 78.8	13.5	66.1	2.3	68.4					
175	449.1	8.2	81.2	2.06	---	2	79.6	- 88.9	28.3	138.6	---	138.6	----	----	39.8	0.4	---
						5	72.6	- 87.7	24.6	120.5	0.4	120.9					
						10	64.3	- 86.6	19.7	96.5	0.8	97.3					
						15	57.4	- 85.0	16.5	80.8	1.0	81.8					
						20	51.4	- 84.4	15.1	74.0	1.1	75.1					
						25	45.5	- 86.4	15.1	74.0	0.8	74.8					

ETHANE (99.84%)

177	446.0	26.75	25.49	0.65	20.2	2	25.3	- 75.5	8.08	39.6	1.76	41.3	---	12.2	12.5	0.5	-0.8
						4	22.97	- 76.1	23.1	113.2	4.83	118.0					
						6	19.0	- 81.6	28.5	139.5	3.27	142.8					
						8	14.3	- 79.0	27.0	132.2	4.31	136.5					
						10	10.4	- 79.0	24.9	121.9	3.97	125.8					

BINARY MIXTURE (98% CH₄; 2% C₂H₆)

227	476.2	26.4	21.34	0.66	20.7	2	21.0	-139.2	9.06	46.2	3.6	49.8	3.2	11.4	10.9	0.4	0.1
						5	18.4	-151.7	12.6	64.3	2.2	66.5					
						8	14.9	-151.8	15.5	79.1	2.7	8.18					
						10	12.5	-150.6	17.0	87.7	3.3	90.0					
						12	9.8	-135.0	18.3	93.4	2.1	95.5					
						15	3.4	-150.6	19.6	100.0	3.8	103.8					
229	476	15.3	26.65	0.82	8.5	2	25.6	-153.2	10.75	54.9	1.5	56.4	3.2	13.35	13.6	0.3	-0.35
						5	23.2	-153.5	12.3	62.8	1.7	64.5					
						8	20.1	-152.8	17.3	88.3	2.6	90.9					
						10	17.9	-153.9	14.8	75.5	1.9	77.4					
						15	11.9	-152.8	17.3	88.3	2.6	90.9					
						20	4.5	-143.9	19.9	101.5	5.3	106.8					
230	475.6	9.5	24.9	0.77	*	2	24.1	-149.9	10.5	53.6	2.1	55.7	0.0	---	12.7	0.4	---
						5	21.5	-153.1	12.1	61.7	2.2	63.9					
						8	18.5	-151.3	13.8	70.4	2.5	72.9					
						10	16.3	-152.1	15.1	77.0	2.5	79.5					
						15	9.8	-149.1	18.6	94.9	4.1	99.0					
						18	5.0	-145.5	20.9	106.6	5.9	112.5					
231	475.8	5.2	25.28	0.78	*	2	24.5	-152.8	12.1	61.7	1.9	63.6	0.0	---	12.9	0.4	---
						5	21.2	-150.6	14.9	76.0	2.8	78.8					
						8	17.6	-151.0	17.4	88.8	3.1	91.9					
						10	14.7	-148.4	18.9	96.4	4.3	100.7					
						12	11.9	-152.4	20.2	103.1	3.2	106.3					
						15	6.8	-148.4	22.0	112.3	4.9	117.2					

BINARY MIXTURES (94.7% CH ₄ ; 5.3% C ₂ H ₆)																	
239	467.7	11.4	34.76	1.07	---	2	33.6	-153.9	11.7	59.7	1.5	61.2	---	---	17.7	0.3	---
						5	30.2	-155.4	16.5	89.2	1.7	90.9					
						8	26.1	-155.0	20.0	102.0	2.2	104.2					
						10	22.9	-160.6	21.7	110.7	0.3	110.0					
						15	14.0	-151.7	23.6	120.4	4.0	124.4					
BINARY MIXTURES (90.9% CH ₄ ; 9.1% C ₂ H ₆)																	
240	442.9	11.9	32.15	1.0	---	2	30.3	-150.9	12.2	62.2	2.1	64.3	---	---	16.4	0.55	---
						5	27.0	-150.6	14.8	75.3	2.5	77.8					
						8	23.6	-149.5	16.9	86.0	2.9	88.9					
						10	20.9	-150.2	18.0	91.1	3.1	94.2					
						15	13.4	-148.0	19.8	99.5	4.1	103.6					
BINARY MIXTURES (81.8% CH ₄ ; 18.2% C ₂ H ₆)																	
241	442.5	12.1	26.65	0.82	---	2	23.8	-138.2	7.1	35.7	1.2	36.9	---	---	13.4	0.9	---
						5	21.1	-138.1	12.9	64.8	2.2	67.0					
						8	18.1	-133.5	16.3	81.9	2.8	84.7					
						10	15.6	-139.5	17.1	85.9	2.9	88.8					
						12	12.7	-137.1	16.7	83.9	2.9	86.8					
						15	8.5	-129.0	14.1	70.8	1.0	71.8					
BINARY MIXTURES (93.2% CH ₄ ; 6.8% C ₂ H ₆)																	
242	450.7	22.2	31.35	0.97	14.3*	2	28.0	-151.0	16.2	81.4	1.1	82.5	25.9	14.9	15.8	0.54	-1.44
						5	24.2	-147.0	16.0	80.4	2.7	83.1					
						8	20.4	-149.1	16.5	82.9	2.3	85.2					
						10	17.6	-49.1	17.1	85.9	2.3	88.2					
						15	10.9	-145.1	19.9	100.0	3.4	103.4					
BINARY MIXTURES (99.45% CH ₄ ; 0.55% C ₂ H ₆)																	
245	463.8	15.0	31.1	0.96	---	2	30.8	-162.4	7.7	39.3	---	39.3	---	---	15.9	0.5	---
						5	28.7	-143.6	10.5	53.6	3.2	56.8					
						10	24.1	-145.9	14.1	71.9	3.8	75.7					
						15	18.1	-151.3	16.6	84.7	2.9	87.6					
						20	11.2	-154.6	20.1	102.6	2.4	105.0					

BINARY MIXTURES (91.5% CH ₄ ; 8.5% C ₃ H ₈)																	
243	450.2	23.0	33.03	1.02	14.05	2	31.8	-150.3	12.2	62.2	2.3	64.5	---	16.9	16.9	0.6	-0.6
						5	28.3	-156.9	14.0	71.4	1.1	72.5					
						8	25.0	-153.2	15.6	79.6	2.2	81.8					
						10	22.5	-148.1	16.4	83.7	3.8	87.5					
						15	15.9	-147.4	18.0	91.8	4.4	96.2					
						20	8.7	-138.8	18.7	95.4	6.4	101.8					
BINARY MIXTURES (99.85% CH ₄ ; 0.15% C ₃ H ₈)																	
246	452.2	13.5	30.2	0.93	4.5*	2	29.7	-154	11.2	57.1	1.4	58.5	---	15.3	15.4	0.8	-0.9
						5	26.5	-145.2	12.4	62.8	3.5	66.3					
						10	21.5	-144.5	14.0	71.4	4.1	75.5					
						15	15.8	-146.6	15.4	78.6	3.9	82.3					
						20	9.8	-140.6	16.6	84.7	6.0	90.7					
BINARY MIXTURES (99.43% CH ₄ ; 0.57% C ₃ H ₈)																	
247	440.6	12.8	30.6	0.94	4.6	2	25.4	-158.4	15.1	77.0	0.8	78.8	2.6	15.1	15.6	0.9	-1.4
						5	26.1	-142.7	14.7	75.0	4.7	79.7					
						8	22.9	-142.4	14.6	74.5	4.8	79.3					
						10	20.5	-147.7	14.7	75.0	3.5	78.5					
						15	14.3	-154.3	15.5	79.1	1.9	81.0					
						20	8.1	-150.6	17.3	88.3	3.2	91.5					
BINARY MIXTURES (99.41% CH ₄ ; 0.59% C ₃ H ₈)																	
248	455.3	12.9	26.5	0.82	6.0*	2	25.7	-142.3	13.6	69.4	4.5	73.9	2.6	13.2	13.5	0.75	-1.05
						5	21.9	-142.8	15.2	77.6	4.9	82.5					
						8	18.7	-145.9	16.4	83.7	4.4	88.1					
						10	16.1	-145.2	16.9	86.2	4.7	90.7					
						15	9.5	-144.8	17.3	88.3	5.0	93.3					
						17	6.7	-144.8	17.1	87.3	4.9	92.2					
BINARY MIXTURES (99.84% CH ₄ ; 0.16% nC ₄ H ₁₀)																	
249	453.5	12.6	28.07	0.86	---	2	27.5	-34.1	12.3	62.8	5.8	68.6	2.6	---	14.3	0.8	---
						5	24.2	-143.4	14.1	71.9	4.4	76.3					
						8	20.7	-141.0	15.7	80.1	5.5	85.6					
						10	18.3	-143.4	16.6	84.7	5.2	89.9					
						12	15.7	-146.2	17.4	88.8	4.6	93.4					
						15	11.5	-149.5	18.4	93.9	3.8	97.7					

5-COMPONENT MIXTURES (98.2% CH₄; 1.62% C₂H₆; 0.112% C₃H₈; 0.043% iC₄H₁₀; 0.03% nC₄H₁₀)

184	471.4	60.2	31.35	0.97	51.8	2	30.65	-152.3	8.3	42.4	1.3	43.7	16.8	16.6	16.0	0.3	0.3	
						5	28.1	-161.8	11.9	60.7	0.0	60.7						
						10	22.7	-161.4	18.8	95.9	0.0	95.9						
						15	13.6	-144.5	26.8	136.7	4.0	140.7						
185	468.4	47.7	40.14	1.24	37.1	2	39.3	} sat.	7.9	39.8	0.0	39.8	9.7	20.8	21.5	0.0	0.3	
						5	36.8		11.7	59.7	0.0	59.7						
						10	30.6		18.5	94.4	0.0	94.4						
						15	22.1		29.1	148.5	0.0	148.5						
						18	15.1		33.4	170.4	0.0	170.4						
						20	9.6	34.2	174.5	0.0	174.5							
186	466.7	36.0	36.75	1.13	26.6	2	36.0	-157.3	8.4	42.9	0.6	43.5	4.5	18.4	18.8	0.2	-0.6	
						5	33.0	-158.8	14.4	73.5	0.7	74.2						
						10	26.2	-161.5	22.5	114.8	0.0	114.8						
						15	15.6	-161.5	28.2	143.9	0.0	143.9						
						18	9.4	-151.5	30.5	155.6	5.2	160.8						
187	465.9	27.3	29.48	0.91	19.7	2	28.5	-148.5	10.3	52.6	2.3	54.9	0.0	14.8	15.0	0.8	-1.0	
						5	25.8	-145.9	14.6	74.5	3.9	78.4						
						8	22.0	-146.2	18.6	94.9	4.9	99.8						
						10	18.8	-146.0	21.0	107.2	5.6	112.8						
						15	9.3	-147.5	26.5	135.2	6.4	141.6						
195	459.1	21.7	23.42	0.72	15.2	2	22.8	-144.5	6.1	31.1	1.8	32.9	0.0	12.5	11.9	0.7	-0.2	
						5	20.8	-144.5	11.4	58.2	3.3	61.5						
						8	17.7	-144.8	16.6	84.7	4.8	89.5						
						10	14.9	-143.4	19.9	101.5	6.2	117.7						
						12	11.4	-144.1	23.2	118.4	6.9	125.3						
223	472.2	6.7	22.66	0.70	*	2	21.9	-148.8	9.9	50.5	2.2	52.7	1.3	---	11.6	0.7	---	
						5	18.9	-147.3	16.9	86.2	4.1	90.3						
						8	14.5	-143.0	20.9	106.6	6.1	112.7						
						10	11.1	-145.5	21.8	;;;/2	7/-	117.2						

5-COMPONENT MIXTURES (98.2% CH₄; 1.62% C₂H₆; 0.112% C₃H₈; 0.043% iC₄H₁₀; 0.03% nC₄H₁₀)

188	457.1	21.0	15.35	.471	16.7	2	14.54	-138.8	11.0	56.3	4.28	60.4	1.68	8.23	7.83	.8	-0.4
						4	12.52	-136.4	13.5	68.7	5.81	74.5					
						6	10.56	-137.8	15.7	80.0	6.39	86.4					
						8	7.73	-138.1	17.7	90.2	7.11	97.3					
189	459.9	55.4	18.15	.56	49.8	2	17.63	-77.0	7.32	37.4	10.60	48.0	4.52	10.8	7.26	1.7	-0.16
						5	15.85	-104.0	8.14	41.6	8.01	49.6					
						8	13.72	-120.8	10.6	54.3	7.41	61.7					
						11	10.88	-124.0	13.6	69.6	8.75	78.3					
						14	7.64	-117.1	15.9	81.3	12.12	93.4					
190	458.0	48.0	16.92	.52	42.7	2	16.50	-91.3	7.43	37.9	10.60	46.8	---	10.14	8.63	1.2	0.31
						5	14.55	-127.3	8.98	45.8	5.27	51.1					
						8	12.18	-126.0	11.2	57.5	6.82	64.3					
						11	9.36	-127.3	14.3	72.9	8.39	81.2					
191	457.6	40.8	16.5	.50	36.0	2	15.73	-121.9	8.13	41.5	5.5	47.0	3.2	9.18	8.42	1.1	-0.34
						4	13.97	-132.0	10.80	55.1	5.6	60.7					
						6	12.32	-126.7	12.9	65.8	7.75	73.6					
						8	10.52	-129.3	14.3	73.0	8.1	81.1					
						10	8.34	-130.3	15.2	77.6	8.1	85.7					
192	457.0	35.7	16.5	.50	30.8	2	15.70	-134.0	12.2	62.2	5.74	67.94	4.3	9.4	8.4	.85	0.15
						4	13.25	-133.7	13.7	69.6	6.5	76.1					
						6	11.22	-132.0	14.5	74.0	7.5	81.3					
						8	9.17	-134.0	14.3	72.9	6.75	79.6					
						10	7.01	-130.6	18.6	94.8	9.86	104.6					
193	457.1	30.9	16.65	.51	36.1	2	15.80	-139.5	9.27	47.3	3.50	50.8	5.8	9.2	8.5	.8	-0.1
						4	14.03	-40.6	12.3	62.9	4.41	67.3					
						6	12.07	-138.1	14.1	72.1	5.66	77.7					
						8	10.24	-136.7	14.7	75.1	6.26	81.4					
						10	7.60	-134.3	14.0	71.6	6.54	78.1					

5-COMPONENT MIXTURES (98.2% CH₄; 1.62% C₂H₆; 0.112% C₃H₈; 0.04% iC₄H₁₀; 0.03% nC₄H₁₀)

194	475.5	26.4	20.24	.620	21.0	2	19.68	-142.7	8.69	44.3	2.89	47.1	4.5	10.75	10.3	.8	-0.35	
						4	17.92	-143.4	11.5	58.6	3.57	62.1						
						6	16.09	-142.0	13.9	71.2	4.65	75.8						
						8	13.72	-142.0	16.1	82.2	5.39	87.6						
						10	11.07	-141.3	17.9	91.7	6.21	97.9						
						12	8.06	-139.2	19.5	99.4	7.46	106.9						
196	443.7	16.2	78.45	2.40	*	2	76.45	-164.5	18.8	96.1	-.97	95.2	---	---	40.0	---	---	
						5	72.08	-163.7	20.7	126.4	-.93	125.5						
						10	62.73	-162.9	30.8	157.5	-.74	156.8						
						15	47.35	-162.9	32.1	164.0	-.77	163.2						
						20	37.44	-162.9	28.7	146.7	-.69	146.0						
						30	20.25	-151.4	9.53	38.4	1.30	39.7						
197	443.7	55.0	64.19	1.97	38.2*	2	62.69	-163.7	14.9	76.4	-.56	65.9	23.2	31.2	32.75	1.13	-0.7	
						5	58.98	-152.9	18.7	95.3	-.45	94.9						
						10	49.95	-162.5	23.9	122.1	-.41	121.7						
						15	41.00	-153.6	27.5	140.0	3.73	143.7						
						20	28.95	-153.6	30.8	157.5	4.18	161.7						
224	452.2	---	12.97	0.4	---	2	12.73	-142.0	7.38	37.6	2.47	40.1	.776	---	6.61	.59	---	
						4	11.07	-140.2	11.6	59.2	4.24	63.4						
						6	9.04	-137.8	15.4	78.6	6.26	84.9						
198	450.7	37.5	63.85	1.97	20.4	2	63.0	} sat. -161.5	9.6	49.0	0.0	49.0	3.9	32.3	32.6	0.1	-0.4	
					5	60.1	15.3		78.1	0.0	78.1							
					10	52.8	22.6		115.3	0.0	115.3							
					15	42.4	27.4		139.8	0.0	139.8							
					20	31.4	29.6		151.0	0.0	151.0							
					25	20.5	29.2		149.0	0.0	149.0							
					30	9.8	-150.7	26.2	133.7	4.9	138.6							

5-COMPONENT MIXTURES (98.2% CH₄; 1.62% C₂H₆; 0.112% C₃H₈; 0.043% iC₄H₁₀; 0.03% nC₄H₁₀)

198	450.7	37.5	63.85	1.97	20.4	2	63.0		9.6	49.0	0.0	49.0	3.9	32.3	32.6	0.2	-0.5
						5	60.1		15.3	78.1	0.0	70.1					
						10	52.8	sat.	22.6	115.3	0.0	115.3					
						15	42.4	-161.5	27.4	139.8	0.0	139.8					
						20	31.4		29.6	151.0	0.0	151.0					
						25	20.5		29.2	140.0	0.0	149.0					
						30	9.8	-150.7	26.2	133.7	4.0	138.6					
199	450.2	22.0	61.5	1.89	7.0*	2	60.6		11.3	57.7	0.0	37.7	1.9	28.3	31.4	0	-3.1
						5	57.7		15.1	77.1	0.0	77.1					
						10	50.3	sat.	23.4	119.4	0.0	119.4					
						15	39.1		30.1	153.6	0.0	153.6					
						20	27.3		29.8	152.1	0.0	152.1					
						25	16.5		24.3	124.0	0.0	124.0					
200	450.0	8.5	64.7	1.99	*	2	63.1		24.6	125.5	0.0	125.5	---	---	33.0	0	---
						5	59.1		26.0	132.7	0.0	132.7					
						10	47.3		26.9	137.3	0.0	137.3					
						15	36.5	sat.	25.8	131.6	0.0	131.6					
						20	28.8		22.8	116.3	0.0	116.3					
						25	20.5		17.8	90.8	0.0	90.8					
						30	14.5	-158.4	10.9	55.6	0.8	56.4					
225	449.9	17.6	13.91	.43	13.8	2	12.77	-146.9	15.3	78.2	3.83	82.0	3.62	7.16	7.	0.5	-0.44
						4	10.35	-145.9	15.6	79.7	4.18	83.9					
						6	7.90	-139.9	15.8	81.1	5.86	87.0					
226	449.6	15.0	11.19	.34	11.6	2	10.87	-133.7	4.72	24.1	2.25	26.3	1.55	6.3	5.7	1.0	-0.4
						4	9.82	-116.4	5.11	26.1	3.96	30.1					
						6	9.09	-101.3	5.51	28.1	5.69	33.8					
						8	8.42	-92.7	5.91	30.2	6.97	37.1					
						10	7.39	-97.6	6.32	32.2	6.93	39.1					

5-COMPONENT MIXTURES (89.2% CH ₄ ; 8.2% C ₂ H ₆ ; 2.0% C ₃ H ₈ ; 0.2% nC ₄ H ₁₀ ; 0.2% iC ₄ H ₁₀)																	
201	432.9	55.0	45.0	1.38	42.6	2	44.00	-169.1	8.84	44.7	---	44.7	8.41	22.5	22.7	---	---
						5	40.19	-166.0	15.9	80.8	---	80.8					
						10	33.33	-163.3	24.3	123.0	---	123.0					
						15	23.40	-133.0	28.2	143.0	0.0	143.0					
						20	10.65	-121.8	27.8	140.0	0.0	140.0					
204	429.5	24.9	39.7	1.22	13.5	2	33.54	-161.0	10.6	53.6	---	53.6	---	20.5	20.1	0.7	-0.3
						5	34.42	-163.7	24.3	122.8	---	122.8					
						10	23.15	-146.9	32.3	163.0	2.7	165.7					
						15	11.57	-135.5	21.7	109.0	3.2	112.2					
208	448.3	25.4	23.5	.720	18.9	2	22.65	-138.1	9.06	45.2	1.2	46.4	---	12.2	11.7	0.6	-0.1
						5	19.35	-136.4	19.5	97.7	2.5	100.5					
						8	14.38	-138.9	23.9	119.0	0.0	119.0					
						11	8.28	-127.4	22.0	110.0	0.0	110.0					
209	448.1	19.4	26.06	.799	12.7	2	25.26	-147.3	6.20	30.9	} sat.	30.9	---	12.6	13.0	0.0	-0.4
						5	22.36	-139.5	16.3	81.5		81.5					
						8	18.25	-141.6	21.7	109.0		109.0					
						11	13.32	-138.1	22.5	112.0		112.0					
						14	7.21	-108.4	18.5	92.7		92.7					
202	429.8	40.5	26.95	0.9	32.5	2	26.2	-139.5	9.4	48.0	3.4	51.4	---	14.4	13.5	0.7	0.2
						5	23.4	-132.3	15.0	76.3	7.3	84.6					
						8	19.2	-132.7	20.9	106.3	5.1	111.4					
						10	15.5	-136.4	25.0	127.2	5.0	132.2					
						12	11.6	-134.7	29.2	148.5	4.3	152.8					
203	429.6	32.8	29.65	1.0	24.5	2	28.9	-143.4	11.9	60.5	3.5	64.0	---	14.9	14.9	0.6	-0.6
						5	25.8	-136.1	14.0	71.2	5.9	77.1					
						8	21.8	-137.1	20.2	103.1	8.1	111.2					
						10	18.1	-136.1	26.6	135.7	1.6	137.3					
						12	13.5	-136.4	34.9	177.5	0.0	177.5					

5-COMPONENT MIXTURES (89.2% CH ₄ ; 8.2% C ₂ H ₆ ; 2.0% C ₃ H ₈ ; 0.2% iC ₄ H ₁₀ ; 0.2% nC ₄ H ₁₀)																		
205	429.3	15.9	33.86	1.1		6.9*	2	32.8	-149.6	14.8	75.3	2.8	78.1	---	16.2	17.0	0.6	-1.4
							5	29.4	-143.1	16.9	86.0	5.3	91.3					
							10	20.4	-141.3	28.8	146.5	4.7	151.2					
							12	15.7	-140.2	25.9	131.8	4.5	136.3					
							15	10.2	-123.8	20.2	102.8	6.5	119.3					
5-COMPONENT MIXTURES (82.0% CH ₄ ; 14.6% C ₂ H ₆ ; 3.0% C ₃ H ₈ ; 0.2% iC ₄ H ₁₀ ; 0.2% nC ₄ H ₁₀)																		
206	442.0	7.6	34.6	1.1	---		2	30.4	-154.7	11.6	59.0	1.4	60.4	---	---	17.4	0.3	---
							5	29.3	-145.9	19.0	96.7	5.1	101.8					
							10	21.4	-140.2	24.2	123.1	4.4	127.5					
							12	17.4	-140.6	23.7	120.6	4.2	124.8					
							15	12.0	-133.4	20.4	103.8	3.5	107.3					
							17	9.8	-125.1	16.5	83.9	2.9	86.8					
5-COMPONENT MIXTURES (82.0% CH ₄ ; 14.6% C ₂ H ₆ ; 3.0% C ₃ H ₈ ; 0.2% iC ₄ H ₁₀ ; 0.2% nC ₄ H ₁₀)																		
207	429.0	17.6	34.05	1.1	---		2	33.1	-144.8	12.3	62.6	3.3	65.9	---	16.0	17.1	0.3	---
							5	29.1	-144.8	22.4	113.9	4.0	117.9					
							10	18.6	-144.8	30.6	155.7	3.9	159.6					
							12	13.7	-131.0	32.8	156.7	3.9	160.6					
							15	10.2	-111.8	28.0	142.4	3.2	145.6					
5-COMPONENT MIXTURES (78.2% CH ₄ ; 8.6% C ₂ H ₆ ; 6.9% C ₃ H ₈ ; 3.1% iC ₄ H ₁₀)																		
244	---	23.3	37.96	1.1	---		2	35.5	-144.5	22.7	109.3	2.1	111.4	---	---	18.3	0.3	---
							5	30.1	-139.5	30.7	147.8	2.9	150.7					
							10	17.6	-137.5	27.8	133.9	3.2	137.1					
							12	13.8	-129.7	21.1	101.6	2.4	104.0					
							15	10.3	-115.1	4.9	23.6	0.6	24.2					

BINARY MIXTURES (98% CH₄; 2% C₂H₆)

228	470.8	20.7	23.51 ⁶	.72	14.7	2	22.81	-145.5	11.0	56.3	3.02	59.3	2.7	11.8	12.0	0.5	-0.6
						5	20.08	-150.9	12.2	62.5	2.22	64.7					
						8	16.99	-151.7	13.5	68.7	2.27	71.0					
						11	13.78	-152.8	14.7	74.9	2.19	77.1					
						14	10.12	-150.6	15.9	81.2	2.97	84.2					
232	470	27.5	19.03	.58	22.0	2	18.55	-140.9	8.32	42.5	2.94	45.4	0.4	10.8	9.7	1.2	0.0
						4	16.55	-139.5	11.8	60.4	4.46	64.9					
						6	14.72	-137.8	14.3	73.2	5.82	79.0					
						8	12.64	-137.4	15.8	80.8	6.54	87.3					
						10	10.21	-137.4	16.3	83.3	6.74	90.0					
233	469.1	22.3	18.05	.55	17.1	2	17.53	-129.0	9.27	47.3	5.17	52.5	---	10.2	9.2	1.0	0.0
						5	15.02	-137.8	11.0	56.2	4.47	60.7					
						8	12.31	-138.8	12.5	63.8	4.87	68.5					
						11	9.27	-135.0	13.7	70.2	6.23	76.2					
234	468.0	17.8	23.86	.73	11.1	2	22.37	-144.4	12.3	63.1	3.61	66.7	---	13.1	12.2	1.0	-0.1
						5	20.13	-142.0	11.0	56.4	3.68	60.1					
						8	17.29	-142.0	13.2	67.5	4.42	71.9					
						11	13.81	-142.3	16.5	83.9	5.44	89.3					
						14	9.90	-138.8	18.3	93.3	7.13	100.4					
235	470.0	12.4	19.4	.6	8.0	2	18.37	-143.7	15.6	79.6	4.76	84.3	---	8.7	9.90	0.98	-2.18
						5	15.15	-139.9	11.7	59.8	5.29	65.1					
						8	12.40	-137.4	13.4	68.3	5.54	73.8					
						11	8.92	-135.7	16.9	86.2	7.48	93.7					
236	468.4	9.0	17.45	.54	5.1*	2	16.34	-139.2	9.8	49.9	3.75	53.6	---	7.65	8.90	0.9	-2.15
						4	14.56	-137.8	12.5	63.7	5.08	68.8					
						6	12.65	-136.4	14.5	74.1	6.25	80.3					
						8	10.56	-135.4	15.9	81.2	7.12	88.3					
						10	7.92	-129.0	16.6	85.0	9.20	94.2					

LIQUID NITROGEN

179	431.3	52.0	53.72	.858	43.6	2	51.99	- 99.9	17.4	34.9	17.5	52.4	19.9	15.17	10.75	4.78	-0.36
						5	48.31	-113.9	16.8	33.7	14.4	48.1					
						10	41.79	-111.7	15.8	31.7	13.9	45.6					
						15	36.06	-117.7	14.9	29.9	12.2	42.1					
						20	30.61	-112.7	14.0	28.1	12.2	40.3					
						30	20.24	-105.4	12.3	24.7	11.7	36.4					
216	465.3	26.1	31.50	.503	21.9	2	29.83	- 86.8	11.1	22.1	12.7	34.8	6.72	8.2	6.30	2.5	-0.6
						5	27.40	-100.1	9.98	19.9	10.0	29.9					
						10	24.13	-102.7	8.58	17.2	8.38	25.6					
						15	20.95	-105.4	7.65	15.3	7.25	22.5					
						20	17.90	-103.9	7.19	14.4	6.93	21.3					
						30	12.39	- 98.1	7.72	15.4	7.91	23.3					
217	463.0	22.0	31.70	.506	18.0	2	30.31	-100.1	10.3	20.6	10.3	30.9	---	7.75	6.34	2.65	-1.24
						5	28.31	-110.0	9.42	18.8	8.48	27.2					
						10	24.89	-107.8	8.28	16.5	7.64	24.1					
						15	21.89	-112.1	7.54	15.1	6.62	21.7					
						20	19.06	-110.1	7.21	14.4	6.48	20.9					
						30	13.55	-100.4	7.77	15.5	7.77	23.2					
218	462.3	18.1	26.77	.427	14.1	2	25.90	- 96.0	8.92	17.8	9.33	27.1	---	7.74	5.35	2.6	-0.2
						5	23.68	-103.0	8.57	17.2	8.34	25.5					
						10	20.78	-106.3	7.99	16.0	7.50	23.5					
						15	17.58	-104.2	7.41	14.8	7.12	21.9					
						20	14.97	-197.5	6.82	13.6	6.32	19.9					
						30	10.18	- 96.7	5.65	11.3	5.87	17.1					
220	461.8	12.25	39.70	.554	8.3*	2	33.52	-101.3	9.48	19.0	9.39	28.4	---	7.64	6.94	2.97	-2.3
						5	30.95	-112.1	9.29	18.5	8.11	26.1					
						10	27.85	-119.3	8.83	17.6	7.09	24.7					
						15	24.43	-116.7	8.42	16.8	6.99	23.8					
						20	21.36	-114.8	8.01	16.0	6.81	22.8					
						30	15.48	-105.4	7.19	14.4	6.82	21.2					

LIQUID NITROGEN

222	456	6.3	27.12	.433	*	2	26.21	- 92.1	9.15	18.3	9.95	28.2	---	---	5.42	2.64	---
						5	23.95	-104.2	8.53	17.1	8.19	25.3					
						10	21.21	-114.9	7.65	15.3	6.49	21.8					
						15	17.93	-107.0	6.04	13.9	6.46	20.3					
						20	15.64	-105.7	6.41	12.8	6.05	18.8					
						30	10.71	- 92.1	5.87	11.7	6.38	18.1					
180	432.9	49.8	64.9	1.04	30.8	2	62.9	-115.5	16.5	33.0	13.8	46.8	31.0	18.1	13.0	5.1	0
						5	58.7	-105.7	15.6	31.2	11.4	42.6					
						10	52.8	-142.8	14.7	29.4	8.15	37.55					
						15	47.4	-133.4	13.8	27.6	9.0	36.6					
						20	41.8	-126.0	12.9	25.8	9.4	35.2					
						30	32.1	-124.1	11.1	22.2	8.3	30.5					
181	429.3	31.4	54.5	0.88	22.6	2	52.7	-127.3	12.4	24.8	8.9	33.7	---	15.8	10.9	5.2	-0.3
						5	50.0	-125.5	12.1	24.2	8.9	33.1					
						10	45.3	-129.1	11.6	23.2	8.1	31.3					
						15	40.8	-122.1	11.1	22.2	8.6	30.8					
						20	36.9	-122.1	10.6	21.2	8.2	29.4					
						30	29.0	-126.7	9.5	19.0	6.9	25.9					
182	427.9	23.5	64.7	1.04	14.5	2	63.2	-139.9	13.9	27.8	8.1	35.9	13.1	16.1	12.9	3.7	-0.5
						5	60.0	-149.5	13.4	26.8	6.5	33.3					
						10	54.7	-148.8	12.7	25.4	6.2	31.6					
						15	50.4	-147.7	12.0	24.0	6.0	30.0					
						20	45.7	-142.7	11.3	22.6	6.3	28.9					
						30	37.3	-140.6	9.9	19.8	5.7	25.5					
183	427	15.2	63.9	1.03	6.7	2	63.9	-129.4	13.1	26.2	9.1	35.3	11.8	15.2	12.8	2.8	-0.4
						5	60.5	-152.3	12.9	25.8	5.9	31.7					
						10	56.3	-148.8	12.6	25.2	6.2	31.4					
						15	51.4	-148.4	12.3	24.6	6.1	30.7					
						20	46.3	-155.4	12.0	24.0	5.1	29.1					
						30	37.5	-153.2	11.4	22.8	5.1	27.9					

LIQUID NITROGEN

219 473.6 14.9

24.4

0.39

11.2

2 23.0 - 84.0
 5 21.3 - 93.9
 10 18.8 -101.6
 15 16.0 -101.0
 20 13.5 - 98.7
 25 11.1 -100.4

7.94 15.9
 7.63 15.3
 7.1 14.2
 6.6 13.2
 6.08 12.2
 5.56 11.1

9.3 25.2
 8.1 23.4
 7.0 21.2
 6.5 19.7
 6.2 18.4
 5.5 16.6

--- 7.34 4.88 2.54 -0.1

221 473.3 8.5

24.8

0.40

5.6*

2 23.6 - 93.6
 5 21.8 - 99.4
 10 18.7 -104.6
 15 15.9 -101.9
 20 13.2 -101.6
 25 11.0 - 97.2

8.5 17.0
 8.15 16.3
 7.57 15.1
 7.0 14.0
 6.4 12.8
 5.8 11.6

9.1 26.1
 8.2 24.5
 7.2 22.3
 6.9 20.9
 6.3 19.1
 6.0 17.6

--- 5.75 4.96 2.6 -1.8

5-4 DISCUSSIONS5-4-1 REVIEW OF RESULTSMethane (Figure 5-4 and Table 5-1)

As indicated for Figure 4-15, the vaporization rates of methane is only weakly dependent on the water temperature. The minor effects have been slightly emphasized by the sensible heat in the vapor evolved. The fluxes generally increased as the initial water temperature was raised. On water whose temperature ranged between 15 and 60°C, the fluxes into pure methane was correlated with

$$Q' = (26.2 + 0.97\theta)T_w^{0.12} \quad (5-57)$$

kW/m²

where θ is time in seconds into the run, and T_w is the initial bulk water temperature in degrees Celsius.

With water at temperatures lower than 15°C, the initial fluxes were generally lower than predicted by Equation (5-57), e.g. runs 162 and 214. The fluxes increased rapidly, however. Runs 168 and 212 with 30.2 and 29.8°C water, respectively, also showed slightly lower initial heat fluxes than expected at the water temperatures. Since the boiling process and associated events are statistical in nature, the deviations noted for experiments 168 and 212 may be taken to be within bounds. Experiment 170 is, however, an exception in that the initial heat flux was much higher than for the other runs. The high fluxes can be explained if ice formed very rapidly on

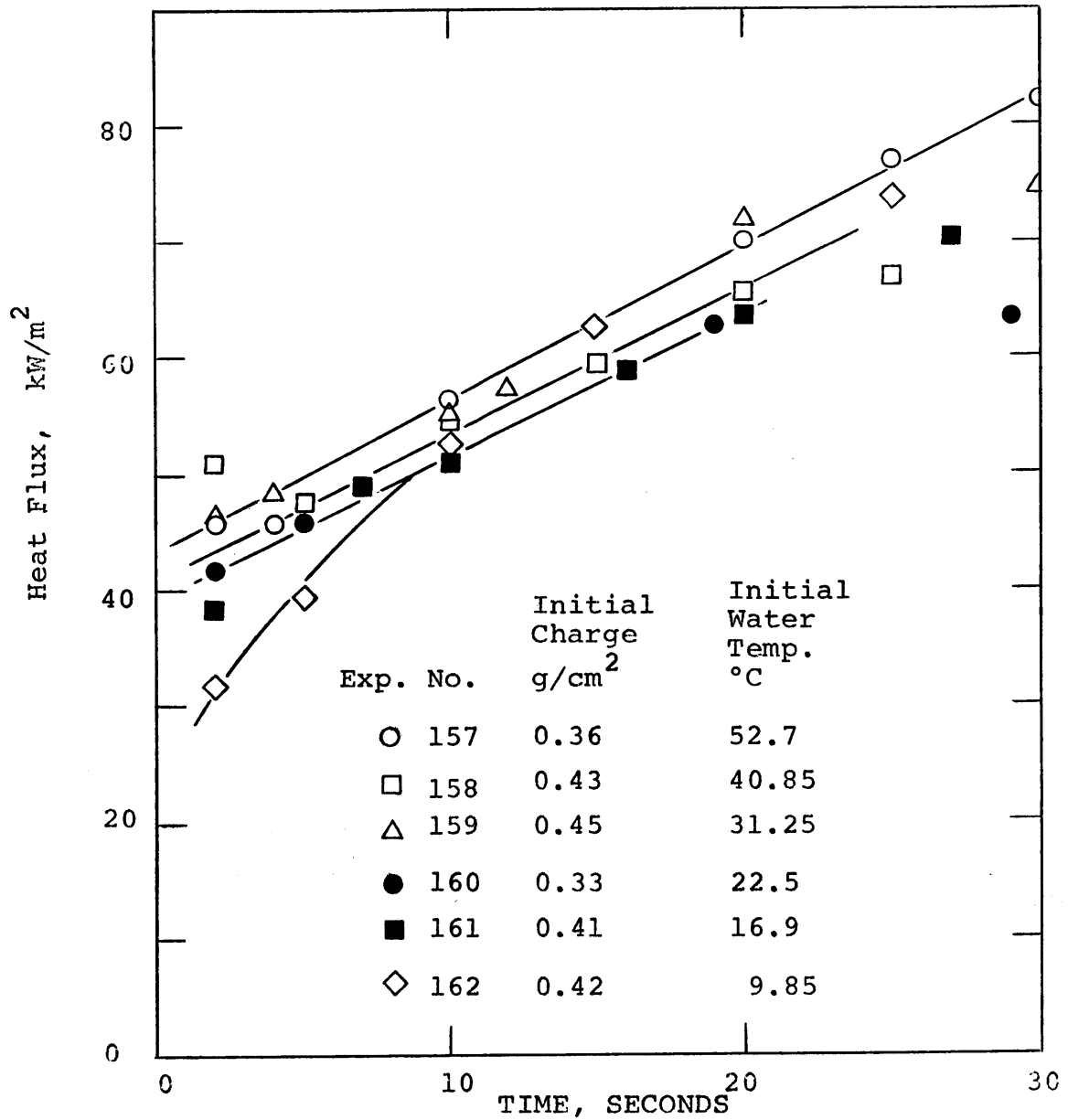


Fig. 5-4

Heat Flux Between Water and Boiling Methane
(99.98%).

low-temperature water with a large quantity of liquid methane spilled. It was observed that the entire boiling cross-section was almost covered with ice at the end of this experiment.

A summary of the total amount of water loss per unit weight of liquid methane input is presented in Table 5-2

TABLE 5-2

Water Loss During Methane Boil-Off

$$(0.8 < W_0 \leq 1.0 \frac{\text{gm}}{\text{cm}^2})$$

EXP #	T_w° Initial Water Temperature $^\circ\text{C}$	$-\Delta$ <u>Weight Water</u> Weight Cryogen Input	Equilibrium* Water Vapor Pressure at T_w° mm Hg
210	50.15	0.065	118.
211	39.5	0.036	53.6
212	29.8	0.028	31.8
213	22.0	0.009	20.0
161	16.9	0.003	14.5
162	9.85	0.003	9.2

*Perry's Handbook (4th Ed.)

The quantity of water lost appears proportional to the vapor pressure at the bulk water temperature. The results are consistent with the fact that water evaporates from the surface at a rate proportional to T_w° and, it diffuses into the vapor film separating the layered liquids. Within this film, water is condensed to produce fog. (See Appendix A.) The latent heat of vaporization for the water vapor is

withdrawn from the water pool, and the heat of sublimation to produce fog (vapor-to-ice) contributes to heating the cryogen vapor within the film . This causes more vaporization of the cryogen than would otherwise have occurred. With water initially at 16.9°C, the heat of sublimation contribution to the total flux was about 1.5 %.

Ethane (Figure 5-5)

The fluxes into boiling ethane are presented in Figure 5-5 and in Table 5-1. The heat transfer rates are noted to rise very rapidly to about 130 kW/m². Furthermore, the curves appear shifted to earlier times as the initial water temperature was lowered. With initial water temperatures at less than 40°C, maxima are noted in the curves. The rate at which the heat flux declined after the maximum has been attained increased as the water temperature was lowered.

It was shown in Chapter 3 that rapidly growing ice discs formed while ethane boiled on water. Moreover, ice formed more readily as the water temperature was lowered. The observed high heat fluxes and rapid rise may, therefore, be attributed to the formation of ice and concomitant nucleate boiling.

Fog was observed at the interface over areas not covered with ice, but the total amount of water evaporated was less than that for the methane runs. This observation can be explained if one remembers that the vapor pressure of water vapor over ice is small and, as soon as the water surface was covered with ice in ethane runs, little water loss occurred. In the course of the experiments, the fog

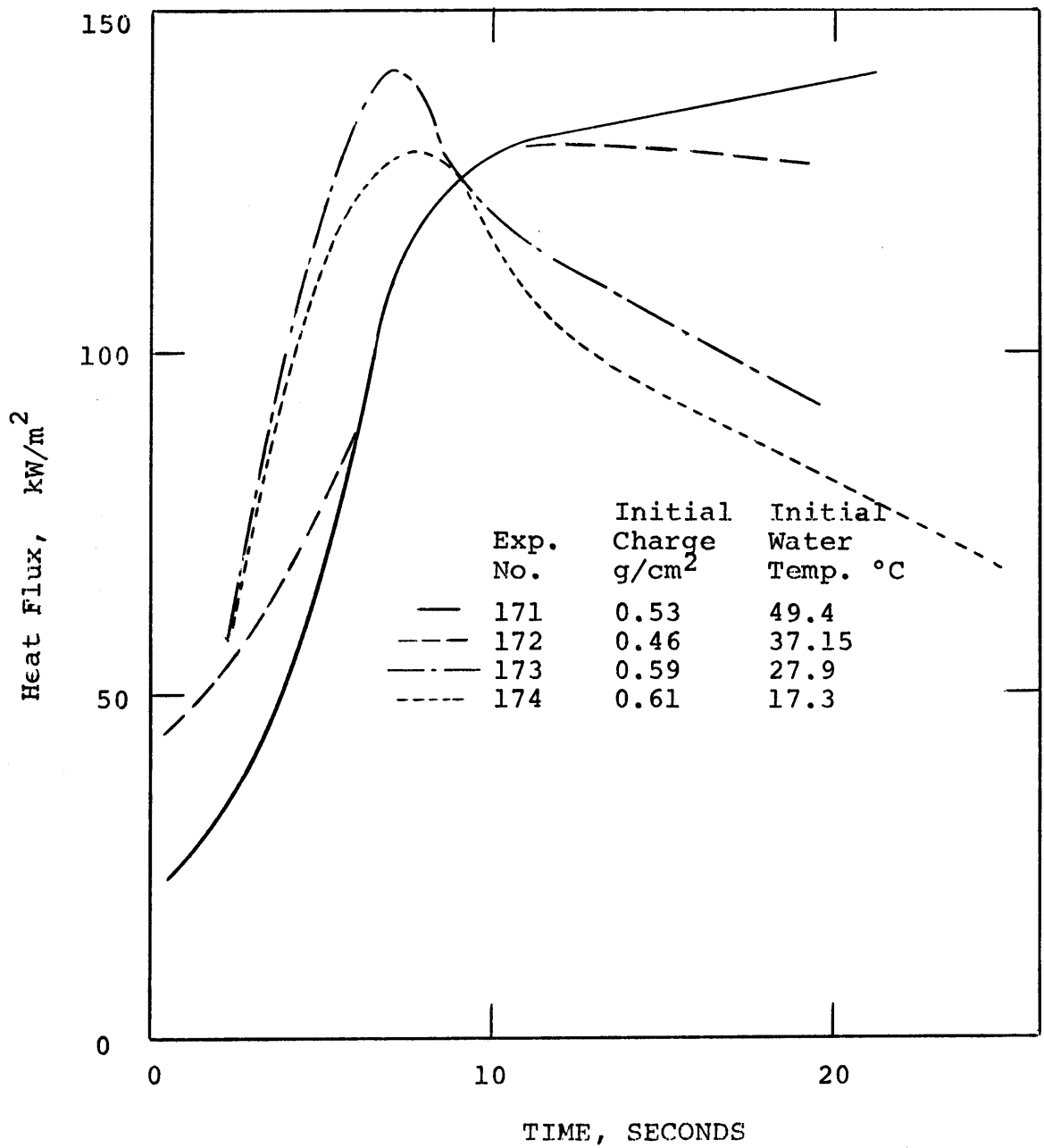


Fig. 5-5

Heat Flux Between Water and Boiling Ethane
(99.86%)

intensity decreased with time.

Binary Mixtures (Figures 5-6 to 5-8)

The boiling fluxes to cryogenic hydrocarbon liquid mixtures which contain methane as the principal component are presented in Table 5-1 and Figures 5-6 to 5-8. Similar to data presented in Chapter 4, methane-ethane mixtures show maxima in the heat flux-composition curves with about 5% ethane initially present in the bulk liquid. The heat fluxes to the mixtures, moreover, were much higher than to pure methane. An 0.55% ethane mixture showed no enhancements at short times, ~ 1 to 2 seconds. Thereafter, the fluxes rapidly increased and enhancements (over pure methane) of 50 to 60% are noted after 20 seconds. With 5.3 mole % ethane initially present, 120% enhancements are noted after 10 seconds, and slightly more at 20 seconds. As the initial ethane concentration was increased above $\sim 5\%$, the heat flux enhancement decreased.

Foams were noted above the boiling mixtures. Opaque white ice discs were also seen in the course of many of the experiments. These floated on the water surface, and the ease with which they nucleated and grew increased as the methane content of the binary mixture was lowered.

Methane-propane, methane-n-butane binary mixtures (Figures 5-7 and 5-8) likewise show heat flux enhancements over pure methane. The relative flux enhancements, for the same methane fractions and similar experimental conditions, were such that n-butane was more

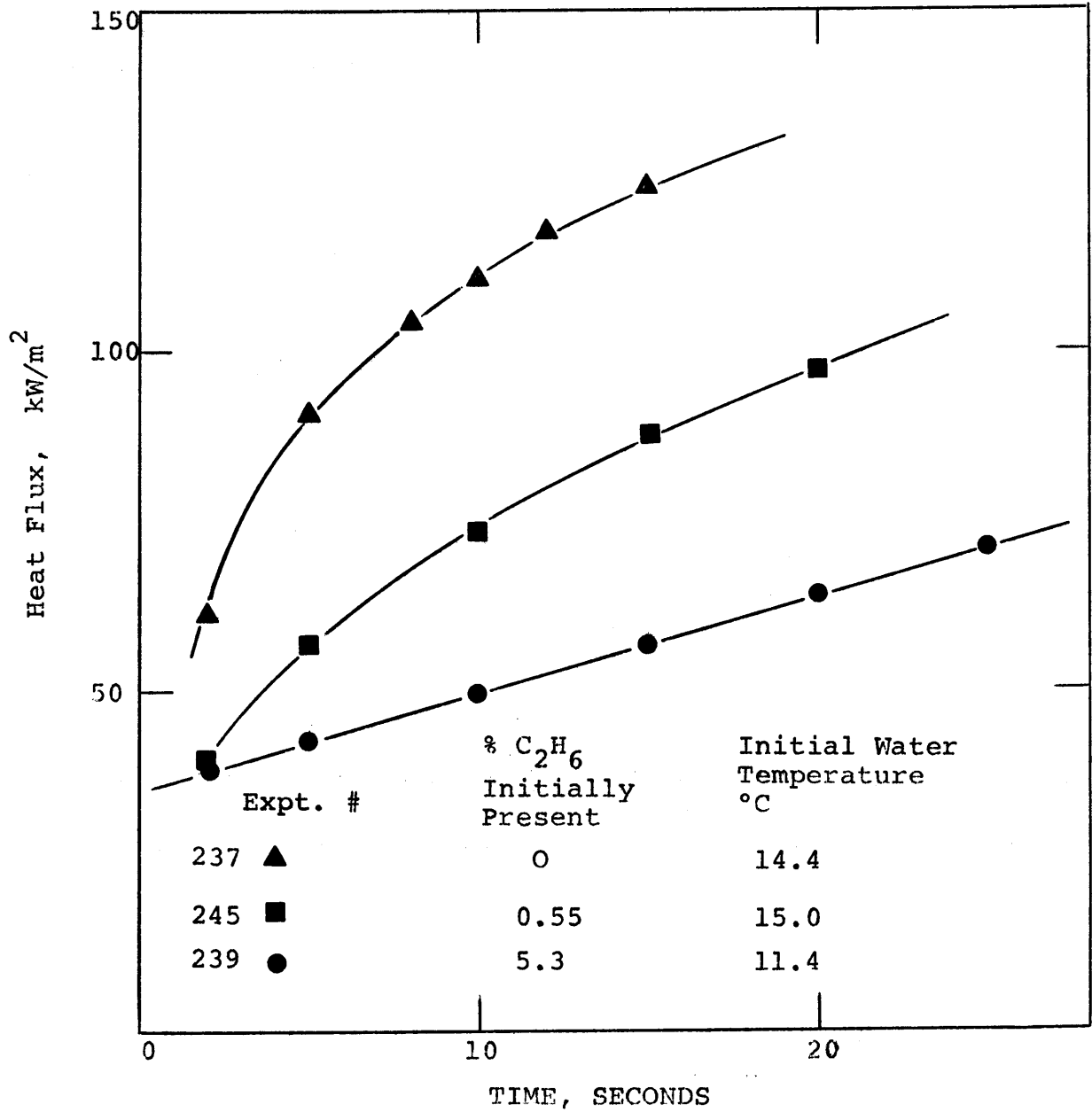


Fig. 5-6

Heat Flux Between Water and Boiling Methane - Ethane Binary Mixtures

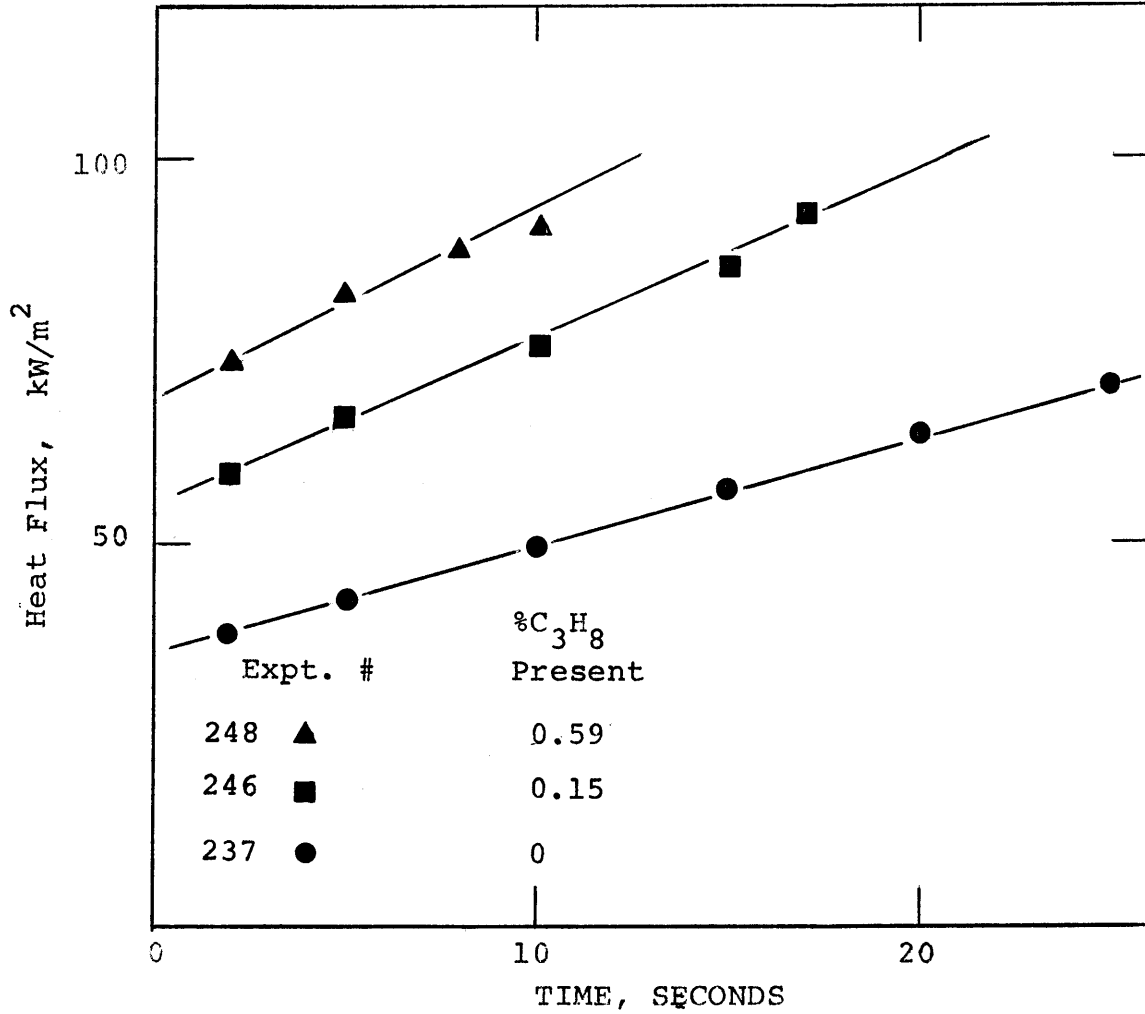


Fig. 5-7

Heat Flux Between Water and Boiling Methane - Propane Binary Mixtures. (Cryogen Charged: 0.4 ± 0.02 g/cm²
Initial Water Temperature: 12 - 15°C)

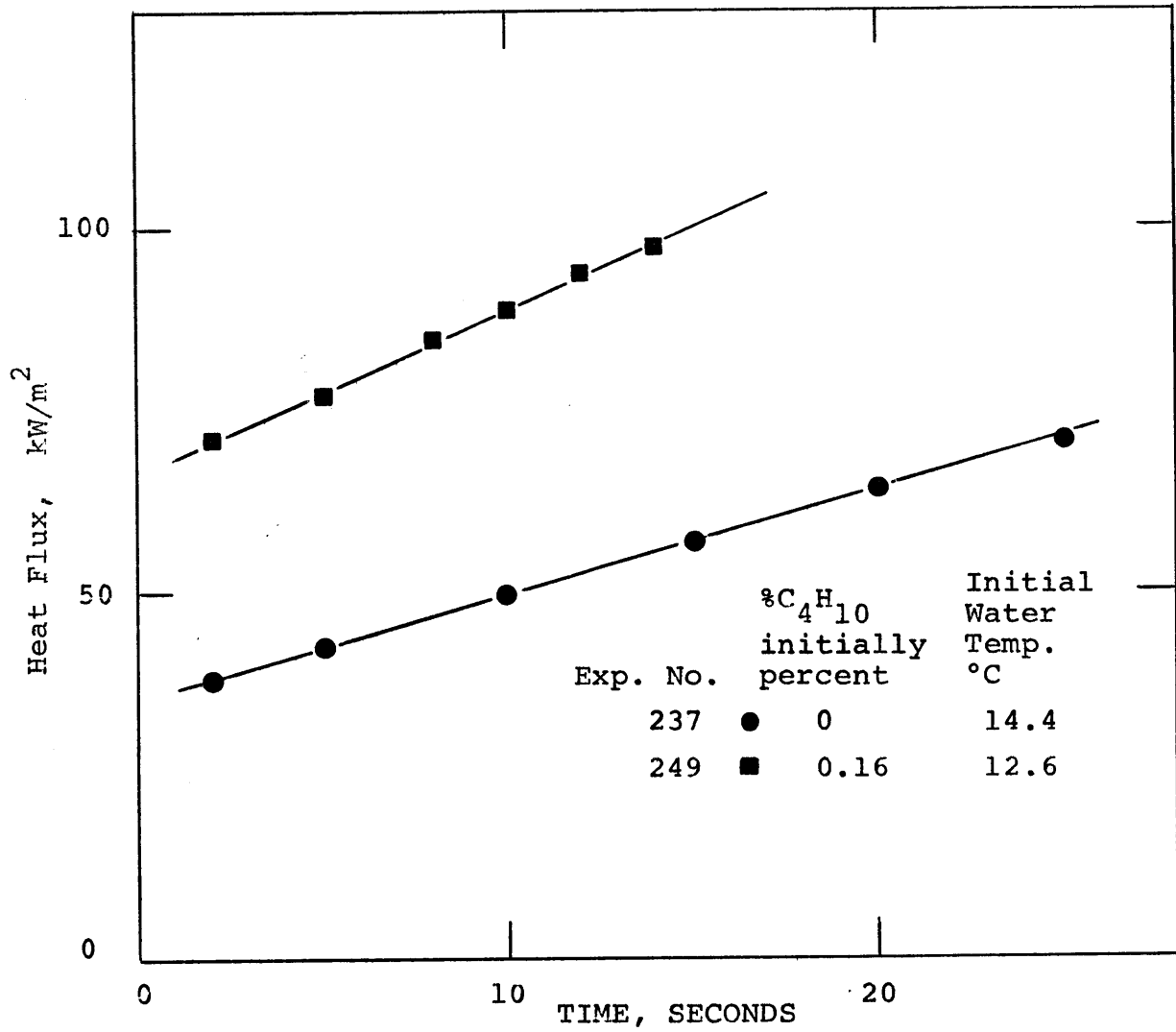


Fig. 5-8

Heat Flux Between Water And A Boiling Methane -
n-Butane Binary Mixture

effective than propane, i.e. heat flux enhancements were higher. Propane, in turn, was more effective than ethane.

5-Component Mixtures (Figure 5-9 and 5-10)

The fluxes calculated for 5-component mixtures are presented in Figures 5-9 and 5-10 (and in Table 5-1). Similar to binary mixtures, the fluxes increased with time and with higher fractions of heavier hydrocarbon present. The rate of rise in the fluxes was, however, much higher with the richer multi-component LNG.

In Figure 5-9, data indicate that the heat flux generally increased slightly as the water temperature was lowered. A combination of low water temperature and large amount of cryogen charged (~ 2 cm), however, affected the fluxes as illustrated in experiment 200; the initial heat transfer rates were high. A similar behavior was noted for pure methane in run 170. The fluxes in run 200 increased slightly to a maximum about 10 s into the run and then declined with time. If ice formed rapidly on the water surface and the boiling mechanism corresponded to that in the nucleate boiling regime, the initial fluxes should be high, especially when the latent heat contribution of the solidification process is taken into account. As soon as the entire surface was covered with ice, the fluxes should drop because the ice layer then constitutes a resistance to heat transfer.

Alternatively, the boil-off rates would decrease when a continuous pool of cryogen no longer exists, i.e. spheroids are formed and actual boiling area decreased. It is not clear which of the two

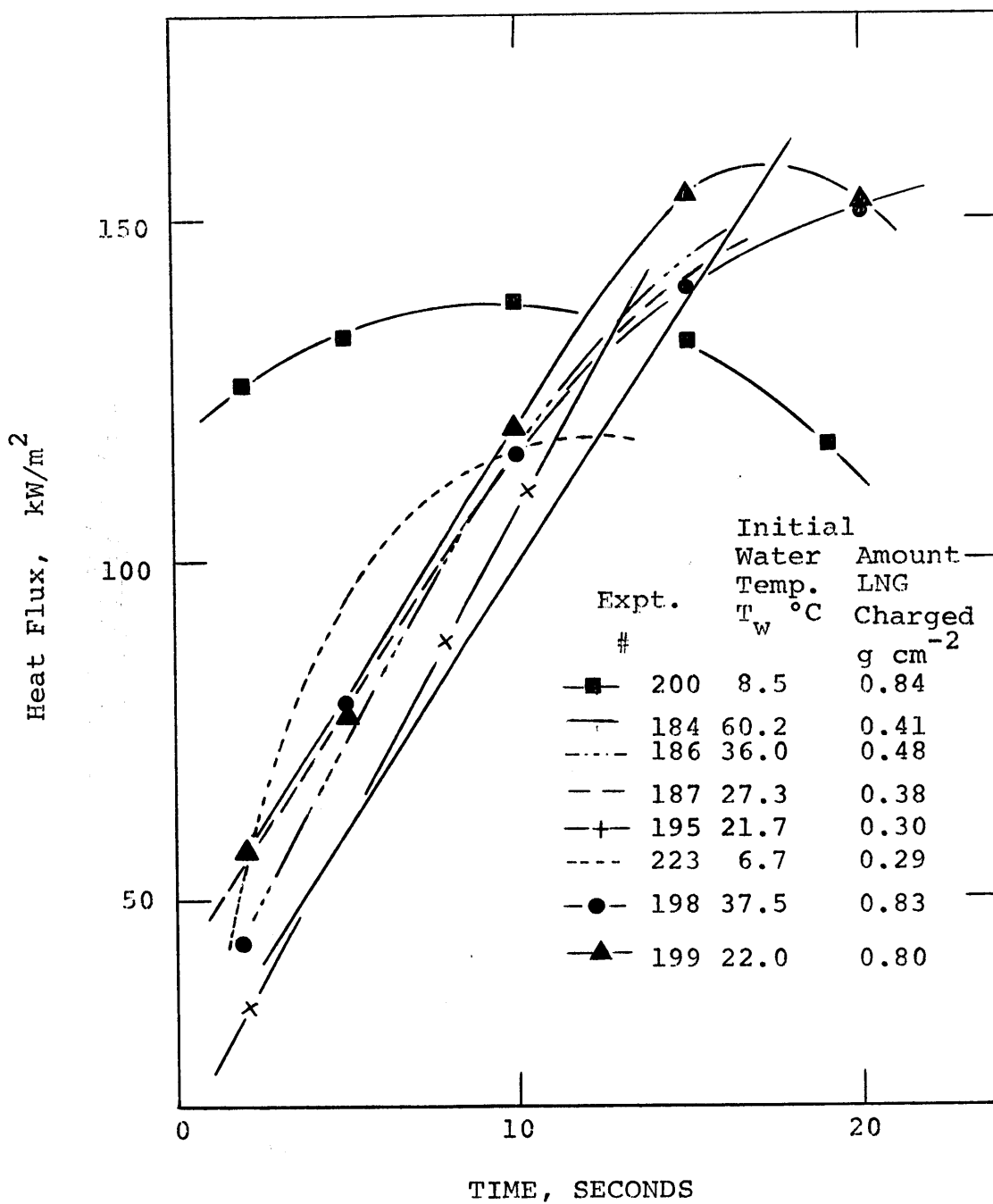


Fig. 5-9

Heat Flux Between Water and Boiling LNG
 (98.2% CH_4 , 1.62% C_2H_6 , 0.11% C_3H_8
 plus trace Butanes)

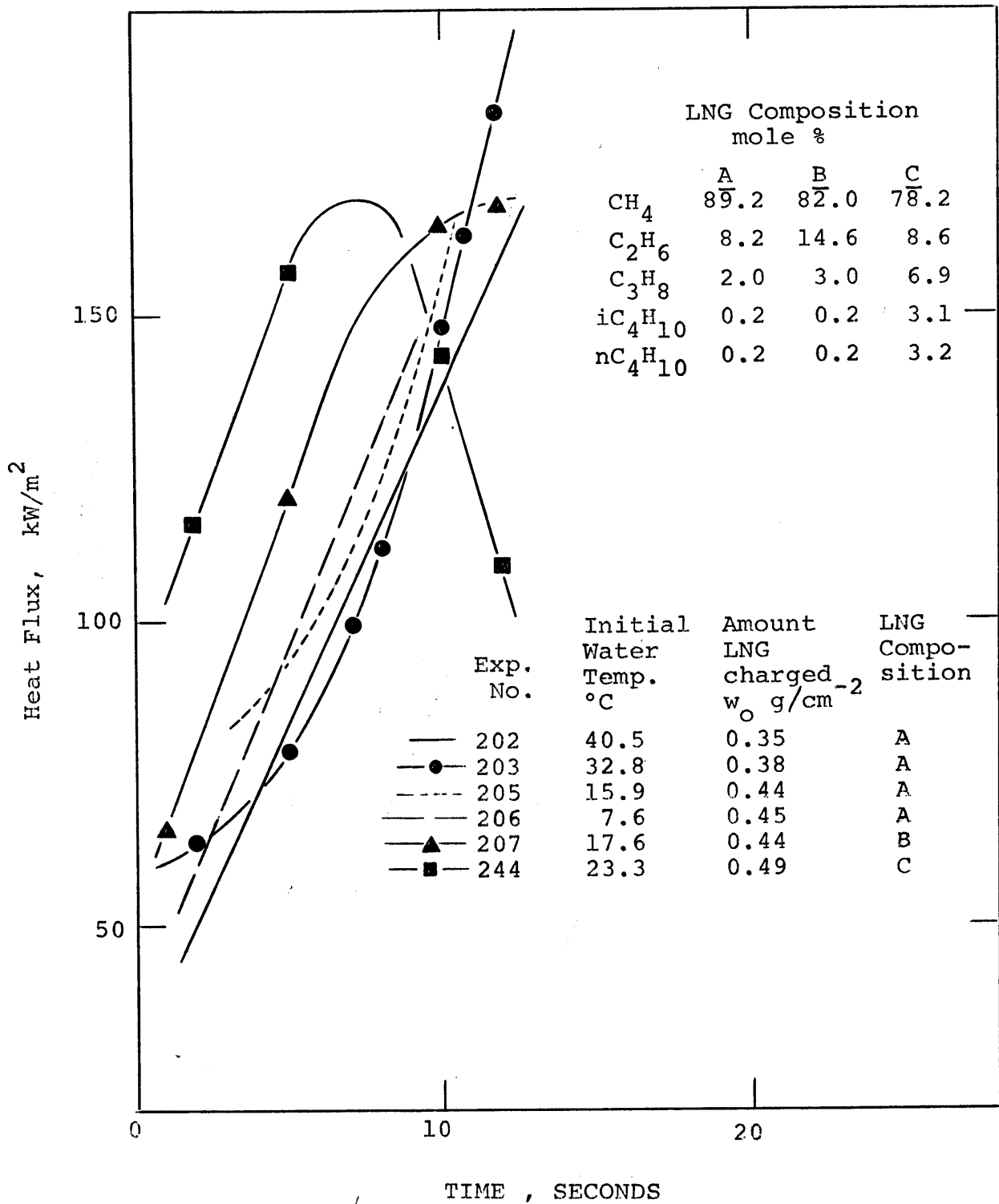


Fig. 5-10

Heat Flux Between Water and Boiling LNG.

explanations is correct, although pictures taken of the interface do not show continuous ice layers.

Small bubbles (and foams) were observed while the LNG boiled, and ice was formed. The ice was opaque, white and contained tiny occluded gas bubbles.

Figure 5-10 shows that the heat flux increased as the methane concentration was lowered. A comparison of runs 205 and 244 which have similar ethane concentration levels indicate that the percentage of higher alkanes affects the fluxes; as the concentration of each member of the homologous series was raised, the heat fluxes increased. A comparison of runs 207 and 244 also indicate that the sum of the ethane and propane fractions, f , do not necessarily determine the heat fluxes. In fact, run 244 has a smaller f than run 207, yet the heat flux was higher.

Nitrogen (Figure 5-11 and 5-12)

Unlike the hydrocarbons, the heat fluxes into liquid nitrogen decreased slowly with time as shown in Figures 5-11 and 5-12. Moreover, the fluxes are a function of the amount of nitrogen spilled.

In experiments 180, 182 and 183, (Figure 5-11) approximately the same amount of nitrogen ($\sim 0.84 \text{ g/cm}^2$) was spilled on water at different temperatures. On 40.8°C water (run 180), the initial flux into nitrogen was about 20% higher than with water at either 23.5 or 15.2°C (runs 182, 183). It was earlier indicated that ice formed very slowly with liquid nitrogen. Therefore ice growth cannot explain

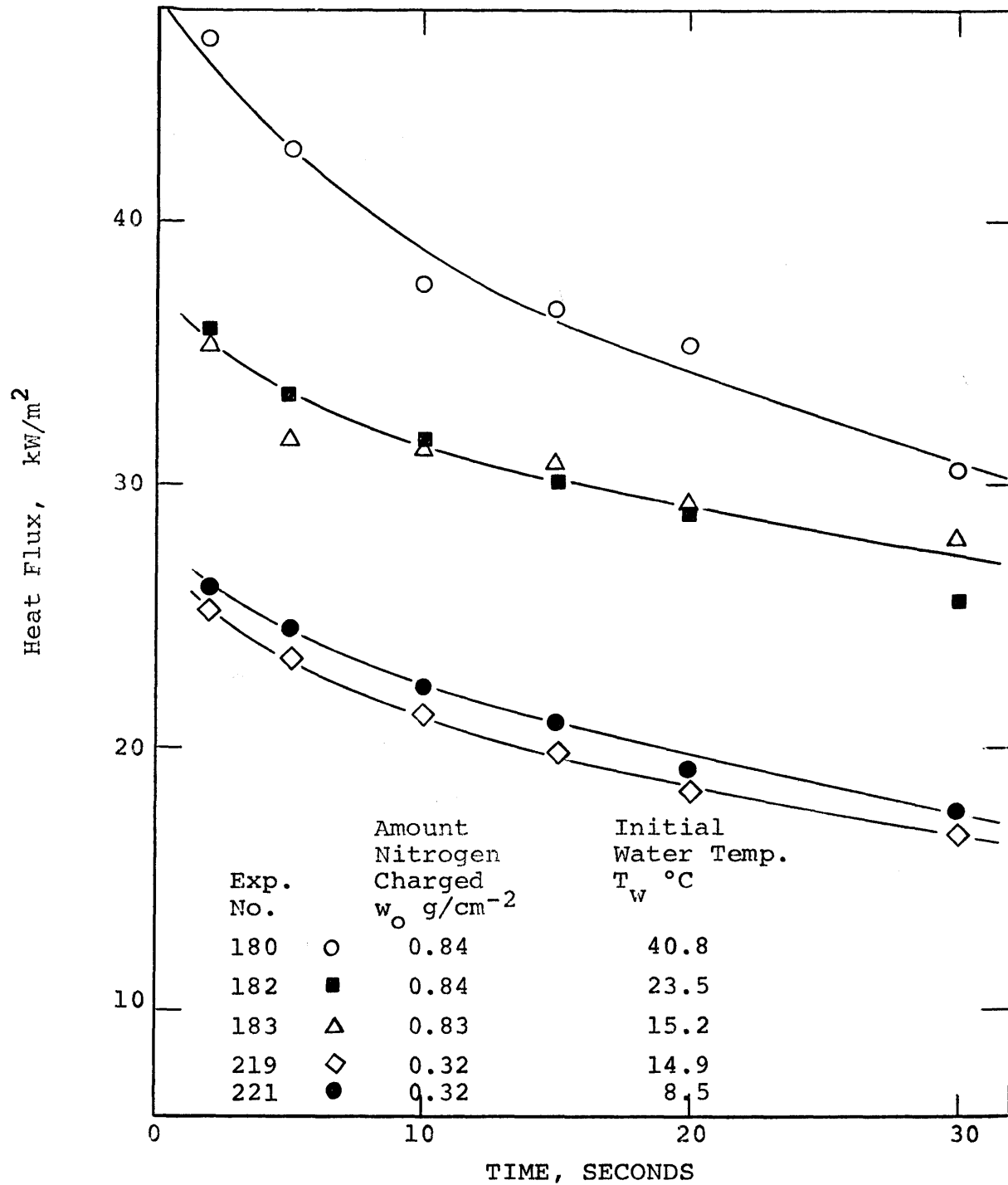


Fig. 5-11

Heat Flux Between Water And Boiling Liquid Nitrogen

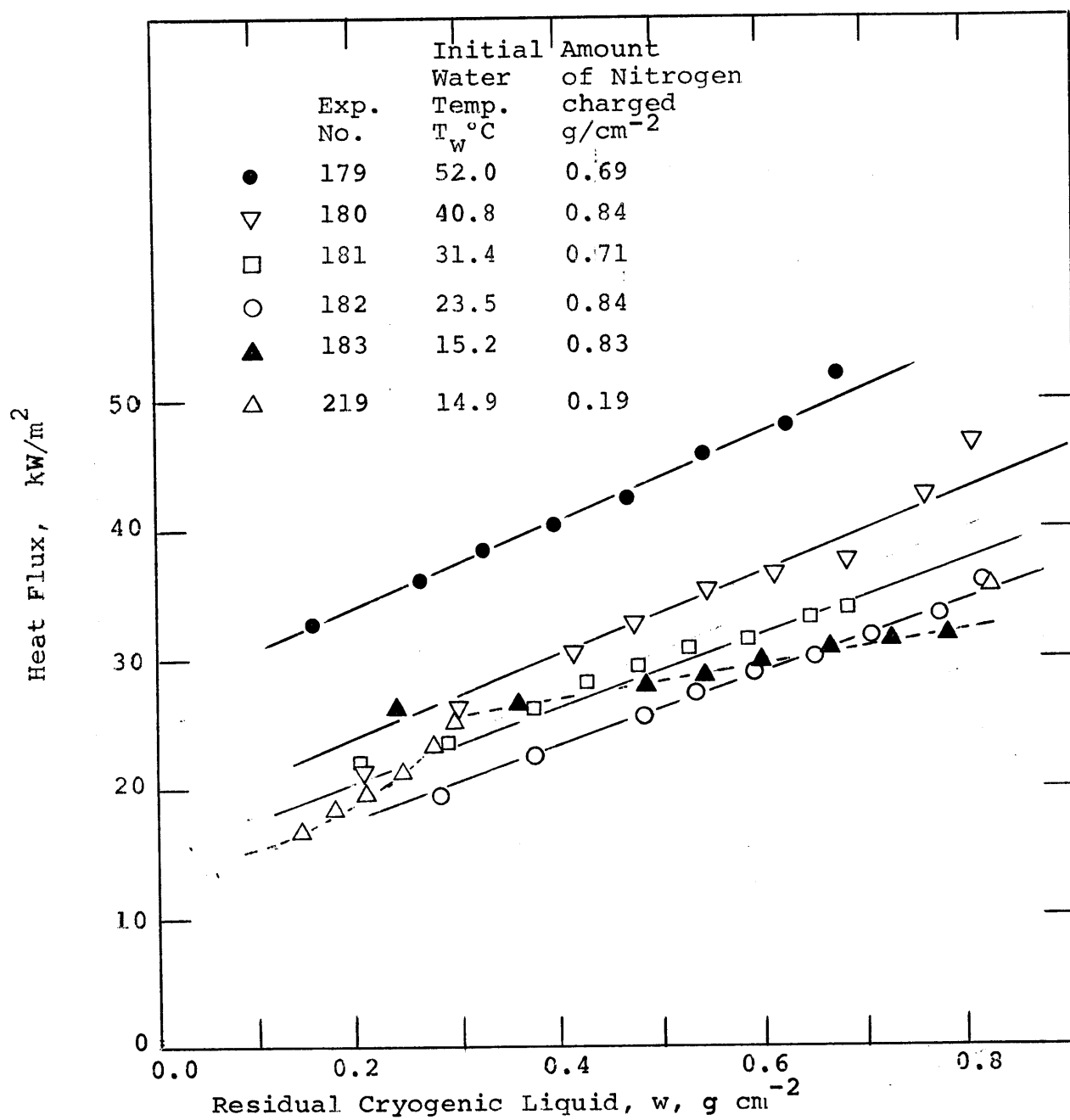


Fig. 5-12

Heat Flux Between Water and Boiling Liquid Nitrogen

the observations. The water loss data (Table 5-3), however, may offer a clue.

TABLE 5-3

Water Loss During Liquid Nitrogen Boil-Off
($\sim 0.84 \text{ g/cm}^2$ spilled)

EXP #	INITIAL Water Temperature °C	$\frac{-\Delta \text{Wt. Water}}{\text{Wt. Cryogen}}$
179	52.0	0.07
180	40.8	0.04
182	23.5	0.02
183	15.2	0.01

Nitrogen's heat of vaporization (200 J/g) is about 7.7% of the heat of sublimation of water. If one assumes that all the water vaporized condensed to fog (a reasonable assumption at the low vapor temperatures observed), it becomes clear that the fog contributes about 34% of the total heat flux when 40.8°C water was used. The corresponding fog contributions were $\approx 21\%$ with 23.5°C water, and 11.5% with 15.2°C water. Since the water-liquid nitrogen temperature difference, ΔT , in the runs are about the same (changes in water temperature are minor relative to the overall ΔT), it appears that the fog contribution alone explains the difference between, e.g., runs 180 and 182. In run 183, with 15.2°C water, a small amount of ice might have been formed.

Thus the noted heat fluxes for this run is higher than can be accounted for by the fog.

A comparison of experiments 183 and 219 shows the effect of the amount of cryogen charged (Figure 5-12). This effect is explained in the next section. The fact that the heat fluxes in run 221 are higher than for run 219 also indicate that the formation and growth of ice particles (which may be recirculated and melted) become more significant as the water temperature was lowered.

5-4-2. DISCUSSION OF RESULTS

In this section, answers are sought and presented for a number of questions that might be posed from the foregoing results. These are (not necessarily in the order of importance):

1. Why do the boil-off rates to methane (and LNG) increase with time while that to liquid nitrogen drop?
2. Why does the vaporization of liquid nitrogen depend upon the amount charged?
3. How does ice formation affect the boil-off rates?
4. How are small bubbles formed in mixtures, and how do these bubbles influence the boil-off rates? The first part of this question has been dealt with earlier in the chapter.

The results (of the present work) are discussed critically in the following as answers are sought for these questions.

Questions 1 & 2. Heat Fluxes

As shown in section 5-2, when two semi-infinite bodies at different temperatures are brought in contact, the heat flux by conduction is given by

$$Q' = \frac{\theta}{1 + \theta} \frac{k_1 T_{\max}}{\sqrt{\pi \alpha_1 t}} \quad (5-58)$$

i.e. $Q' \propto t^{-1/2}$ or the heat flux decreases with time. If one or both of the bodies have convective flows up to the interface, the heat flux is enhanced over that predicted by Equation (5-58) (see Figure 2-14), but the heat fluxes still decrease with time unless the heat transfer coefficients are infinite. If a low thermal conductivity vapor film separates the bodies, such as the case during film boiling, the heat flux becomes much less than obtained with direct contact.

For the case of cryogenics film boiling on water, convective flows occur in both liquids and heat is transferred across the vapor of the cryogen. In transient experiments, the temperature difference ΔT , across the vapor film, and the head of cryogenic liquid remaining, should continuously decrease with time with the following possible results. These are based on the assumption that the vapor film thickness, δ , changes as a boiling experiment progressed.

Since the two superposed liquids are in continuous oscillations (driven by bubble production mechanisms), the probability of the liquids touching each other frequently, intermittently and at

random locations is increased as δ decreases. Even without bubbles being produced (together with the associated hydrodynamic instabilities), boiling liquid-heating surface contacts may be obtained as shown by Bradfield (1966). High local fluxes are realized when such direct contacts are made, and the total heat transferred per unit area at a contact site is obtained by integrating Equation (5-58), i.e.

$$Q = 2\theta \frac{k_1 \Delta T}{1 + \theta} \left(\frac{\tau_c}{\pi \alpha} \right)^{1/2} \quad (5-59)$$

where τ_c is the contact time.

The overall heat flux, at any instant, between the liquids is obtained by integrating Equation (5-58) over the entire liquid-liquid interface, (wherever contacts occur). One must take into account the fact that the different contact sites have different life times (i.e. t varies with site), and the fact that each site may have a time-dependent area of contact. To this flux, the contribution due to conduction across the vapor film where liquid-liquid contacts do not exist must be added.

Apart from the high average heat fluxes that may be realized by intermittent direct liquid-liquid contacts, the probability of ice forming on water is enhanced as δ decreases. If liquid-liquid contacts are obtained for sufficiently long durations, ice nucleation occurs. The nucleation theory (Fletcher, 1966) indicates that the number of embryos produced is given by:

nitrogen and pure methane boiled on water for the experiment durations (<60 s). A close examination of Plate 6 of Figure 3-6, however, show that some tiny ice particles (or nuclei) are present at the water surface. Moreover, Plates 5 and 6 show some dark patches where the liquids touch. It is here suggested that ice particles were on the water surface but they are of such sizes that they are not visible in the pictures (except, maybe in Plates 5 and 6). These ice particles were apparently recirculated into the bulk and melted.

Pictures of boiling nitrogen (Figure 305) do not show the patches or ice particles on water surface. Some pieces of ice are noted, however, within the cryogen.

The differences between the boiling of nitrogen and methane may be explained thus. With a ΔT of $>200^\circ\text{C}$ while nitrogen boiled, stable film boiling is obtained. The minimum film boiling ΔT is $\sim 48^\circ\text{C}$ (Flynn et al., 1961). The formation and departure of bubbles cause oscillations of the lower free surface of the cryogen (adjacent to the water), but, apparently, the amplitudes of oscillations were sufficiently low and little liquid-liquid contact occurred. (The facts that the bubbles noted in nitrogen during film boiling are small relative to the hydrocarbon bubbles, and are produced with small inter-bubble spacings (see Figure 3-4) may be important.) If negligible liquid-liquid contact occurred, then the heat flux depends primarily on the resistance of the vapor film.* The heat flux is

*It may be readily shown that the vapor film resistance control the flux of heat. An order of magnitude analysis of the ratio, J , of

therefore prescribed by

$$Q \cdot = h^{\#} (T_w - T_c) \quad (5-61)$$

where the effective heat transfer coefficient, $h^{\#}$, is evaluated from

$$\frac{1}{h^{\#}} = \frac{1}{h_c} + \frac{\delta}{\bar{k}_v} + \frac{1}{h_w} \quad (5-62)$$

conductance
conductance
conductance
in cryogen
within vapor
within water

film

For nitrogen boiling on water, $h_c \gg \frac{\bar{k}_v}{\delta}$ or h_w , and $h_w \sim 0.1 \frac{\bar{k}_v}{\delta}$ (see footnote).

*resistance in the vapor to that in water is given by:

$$J \approx \frac{Q \cdot}{k_w \frac{\Delta T^{\#}}{\Delta z}} \times \frac{\Delta T^{\#}}{\Delta T_{\text{film}}} = \frac{h \Delta z}{k}$$

water
boundary
layer

where, the heat flux, $Q \cdot = h \Delta T_{\text{film}}$ is temperature across the vapor film, and $\frac{\Delta T^{\#}}{\Delta z}$ is the temperature gradient in water, at the surface.

e.g. in experiment 216, $\Delta T^{\#} \sim 20^{\circ}\text{C}$ for $\Delta z \sim 0.5 \text{ mm}$. $Q \cdot \sim 28 \text{ kW/m}^2$, $\Delta T_{\text{film}} \sim 200^{\circ}\text{C}$, and $k_w \sim 0.6 \text{ W/mK}$.

Hence

$$J \sim 0.1 \quad (< 1)$$

This means that the resistance within the vapor film is limiting.

Hence

$$Q \cdot \approx 0.9 \frac{\bar{k}_v}{\delta} (T_w - T_c)_{\text{bulk values}} \quad (5-63)$$

This means that the heat flux to liquid nitrogen is inversely proportional to the film thickness. Experimental data (Appendix F) indicate that $T_w - T_c$, i.e. the temperature difference across the film, does not decrease by much in a run ($\bar{k}_v \propto |T_w|$ and $|T_c|$), hence other factors that determine δ , such as the liquid hydrostatic head or external pressure, will also determine the heat flux values.* It is noted in Figure 5-12 that the heat transfer rates to liquid nitrogen decreased as the hydrostatic head decreased. Since the hydrostatic head exerts a compressive force on the vapor film, a relaxation of the film should occur as nitrogen vaporized, i.e. δ increases with time and the flux decreases.

This film relaxation hypothesis explains why the flux to nitrogen should decrease with time. It also explains why the noted initial heat fluxes should depend on the quantity of nitrogen introduced. The fact that very high heat fluxes are achieved if pressure is applied to liquid cryogenics in film boiling (Sciante et al., 1967; Park et al., 1966) support the hypothesis.

The steady state heat fluxes to liquid nitrogen film boiling on solid surfaces at a $\Delta T \sim 220$ K has been measured to be between 25

*The absolute value of water surface temperature is also important. As shown earlier, the amount of water lost and the contribution of the heat of sublimation of the water vapor-fog phase changes to the total flux may be appreciable.

to 30 kW/m^2 (Sauer and Ragsdell, 1971; Flynn et al., 1961). This is in the range noted in the present study for boiling on water. (Figure 5-9.) The transient heat fluxes obtained with water were, however, dependent on the initial water temperature and generally increased as the initial water temperature was increased. The difference in results (for boiling on a solid and on water) has been earlier explained as due to the heat of sublimation released by water vapor as it formed a fog.

The heat transfer coefficient, h , calculated from Equation (5-49) for nitrogen (constants evaluated at 165K) is about $130.6 \text{ W/m}^2\text{K}$. This means that the heat flux calculated from theoretical considerations (modified Berenson's equation) is about 27 kW/m^2 at a $\Delta T \sim 220\text{K}$. This is within the range of experimental data and the correlation may be considered good.

Liquid methane, with a lower temperature difference across the vapor film, ($\Delta T \sim 170^\circ\text{C}$), releases large bubbles, and it probably experiences large amplitude and lower frequency oscillations than nitrogen at the free surface adjacent to water ($\Delta T_{\text{min}} \sim 72^\circ\text{C}$ for film boiling). The consequence, as noted earlier, is that liquid-liquid contact of short duration would frequently occur. The frequency and duration of such contacts determine the extent of enhancement above the condition of complete liquid-liquid separation. The heat fluxes (Figure 5-4) obtained indicate that the frequency and/or duration of contact increases with time as the fluxes show upward trends. The formation, recirculation and melting of microscopic ice nuclei are

probably very significant factors in the noted fluxes. (In experiments of long duration, large ice pieces are noted on the water surface.)

Heat fluxes to methane boiling on solid surfaces ($\Delta T \sim 170$ K) were reported by Sciance et al. (1967) and Sliepcevich et al. (1968) to be about 35 kW/m^2 . This value is in the range of initial heat fluxes from water in Figure 5-4 as might have been expected. Again, the actual water-liquid methane fluxes were probably slightly higher than with a solid heating surface because of the contribution of the water vapor which sublimed into fog.

The heat flux calculated from theory (Equation 5-49) with $\Delta T \sim 170$ K is about 27 kW/m^2 , the same noted for nitrogen. This is about 20% too low. Correction for fog effects would slightly reduce the margin of error.

Questions 3. Formation of Ice

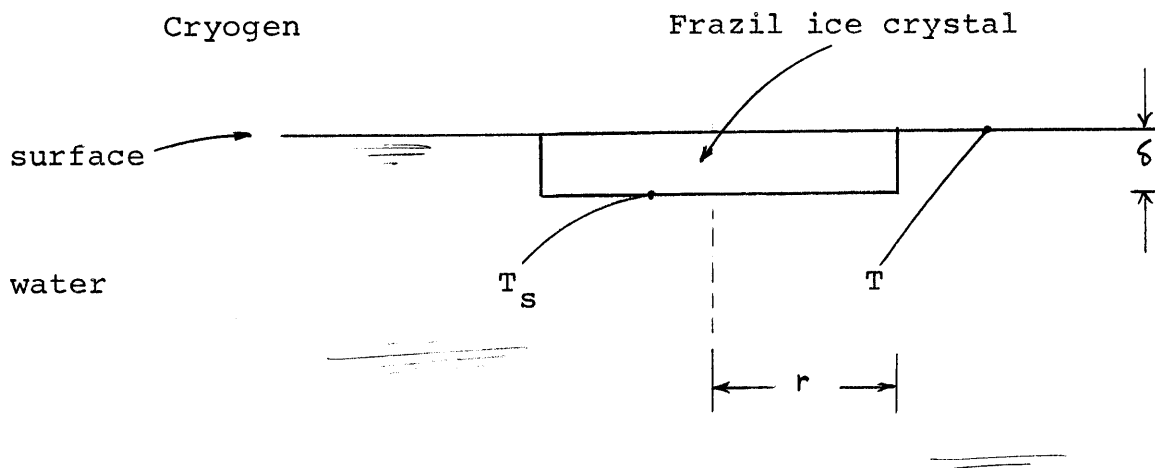
When ethane (b.pt. -88.3°C) was poured on water ($<50^\circ\text{C}$), ice platelets were noted on the water (Figures 3-7 and 3-8). The rapidity of formation of these platelets, and rate of growth, were noted to increase as the water temperature approached 0°C . Moreover, the heat fluxes noted into boiling ethane rose very sharply from ~ 40 to 50 kW/m^2 to $\sim 130 \text{ kW/m}^2$ in about 10 s (Figure 5-5). Furthermore, film boiling appear to be the mode of heat transfer where ice was not present. The latter was suggested by the fog in the pictures, e.g. Figure 3-7. Film boiling might also have been pre-

dicted since the data of Sliepcevich (1968) indicate that the Leidenfrost ΔT for ethane is about 22°C .

The initial formation of the ice may be attributed to a small film thickness, δ , and extensive liquid ethane-water contacts. After ice is formed, a change of boiling regime from film to nucleate occurs over the solid. This is accompanied by an increase in heat flux. The fact, though, is that the peak (or highest) nucleate boiling flux recorded for ethane (at 1 atm) on a solid surface is $\sim 48 \text{ kW/m}^2$ (Sliepcevich et al. 1968). This is only one third the highest flux measured while this alkane boiled on water, but it is about 20 times the flux for film boiling ($\Delta T \sim 100 \text{ K}$).

Apart from the large latent heat (of ice) released, microscopic irregularities on the surface of the ice formed may influence the results. To maintain the high fluxes, growth of ice occurred primarily, and rapidly in the subcooled surface layers of the water, and wafers were formed. The fact that nucleate boiling should occur on the ice wafers may be established from a simple calculation based on the measured rate of growth of the ice discs or platelets. A typical ice platelet surface temperature may be estimated as follows:

One may assume that the ice platelet is stationary (except for radial growth) and just neutrally bouyant as indicated in the sketch below:



The energy balance is given by

$$(C_{p_w} \Delta T_w + \Delta H_f) \frac{dm}{dt} = k a^+ (T_s - T) \quad (5-64)$$

[Heat released during solidification] [Heat released into the cryogen]

where a^+ is a shape factor for the disc. This equals $8.88r$ (Kutateladze, 1963; Sunderland and Johnson, 1964). Thus Equation (5-64) becomes, approximately ,

$$\frac{dr}{dt} \doteq \frac{4.44k(T_s - T)}{\pi \rho_s \Delta H_f \delta} \quad (5-65)$$

where $\delta \sim 750 \mu\text{m}$ (measured in experiments), $T_s \sim 0^\circ\text{C}$ and $k \sim 3.5 \text{ W/mK}$

(Ratcliffe, 1962). $\frac{dr}{dt}$ was measured (average of 5 independent discs) to be $\sim 0.13 \text{ cm S}^{-1}$. The temperature of the ice upper surface, T , is $\sim -70^\circ\text{C}$, when Equation (5-65) is solved.* This is also the average temperature apparently imposed on the water surface. The conditions for platelet or frazil ice formation are, therefore, similar to, but more severe than those reported by Schaefer (1950) and Arakawa (1954).

Even though ethane boils at a higher temperature than methane or nitrogen, ice platelets (or frazil ice) were not noted with the latter cryogens. The reasons for the difference are not clear, but they may be related to the fact that thicker vapor layers are obtained as ΔT increased in film boiling. Most of the temperature drop occurs across this vapor layer. With nitrogen and methane boiling, the water experiences some surface subcooling. (See Thermocouple reading in Appendix F). Platelets should probably grow, but at slow rates, if the duration of the experiments were sufficiently long. But as soon as the platelets form, nucleate boiling should occur and extremely high heat fluxes may be obtained. High heat fluxes were readily obtained when pressure was applied on methane or nitrogen in film boiling on water, i.e., when the liquids are forced close together.

*Thermocouples embedded within the ice read temperatures $\sim -80^\circ\text{C}$.

(See Appendix F, exp. 171 to 177).

Another mechanism by which ice production may be enhanced involve hydrates. Very little data exist on hydrate formation at low cryogenic temperatures. If one extrapolates the curves in Figure 2-13 to low temperatures, one may predict that hydrates should form readily at low pressures. In that case, since ethane form hydrates more readily than either methane or nitrogen (Katz, 1959), the rate of production of ice nuclei on the water surface, or within the vapor film, should be highest for ethane. Presumably those nuclei develop into platelets with ethane, but are recirculated and melted in water above which methane and nitrogen boiled.

In prolonged methane boil-off runs, and when LNG was boiled, white opaque ice discs were noted on the water surface. The ice occluded tiny gas bubbles, and the rate of ice growth increased as the methane concentration in LNG was reduced. Growing ice discs are seen in Figures 3-5 and 3-10. The ice discs were thicker and they grew more slowly than the platelets noted while ethane boiled. The origin of the bubbles occluded in the ice is not known. It may be that gases dissolved originally in the water were trapped as the ice formed. The ice (hydrates ?), however, promote nucleate boiling and help explain the high fluxes noted into LNG as discussed next.

Question 4: Boiling of Mixtures

In earlier sections, two basic hypotheses were advanced on the formation of small bubbles in LNG.

The first involved the mechanism of production of the

bubbles. It was suggested that the bubbles originated in a 'nucleate boiling' type process when the LNG comes in direct contact with water, presumably on omnipresent dust particles originally on the water. Bubbles were also suggested formed when pure liquids (e.g. nitrogen, methane) contact water. The primary difference between the bubbles formed in single-component liquids and in mixture was suggested to be the ease of coalescence of adjacent bubbles. When the bubbles coalesce readily, film boiling is quickly initiated. Such is believed to be the case with pure liquids. With mixtures, the bubbles formed are smaller and they do not coalesce as readily. Concentration gradients should exist around the bubbles, and the gradients may cause convective flows between adjacent bubbles (Marangoni effect)*. The net effect is that the bubbles are maintained apart, and film boiling would be initiated only when dense clusters of the bubbles were formed.

The second hypothesis is on the formation of small bubbles in mixtures but not in pure liquids. A simple theory was proposed on

*In mixtures, a concentration gradient probably exist around each bubble. Therefore, convective flows driven by surface tension which is a function of concentration (Hovestredjt, 1963; Saville, 1973) may occur. Liquid flow between bubbles tend to keep them apart and hinder their coalescence. The significance of convective flows may be estimated by calculating a Marangoni number defined as:

$$M = \frac{\frac{d\alpha}{dx} \Delta x}{\mu} \left(\frac{t}{\rho}\right)^{1/2}$$

For a binary methane-ethane mixture at -160°C , $M \sim 10^{11} t^{1/2}$ where t is in seconds. Convection is important when $M > \sim 80$ (Pearson, 1958). Hence, flows may be initiated at $t \sim 30 \mu\text{s}$ after a bubble forms.

how hydrodynamic forces affect the early growth of a bubble in Section 5-2-2. In Section 5-2-1, a survey of growth rate equations in the literature was presented. It was shown that most derivations were on the asymptotic growth stage. (This is the growth stage of the bubbles noted in the pictures - Figures 3-9 and 3-10.) Pictures presented by van Strahlen (1968), however, show that within 0.2 ms, large bubbles were formed from microscopic sizes. Moreover, 50 to 80% of the bubble diameters 10 ms after bubble nucleation were realized within the short early stage.

Since it has been hypothesized that the bubbles are formed primarily in the short duration initial liquid-liquid contact (may be 10 ms after the spill) it is most appropriate to consider how the bubble sizes would be limited in the early growth stage. One of the ways was examined in Section 5-2-2. The fact that the theory presented is tentative must be emphasized in view of the very limited experimental data. Primarily, the pressure differences across the boundaries of growing bubbles are not known.

In surface boiling problems (with subcooled liquids), the bubbles released from a boiling interface collapses in the bulk liquid. Then it is usually assumed that large ΔP values are obtained, $\Delta P \gg \sigma/R_{\text{bubble}}$, and ΔP may be estimated from data on bubble collapse rates. Bankoff (1966) includes a review on such calculations. For a bubble in a saturated liquid mixture, $\Delta P, (P_b - P_{\text{amb}})$, in the early growth stage is not known. It may be small and negative if P_b is slightly

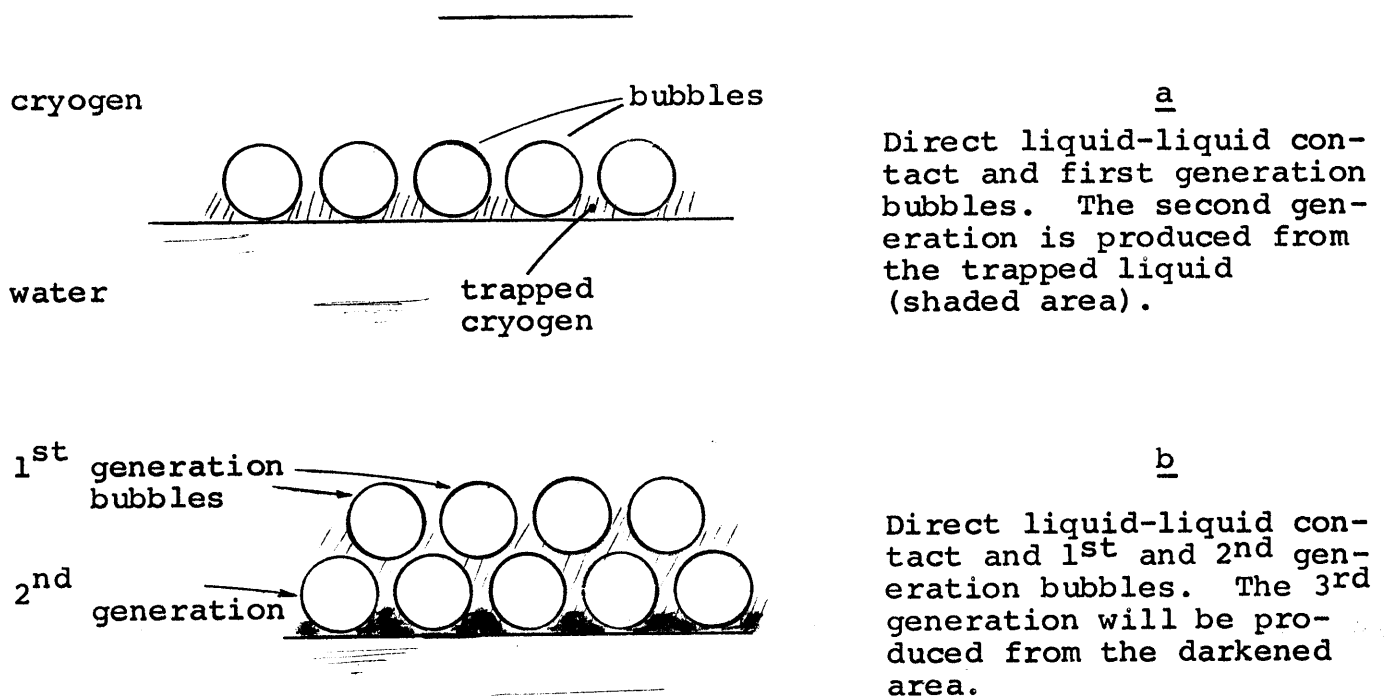
less than the vapor pressure. When ΔP is in the same order of magnitude as σ/R_f (R_f is equilibrium bubble radius), as was implicit in the analysis in Section 5-2-2, then variations in surface tension values, σ , as one moves from one liquid to another may be used to explain the differences in bubble sizes.

With pure methane ($\sigma=0.014$ N/m) or ethane ($\sigma=0.017$ N/m) at their saturation temperatures, relatively big bubbles should be produced. These bubbles may merge readily at the boiling interface to initiate film boiling. The big bubbles will also be bouyant. A bubble formed in a binary mixture of methane and ethane would have essentially pure methane within the cavity. This methane would have been removed from the bubble walls which will, therefore, be richer in ethane than the bulk liquid. If the bubble boundary is assumed to contain pure ethane, and the wall is maintained at the temperature of the bulk liquid (e.g. $\sim -160^\circ\text{C}$), the effective surface tension obtained by extrapolation (Figure 3-11) is ~ 0.028 N/m. Hence, the bubbles formed will be smaller with the mixtures on account of the larger growth resisting forces. Similar reasoning is applied to other 'positive' mixtures.

The sequel to the foregoing hypotheses is a description of how the small bubbles formed in mixtures (by whatever mechanism) cause the high fluxes noted in Figures 5-6 to 5-10.

As suggested in Section 5-2-3, the minimum bubbles separation without coalescence may be very small, ~ 4 μm . The bubble

packing a short while after the two liquids are contacted could be as shown in the sketch below. Generations of bubbles are stacked up on each other, and more bubbles form from the small liquid pockets trapped at the liquid-liquid interface. Eventually, these bubbles coalesce after the concentration gradients between adjacent bubbles are destroyed, and film boiling would result. The time scale for the complete process may be extremely short ($< \sim 10$ ms).

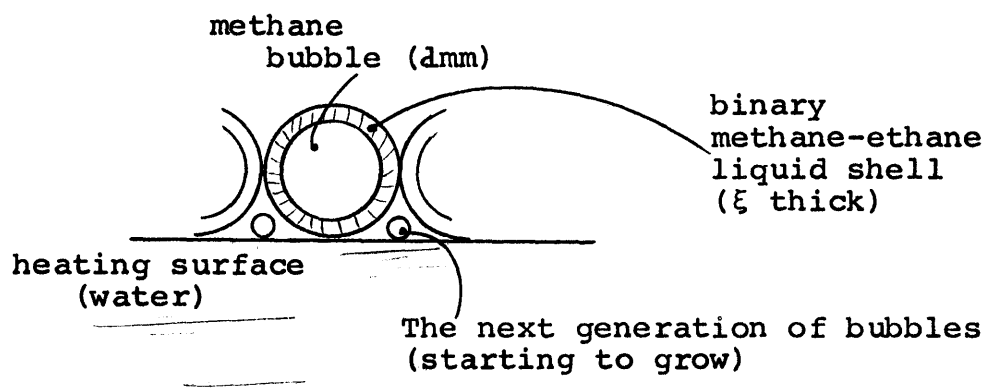


Sketch of bubble growth in liquid mixtures. Many generations may be produced before film boiling is established. In the meanwhile, the liquid adjacent to the water is continuously depleted of volatiles.

The consequence of the formation of several bubbles at the liquid-liquid interface, bubbles which contain primarily one component

of the liquid mixture, e.g., methane in LNG) is that localized enrichment of the less volatile components occur. For fixed bubble sizes and lattice arrangement, the average concentration of a component in the liquid films surrounding the bubbles, may be estimated for a specified number of generation of bubbles.

If, for example, several d mm i.d. methane bubbles are assumed formed from a spherical methane-ethane binary liquid shell of thickness, ξ ,



The methane concentration by weight, X_A , is related to the number of bubbles produced, n , by

$$X_A = X_{Ao} - n \frac{\rho_v}{\rho_L} \frac{d^3}{[(d + 2\xi)^3 - d^3]} \quad (5-66)$$

or

$$X_A = X_{Ao} - n \frac{\rho_v}{\rho_L} \frac{1}{(1 + 2\xi/d)^3 - 1} \quad (5-67)$$

For $d \sim 1$ mm, $\xi \sim 2$ μ m (an approximate concentration displacement

thickness), $\rho_v \sim 10^{-3} \text{ g/cm}^3$ and $\rho_L \sim 0.5 \text{ g/cm}^3$

$$\xi/d \approx 2(10^{-3})$$

and

$$X_A \approx X_{A0} - n(0.166)$$

Hence, for a boiling methane-ethane binary mixture which contains initially 95.8% by weight methane (98 mole %), about 6 generations of bubbles should completely remove methane from a zone ($\sim 1 \text{ mm}$ thick with 1 mm bubbles present as in the sketch) at the liquid-liquid interface.

When bubbles smaller than 1 mm are produced, a larger population of bubbles may form, and more methane can be removed from a thinner zone (\sim bubble diameter) in each generation. Therefore, as one replaces ethane with propane (in binary mixtures with methane), and smaller bubbles are produced (higher effective σ), fewer bubble generations will remove the methane from the interface. When methane is evaporated from the interface, the ΔT across the vapor film between the liquids, is lowered and the intermittent liquid-liquid contacts described earlier should occur more frequently. (See Section 5-1.) High heat fluxes would be realized, especially when some ice forms at the interface and nucleate boiling occurs.

The basic concepts are summarized as follows:

1. Bubbles form by a 'nucleate boiling' type process.

2. Bubble sizes may be influenced to a large extent by the surface tension forces, σ , at the bubble boundary.
3. As σ increases, smaller and smaller bubbles are formed at the boiling liquid-liquid interface. Bouyant bubbles depart the interface.
4. The ease with which bubbles coalesce to initiate film boiling is a function of the initial bulk liquid constituents and compositions. Coalescence would occur least readily at certain mixture compositions at which the concentration gradients (around the bubbles) are largest. Induced convective flows between bubbles depend on the gradients.
5. At these compositions, many generations of bubbles are produced from the same site and the boiling liquid lower free surface will be depleted in its most volatile components. When a dense cluster of bubbles is formed, coalescence may occur at the liquid-liquid interface.
6. The ΔT across the boiling interface becomes lower than without enrichment, and transition boiling may occur. This is accompanied by high heat fluxes.
7. The fluxes realized would be dependent on the extent of short duration liquid-liquid contacts. The frequency of these contacts, area of contact and time period for each contact should increase as ΔT decreases. This

idea may be used to explain the differences in heat fluxes to binary mixtures of different compositions, or different components. For binary mixtures of different compositions, the extent of volatile liquid depletion at the interface (before film boiling is initiated) will determine the ΔT across the interface. The constituents of the mixture also determine the ΔT that would be obtained.

8. After ice is formed, nucleate boiling should occur with some concentration effects exhibited. (Van Strahlen, 1967, 1968).

Sliepcevich et al. (1968) presented data on the boiling of LNG (87% methane, 4% nitrogen, 5% ethane with the balance propane and higher alkanes) from horizontal cylinders. Unfortunately data in the range $35 < \Delta T < 400^\circ\text{C}$ were not obtained at 1 atm pressure. If the film boiling and nucleate boiling curves are extrapolated, however, the fluxes at a $\Delta T \sim 170^\circ\text{C}$ (LNG saturation boiling point $\sim -160^\circ\text{C}$) are 15.8 kW/m^2 and 950 kW/m^2 respectively in the regimes. The data in Figures 5-6 and 5-7 are within these extreme values.

5.5 COMPARISON OF RESULTS WITH PREVIOUS WORK

The available literature on the boiling of cryogenics on water has been reviewed in Section 2-2. There it was shown that the data available were obtained from exploratory experiments which did not involve careful design of apparatus. For this reason, a

qualitative comparison is deemed most appropriate.

Contrary to the conclusions of Burgess et al. (1970, 1972), but in partial agreement with Boyle and Kneebone (1973), the boil-off rates of the cryogenics (except nitrogen) increased with time. A large scatter was noted in Burgess et al.'s data. It is thus easy to conclude that the true behavior of the liquid systems were obscured in their data. Boyle and Kneebone (1973) obtained a heat flux which increased with time while LNG boiled on water, except when the amount of LNG introduced was less than 0.17 gcm^{-2} . Then the 'apparent' boil-off rates decreased with time. As stated earlier, the entire boiling cross-section was most probably not covered in the experiments with low charges. The superficial area used is therefore not the true value.

The results of this work indicate that the amount of liquid hydrocarbon ($0.5 < \xi \leq 2.5 \text{ cm}$) did not influence the vaporization rates, but the reverse was the case for liquid nitrogen in that its boil-off rates increased as the charge was increased. Boyle and Kneebone on the other hand found a strong dependence of the amount of LNG layered; the boil-off rates increased as the charge was increased. However, in the same set of data, their boil-off rates ($\text{gcm}^{-2}\text{s}^{-1}$) for approximately the same LNG head (in cms or gcm^{-2}) did not coincide for the different diameter vessels. That is the vaporization rate was $\sim 20\%$ higher in the 1.04 m I.D. vessel than in the 2.18 m I.D. vessel. It may, therefore, be suggested that

heat contribution from the vessel walls (material of construction not provided) are significant in their experiments. For this reason, the noted effect of the charge may be artificial. The amount-spilled dependence observed by Burgess et al. (1972) (Table 2-1) for methane appears to be by coincidence since the reported values were within the scatter of their data, wall effects might have been important as well.

In partial, but qualitative agreement with Boyle and Kneebone, a strong dependence of water temperature was noted only when cold water ($< 10^{\circ}\text{C}$) was used. They noted $\sim 200\%$ enhancements in heat flux from water at 0.5°C , $\sim 100\%$ for water at 4°C and $\sim 60\%$ for 10°C water over that for 15°C water 10-15s into the runs. The heat flux reported from the 0.5°C water into LNG (95.85% CH_4 , 2.75% C_2H_6 , 0.25% C_3H_8 , 0.15% C_4H_{10} and the balance nitrogen) was about 25 kW/m^2 , 5s into the runs. This rose to $\sim 88 \text{ kW/m}^2$ at 15s (6 mm LNG charged). These values are 40% to 70% lower than obtained on warmer water in the present work with leaner LNG. (See Figure 5-6).

It is not clear how to reconcile their results with the present work.

With respect to the effect of the composition of mixtures on the vaporization rates, the present results agree qualitatively with those of Nakaniski and Reid (1971), and Boyle and Kneebone (1973). Heat fluxes into mixtures of methane with higher alkanes were higher than into pure methane. Moreover, the enhancement increased as the

fraction of methane in the mixtures was lowered. Nakanishi and Reid (1971) observed that the presence of traces of pentane or hexane in methane caused the latter to boil-off at faster rates. This observation was confirmed for ethane, propane and butane in methane. Furthermore, it was established that the enhancement to methane increased as the additive level in the alkane homologous series increased.

CHAPTER 6CONCLUSIONS AND RECOMMENDATIONS

The conclusions of this work are summarized as follows:

1. The heat flux from water into a cryogenic hydrocarbon liquid mixture which has methane as its principal component is much higher than that into pure methane.
2. The vaporization rates of such mixtures increase as the fraction of methane present is decreased.
3. Traces of ethane, propane and butane in methane cause large enhancements in the observed heat flux into methane (50 - 100%). It is noted that butane is more effective in enhancing the heat flux than either propane or ethane. In turn, propane is more efficient than ethane.
4. With binary mixtures of methane and ethane, a maximum in the heat flux-methane fraction plot is obtained when the mixture initially contained about 5% ethane.
5. The heat flux to hydrocarbon liquids, single component and mixtures, increases with time as the liquids boil on water.
6. Boil-off rate-time curves for nitrogen, however, show that the rate of evaporation decreases with time.
7. The boil-off rates of the hydrocarbons are essentially independent of the amount of the liquid cryogens

initially poured on water.

8. Nitrogen vaporization rates, however, increase as the charged liquid quantity is raised.
9. The boil-off rates of nitrogen and the hydrocarbons are essentially independent of the temperature of the water ($10 \leq T_w \leq 60^\circ\text{C}$).
10. Some water is carried off as fog by the vapors of the boiling liquids. The amount of water loss is almost proportional to the vapor pressure at the bulk water temperature.
11. Numerous small bubbles (< 4 mm diameter) are produced and observed at the interface of mixtures when the liquids boil on water. No such small bubbles are seen in pure boiling liquids.
12. Big bubbles are noted produced at the liquid-liquid interfaces. In nitrogen, the average diameter is about 8.7 mm. The diameters are about 1.35 cm in the hydrocarbons, single-components or mixtures.
13. Pure ethane boils-off quite rapidly on water.
14. Ice is sometimes noted at the interfaces. On water at low temperatures, nitrogen forms ices slowly and the ice pieces are thin and transparent. With the hydrocarbons, the ice is opaque white. Mixtures form ice more readily than pure methane. With ethane, rapidly

growing ice wafers are noted.

15. Heat fluxes to nitrogen are in the range observed for boiling on solid surfaces, i.e., 25 to 35 kW/m². This also agrees with results of a hydrodynamic model of film boiling heat transfer.
16. Vapors leaving boiling pools of nitrogen are superheated. The calculated sensible heat transported, including the heat of sublimation of the fog, may be as much as 40% of the total flux.
17. The vapors above methane rich hydrocarbon pools are also superheated ($T_v \sim -130^\circ\text{C}$). The vapor sensible heat is in the order of 5% of the total flux.
18. Vapors above boiling ethane pools are almost saturated, $T_v \sim -86^\circ\text{C}$. The exception is when hot water ($\sim 50^\circ\text{C}$) and a small quantity of ethane is layered. Then superheat of up to 20°C are noted.
19. Temperatures at the water surface do not drop much below 0°C while nitrogen and methane boiled. Mixtures and ethane, however, give low surface temperatures when the thermocouple junction is encapsulated in ice.
20. The structures at the interface of nitrogen with a warm smooth glass surface is different from that noted at a glass-water interface. The cryogen lower free surface is smoother with the latter system.

It is recommended that continuing research include examination of the following points.

1. The surface tension of binary mixtures of methane and the higher alkanes should be determined as a function of liquid composition (at the equilibrium temperatures). Both static and dynamic surface tension values should be established if possible. This should permit a better understanding of small bubble production in positive liquid mixtures.
2. Formation of hydrates by cold hydrocarbon gases should be studied. The conditions of hydrate formation above a water surface at low vapor temperatures and pressures should be established.
3. The turbulence at the water surface should be closely examined for its efficiency of ice particle recirculation. The lack of sharp resolution of ice particles with 1 ms exposure suggest very high velocities are achieved.
4. The rate of growth of bubbles in hydrocarbon mixtures, concentration profiles around the bubbles and the break-off volumes should, also, be studied. Knowledge of these could suggest why vapor explosions are obtained with mixtures of certain compositions.

APPENDICES

APPENDICES

- A. FOG FORMATION
- B. EQUIPMENT OPERATIONAL PRINCIPLES, DESIGN DETAILS AND PERFORMANCE DATA
- C. AUXILIARY RESULTS
 - Bursting of Bubbles
 - Vapor Hold-Up in Boiling Cryogens
- D. ERROR ESTIMATE (HEAT FLUX) AND THERMOCOUPLE CALIBRATION DATA
- E. SAMPLE DATA TREATMENT
 - Computer Program
 - Coefficients of Least Square Fit
- F. EXPERIMENTAL DATA
 - List of Experiments and Variables
 - DATA
- G. BIBLIOGRAPHY
- H. NOMENCLATURE

APPENDIX A

FOG FORMATION

Generation of fog within the vapor film separating water from the cryogens is believed to be a vaporization-freezing process, i.e. water vapor is condensed to ice particles within the film. In the following, the conditions necessary and the location above the water surface that fog is produced are determined. The assumptions made in the analysis and justifications for them are presented as follows:

1. The average film thickness, δ , is about 100 μm (Bradfield, 1966).
2. Flow within the film is laminar. This would be expected unless the vapor velocities are very large.
3. The film thickness is essentially constant with time and in space.
4. The film has a negligible thermal capacity.

If one performs a differential energy balance on an element dz in Fig. A-1, one obtains (Bird et al., 1960)

$$\rho_v \frac{DU}{Dt} = -\nabla \cdot q + Q'' \quad (\text{A-1})$$

where $\frac{DU}{Dt}$ is the substantial time derivative of the internal energy of the film per unit volume, and q is the conductive heat flux. Q'' is the generation term. The vapor has been assumed to be incompressible and viscous dissipation is neglected. At $z = \delta$, both fresh vapor

produced at the cryogen surface, and water vapor diffusing from $z = 0$ are assumed to depart in bubbles without affecting the film.

The first step in the analysis is to determine the temperature profile that will exist within the film if there were very small convective flows in the z -direction, i.e. that due to diffusing water vapor alone, and no phase transformations (vapor-ice) are allowed, that is, $Q'' = 0$. In that case, since $\rho_v \cdot \frac{DU}{Dt}$ is small, at steady state

$$q \approx \text{a constant} \quad (\text{A-2})^*$$

Since the temperature difference across the film is large, and the thermal conductivity of the vapor is a function of temperature, (A-2) becomes

$$k(T) \frac{dT}{dz} = \text{constant} \quad (\text{A-3})$$

The subsequent steps involve the determination of the temperature profile, the saturation vapor pressure of water, P_A° , at different

 *It is recognized that this relation will not be accurate near $z = \delta$ due to the cryogen vapor production. $V_z|_{z=\delta}$ may be substantial there. Within the film and close to $z = 0$, $V_z|_{z=\delta}$ however, the assumptions should be good if the cryogen does not diffuse into the water.
 Note that:

$$\rho_v \frac{DU}{Dt} \approx \rho C_p \frac{\partial T}{\partial t} + V_z \frac{\partial T}{\partial z}$$

for the one-dimensional problem.

z positions corresponding to the local temperatures, and the actual water vapor concentration or pressure, P_A , by solving the diffusion equation. At a critical P_A/P_A° , spontaneous transformation from water vapor to ice particles (fog) occurs. Since P_A/P_A° is a function of z , the position of fog formation above the water, z_c , can, therefore, be determined. (The derivations assume that the temperature profiles are first established. Then spontaneous fog formation occurred.)

The boundary conditions are

$$T(\delta) = T_c$$

and $T(0) = T_w \quad (= T_0, \text{ a reference temperature})$

Equation (A-3) can be non-dimensionalized with

$$\phi = \frac{T - T_w}{T_c - T_w}$$

and $\zeta = z/\delta$

An integral approach for solving (A-3) is adopted. Polynomials are assumed for both the temperature profile and the vapor thermal conductivity as

$$\phi(\zeta) = a_0 + a_1\zeta + a_2\zeta^2 \quad (\text{A-4})$$

and $k(\phi) = k_0(\alpha + \beta\phi) \quad (\text{A-5})$

Hence for liquid nitrogen at -196°C on water at 0°C , the average film temperature is $\sim -81.1^{\circ}\text{C}$.

Equation (A-9) is an approximate temperature profile within the film. The heat flux can then be calculated from this profile from

$$q' = -k_0 \frac{d\phi(0)}{d\zeta} \frac{T_c - T_w}{\delta} \quad (\text{A-11})$$

For nitrogen on water at conditions given earlier, and $\delta \sim 100 \mu\text{m}$,

$$q' \sim 24 \text{ kW/m}^2$$

This flux is a good approximation of the experimental value (25 to 35 kW/m^2). The result gives some confidence in the chosen profile.

Next, the water vapor concentration profile within the film is determined. The flux equation is

$$N_{A_z} = \frac{-C D_{AB}}{1 - y_A} \frac{dy_A}{dz} \quad (\text{A-12})$$

if the vapor diffuses into a stagnant film or into a fluid in laminar flow in a direction perpendicular to the diffusion direction.

Schwartz and Brow (1950) showed that the diffusion coefficient of water vapor into nitrogen gas can be described with

$$D_{AB} = D_{AB}^{\circ} (a_1 + a_2 \phi)^S \quad (\text{A-13})$$

where $s = 2.334$ and ϕ is the dimensionless temperature defined earlier. A numerical value of $6.54(10^{-7}) \text{ cm}^2/\text{sK}^{2.334}$ was given for D_{AB}° .

When (A-13) is substituted into (A-12), the latter can be integrated, i.e.,

$$\int_0^{\zeta} \frac{\Gamma d\zeta}{(a_1 + a_3\zeta + a_4\zeta^2)^s} = \int_0^{\ln(1-y_A)} \frac{d(\ln(1-y_A))}{d(\ln(1-y_A))} \quad (\text{A-14})$$

$$\Gamma = \frac{N_{AZ} \delta}{D_{AB}^{\circ} C}$$

$$a_1 = T_w$$

$$a_3 = (1 + \psi)(T_c - T_w)$$

and $a_4 = -\psi(T_c - T_w)$

In the present problem

$$T_w = 273\text{K}$$

$$T_c - T_w = -196\text{K}$$

$$\psi = -0.516$$

$$\delta \sim 100 \mu\text{m}$$

$$c \sim 10^{-3} \text{ g/cm}^3 \quad (= \rho_v)$$

and $N_{AZ} \sim 10^{-4} \text{ g/cm}^2\text{-s}$

N_{AZ} is an approximate value based on the water loss in the experiments. (See Table 5-3.)

Equation (A-14) is most readily solved graphically. The final results is presented in Figure A-2 as the partial pressure of

water vapor, $P_A (= y_A P_T)$ versus the dimensionless distance. In the same figure, the saturation vapor temperature of water corresponding to the local temperature within the film (based on the profile in (A-9)) has been plotted. (Vapor pressure data was taken from Weast (ed.), Handbook of Chemistry and Physics, 53rd edition.)

In Table A-1, at $\zeta = 0.09$, the saturation ratio is 2.2 at -10°C . This is less than required for nucleation as shown in Figure A-3. Calculations and data correspond at $\zeta \sim 0.25$ when (P_A/P_{A0}) equals about 7. Hence the fog is generated at a distance of about $25 \mu\text{m} (= \zeta\delta)$ from the water surface.

The foregoing derivations show that fog is produced within the film very near the water surface. In a real situation, after the initial ice particles are formed, some degree of mixing may occur within the film. The consequence is that any concentration and temperature profiles are destroyed and fog would start forming very close to the water surface.

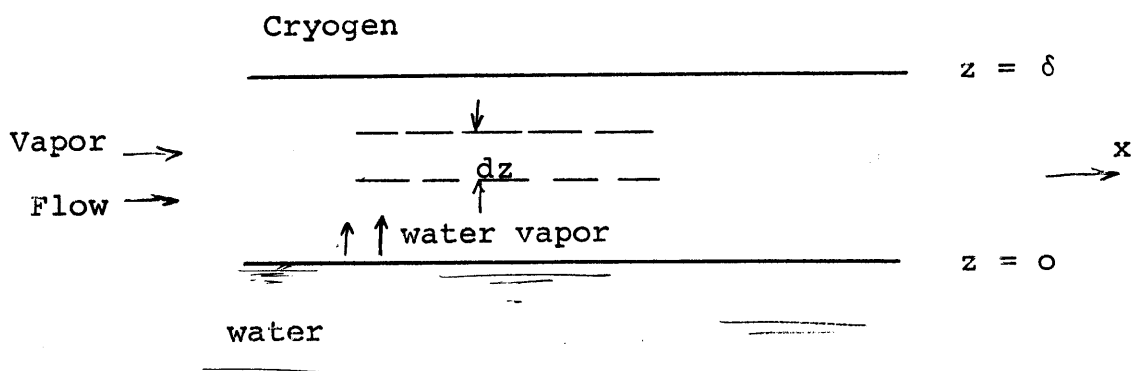
TABLE A-1
Saturation Ratio within the Vapor Film

Dimensionless Distance	Temperature	Saturation* Vapor Pressure	Saturation Ratio
ζ	T°C	P_A° mm Hg	P_A/P_A°
0	0	4.58	1
0.09	-10	1.95	2.2
0.252	-30	0.286	13.6
0.384	-50	0.0296	115.5

* Weast (53rd ed., 1972-73)

A few values of the saturation ratio, P_A/P_A° , are presented in Table A-1. Pound et al. (1951) and others presented data on the critical saturation ratios, $(P_A/P_A^\circ)_{\text{critical}}$, for homogeneous nucleation of water vapor. The data are reproduced in Figure A-3.

Fig. A-1 Vapor Film Between Water and Cryogen



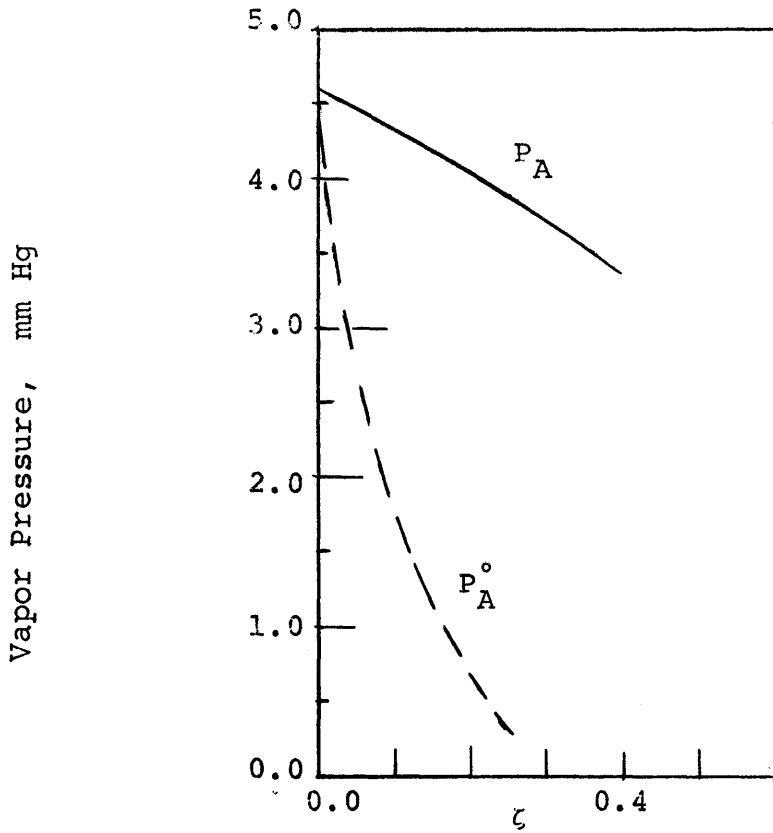


Fig. A-2
 Vapor Pressures And Partial Pressures
 Of Water As A Function Of Position Within
 The Film

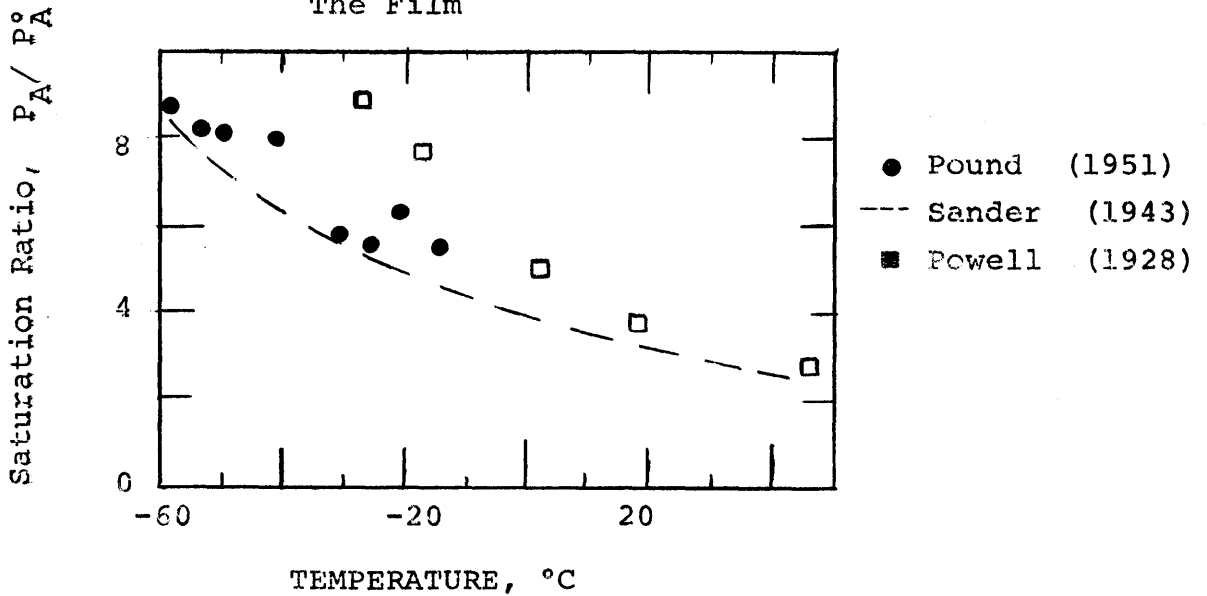


Fig. A-3
 Experimental Values Of The Critical Saturation
 Ratio For Homogeneous Nucleation Of Water Vapor

APPENDIX B

EQUIPMENT OPERATIONAL PRINCIPLES, DESIGN DETAILS AND PERFORMANCE DATA

1. THE BALANCE

The weight-measuring device used in this thesis is a Mettler PE 11 top-loading balance. An electrical output signal linearly proportional to the applied load is generated by the equipment. The block diagram of the balance which operates on a force compensation principle is presented in Figure B-1.

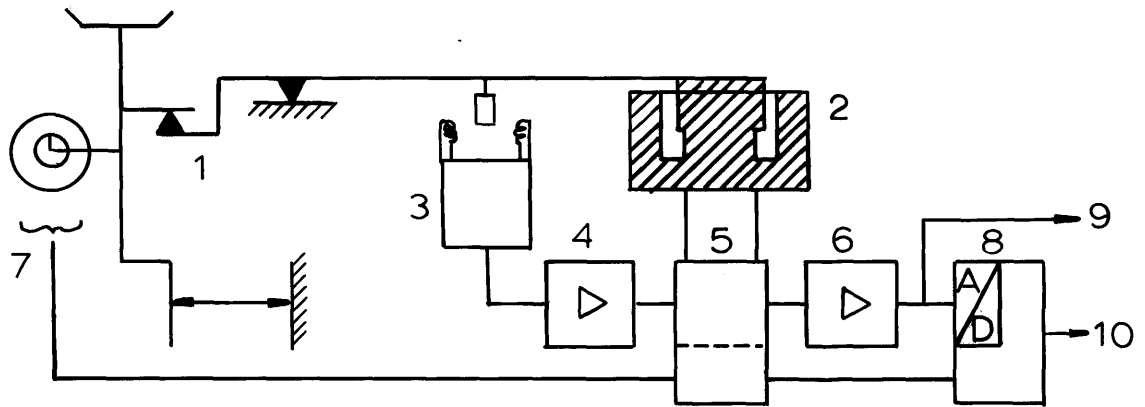
A sensor 3 determines the deflection of the balance beam which occurs when a weight is applied on the pan. The output signal of the sensor is amplified in a variable-gain amplifier 4. The amplifier generates a compensating force in device 2 via a range-selector switch 5. It is this force which produces the counter-rotational torque which keeps the balance beam at rest in its original position.

A voltage proportional to the compensating force is produced at the range selector switch 5, and the signal is amplified at 6. The analog output signals can be directly fed into a recorder and/or into an Analog-Digital Converter 8 for digitalization of output.

The performance data are presented in Table B-1.

2. SANBORN RECORDING SYSTEMS

To receive and record the analog signals output by the balance and the thermocouples, Sanborn recorders were employed. Each consists of a DC Plug-in general purpose coupling unit (Model 350 - 2),



Legend

- 1 Mechanical Top - Loading Balance System
- 2 Compensation System
- 3 Beam Sensor
- 4 Variable Gain Amplifier
- 5 Range Selector Switch
- 6 Output Amplifier
- 7 Digital Detection of the Built - in Weight
- 8 Analog - Digital Converter
- 9 Analog Output Signal
- 10 Digital Output Signal

Figure B-1 Block Diagram of Balance

TABLE B-1
 PERFORMANCE DATA FOR METTLER PE 11 BALANCE

Weighing

1. Range	-1 to 10 kg.
2. Taring System	
by rapid tare adjustment device	0 to 1 kg.
maximum tare (with built-in weights)	0 to 9 kg.
3. Linearity (standard deviation)	± 0.05 g
4. Precision	± 0.05 g
5. Measured Response Time (0 - full scale)	< 20ms
6. Severe Oscillations damped out in	~ 1 s

Electrical

7. Analog Output	
Output 0.1 V ungrounded, range	-100 to 100 mv
Source impedance	50 Ω
(2 other ranges provided but not used)	
8. Digital Output	
Parallel including decimal pt. and sign	0.1 mv \equiv 1 g
Digital code	1,2,4,8 (BCD)
Level : 0	0... +0,4V
L (TTL/DTL - compatible)	+2, 4V... + 15V
9. Power Supply	110V $\pm 10\%$ 60 H _z

a low-level preamplifier (Model 350 - 1500) and a recording system.

The signal to be recorded enters via INPUT connectors into the Plug-in unit. This device includes a guarded input circuit a calibration signal of $200 \text{ V} \pm 0.25\%$, zero suppression facilities with ranges of $\pm 2 \text{ mv} (\pm 0.5\%)$, $\pm 20 \text{ mv} (\pm 0.5\%)$ and $\pm 100 \text{ mv} (\pm 1\%)$ and provisions for standardizing the zero suppression circuit against a cadmium standard cell. The primary function of this device is to protect the low voltage signals from stray potentials in the external circuit which may prevent the full use of the preamplifiers capabilities, or cause difficulties in distinguishing the effects or values being measured from superimposed noise signals, or base-line drifts.

The Low-Level Preamplifier is a multipurpose DC chopper amplifier, it operates with an internally-generated 440-cycle excitation.

A 440 cycles/second mechanical chopper in the input circuit reverses the polarity of the input signal 880 times per second. The resulting signal is a 440-cycle amplitude-modulated square wave. The amplitude of this square wave is proportional to the amplitude of the input signal to the preamplifier from the Plug-in. This square-wave signal is amplified and then demodulated by a synchronous transistor phase sensitive detector circuit. This provides an output which is a replica of the original input signal to the preamplifier. Thus the preamplifier may be divided into the power circuits, input circuits, amplifier circuits, demodulator and oscillator circuits and output circuits. Detailed descriptions of these circuits are presented in the "350-1500A Low Level Preamplifier" manual prepared by Hewlett-

Packard Company.

The Preamplifier specifications are provided in Table B-2.

The Sanborn recorders are direct-writing oscillographic units which provide rapid and permanent records of input variables against a time base. In each channel, a galvanometer moves a heated stylus over the plastic-coated Sanborn Permapaper as the paper is drawn over a sharp edge platen at a preset constant speed.

Recording is done by moving-coil galvanometers with permanent magnets and each coil has two windings; the outside winding carries feedback voltage which are applied to the power amplifiers for damping; the inside winding carries the signal currents.

The recorder characteristics are provided in Table B-3.

3. THE DATA LOGGER

Used in parallel with the Sanborn recorders is a Hewlett-Packard Data Acquisition System (Model 2014B) which can record signals from one to 600 separate input sources. The signals are recorded on 8-level IBM coded punched tape and/or on print paper tape. The device is also capable of recording the time and channel number corresponding to the signal sources.

The instrument consists of a scanner, a digital voltmeter, a coupler and dock, tape punch facilities and a digital paper printer.

The Guarded Crossbar Scanner (Model HP2911) is an electronically controlled crossbar switch which sequentially scans the signal sources, and successively supplies the signals via a single set

TABLE B-2
 SANBORN PREAMPLIFIER SPECIFICATIONS

Bandwidth	
HI/FREQ CUT-OFF Switch	
HIGH	DC to 90 H _Z (-3dB)
MED	DC to 30 H _Z (-3dB)
LOW	DC to 15 H _Z (-3dB)
Measured Response Time (99% full scale)	15 ms
Input Impedance	10 ⁵ Ω
Isolation Impedance	2 (10 ¹²) Ω in parallel with 0.6 pico F with guard connected to com- mon mode source
Output Impedance	350 Ω
Overload Recover (at X 100)	50 ms
Sensitivity	20μV input for 1V out- put maximum Gain is 50,000

TABLE B-3

SANBORN RECORDER GALVANOMETER CHARACTERISTICS

Sensitivity at ATTENUATOR settings

X 20	40 μ V/division
X 50	100 μ V/division
X 100	200 μ V/division
X 200	400 μ V/division
Maximum	2 μ V/division deflection

Response (90% full scale) 7 ms

Bandwidth same as preamplifier

Frequency Response of galvanometer
(damped 70% of critical) -3dB

Damping source impedance 3 Ω

Linearity (standard deviation) \pm 0.25 division

Torque 0.025 N-m developed by 160 ma
for a 10-division deflection

Coil Resistance

Signal winding 15 Ω cold 17.5 Ω hot

Feedback winding 15 Ω

Hysteresis

Previous signals do not affect
the recorded data by more than
 \pm 0.15 divisions

of switch into the system voltmeter. The scanner allows all or a selected group of data sources to be scanned in a continuous cycle or one step at a time upon command. UPPER and LOWER LIMIT switches determine scan excursion as desired.

The digitizing functions are performed by an integrating digital voltmeter, HP-3450A. This device utilizes a dual-slope integrating technique and is equipped with fully guarded measurement circuitry which provide excellent noise and common-mode voltage immunity.

Analog input voltage is charged for a fixed precise 1/10 or 1/60 secs timing interval into the integrator. This is then discharged to zero by a fixed reference voltage. Since the charge rate is proportional to the input voltage, and the discharge rate fixed, the time taken for discharge is proportional to the input voltage. Thus a voltage-to-time conversion is achieved. A voltage read-out is then obtained by counting pulses from a 1 m H_z crystal oscillator during the discharge time.

The voltmeter specifications are presented in Table B-4 for detailed operational principles, reference is made to the Hewlett-Packard Model 3450A multi-function meter manual, number 03450-90002.

The coupler, HP2547A, is an interface device which operates with digital recording devices to translate the binary-coded-decimal (BCD) outputs of instruments such as digital voltmeters into serially-coded records. It also generates the signal that controls the operations of the scanner and recording devices.

The HP-2753A high speed tape punch is a perforator which punches

TABLE B-4

HEWLETT-PACKARD INTEGRATING DIGITAL VOLTMETER SPECIFICATIONS
(D.C. VOLTAGE)

Full Range Display	± 1.0 V
Accuracy	$\pm 0.003\%$ of reading
Measuring Speed	
Single Scan	
Integrating period	100 ms
Reading period	380 ms
Continuous Scan	
Integration period	16.6 ms
Reading period	65 ms
Input Resistance	10^{10}

input data on tapes of one inch width. It records five to eight-level codes at speeds of up to 115 characters per second. Tape supply and take-up assemblies are integral parts of the unit. Further details on the operational principles and performance data are presented in the manual prepared by the Hewlett-Packard Company.

4. GAS CHROMATOGRAPH

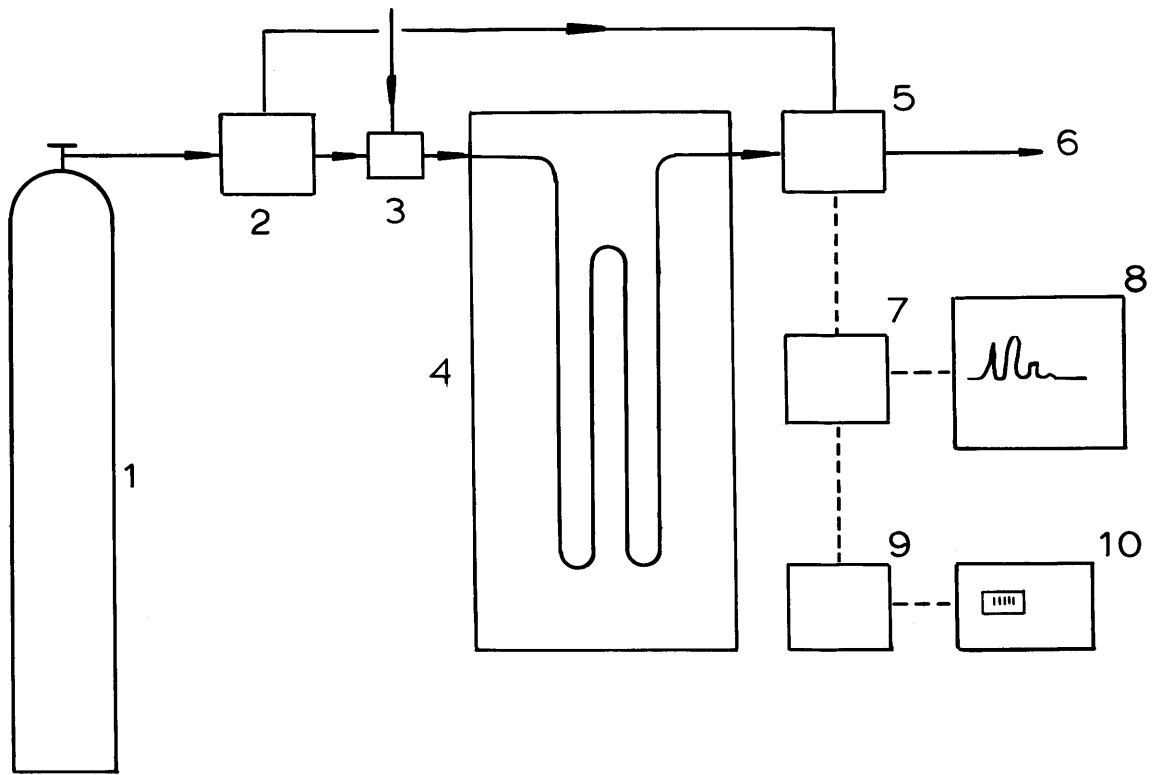
Analyses of the hydrocarbon mixtures were carried out with gas chromatographic equipment which effect a physical separation of a mixture into its components in elution columns. The basic principle of operation is that gases have different distribution coefficients between a fixed and a mobile phase. The separated gases are then passed into suitable detectors to determine the relative quantities of the components.

The essential features of any G.C. are shown in Figure B.2 which is self explanatory. There are three distinct parts: the injection system, the column, a long thermostated narrow tube, usually packed with a granular solid, and the detector.

The output integration was performed automatically and directly with the aid of the Varian Aerograph Model 477 Digital Integrator. This device features voltage to frequency conversions, automatic base-line correction, slope detection and print-out.

A MICROCORD 44, self-balancing potentiometric strip chart recorder was used to obtain the chromatograms.

Calibration data for the hydrocarbons under study are presented



Legend

- | | |
|----------------------|--------------------|
| 1 Carrier Gas Supply | 6 Vent |
| 2 Flow Regulator | 7 Amplifier |
| 3 Injection Port | 8 Recorder |
| 4 Columns and Oven | 9 Integrator |
| 5 Detector | 10 Digital Printer |

Figure B-2 Schematic of Gas Chromatograph

Perkin-Elmer 990

A flame ionization detector was supplied with this instrument. The device can detect trace amounts of hydrocarbons but it is insensitive to inorganic compounds, and it will not measure the amount of nitrogen in a mixture.

The column packing used with the Perkin-Elmer instrument was different. Excellent separation of the hydrocarbon components were achieved with 80 100 mesh (147-175 μm diameter particles) Durapak C8 polyaromatic resins in a 2.44 m long stainless steel tube of 2.36 mm I.D. A typical chromatogram is presented in Figure B.3.

Two chromatographic units were employed in this study, differing primarily in the column length and packing material, and the detection technique. These are the Hewlett-Packard series 700 and the Perkins-Elmer Model 990 Gas Chromatographs.

HP-700 G.C. Unit

The Hewlett-Packard unit is equipped with a 3.66 m long and 3.94 mm I.D. stainless steel tube packed with 50/80 mesh Porapak Q beads. Porapak are macroreticular resins with good column characteristics, good selectivity and efficiency. The resins act as an extended liquid phase with a rigid open structure and very high surface area. Application is limited to temperatures below 250 C.

A Katharometer (thermal conductivity detector) used with the unit.

5. GAS SAMPLING FOR CHROMATOGRAPHIC ANALYSIS

The device for taking gas samples of the same compositions as the cryogenic liquid mixtures is shown schematically in Figure B.4. It consists of a 20 gage (0.91 mm I.D.), 8 cm long, stainless steel cannula sealed into the entrance of a gas sampling bottle, below Stopcock 1. To the opposite end of the bottle is attached a self-sealing, thick walled, rubber tube. The bottle is first evacuated to about 1 mm Hg with Stopcock 1 closed. Then Stopcock 2 was closed and 1 opened. A small liquid volume (of the same composition as the bulk) is drawn through the cannula and into the bottle at room temperature where it is very quickly vaporized. Since about 4 cm of the cannula was inserted into the cryogen and allowed to attain its temperature, no vapors are drawn into the bottle. Stopcock 1 is again closed and 2 opened to evacuate the bottle in a 'flushing' process. The process is repeated as many times as required until any residual air in the bottle has been removed. Two or three flushes are usually sufficient. Too many flushes causes Stopcock 1 to contract appreciably, thereby allowing air to leak into the sample bottle. In addition, the sample bottle wall temperature decreased and a long time is then required for the walls to warm up to a temperature where homogeneity in the mixture, especially the higher boiling components such as the butanes is assured. The pressure in the bottles are slightly above atmospheric (by 0.2 - 0.5 atmospheres) and direct heating of the bottle is not recommended.

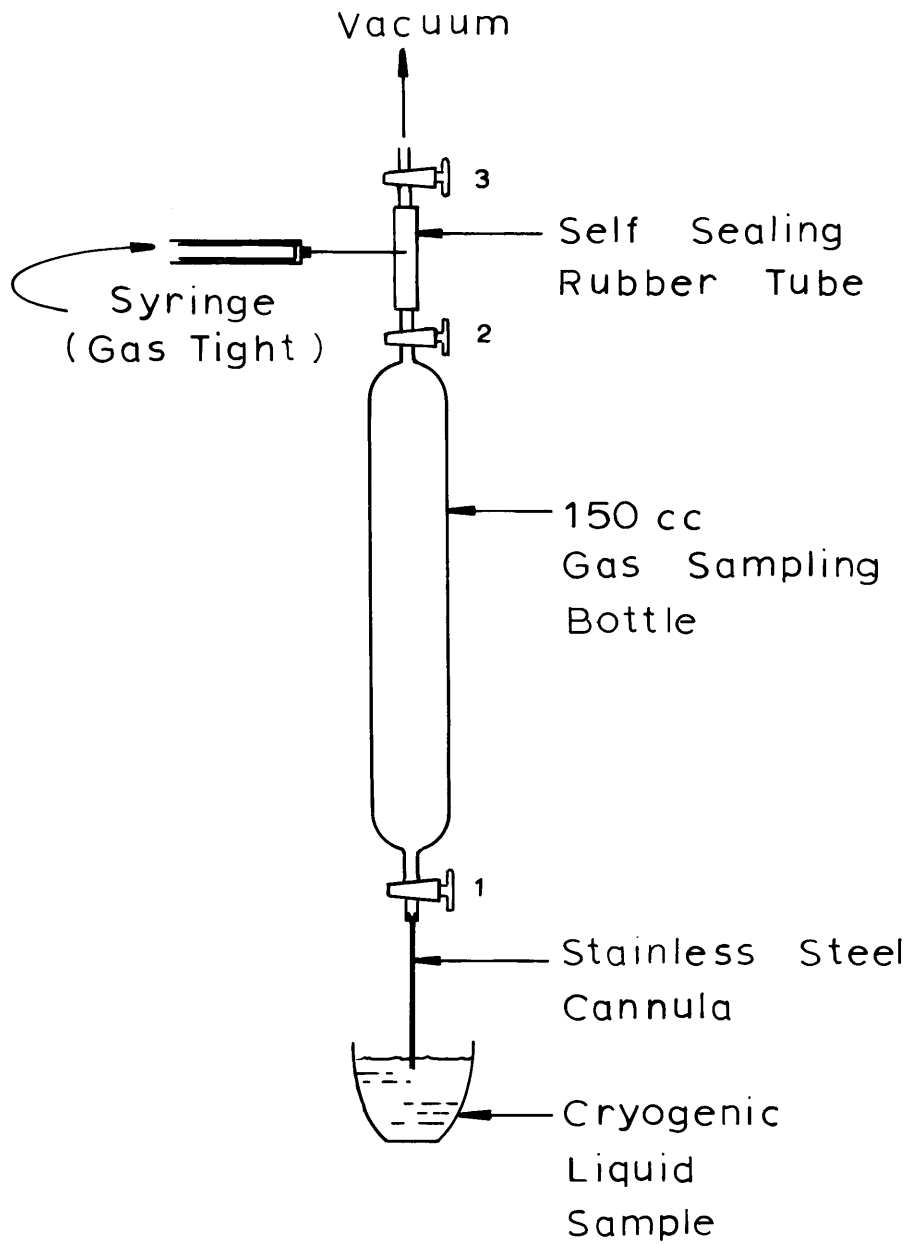


Figure B-4 Apparatus for Sampling Cryogenic Liquids

To withdraw a gas sample, Stopcock 3 is closed and 2 opened to admit the mixture into the rubber tube. (Note that Stopcock 1 is closed). The syringe is flushed several times as quickly as possible and the sample withdrawn. To take another sample, (Stopcock 2 is closed after sample is withdrawn) the space between 2 and 3 must be re-evacuated. Several samples taken of the same gas within 12 hours gave the same results within the resolutions of the Gas Chromatographic units, therefore, the gases are well mixed.

6. THERMOCOUPLE HEAT-STATIONING REQUIREMENTS IN MEASURING TEMPERATURES IN THE VAPOR DEPARTING A BOILING POOL OF LIQUID

To reduce conduction heat leak to vapor phase thermocouples, all were heat stationed as illustrated in Figure B.6. The length of thermocouple wire coiled in the phase of measurement was chosen to prevent errors in excess of 0.5 °C. The error was estimated using a simple fin model as illustrated below.

The thermocouple wires were copper and constantan, 25.4 μm meters (1 mil) in diameter and not insulated. The maximum temperature difference that parts of the thermocouples can be exposed to is about 220°C. This is attained when nitrogen (boiling point -196 C.) boils in a pool and the ambient is at about 25°C. The thermal conductivities of copper and constantan (55% copper and 45% nickel) are 130 W/m K (225 Btu/hr-ft-°F) and 7.5 W/m K (12.9 Btu/hr-ft-°F) respectively. Hence the heat leak into the copper wire will be larger. For this reason, the calculations will be made as if pure

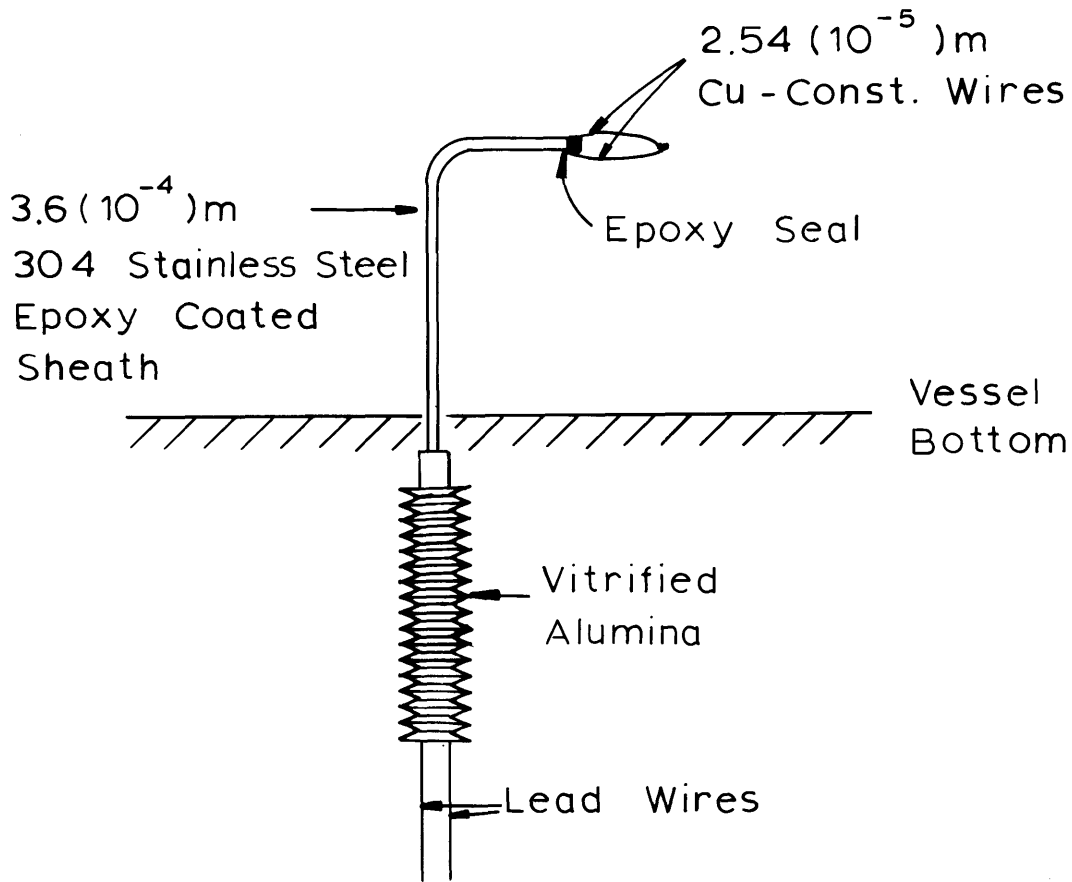


Figure B Thermocouple Probe in Water

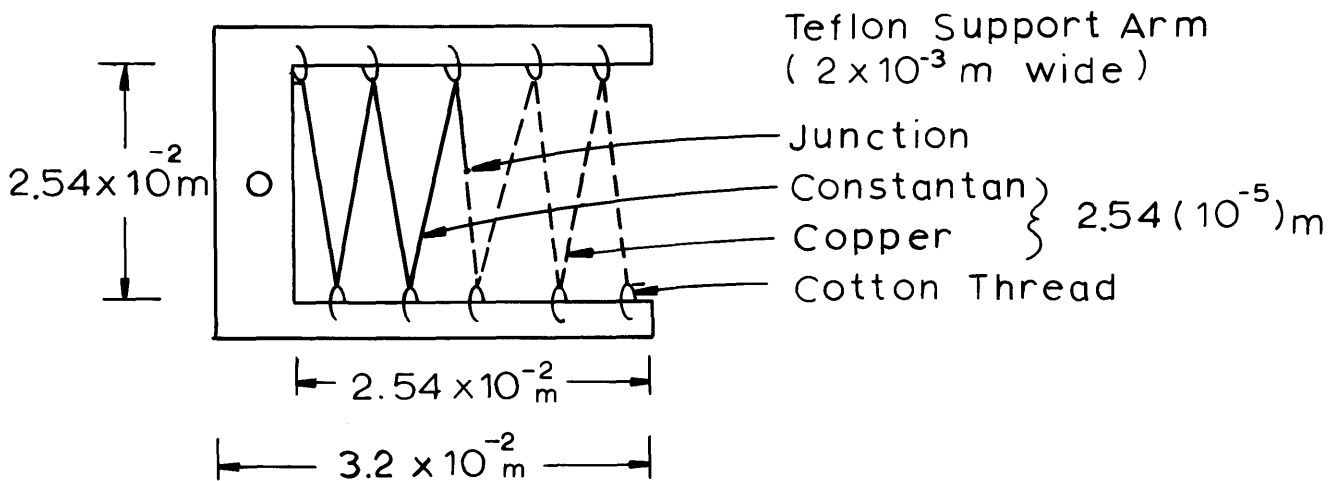


Figure B-6 Vapor Thermocouple : Heat Stationed on the Holder (Bottom or Top View)

copper wires were present on both sides of the junction, to simulate the worst possible situation. Since the heat flow is then symmetric about the junction when equal lengths of lead-wires are used, the geometry of heat conduction into a circular rod (or wire) insulated at one end (the junction) and maintained at a constant temperature at the other end can be adopted, as shown in Figure B-5.

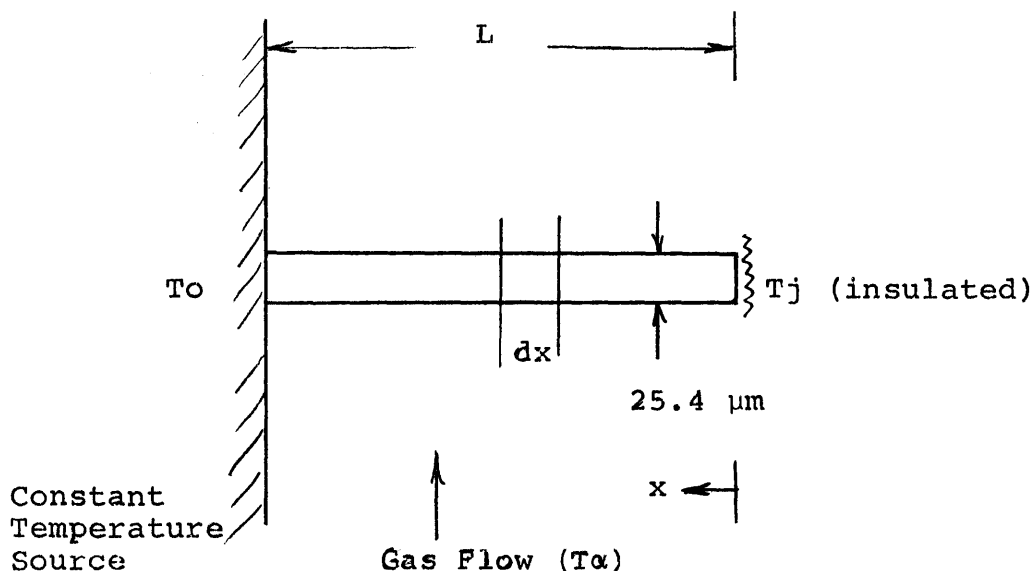


Figure B-5

The problem is that of estimating L such that $T_j = T_\alpha \pm 0.5^\circ\text{C}$.

Performing a differential energy balance on an element, dx , and assuming a steady state process and temperature independent physical properties, the equation obtained is

$$\frac{d^2\theta}{dx^2} - m^2\theta = 0 \quad (\text{B-1})$$

$$\text{Where } m^2 = \frac{4h}{kD}$$

$$\theta = T(x) - T_\alpha$$

and h , is the heat transfer coefficient, k , the thermal conductivity of copper, D , the diameter of wire and T , the temperature.

The boundary conditions are

$$\frac{d\theta(0)}{dx} = 0 \quad (\text{B-2})$$

$$\text{and } \frac{\theta(L)}{\theta_0} = 1 \quad (\text{B-3})$$

The solution is given by

$$\frac{\theta}{\theta_0} = \frac{T(x) - T_\alpha}{T_0 - T_\alpha} = \frac{\cosh(mx)}{\cosh(mL)} \quad (\text{B-4})$$

The location of interest is at $X=0$. Hence the relation sought is given by

$$T_j - T_\alpha = \frac{(T_0 - T_\alpha)}{\cosh(mL)} \quad (\text{B-5})$$

Assume a heat transfer coefficient of $0.35 \text{ W/m}^2\text{K}$ ($2 \text{ Btu/hr-ft}^2\text{°F}$) between the gas and the wires.

$$m = 67.77 \text{ m}^{-1} \quad (\text{B-6})$$

For a maximum error of 0.5°C . and $T_0 - T_\alpha$ of 220°C .

$$L \sim 9 \text{ cm (0.29 ft)} \quad (\text{B-7})$$

(For a maximum error of 0.1°C ., a length of slightly more than 11 cm is required).

The calculations suggest that each of the lead-wires of the thermocouples exposed to the vapor whose temperatures are required to be measured must be at least 10 cm long.

7. LIQUID AND VAPOR THERMOCOUPLES

The basic requirements for measuring local temperatures in the fluids involved in this study are

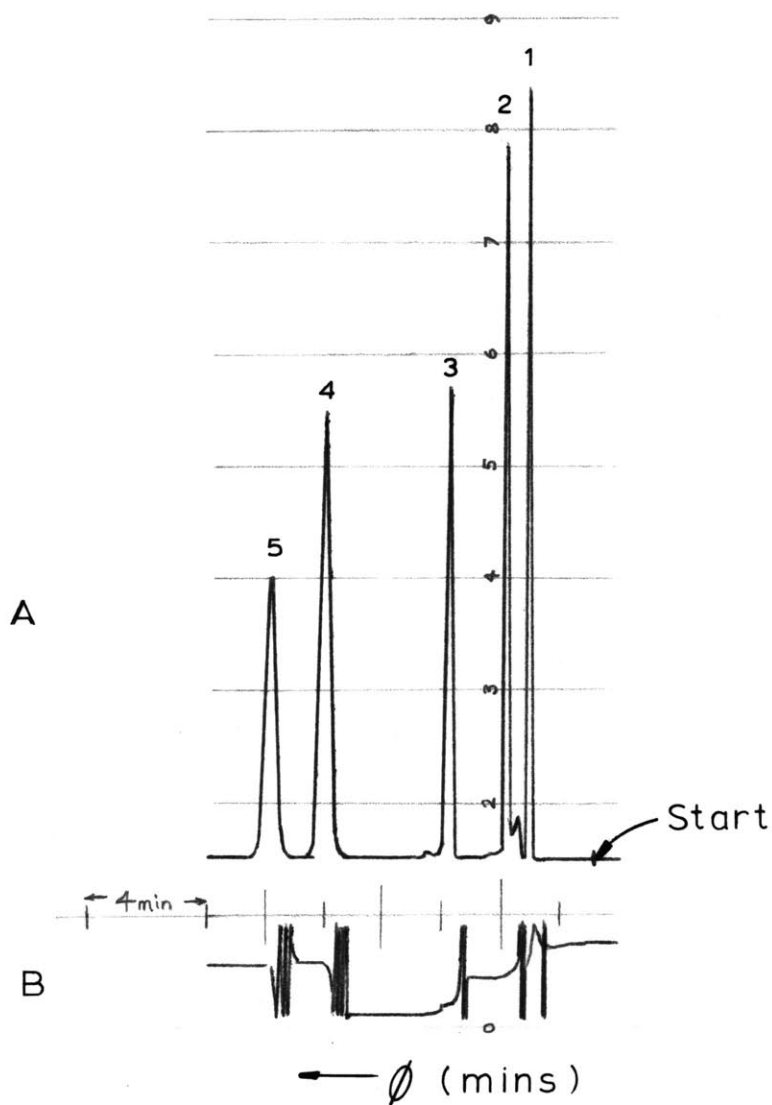
fast response

and minimal thermal and flow disturbance of the fluid bodies.

For this reason 25.4 μm O.D. (1 mil) Copper-Constantan wires were employed in the fabrication of the thermocouples. For ease of manufacture and improved strength during application, the junctions were beads of diameter between 60 and 80 μm .

Temperatures in Water

Water temperatures were measured with the thermocouples inserted through the bottom of the boiling vessel. In this way, the interface is not penetrated by any solid conductor. Fine wires, however, are not rigid and cannot be made to stay at a predetermined location. For this reason, the thermocouples in the water had to be enclosed in a metallic sheath for support. A standard design of the 'HT micro-miniature thermocouples' of the Balwin-Lima-Hamilton (BLH) Corporation was modified for the present application. The probe (shown schematically in Figure B.6) consists of an 360 μm O.D. stainless steel tube through which 2 fused ceramic tubes 76.2 μm O.D. X 50.8 μm I.D.) were



	Atten.	
1 Methane	x 256	Carrier Gas (Nitrogen)
2 Ethane	x 64	Flow Rate
3 Propane	x 64	Oven Temperature = 25 °C
4 i-Butane	x 32	
5 n-Butane	x 32	A: Recorder Output
		B Disc Integrator Output

Figure B-3 Chromatogram of Low Molecular Weight Hydrocarbons in Durapak Filled Columns in G.C. With a Flame Ionization Detector.

threaded. The thermocouple wires were threaded through the ceramic tubes and the junctions made. The ends of the steel tube constituting the sheath were sealed with epoxy. A thin coating of epoxy was also applied on the outside wall. The junction distance to the sheath, that is, the exposed wire sections, varied between 20 mm for the thermocouples located near the water surface to 2 mm for the others.

The sheaths were supported in vitrified threaded alumina rods which were located outside the vessel. Lead wires emerging from the alumina were 0.254 mm in diameter.

The thermocouple response times, determined with photo-oscillographic techniques and the Sanborn recorders independently, ranged between 24 ms for the thermocouple at the water surface to 250 ms for the ones below the surface.

Vapor Temperature Measurements

Temperatures of the vapor evolved during boiling were measured with the aid of the 'thermocouple tree' described in section. It was demonstrated there that about 0.1 m lengths of lead wires are required for heat stationing each thermocouple in the plane of the junction, i.e., perpendicular to the direction of vapor flow.

The final design is shown in Figure B.6. Each consists of a bare thermocouple (fabricated by Omega Engineering, Inc.) suspended in a horizontal plane by a Y-shaped Teflon support and cotton-wool threads. The threads were looped into the Teflon arms, and the thermocouple wires inserted through the loops to form a web. The minimum arm

length of the thermocouple wires in the web was 11.5 cm.

The thermocouple response times were 21 ± 5 ms.

8. THERMOCOUPLE TREE

An accurate measurement of the transient temperatures of the vapor evolved from the boiling pool depends on preventing both the recirculation of ambient air into the boiling vessel, and backmixing in the vapor space above the pool itself.

For this reason, an arrangement shown in Figure B-8 was designed and constructed. It consists of an acrylic double cone, a supporting rod and thermocouple holders.

The double cone serves two purposes. It directs the volatile liquid introduced at the start of each run towards the vessel walls where it flows down onto the heat source liquid. Splashing is thereby minimized during the short duration delivery. The tangential flow towards the wall and water surface also causes the normal forces directed at time zero on the balance to be minimal, thereby decreases the period of initial oscillations in the balance to less than 0.2 s after complete delivery. The second function of the cone is to direct the vapor generated during boiling out of the vessel without backmixing, and at the same time keep the ambient air out of the vessel. An analysis of the performance is shown below.

Flow Around Obstacles

The flow conditions which might affect temperature measurements

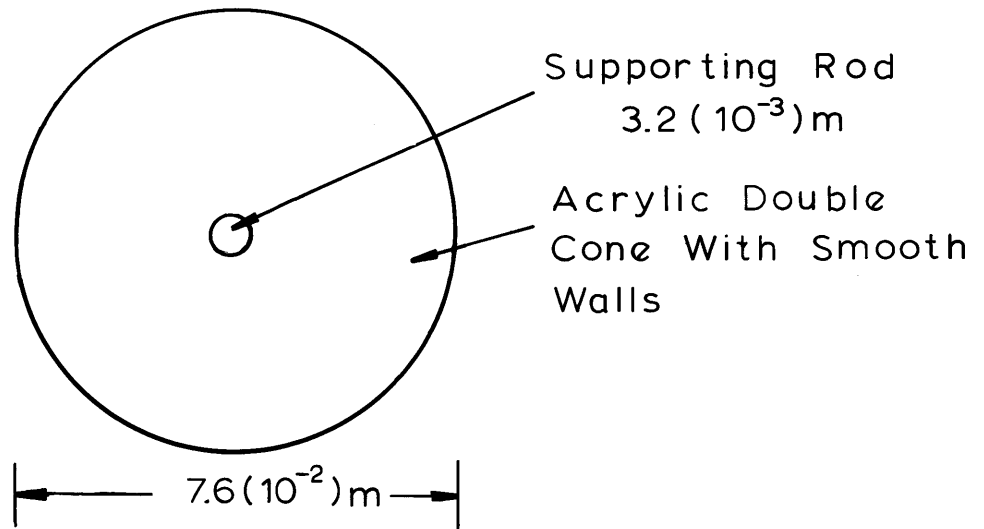


Figure B - 7 a

B Fluid-Directing Double Cone (Bottom View)

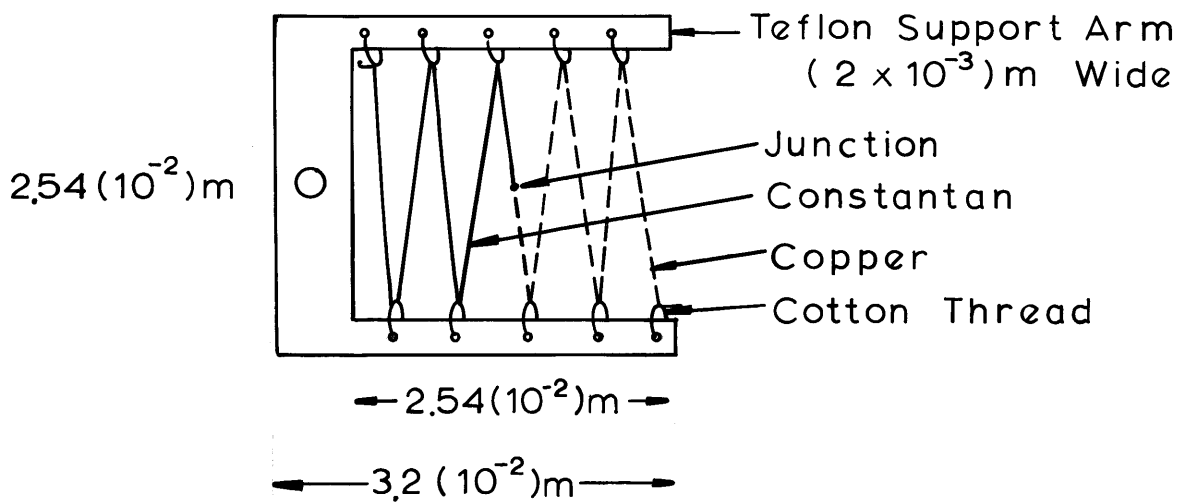


Figure B - 7 b

C. Thermocouple : Heat Stationed on the Holder
 (Bottom or Top View)

in the vapor phase beneath the cone are:

the accumulation of fluid in front of an obstacle, or stagnation

separation at the cone surface, the thermocouple holder and along the supporting rod. Flow separation leads to eddies and therefore backmixing

or downward flow of vapor. This has been eliminated in the design.

The situation of particular interest are the plane stagnation flows at the thermocouple holders, and the flow around the fluid directioning cone.

Foettinger (1939) demonstrated photographically (reproduced in Schlichting, 1968, p.35) that adverse pressure gradients together with friction at a wall determine the process of separation with plane stagnation flows. In flows at right angles to a wall, fluid is dammed-up in a small pocket at the centre of the surface but no separation occur since there is no frictional force in the direction of bulk flow. The pressure in the pocket is higher than anywhere else in the stream. Along the wall, the redirected fluid particles move in a field of decreasing pressure (and increasing fluid velocities), therefore separation again does not take place. The location of a narrow or circular object at the wall, normal to the surface, causes the formation of a new boundary layer which (the boundary layer) has a pressure increase in the direction of flow. Consequently, separa-

tion occurs and vortices are formed. The distance of the boundary layer separation point to the plane wall determines the eddy size or 'dead space' which does not normally extend beyond the bounds of the plane wall.

Two suggestions can be made immediately. One is that the thermocouple junctions must neither be directly under a plane horizontal surface nor very near the horizontal thermocouple Teflon supporting strips (Figure B-7 , b). The second is that large scale dead space would be prevented if the fluid directing device had a conical instead of planar bottom face.

Since the thermocouple holder strips are narrow and widely spaced, they can not be considered to be significant recirculating vortex generating objects. Karman vortex streets (Schlichting, 1968) in the direction of flow will probably be present, however.

Mathematical analyses of potential flow over conical surfaces have been carried out by Lenteritz and Mangler (1945), and Mangler (1943). Evans (1968) presented their derivations and extended the analysis to account for the boundary layers in real fluid flows over such surfaces. From the calculations, it was demonstrated that stagnation is only obtained for flows perpendicular to a flat surface, that is a half cone angle of 90° , except along the line of axis of symmetry of the cone. Flow separation from the wall is not obtained except for flows into diffuser cones of half cone angles greater than 17.8° , or over sharp edges.

It is thus apparent that the half cone angle of 71.6° of the fluid director used in the experiments is a safe one. On applying the analysis presented by Evans, it can be shown that the vapor velocity near the cone surface (outside of the boundary layer), v , is related to the distance along the cone surface from the apex, r , by the proportionality

$$v \propto r^{0.6}$$

and the displacement thickness, δ_1 , is given by

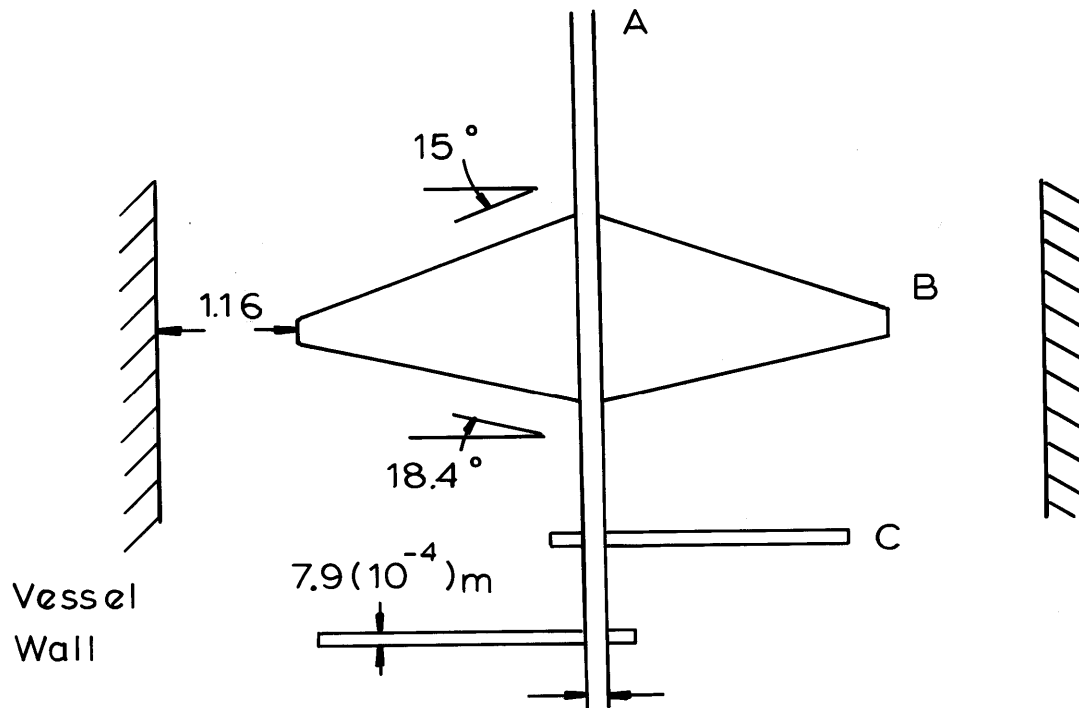
$$\delta_1 = 0.892 \quad (\text{boundary layer thickness})$$

in a field whose pressure decreases with increasing distance from the apex and is therefore non-supportive of flow separation.

9. THE 'BOILING' VESSEL

The following factors were important considerations in the design and construction of the 'boiling' vessel shown in Figure B.9.

1. The total weight of the vessel, empty, must be kept as low as possible since the maximum measurable load on the balance is 11 kg.
2. Heat transport between the fluids of interest and the surroundings must be kept at a minimum.
3. Rapid attainment and sustenance of pool boiling over a period greater than 30 seconds is desired to eliminate the processes of volatile liquid spreading, and/or pool break-up in short time scales.



Legend

- A Acrylic-Coated Brass Supporting Rod
- B Acrylic Fluid-Directing Double Cone
- C Teflon Thermocouple Holder

Figure B-8 Thermocouple Tree
(Side View)

4. Wall effects both as heat source or nucleating sites must be minimized.
5. Accurate and representative measurements of weights and temperatures are desired, and are more readily achieved in small scale experiments.

The vessel is essentially a triple-walled container of plastic construction, an inside diameter of (9.92 ± 0.02) cm and an internal depth of 17.8 cm. The inside wall comprises a scratch-free $127 \pm 2 \mu$ thick cellulose acetate lining separated from the adjacent wall by $400 \pm 50 \mu$, highly porous rigid foam spacers of very low thermal conductivities (< 0.02 W/m K at 25 C. and lower temperatures). The bottom of the inside wall is also of the cellulose acetate sheet suspended on air pockets trapped in thin polyethylene films. Seals connecting the vessel bottom lining to the walls were made with thin coats of epoxy. The inlet ports for the thermocouple probes were also sealed with the thermocouples in place.

The outer two walls were 0.635 cm thick cast acrylics tubes, 10 cm and 12.5 cm I.D. The annular space was compression sealed-in by two circular gasket rings of the same material at both ends. The space was then evacuated to a pressure of about 1 mm Hg.

The thermocouple holders are fixed in position as shown in the figure to an aluminum bottom plate shown from two perspectives in Figure B.10. The plate contains 7 drilled-through holes and 7 tapped holes. The dimensions are given in the figure. With the shown hole



Room 14-0551
77 Massachusetts Avenue
Cambridge, MA 02139
Ph: 617.253.2800
Email: docs@mit.edu
<http://libraries.mit.edu/docs>

DISCLAIMER

**Page has been omitted due to a pagination error
by the author.**

(p.306)

locations, thermocouple junctions can be positioned, in the water, at varied levels below the interface and desired lateral distances from the wall.

The threaded aluminum supports were used to adjust the vessel to a vertical orientation when used in conjunction with a bubble level. This is necessary because the surface area used in the analysis is the vessel cross-section.

APPENDIX C

AUXILIARY RESULTS

This appendix contains some experimental results on sputtering from large bubbles when they burst, and vapor hold-up in boiling cryogenes.

§1. SPUTTERING FROM LARGE BUBBLES

Sputtering is a phenomenon in which liquid droplets are produced as a result of gas bubbles bursting at a gas-liquid interface. (Woodcock et al., 1953; Day, 1964, 1967.) It has been observed during boiling, gas-liquid contacting operations and has been hypothesized as one of the principal methods air-borne salt crystals are produced from the ocean. (Blanchard, 1963.)

Kientzler et al. (1954) photographically studied the intricate hydrodynamic processes accompanying the bursting of small bubbles ~ 0.2 to 1.88 mm diameter. Bigger bubbles, 0.3 to 6.0 mm diameter were studied by Newitt et al. (1954), Toba (1958) and Day (1967). These studies have identified two explosive events whereby liquid droplets are formed. The first is that the liquid surface of the ruptured bubble contacts very quickly to re-establish a configuration of minimum surface energy. The resulting overshoot of the surface tension forces causes a liquid jet to develop from what was the base of the bubble. The jet then necks into the several droplets and drops thrown upwards. The second method of droplet production is that

fragments of the liquid, originally part of the bubble cap, become atomized by the rapid release of the excess pressure within the bubble. The resulting bubble-film droplets may then be carried off by the gas released.

In the present work, the hydrodynamic processes are examined when large bubbles, 7 mm to 14 mm diameter, in the size range produced during the film boiling of cryogenic liquids, burst at the upper liquid-vapor interface. The motivation has been to determine whether a significant quantity of the cryogen can be lost as the liquid. It is necessary to establish this fact in order to analyze the results of this study correctly.

The results for helium bubbles released from a nozzle (5 mm i.d.) in n-hexane are presented in Figure C-1. The surface tension of hexane is 0.018 N/m; this value is the same order of magnitude as for the cryogenic liquids. As shown in Plate 1, the big bubbles undergo a series of deformations if the injection point is well below the surface. The ultimate shape is an oblate spheroid. The spheroids, however, undergo continuous rapid distortions and oscillations as they spiral upwards in the liquid. At the interface, they only erupt and do not produce droplets.

When the distance of travel is reduced, the anterior of the bubble touches the free liquid surface before the bubble becomes oblate. A hemispherical cap of liquid film is then projected above the level of the surrounding liquid. Plate 2 shows one hemispherical cap in the process of disintegration after rupture. The bright spots



Plate 1

Transient Bubble Shapes
No Atomization



Plate 2

Bubble Just Burst
Flying Liquid Film
Pieces.



Plate 3

Liquid Surface After
Dome Remnants Have
Retracted. A Hexagram
Centre Piece Develops



Plate 4

Centre Piece Ejects
Droplets



Plate 5

Hexagram Spilling Over
In The Process of Destruction

The Sequence in Plates 2-5 is Estimated to Have a Duration of About
 0.3 ± 0.1 Seconds

Figure A-2 Reconstituted Sequence of Sputtering from Helium Bubbles
Released from a 5mm ID Nozzle in n-Hexane. In Plate 1, the Bubble
Distance of Travel is About 2.5 cms. The Distance is Less Than 1.5 cm
In The Other Pictures

on the right of the opening are reflections from flying liquid drops (and sheets) which were originally part of the dome. The drops are large (~ 1 mm diameter) and they fall back onto the liquid surface.

Plates 3, 4 and 5 show the sequence of events after the bubble dome has ruptured. This sequence has been reconstituted from still photographs of 1 ms exposure. Plate 3 shows the liquid surface structure after the dome remnant in a symmetrically burst bubble has retracted. A folded hexagram pattern is noted. The apex developed into a jet which usually released no droplets. When droplets were produced, up to eight have been counted. Figure 4 shows one of the exceptional cases. The droplets are 0.4 to 0.6 mm diameter and they fall back onto the liquid after travelling about 1 to 3 cm above the surface. The hexagram structure is seen spilling-over in the process of destruction in Plate 5.

It can be concluded from these results on the bursting of single bubbles that

1. a large bubble will only erupt if it bursts after it has achieved a flat conformation.
2. a large bubble may (but seldom will) cause droplets to be ejected from the liquid surface if it bursts before it flattens out. Any droplets produced are large and they fall back onto the liquid.

If the liquid were a boiling cryogen and the vapor evolved were superheated, the droplets, when they form, would partially vaporize while in their trajectory. Analysis of the rate of vaporization of such

droplets have been carried out by Marshall (1954). If a droplet were assumed suspended in a stagnant warm gas, the time for complete vaporization is given by:

$$\theta = \frac{\Delta H_v \rho_L d^2}{8k_v \Delta T} \quad (C-1)$$

where ΔT is the temperature difference between the droplet and the ambient, d is initial droplet diameter, ρ_L is density of liquid, k_v is the vapor thermal conductivity and ΔH_v is the heat of vaporization.

For a liquid nitrogen droplet, 0.5 mm diameter, in nitrogen vapor at -96°C (i.e. $\Delta T = 100^\circ\text{C}$), the droplet will vaporize completely in 3 s.

The flight time of a droplet, however, is given by

$$\theta_{fl} = \sqrt{\frac{8s^*}{g}} \quad s^* \text{ is height of drop travel} \quad (C-2)$$

Hence, for a droplet thrown 3 cm above the liquid,

$$\theta_{fl} = 0.16 \text{ s}$$

The droplet would have vaporized very little in flight.

From the foregoing, it may be concluded that when large bubbles burst at the surface of organic liquids ($\sigma \sim 0.015 \pm 0.005 \text{ N/m}$), drops produced are large or no drops are produced at all. Furthermore,

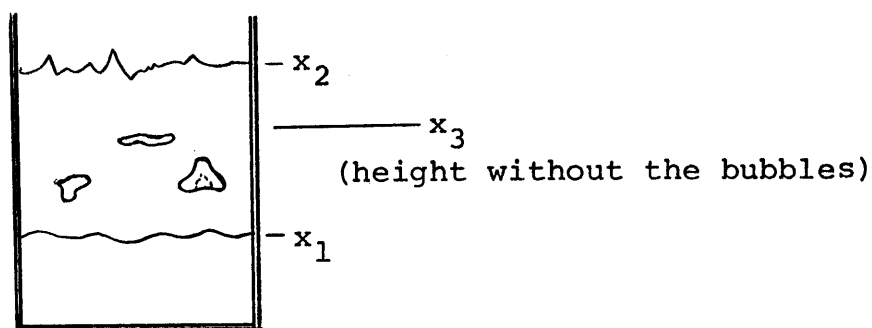
if drops were produced in the apparatus of this study, they would not vaporize appreciably in flight and they would fall back onto the boiling pool.

§2. VAPOR HOLD-UP IN BOILING CRYOGENS

A liquid boiling in the nucleate, transition or film boiling regime contains bubbles within its bulk. These bubbles expand the liquid height above the actual hydrostatic head.

The void fraction in liquid nitrogen ($\rho \sim 0.8 \text{ g/cm}^3$), methane ($\rho \sim 0.42 \text{ g/cm}^3$), and ethane ($\rho \sim 0.51 \text{ g/cm}^3$) as they boiled on water, has been plotted in Figure C-2 as a function of the liquid hydrostatic head. The values were obtained from experimental results as follows:

Consider the boiling vessel to appear as shown below in the course of a run.



SCHMATIC OF BOILING VESSEL

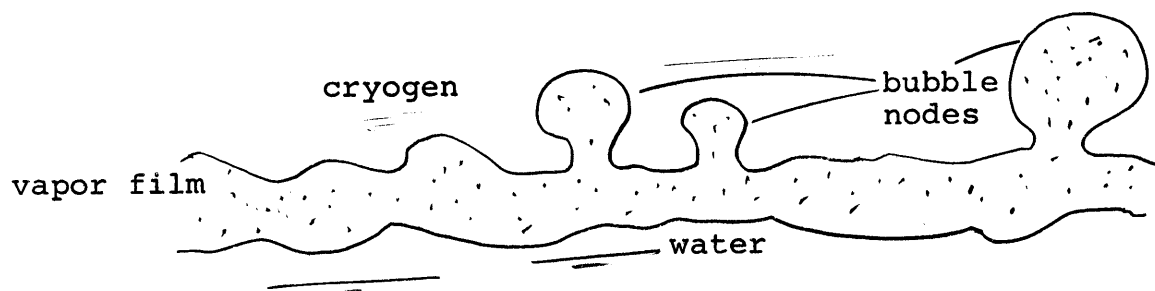
At the start of a run, the quiescent level of the water surface, x_1 , was measured. After the cryogen has been layered, x_2 , the average height of the cryogen, was measured with a cathetometer as a function

of time after the liquids were contacted. The hydrostatic head of liquid, $x_3 - x_1$, is determined from the residual weight versus time data in Appendix F for the time an x_2 value was recorded. The void fraction, ϵ , is then evaluated for the particular $x_3 - x_1$, from

$$\epsilon = \frac{x_2 - x_3}{x_2 - x_1} \quad (c-3)$$

The procedure is then repeated for other hydrostatic liquid heads.

The results show that the liquid void fraction increased as the hydrostatic head of liquid decreased. This appears logical if film boiling is the mode of heat transfer. In addition to the vapor within the thin film, there are numerous incomplete bubbles or bubble nodes which, at any instant, constitute part of the film. This is as shown in the sketch below.



The relative significance of the volume within the nodes increase as the hydrostatic head of cryogen decreases. This effect is reflected in Figure C-2. For large cryogenic liquid heads, $\epsilon \sim 0.15$. It should be remembered that the bubble diameters are large. Hence errors in the measurements of x_2 for hydrostatic heads less than 6 mm might be expected.

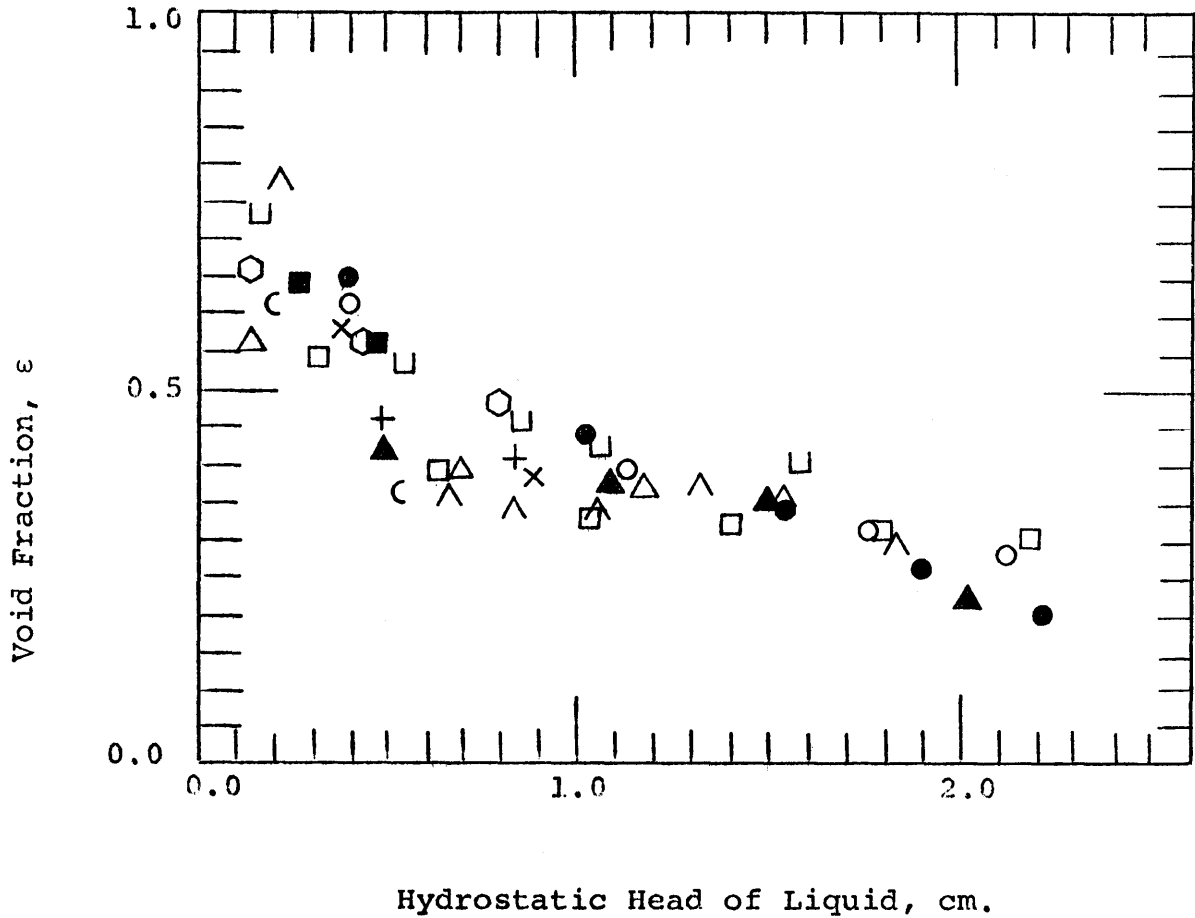


Fig. C-2

Void Fraction in Boiling Cryogenic Liquids

Liquid Nitrogen		Liquid Methane		Liquid Ethane	
Run#	Symbol	Run#	Symbol	Run#	Symbol
149	○	164	■	173	×
150	△	169	●	174	+
151	○	170	▲	175	□
152	□			177	⊂
				178	∧

APPENDIX D

ERROR ESTIMATE (HEAT FLUX) AND THERMOCOUPLE CALIBRATION DATA

In this appendix, the contribution of the vessel walls and the environment to the experimental heat fluxes is estimated. Next, the calibration data of the thermocouples are presented.

D-1 ERROR ESTIMATE

The vessel was described in Chapter 4 and Appendix B to be a triple-walled container. The innermost wall was fabricated out of a cellulose acetate sheet which was $127 \mu\text{m}$ thick, and it was separated from the adjacent wall by a $400 \pm 40 \mu\text{m}$ air gap. The total mass of inner wall, including the bottom was $8.4 \pm 0.1 \text{ g}$. Since the thermal capacity of cellulose acetate is $\sim 1.5 \text{ J/gK}$ (Perry, 4th ed.), one obtains the total heat capacity of this lining to be $\sim 12.6 \text{ J/K}$. This means that if the wall was cooled by $\sim 220^\circ\text{C}$, e.g. with liquid nitrogen, 4.2 J/cm^2 energy is liberated. In the large spill runs, $\sim 100 \text{ cm}^2$ of the wall comes in direct contact with the cryogenics. Hence the heat released from the wall will vaporize $\sim 2 \text{ g}$ nitrogen or $\sim 1 \text{ g}$ methane, ethane, or LNG. (These weights are about 1-2% of the total amount of cryogenic liquid spilled.) From preliminary experiments in which pieces of the cellulose acetate (at $\sim 25^\circ\text{C}$) were immersed into saturated liquid nitrogen, it is estimated that the acetate's heat content was released in $\sim 1 \text{ s}$ or less. Hence in the present work, no contribution to the heat fluxes are expected from the

wall itself 1 s after the spill.

The rate at which energy was conducted across the air gap separating the two innermost walls during a run is also important. Cold water (at about 6°C) was poured into the empty vessel. The temperature of the water (3.8 cm deep) was then monitored as a function of time. The Sanborn recorder output is presented in Figure D-1.

A gain in water temperature of about 0.6°C was noted at the end of 140 s. This is equivalent to a flux of about 0.27 kW/m² at a ΔT across the two inner walls of about 20°C. For a ΔT ~220°C (e.g. with liquid nitrogen boiling), the heat flux into the vessel should be ~3 kW/m² or less.

The fraction of total heat transfer into the cryogen supplied through the wall

$$T = \frac{H_{\text{amb}}}{H_{\text{amb}} + H_w (A_w/A_{\text{amb}})} \quad (\text{D-1})$$

where H is the heat flux and A the appropriate surface area. Subscripts amb and w refer to the ambient and the water.

In a run in which 1 cm deep pool of liquid nitrogen was spilled, run 182,

$$H_w \sim 30 \text{ kW/m}^2$$

$$H_{\text{amb}} \sim 3 \text{ kW/m}^2$$

$$A_w/A_{\text{amb}} \sim 2.5$$

Hence $T \approx 0.038$

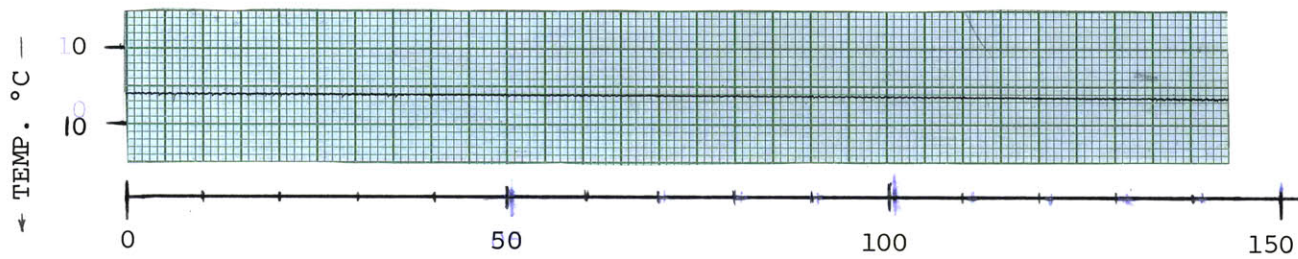


FIG. D-1 Change in Temperature of Cold Water Poured into the Boiling Vessel Initially Empty. Weight of Water was 300g

i.e. the contribution from the surroundings to the total heat flux was less than 4%. With hydrocarbons, this contribution from the surroundings was less than 2%.

A low contribution to the heat flux from the ambient could have been predicted. The calculated Ra number for a convective flow within the 400 μm air gap is given by

$$\text{Ra} = \frac{g\beta\Delta T\delta^3}{\alpha\nu} = 1.96$$

where δ is the gap thickness and $\Delta T \sim 220^\circ\text{C}$, i.e. the inner wall was assumed to be at -196°C (b.pt. nitrogen) and the outerwall at room temperature. The very low Ra indicates that the flow will be laminar and stable against perturbations (Pan, 1970; Batchelor, 1955). Hence heat transfer across the air gap ($k \sim 0.024 \text{ W/mK}$) will be by conduction. (The corresponding k for water is $\sim 0.59 \text{ W/mK}$ at 0°C .)

D-2 THERMOCOUPLES CALIBRATION

The calibration data for the thermocouples are presented in Tables D-1 and D-2. These have been fitted with polynomial regression equations of the form

$$Y = a_0 + a_1x + a_2x^2 + a_3x^3$$

where Y is temperature in $^\circ\text{C}$ and x is the thermocouple readings in millivolts. Inclusion of higher order terms did not cause improvements

in the sum of the squares (of the deviation of the curves from the data). The polynomial coefficients and the mean square deviation are presented in Table D-3. Thermocouples 1, 2, 3 and 4 were in the water. (Positions cited in Appendix F.) Thermocouples 5 and 6 were in the vapor above the boiling pools.

TABLE D-1

Calibration Data for Thermocouples in Water

Temperature* °C (mercury-in-glass thermometer)	Emf Readings (mV)			
	#1	#2	#3	#4
50.6	2.01	2.02	2.02	1.96
45.1	1.77	1.77	1.78	1.68
33.58	1.30	1.31	1.31	1.28
30.7	1.19	1.12	1.19	1.17
28.3	1.10	1.09	1.09	1.10
26.5	1.02	1.03	1.03	1.01
24.7	0.95	0.96	0.96	0.95
22.0	0.84	0.85	0.85	0.85
20.28	0.77	0.79	0.80	0.80
17.1	0.66	0.66	0.67	0.67
15.3	0.59	0.59	0.59	0.61
13.1	0.50	0.50	0.50	0.51
11.0	0.42	0.42	0.42	0.46
9.3	0.35	0.35	0.36	0.39
7.1	0.28	0.28	0.28	0.31
5.5	0.21	0.21	0.21	0.27
3.2	0.13	----	0.11	----
0.4	0.01	0.00	0.01	0.02

*Thermocouple calibrated against the temperature of saturated steam and ice-water baths at 756 mm Hg.

TABLE D-2

Calibration Data* for Thermocouples in Vapor

Temperature °C	#5	Emf Readings (mV) #6	NBS
-195.6	-5.52	-5.50	-5.536
-161.5	-4.96	-4.94	-4.896
-88.3	-3.03	-3.00	-3.037
0.0	0.01	-0.01	0.00
30.3	1.22	1.23	1.21

*The number of points are few because available pure cryogenic liquid were used for the calibration. Pure liquid nitrogen, methane and ethane were used at a barometric pressure of 756 mm Hg.

TABLE D-3

Regression Coefficients for the Thermocouples

Thermocouple Number	a_0	a_1	a_2	a_3	Rms Deviation °C
1	-0.115	26.86	-0.786		0.1
2	-0.172	26.74	-0.752		0.2
3	-0.232	26.821	-0.771		0.2
4	-1.912	28.986	-0.955		0.4
5*	-1.083	25.56	0.129	0.327	1.0
6*	-1.132	25.52	-0.026	0.308	1.1

*See comments with Table D-2

APPENDIX E

SAMPLE DATA TREATMENT

The method of obtaining the heat fluxes from the data is presented in this appendix. The method is illustrated with a typical experiment-run #161 in which liquid methane (~ 1 cm deep) was spilled on 16.9°C water. Following this, the coefficients of the regression equation with which the data are fitted are listed. (Table E-3)

Raw data compiled by the data logger during experiment 161 are presented in Table E-1. These show the record of the actual time in seconds, and the weight of the vessel in which the cryogen boiled (pure methane in this case) and the thermocouple readings in microvolts. The emf reading of the vessel weight in channel 112 is directly convertible to grams. That is, a reading of 006046632 is equivalent to 466.32 g. The third digit from the left in 006046632 specifies that the subsequent digits belong to a number to be multiplied by 10^{-6} with the results in volts. This last point applies to the thermocouple readings (Channels 113-118) as well. Due to a minor fault in the electrical connections, channel 114 (on data logger) was experimentally found to read about $35 \mu\text{V}$ too low. This constant was added to every number from that channel.

The emf readings are converted into physical parameters, grams and degree Celsius, with the aid of the computer. The calibration data presented in Appendix D were used to determine the temperatures. The results are presented in Table E-2. The location of the



Room 14-0551
77 Massachusetts Avenue
Cambridge, MA 02139
Ph: 617.253.2800
Email: docs@mit.edu
<http://libraries.mit.edu/docs>

DISCLAIMER

**Page has been omitted due to a pagination error
by the author.**

(p.325)

thermocouples have been included in the table. (Note that the weight of the vessel and water, at zero time, has been subtracted from the total weight to generate the second column, i.e., the residual weight of cryogen.)

Next, the residual weight of cryogen is fitted with a polynomial regression equation as a function of time. The computer program for this is presented in Table E-4. It is a modified version of the IBM scientific subroutine program POLRG. Briefly, the computer takes the first degree equation

$$y = a_0 + a_1x \quad (E-1)$$

and generates the regression coefficients a_0 and a_1 . (Y is the weight, and x is time.) Then, an analysis of variance is carried out. The computer calculates the sum of the squares of the deviation from the data, Σ , and determines the root mean square deviation, ψ . Then it takes the equation

$$y = a_0 + a_1x + a_2x^2 \quad (E-2)$$

and repeats the process. If there is an improvement in the Σ value, it then adds the term a_3x^3 to equation E-2. Successive terms of the polynomial are added until there is only very little improvement in Σ . Then the calculation stops and the best fit equation has been found. Usually a second or third degree equation was sufficient.

TABLE E-3

The Coefficients of the regression Equation Describing $M_L(t)$

$$M_L(t) = a_0 + a_1t + a_2t^2 + a_3t^3 + a_4t^4$$

M_L is in grams and t is in seconds.

Note:

To keep the order of regression equation low, some of the data were treated in two parts. That is, for a run with long duration or sharp curvature in the M_L versus t plot, the data may be divided into two halves and each half fitted with an equation. The resulting equations are subject to conditions that M_L and dM_L/dt values, calculated at the point of data division, must match, approximately.

*Slope at short times ($< \sim 2-3$ s) incorrect.

EXP. #	Time Range Regressed 0-t s	a ₀	a ₁	a ₂	a ₃	a ₄	Rms Deviation ψ g
157	30	28.6	-0.482	-0.015	0.00013	---	0.11
158	30	34.05	-0.627	-0.007	---	---	0.17
159	30	35.36	-0.6	-0.0085	---	---	0.03
160	30	26.12	-0.508	-0.0147	0.00019	---	0.12
161	30	31.71	-0.467	-0.0131	0.00008	---	0.24
162	30	32.88	-0.347	-0.0231	0.00024	---	0.14
163	30	59.5	-0.732	-0.0067	-0.00034	---	0.25
164	30	71.22	-0.584	-0.0067	-0.00008	---	0.26
165	24	17.87	-0.67	-0.0343	-0.00355	0.00009	0.09
166	20	14.54	-0.394	-0.0155	0.00097	-0.00001	0.07
167	20	15.04	-0.449	-0.0255	0.00163	-0.00001	0.16
168	20	14.484	-0.3510	-0.044	0.00349	-0.00007	0.13
169	30	78.37	-0.701	0.00337	-0.00023	---	0.25
170	30	71.9	-0.88	-0.0195	0.00027	---	0.2
171	18	41.5	-0.126	-0.0922	0.00126	---	0.23
172	15	35.5	-0.343	-0.082	---	---	0.18
173*	1-10	45.4	0.45	-0.348	0.0155	---	0.25
	10-25	48.6	-1.675	-0.01474	0.0007	---	
174*	1-10	46.9	0.358	-0.31	0.0133	---	0.17
	10-30	50.4	-1.784	0.0054	0.00025	---	
175	30	83.59	-2.405	0.057	-0.00086	---	0.33
176*	14	23.05	0.882	-0.391	0.0158	---	0.2
177*	18	24.6	1.49	-0.667	0.0488	-0.00111	0.24
178	30	84.2	-1.308	-0.0353	0.00105	---	0.45
179	30	54.95	-1.379	0.008	-0.00002	---	0.13
180	30	65.14	-1.305	0.007	---	---	0.32
181	30	55.01	-1.066	0.011	-0.00015	---	0.2
182	30	65.31	-1.094	0.0055	---	---	0.16
183	30	66.06	-1.021	0.00255	---	---	0.29
184	20	31.7	-0.469	-0.0405	-0.00057	---	0.2
185	24	41.64	-1.39	0.1224	-0.0116	0.00024	0.16
186	20	36.8	-0.304	-0.0899	0.00122	---	0.3
187	18	29.92	-0.558	-0.0606	0.00048	---	0.17
188	12	16.03	-0.648	-0.053	0.0007	---	0.22
189	16	18.46	-0.388	-0.0268	---	---	0.12
190	15	17.53	-0.526	-0.0088	-0.0011	---	0.13

191	16	16.71	-0.374	-0.0695	0.00195	----	0.3
192	16	17.22	-0.761	-0.0528	0.00257	----	0.19
193	15	16.98	-0.385	-0.095	0.004	----	0.24
194	16	20.69	-0.431	-0.063	0.00102	----	0.09
195	16	23.61	-0.239	-0.0646	----	----	9.13
196	30	79.8	-1.075	-0.102	0.00246	----	----
197	30	64.73	-0.947	-0.0543	0.00061	----	0.4
198	30	64.1	-0.41	-0.087	0.00133	----	0.3
199	0-10	62.24	-0.714	-0.357	-0.00126	----	0.24
	10-30	61.1	0.0073	-0.1377	0.00265	----	----
200*	30	67.7	-1.794	-0.0292	0.001	----	----
201	24	44.77	-0.247	-0.116	0.00228	----	----
202	12	27.4	-0.442	-0.07	-0.00034	----	0.1
203	12	30.64	-0.996	0.0359	-0.00594	----	0.18
204*	17	39.34	-0.177	0.277	-0.0096	----	0.4
205	10	34.99	-1.1994	0.0304	-0.00546	----	0.24
206	17	34.65	-0.382	-0.143	0.00488	----	0.4
207	12	34.34	-0.264	-0.1886	0.00557	----	0.27
208*	17	23.37	0.106	-0.228	0.00885	----	0.36
209*	17	25.56	0.245	-0.201	0.0067	----	0.46
210	30	26.86	-0.413	-0.0239	0.00036	----	0.21
211	30	34.6	-0.5	-0.014	0.00006	----	0.16
212	30	28.45	-0.3	-0.0234	0.00027	----	0.14
213	30	29.26	-0.536	-0.00917	----	----	0.09
214	30	29.6	-0.306	-0.0257	0.00039	----	0.15
215	20	15.97	-0.395	-0.0155	0.00023	----	0.17
216	30	31.76	-0.919	0.0165	-0.00024	----	0.19
217	30	32.14	-0.849	0.0138	-0.00021	----	0.19
218	30	27.3	-0.708	0.00452	----	----	0.18
219	30	24.5	-0.631	0.004	----	----	0.17
220	30	34.95	-0.746	0.00317	----	----	0.17
221	30	25.13	-0.728	0.00866	-0.00008	----	0.15
222	30	27.62	-0.742	0.00884	-0.00009	----	0.13
223	15	23.06	-0.279	-0.135	0.0043	----	0.14
224	10	13.44	-0.315	-0.0714	----	----	0.11
225	10	15.08	-1.163	-0.00545	----	----	0.05
226	20	11.44	-0.334	-0.00772	----	----	0.14
227	16	22.05	-0.491	-0.0557	0.00095	----	0.1
228	20	24.34	-0.79	-0.0157	----	----	0.09
229	20	27.34	-0.753	-0.01956	----	----	0.17
230	20	25.69	-0.734	-0.018	-0.00024	----	0.11

231	18	26.18	-0.776	-0.0413	0.00047	---	0.11
232	20	19.37	-0.294	-0.097	0.0032	---	0.18
233	17	18.72	-0.617	-0.026	0.00034	---	0.13
234	20	24.82	-1.265	0.1074	-0.0108	0.00029	0.16
235	16	21.107	-1.795	0.194	-0.017	0.00045	0.09
236	15	17.76	-0.5	-0.071	0.0021	---	0.23
237	30	32.4	-0.447	-0.0139	0.00007	---	0.14
238							
239	20	35.08	-0.607	-0.08	0.00174	---	0.29
240	22	31.91	-0.79	-0.0405	0.0007	---	0.22
241	2-22	24.53	-0.13	-0.114	0.0035	---	0.24
242	20	30.5	-1.282	0.0103	-0.00082	---	0.2
243	22	33.25	-0.831	-0.0285	0.00043	---	0.19
244	0-15	38.83	-1.0396	-0.211	0.0102	---	0.4
245*	25	32.14	-0.627	-0.0183	-0.00016	---	0.17
246	25	31.04	-0.808	-0.0157	0.00013	---	0.16
247	20	31.8	-1.21	0.0102	-0.00045	---	0.27
248	17	27.56	-0.952	-0.0274	0.00065	---	0.16
249	16	29.05	-0.843	-0.0277	0.00037	---	0.12

In run 161, the coefficients are $a_0 = 31.71$, $a_1 = -0.467$, $a_2 = -0.013$, and $a_3 = 8(10^{-5})$. The root mean deviation (ψ) was 0.24 g. We now have a function $M_L(t)$ which the computer is made to plot together with the actual data. The plot for run 161 is presented in Figure E-1.

In the next step, $M_L(t)$ is differentiated with respect to time, t . Hence we obtain dM_L/dt . The heat flux as given by Equation (5-6) is

$$Q' = \frac{dM_L}{dt} (\Delta H_v + C_p (T_v - T_{sat})) \quad (E-3)$$

T_v is obtained by averaging the vapor temperature at the desired time. The heat flux as a function of time for run 161 is plotted in Figure E-2.



Room 14-0551
77 Massachusetts Avenue
Cambridge, MA 02139
Ph: 617.253.2800
Email: docs@mit.edu
<http://libraries.mit.edu/docs>

DISCLAIMER

**Page has been omitted due to a pagination error
by the author.**

(Pages 332-334)

COMPUTER PROGRAM

APPENDIX F

EXPERIMENTAL DATA

This appendix contains the list of the experiments performed, and the variable of each run in Tables F-1 and F-2. The data recorded on the Hewlett-Packard acquisition system are presented in the sequence of the runs in Table F-3.

TABLE F-1

Set of Experiments

HYDROCARBONS (%)

RUN #	CH ₄	C ₂ H ₆	C ₃ H ₈	nC ₄ H ₁₀	iC ₄ H ₁₀
157-170 210-215 237	99.98	---	---	---	---
171-178	---	99.84	---	0.16	---
227-236	98	2	---	---	---
239	94.7	5.3	---	---	---
240	90.9	9.1	---	---	---
241	81.8	18.2	---	---	---
242	93.2	6.8	---	---	---
245	99.45	0.55	---	---	---
243	91.5	---	8.5	---	---
246	99.85	---	0.15	---	---
247	99.43	---	0.57	---	---
248	99.41	---	0.59	---	---
249	99.84	---	---	0.16	---
184-200 223-226	98.2	1.62	0.112	0.03	0.043
201-206	89.2	8.2	2.0	0.2	0.2
207-209	82.0	14.6	3.0	0.2	0.2
244	78.2	8.6	6.9	3.1	3.2

TABLE F-2

Variables of the Experiments

§1. ULTRA-PURE METHANE (99.98%)

RUN #	\bar{T}° Initial ^W Water Temperature °C	M_L Mass ^L of Cryogen Spilled g
157	52.7	28.05
158	40.85	33.4
159	31.25	34.75
160	22.5	25.6
161	16.9	31.75
162	9.85	32.5
163	30.1	58.85
164	16.8	70.4
165	27.8	17.45
166	23.2	14.0
167	35.3	14.66
168	30.15	14.18
169	26.05	77.96
170	9.3	71.1
210	50.15	26.53
211	39.5	34.14
212	29.8	28.09
213	22.0	28.54
214	15.0	29.5
215	8.3	15.48
237	14.4	32.19

§2. CHEMICALLY PURE ETHANE (contains 0.16% nC₄H₁₀)

171	49.4	41.06
172	37.15	35.21
173	27.9	45.32
174	17.3	47.05
175	8.2	81.2
176	32.6	23.65
177	26.75	25.49

§3. BINARY MIXTURES

RUN #	% COMPONENT				\bar{T}_W ° Initial Water Temperature °C	M_L Mass ^L of Cryogen Spilled g
	CH ₄	C ₂ H ₆	C ₃ H ₈	nC ₄ H ₁₀		
227	98	2	---	---	26.4	21.34
228	---	---	---	---	20.7	23.51
229	---	---	---	---	15.3	26.65
230	---	---	---	---	9.5	24.91
231	---	---	---	---	5.2	25.28
232	---	---	---	---	27.5	19.03
233	---	---	---	---	22.3	18.05
234	---	---	---	---	17.8	23.86
235	---	---	---	---	12.4	19.4
236	---	---	---	---	9.0	17.45
239	94.7	5.3	---	---	11.4	34.76
240	90.9	9.1	---	---	11.9	32.15
241	81.8	18.2	---	---	12.1	26.65
242	93.2	6.8	---	---	22.2	31.35
243	91.5	---	8.5	---	23.0	33.03
245	99.45	0.55	---	---	15.0	31.1
246	99.85	---	0.15	---	13.5	30.21
247	99.43	---	0.57	---	12.8	30.6
248	99.41	---	0.59	---	12.9	26.5
249	99.84	---	---	0.16	12.6	28.07

§4. 5-COMPONENT MIXTURES

RUN #	% COMPONENT					\bar{T}_W ° Initial Water Temperature °C	M _L Mass ^L of Cryogen Spilled g
	CH ₄	C ₂ H ₆	C ₃ H ₈	nC ₄ H ₁₀	iC ₄ H ₁₀		
184						60.2	31.35
185						47.7	40.14
186						36.0	36.75
187						27.3	29.48
188						21.0	15.35
189						55.4	18.15
190						48.0	16.92
191						40.8	16.5
192	98.2	1.62	0.112	0.03	0.043	35.7	16.5
193						30.9	16.65
194							
195						21.7	23.42
196						16.2	78.45
197						55.0	64.10
198						37.5	63.85
199						22.0	61.5
200						8.5	64.7
223						6.7	22.66
224						---	12.97
225						17.6	13.91
226						15.0	11.19
201						55.0	45.0
202						40.5	26.95
203						32.8	29.65
204	89.2	8.2	2.0	0.2	0.2	24.9	39.7
205						15.9	33.86
206						7.6	34.6
207						17.6	34.05
208	92.0	14.6	3.0	0.2	0.2	25.4	23.5
209						19.4	26.06
244	78.2	8.6	6.9	3.1	3.2	23.3	37.96

§5. LIQUID NITROGEN

RUN #	\bar{T}_w ° Initial Water Temperature °C	M_L Mass of Cryogen Spilled g
179	52.0	53.72
180	40.8	64.85
181	31.4	54.53
182	23.5	64.69
183	15.2	63.86
216	26.1	31.5
217	22.0	31.7
218	18.1	26.77
219	14.9	24.4
220	12.25	34.7
221	8.5	24.78
222	6.3	27.12

Table F-3
Experimental Data

On File With:

Professor Robert C. Reid
Department of Chemical Engineering
Massachusetts Institute of Technology
Cambridge, Massachusetts 02139

LITERATURE CITED

1. Alfred, J.C. and G.H. Blount, (1954) "Experimental Studies of Taylor Instability" Univ. California, Los Alamos Lab., Rep. LA - 1600.
2. Anonymous, "Study on LNG Safety 1 and 2", Informal reports dated February 1971. Tokyo Gas Company Limited.
3. Arakawa, K., (1954) "Studies on the Freezing of Water: II Formation of Disc Crystals" J. Fac. Sci., Hokkaido Univ. Japan, Ser II, Vol IV (5), 311.
4. Ibid, (1955) "Studies on the Freezing of Water: III Crystallography of Disc Crystal and Dendrites Developed from Disc Crystals" J. Fac. Sci., Hokkaido Univ. Japan, Ser II, Vol IV (5), 355.
5. Bankoff, S.G., (1966) "Diffusion - Controlled Bubble Growth", Adv. Chem. Engr. 6, 1-60.
6. Bankoff, S.G. and Mehra, V.S., (1962) "A Quenching Theory for Transition Boiling" Ind. Engr. Chem. Fund. 1, 38-40.
7. Batchelor, G.K., (1954) "Heat Transfer by Free Convection across a Closed Cavity between Vertical Boundaries at Different Temperatures" Quart. Appl. Math. 12 (3), 209.
8. Beer, H. and P. Burow, (1971) "Bubble Dynamics and the Interferometric Determination of Temperature Fields in the Vicinity of Growing Bubbles in Nucleate Boiling" Proc. First Nat. Heat Mass Transf. Conf., Indian Inst. Teh. Madras. HMI - 42-71.
9. Bellman, R. and R.H. Pennington, (1954) "Effects of Surface Tension and Viscosity on Taylor Instability" Quart. Appl. Math. 12, 151.
10. Berenson, P.J., (1960) On Transition Boiling Heat Transfer from a Horizontal Surface Ph.D. Thesis. Mech. Engr. Dept. M.I.T.

11. Berenson, P.J., (1961) "Film-Boiling Heat Transfer from a Horizontal Surface" J. Heat Transfer, August. 351-358.
12. Berenson, P.J., (1962) "Experiments on Pool Boiling Heat Transfer" Int. J. Heat Mass Transfer 5, 985.
13. Berg, J.C., A. Acrivos and M. Boudart, (1966) "Evaporative Convection" Advances in Chemical Engineering 6, 61-123.
14. Bigg, E.K., (1953) "The Supercooling of Water" Proc. Phys. Soc. B. 66, 688.
15. Blair, L.M. and J. A. Quinn, (1969) "The On-set of Cellular Convection in a Fluid Layer with Time-Dependent Density Gradients" J. Fluid Mech. 36 (pt 2), 385.
16. Blanchard, D., (1963) Progress in Oceanography, Vol 1 (Editor M. Sears) MacMillan Co., 70 ff.
17. Bonilla, C.F. and Eisenberg, A.A., (1948) "Heat Transfer to Boiling Styrene, Butadiene and their Mixtures with Water" Ind. Engr. Chem. 40 (6), 1113.
18. Borishansky, V.M., (1959) "Heat Transfer to a Liquid Freely Flowing Over a Surface Heated to a Temperature Above the Boiling Point" AEC-tr-3405 ed. Kutateladze S.S.
19. Borishansky, V.M. and B.S. Fokin, (1965) "Correlation of Heat Transfer Data on Stable Film Pool Boiling at Vertical Surfaces for Free Convection" Int. Chem. Eng. 5 (4), 666.
20. Bošnjakovic, F., (1930) "Verdampfung und Flüssigkeitsüberhitzung" Tech. Mech. Thermo-Dynam. Berl. 1, 358-62.
21. Boyle, G.J. and Kneebone, A., (1973) "Laboratory Investigations into the Characteristics of LNG Spills on Water: Evaporation, Spreading and Vapor Dispersion" Shell Research Limited, Thorton Research Centre, Chester, England. API Report 6Z32.

22. Bradfield, W.S., (1966) "Liquid-Solid Contact in Stable Film Boiling" Ind. Engr. Chem. Fund. 5 (2), 200-204.
23. Bragg, J.R. and Westwater, J.W., (1970) "Film Boiling of Immiscible Liquid Mixtures on a Horizontal Plate" Proc. Heat Transfer Conf.
24. Bromley, L.A., (1950) "Heat Transfer in Stable Film Boiling" Chem. Engr. Prog. 46 (5), 221-7.
25. Burgess, D.S., Murphy, J.N. and Zabetakis, M.G., (1970) "Hazards of LNG Spillage in Marine Transportation" SRC Report No. S-4105, Bureau of Mines, Pittsburgh, Pa.
26. Burgess, D., Biordi, J. and Murphy, J., (1972) "Hazards of Spillage of LNG into Water" MIPR No. Z-70099-9-12395.
27. Chambré, P.L., (1956) "On the Dynamics of Phase Growth" Quart. J. Mech. and Appl. Math., IX, pt 2, 244-233.
28. Chandrasekhar, S., (1960) Hydrodynamic and Hydromagnetic Stability, Oxford University Press, London.
29. Chang, Y., (1959) "Wave Theory of Heat Transfer in Film Boiling" J. Heat Transf. 81, February, 1-12.
30. Carslaw, H.S. and J. C. Jaeger, (1959) Conduction of Heat in Solids 2nd ed. Oxford Univ. Press, London.
31. Clements, L.D. and C. P. Colver, (1970) "Natural Convection Film Boiling Heat Transfer" Ind. Engr. Chem. 62 (9), 26-46.
32. Clements, L.D. and C. P. Colver, (1972) "Generalized Correlation on Boiling" J. Heat Transfer 94, 324.
33. Corty, C. and A. S. Fourst, (1955) "Surface Variables in Nucleate Boiling" Chem. Engr. Symp. Ser. 17 (51).

34. Davies, J. T. and E. K. Rideal, (1963) Interfacial Phenomena, Academic Press, N.Y.
35. Day, J.A., (1964) "Production of Droplets and Salt Nuclei by the Bursting of Air-Bubble Films" Quart. J. Roy. Met. Soc. 90, 72.
36. Ibid., (1967) "Bursting Air Bubbles Studied by the Time Exposure Technique" Nature 216, 1097.
37. Deaton, W.M. and Frost, E.M., Jr., (1946) "Gas Hydrates and Their Relation to the Operation of Natural-Gas Pipelines" Mono 8, U.S. Department of Interior, Bureau of Mines.
38. Denbigh, K., (1966) Chemical Equilibrium Cambridge Univ. Press. London, 2nd ed.
39. Dergarabedian, P., (1953) "The Rate of Growth of Vapor Bubbles in Superheated Water" J. Appl. Mech. 20, 537.
40. Dergarabedian, P., (1960) "Observations on Bubble Growths in Various Superheated Liquids" J. Fluid Mech. pt 1, 9, 39-48.
41. Drew, T.B. and Mueller, A.C., (1937) "Boiling" AIChE Trans. 33, 449.
42. Eckert, E.R.G. and M.R. Drake, Jr., (1972) Analysis of Heat and Mass Transfer McGraw-Hill Book Co., N.Y.
43. Evans, H.L., (1968) Laminar Boundary-Layer Theory Addison-Wesley Co., Reading, Mass. U.S.A.
44. Fletcher, N.H., (1966) The Physics of Rain Clouds, Cambridge University Press. England.
45. Flynn, T.M., J.W. Draper and J.J. Roos, (1961) "The Nucleate and Film Boiling Curve of Liquid Nitrogen at One Atmosphere", Adv. Cryogenic Engr., 7, 539-45.

46. Froesshing, N., (1940) "Verdunstung, Wärmelübergang und Geschwindigkeitsverteilung bei Zweidimensionaler und Rotationssymmetrischer Laminarer Grenzschichtströmung. Lunds. Univ. Avsskr. N.F. Avd. 2, 35, #4.
47. Foettinger, H., (1939) "Strömungen in Dampfkesselanlagen", Mitt. der. Ver. Groß-Kesselbesitzer, 73, 151.
48. Forster, H.K. and N. Zuber, (1954) "Growth of a Vapor Bubble in Superheated Liquid" J. Appl. Phys. 25, 474-8.
49. Forster, K. and Zuber, N., (1955) "Dynamics of Vapor Bubbles and Boiling Heat Transfer" AIChE J. 1, 531-5.
50. Frost, E.M., jr. and Deaton, W.M., (1946) "Gas Hydrates Composition and Equilibrium Data" The Oil & Gas Journal, July 27, 170-8.
51. Gallant, R.W., (1968) Physical Properties of Hydrocarbons, Vol 1, Gulf Publ. Co., Houston, Texas
52. Gibbons, R.M., (1973) "Thermophysical Data for Cryogenic Material", Chapter 12 of Cryogenic Fundamentals by Haselden, G.G.
53. Gibson, D.C., (1972) "The Kinetic and Thermal Expansion of Vapor Bubbles" J. Basic Engr., March 89-96.
54. Gordon, K.F., Singh, T. and Weissman, E.Y., (1961) "Boiling Heat Transfer Between Immiscible Liquids" Int. J. Heat Mass Transfer 3, 90.
55. Hammerschmidt, E.G., (1934) "Formation of Gas Hydrates in Natural Gas Transmission Lines" Industrial and Engineering Chem. 26, (8), 851-5.
56. Hayami, S. and Toba, Y. "Drop Production by Bursting Air Bubbles on the Sea Surface" J. Oceanog. Soc. Japan 14, 145, 1958.
57. Hovestreibdt, J., (1963) "The Influence of the Surface Tension Difference on the Boiling of Mixtures" Chem. Engr. Sci., 18, 631-9.

58. Jakob, M. and Fritz, W., (1931) "Versuche über den Verdampfungsvorgang", Forshung a.d. Ger. d. Ingenieurwes 2, 435-447.
59. Jakob, M., (1949) Heat Transfer, Vol 1, 621-30, N.Y., J. Wiley & Son.
60. Katz, D.L. et al, (1959) Handbook of Natural Gas Engineering. McGraw-Hill Co., Inc., N.Y.
61. Kantsky, D.E. and Westwater, J.W., (1967) "Film Boiling of a Mixture on a Horizontal Plate" Int. J. Heat Mass Transfer 10, 253-6.
62. Kientzler, C.F. A.B. Arons, D.C. Blanchard and A.H. Woodcock, (1954), "Photographic Investigation of the Projection of Droplets by Bubbles Bursting at a Water Surface" Tellus 6, 1.
63. Knelman, F., Dombrowski, N. and Newitt, D. "Mechanism of the Bursting of Bubbles" Nature 173, 261 (1954).
64. Kutateladze, S.S., (1963) Fundamentals of Heat Transfer, Academic Press. N.Y.
65. Lenteritz, R. and Mangler, W., (1945) "Die symmetrische Potentialströmung gegen einen Kreiskegel" Untersuch. Mitt. dtsh. Luftfahrft 3226.
66. Levich, V.G., (1962) Physicochemical Hydrodynamics, Prentice-Hall, Inc., Englewood Cliffs, N.J.
67. Lewis, D.J., (1950) "The Instability of Liquid Surfaces when Accelerated in a Direction Perpendicular to their Plane", pt II, Proc. Roy. Soc. London 202(A), p. 81.
68. Lock, R.C., (1951) "The Velocity Distribution in the Laminar Boundary Layer between Parallel Streams" Quart. J. Mech. Appl. Math. 4, 42-63.
69. M. S. Longuet-Higgins, (1953), "Mass Transport in Water Waves", Phil. Trans. Roy. Soc. London A245, 66.

70. M. S. Longuet-Higgins, (1960) "Mass Transport in the Boundary Layer at a Free Oscillating Surface" J. Fluid. Mech. 8, pt 2, 293.
71. Lord, Rayleigh, (1916) "On Convective Currents in a Horizontal Layer of Fluid when the Higher Temperature is on the Underside" Phil. Mag., 32, 529-46.
72. Luborsky, F.E., (1959) "The Kinetics of Growth of Spherical Iron Crystallites in Mercury" J. Phys. Chem. 61, 1336-1340.
73. Mangler, W., (1943) "Die ähnlichen Lösungen der Prandtlschen Grenzschtichtgleichungen" Zeitschrift für angewandte Mathematik und Mechanik 23, 241.
74. Marshall, W.R., Jr., (1954) "Evaporation from Drops and Sprays", Chapter 10 in "Atomization and Spray Drying" Chem. Engr. Prog. Mono. Ser. 50, 2.
75. Mason, B.J., (1955) "Bursting of Air Bubbles at the Surface of Sea Water" Nature 174, 470.
76. Mason, B.J., (1958, a) "The Supercooling and Nucleation of Water". Advances in Physics 7, 211.
77. Ibid., (1958) "The Growth of Ice Crystals from the Vapor and the Melt" Advances in Physics 7, 235.
78. May, W.G., W. McQueen and R.H. Whipp, (1973) "Spills of LNG on Water", Esso Research and Engr. Co., Florham Park, N.J. Presented at API Conference, March 26.
79. McAdams, W.H., (1954) Heat Transmission. 3rd. ed. McGraw-Hill Book Co., Inc.
80. Milne - Thomson, L.M., (1960) Theoretical Hydrodynamics, MacMillan Co., N.Y. 4th Ed.

81. Morozov, V.G., (1963) "An Experimental Investigation of the Cessation of Film Boiling of a Liquid on a Submerged Heating Surface" Inzh-niz. Zh. 4, 15; and Inst. Chem. Engr. 3 (1), 48-51.
82. Nakanishi, E. and Reid, R.C., (1971) "Liquid Natural Gas - Water Reactions" Chem. Engr. Progr. 67 (12), 36.
83. Newitt, D.M., Dombrowski, N. and Knelman, F.H. "Liquid Entrainment, 1. The mechanism of drop formation from gas or vapour bubbles" Trans. Instn. Chem. Engrs. 32, 244, 1954.
84. Novakovic, M. and Stefanovic, M., (1964) "Boiling from a Mercury Surface" Int. J. Heat Mass. Trans. 7, 801.
85. Nukiyama, Shiro, (1934) "Maximum and Minimum Values of Heat Transmission from Metal to Boiling Water Under Atmospheric Pressure", J. Soc. Mech. Engr. Japan, 37, 367.
86. Pan, P.C., (1970) Stability of Natural - Convection between Two Vertical, Parallel Plates at Different Temperatures Sc.D. Thesis, Chem. Engr. Dept. M.I.T.
87. Pearson, J.R.A., (1958) "On Convection Cells Induced by Surface Tension" Journal Fluid Mech. 4, 489-500.
88. Perry, J.H., (1963) Chemical Engineer's Handbook, McGraw-Hill Book Co., 4th Ed.
89. Phillips, O.M., (1969) The Dynamics of the Upper Ocean, Cambridge Univ. Press. London.
90. Plesset, M.S. and S.A. Zwick, (1952) "A Non-steady Heat Diffusion Problem with Spherical Symmetry" J. Appl. Phys. 23 (1), 95-98.
91. Plesset, M.S. and S. A. Zwick, (1954) "The Growth of Vapor Bubbles in Superheated Liquids" J. Appl. Phys. 25 (4), 493-500.

92. Pound, G.M., L.A. Madonna and C. Sciulli, (1951) "Kinetics of Nucleation in Atmospheric Phase Transitions" Carnegie Inst. Tech. Metals Res. Lab. Quart. Rep 5.
93. Powell, C. F., (1928) "Condensation Phenomena at Different Temperatures", Proc. Roy. Soc. London 119 (A), 553.
94. Park, E.L., Colver, C.P., Slipevich, C.M., (1966) "Nucleate and Film Boiling Heat Transfer to Nitrogen and Methane at Elevated Pressures and Large Temperature Differences" Adv. Cryo. Eng. 11, 516-529.
95. Ratcliffe, E.H., (1962) "The Thermal Conductivity of Ice: New Data on the Temperature Coefficient" Phil. Mag. Ser. 8, 7, 1197-1203.
96. Rohsenow, W.M., (1952) "A Method of Correlating Heat Transfer Data for Surface Boiling of Liquids" ASME Trans. 74-969-76.
97. Rohsenow, W.M., (1971) "Boiling" Annual Review of Fluid Mechanics, Vol 3.
98. Roll, J. B. and J. E. Myer, (1964) "The Effect of Surface Tension on Factors in Boiling Heat Transfer" A.I.Ch.E. J. 10, 530.
99. Ruzicka, J., (1959) "Heat Transfer to Boiling Nitrogen" in Problems of Low Temperature Physics Vol 1, Pergamon Press, N.Y., 323-9.
100. Saito, S., Shazaburo, Marshall D.R. and Kobayashi, R. "Hydrates at High Pressures: Pt II, Application of Statistical Mechanics to the Study of Hydrates of Methane, Argon, and Nitrogen" AICHE J. 10 (5), 734-40.
101. Saito, S., Shazaburo and Kobayashi, R., (1965) "Hydrates at High Pressure: Pt III, Methane - Argon - Water, Argon - Nitrogen - Water Systems" AICHE J. 11 (1), 96-9.

102. Sander, A. and E. Damköhler, (1943) "Übersättigung bei spontanen Keimbildung in Wasserdampf" Naturwissenschaften 31, 460.
103. Sauer, H.J., Jr., and Ragsdell, K.M., (1971) "Film Pool Boiling of Nitrogen from Flat Surfaces" Adv. in Cryogenic Engr. 16.
104. Saville, D.A., (1973) "The Effects of Interfacial Tension Gradients on the Motion of Drops and Bubbles" Chem. Engr. J., 5, 251-9.
105. Schaefer, V.J., (1950) "The Formation of Frazil and Anchor Ice in Cold Water" Trans. Am. Geophys. Un. 31 (6), 885.
106. Schlichting, H., (1968) Boundary Layer Theory McGraw-Hill Book Co., N.Y. 6th Ed.
107. Schwertz, F.A. and Brow, J.E., (1951) "Diffusivity of Water Vapor in Some Common Gases" J. Chem. Phy. 19 (5), 640.
108. Science, C.T., Colver, C.P. and Sliepcevich, C.M. "Pool Boiling of Methane between Atmospheric Pressure and the Critical Pressure", Adv. in Cryogenic Engr. 12, 395.
109. Scriven, L.E., (1959) "On the Dynamics of Phase Growth" Chem. Engr. Sci. 10(1/2), 1-13.
110. Scriven, L.E., (1960) "Dynamics of a Fluid Interface" Chem. Engr. Sci. 12, 98-108.
111. Scriven, L.E., (1962) "On the Dynamics of Phase Growth" Chem. Engr. Sci. 17, 55.
112. Sideman, S., (1966) "Direct Contact Heat Transfer between Immiscible Liquids" Adv. in Chem. Engr. 6 Academic Press., N.Y.
113. Silveston, P.L., (1958) "Wärmedurchgang in waagerechten Flüssigkeitsschichten" Pt 1 Forsh. Ing. Wes. 24, 29-32 and 59-69. (See also Schmidt E. and Silveston, P.L. (1960) "Natural Convection in Horizontal Liquid Layers" Chem. Engr. Symp. Ser. 29, 55).

114. Skinner, L.A., (1963) Ph.D. Thesis, Northwestern Univ., Evanston, Illinois.
115. Slipecevich, C.M., Hashemi, H.T. and Colver, C.P. "Heat Transfer Problems in LNG Technology" Chem. Engr. Symp. Ser. 64 (87), 120-126.
116. Spangenberg, W. and W. Rowland "Convective Circulation in Water Induced by Evaporative Cooling" The Physics of Fluids. 4 (6), 743 (1961).
117. Sunderland, J.E. and Johnson, K.R., (1964) "Shape Factors for Heat Conduction Through Bodies with Isothermal or Convective Boundary Conditions" Trans. Am. Soc. Heating, Refrigerating and Air Conditioning engineers. 70, 237.
118. Taylor, G.I., (1950) "The Instability of Liquid Surfaces when Accelerated in a Direction Perpendicular to their Plane" Pt 1, Proc. Roy. Soc. London 201 (A), 192.
119. Toba, Y., (1959) "Drop Production by Bursting of Air Bubbles on the Sea Surface (II), Theoretical Study of the Shape of Floating Bubbles" J. Oceanog. Soc. Japan 15, 121.
120. Tong, L.S., (1965) Boiling Heat Transfer and Two Phase Flow. J. Wiley and Son, N.Y.
121. Turner, J.S., (1973) Buoyancy Effects in Fluids, Camb. Univ. Press., London.
122. van Strahlen, S.J.D., (1966, 1967) "The Mechanism of Nucleate Boiling in Pure Liquids and in Binary Mixtures" Pt. I - IV. Int. J. Heat Mass Transfer, 9, 995-1046 (1966) 10, 1469-1498 (1967)
123. van Strahlen, S.J.D., (1968) "The Growth Rate of Vapor Bubbles in Superheated Pure Liquids and Binary Mixtures" Pt I and II. Int. J. Heat Mass Transfer, 11, 1467-1512.

124. Vos, A.S. and van Strahlen, S.J.D., (1956) "Heat Transfer to Boiling Water - Methylethylketone Mixtures" Chem Engr. Sci. 5, 50-6.
125. Weast (Ed.) (1972-3) Handbook of Chemistry and Physics, 53rd Ed.
126. Wehmeyer, D.P. and T.W. Jackson, (1972) "Transient Film Boiling of Carbon Tetrachloride and Freon-113 on a Horizontal Cylindrical Surface" J. Heat Transfer, November.
127. Westwater, J.W. and J. G. Santangelo, (1955) "Photographic Study of Boiling" Ind. Engr. Chem. 47 (8), 1605 - 1610.
128. Wijk, W.R. van, Vos, A.S., van Strahlen, S.J.D., (1956) "Heat Transfer to Boiling Binary Liquid Mixtures" Chem. Engr. Sci. 5, 68-80.
129. Woodcock, A.H., Kientzler, C.F., Arons, A.B., and Blanchard, D.C., (1953) "Giant Condensation Nuclei from Bursting Bubbles" Nature, 172, 1144.
130. Zuber, N., (1958) "On the Stability of Boiling Heat Transfer", Trans. ASME 80 (3), 711-720.

BIOGRAPHICAL NOTE

The author was born February 13, 1948 at Erijiyan-Ekiti, Nigeria. He received his primary education at Ibadan (1953-1959), and attended Christ's School, Ado-Ekiti, Nigeria, for secondary education (1960-1966).

In September 1966, he was enrolled as an undergraduate with an ASPAU scholarship at the Department of Chemical Engineering at Purdue University, Lafayette, Indiana. Upon being graduated with distinction 2 1/2 years later, he was admitted to M.I.T. with an assistantship. He was awarded an M.S. in 1970 upon submission of a thesis. He also attended M.I.T. Practice Schools. He worked for the G. E. Company between 1970 and 1972. He is currently on leave of absence from Polaroid Corporation. He is a member of Tau Beta Pi, Omega Chi Upsilon and Sigma Xi.

The author is married and has a son.